INTERACTION BETWEEN STRUCTURAL WALLS, FLOORING SLABS AND GRAVITY FRAMES IN REINFORCED CONCRETE BUILDINGS

A thesis submitted in partial fulfilment of the requirements for the Degree

of Doctor of Philosophy in Structural Engineering

in the University of Canterbury

by Reza E. Sedgh

Supervisor: Prof. Rajesh Dhakal

Associate Supervisors: Prof. Athol Carr and Dr. Chin-Long Lee

University of Canterbury

2018

ABSTRACT

Reinforced concrete (RC) wall structures are generally relied to perform adequately in resisting the lateral forces during strong earthquake ground motions. However, recent earthquakes have indicated that several RC structural walls were damaged or failed because of the deformation compatibility issues between the structural walls and secondary gravity systems. This failure mode is caused by interaction between the structural walls, floor systems and gravity columns under the severe earthquake actions. Hence, in order to predict the inelastic response of such structural systems under seismic loads, the hysteretic response of critical zones in structural walls and their interactions with other structural components should be accurately described by reliable numerical models.

A review of available literature confirmed that the interaction mechanism between the structural walls with neighboring structural subsystems is not yet well understood, particularly in the nonlinear response range. The research presented in this Thesis seeks to investigate the interaction mechanism between the structural walls, floor systems and gravity columns in multi-story shear wall buildings. The consequences of such interaction is also explained, which raise some concerns regarding the reliability of current design code provisions.

A numerical modelling approach is developed in this research, which is capable of successfully capturing the dynamic response of multi-storey structural wall systems under ground motion excitations. Experimental results of scaled isolated RC wall specimens and a full-scale multi-storey RC wall system tested under static and dynamic loads are used for verification of the adopted modelling and analysis approach. The mechanism of three-dimensional spatial interaction between the structural walls, floor systems, and gravity columns under in-plane static and dynamic loadings was scrutinized by using the validated numerical model. The main parameters controlling this interaction mechanism are identified to be the flexural/torsional

stiffness of the floor systems, the bay length between the walls and gravity frames, and the wall height, and the design base rotation.

Thus, this thesis reports the insight gained into the nature of this interaction through an extensive numerical analysis conducted using a verified and validated constitutive shear wall model employing multilayered shell elements. Several important aspects of this interaction in typical multi-storey shear wall buildings have been addressed in this Thesis. For example, based on an extensive parametric analysis of multiple case study shear wall buildings, typical values of system overstrength factor have been proposed for design of shear walls. Using the proposed system overstrength factors in capacity design of structural walls improves the seismic performance of RC shear wall buildings. Additionally, the impact of three-dimensional interactions on the amount of the axial forces in the gravity columns and shear walls is also examined in this Thesis. Finally, a practical approach for appropriate modelling of structural damping in nonlinear dynamic analysis of ductile walls is recommended.

The proposal of a simplified method for the estimation of system overstrength factor (caused by the spatial vertical interaction) in multi-storey structural walls is another outcome of this Thesis. The proposed simplified method is found to be reasonably accurate when compared to the numerical analysis results.

ACKNOWLEDGEMENTS

This thesis is the product of a long journey that would not have been possible without the help of many. Therefore, I would like to acknowledge all the support and encouragement I have received during my doctoral research.

First and foremost, I am deeply indebted to my primary supervisor, Professor Rajesh Dhakal, for his continued support and advice. I am also grateful to my associate supervisors, Emeritus Professor Athol Carr and Dr. Chin-Long Lee for their guidance and encouragement during my study.

I would like to thank the University of Canterbury for funding my research with the UC Doctoral Scholarship. The entire Civil and Natural Resource Engineering Department at the University of Canterbury deserves praise for providing me with several teaching assistant roles over the past four years.

I am thankful to my parents for their life-long love, encouragement, and support. My special thanks go to my wife, Dr. Nazila Alinaghi for her unwavering support and love. She kindly proofread some sections of this thesis. Finally, thanks to my fellow PhD students at the University of Canterbury for being such amazing friends. I would like to dedicate this thesis to my family.

TABLE OF CONTENTS

LIST OF TABLES

LIST OF FIGURES

1 Introduction, Motivation and Literature Review

1.1 Introduction

Reinforced concrete (RC) structural walls are very efficient components for resisting lateral loads imposed by earthquakes. They provide considerable strength and stiffness as well as the deformation capacity needed to resist the demands induced by strong earthquake ground motions. In regions where strong earthquake ground motions are expected to occur, it is not feasible or economical to design a structural wall to remain fully elastic during a severe earthquake. Thus, inelastic deformations are expected, mostly at the base of the structural walls. Allowing occurrence of inelastic deformations reduces the elastic force that a structural wall must resist, and consequently, the RC structural wall must be specifically detailed at its critical zones, i.e., special transverse reinforcement must be provided within the critical zones where significant inelastic deformations and energy dissipation are expected to be concentrated.

RC structural walls with different shapes of cross sections such as I, T, L, and C are used in the centre or the perimeter of a building plan to resist the lateral forces. In shear wall buildings, the gravity loads are commonly resisted by floor slab-column gravity frames or beam-column gravity frames. Such systems are preferred for moderate and high-rise buildings.

RC structural walls are employed to resist both vertical and horizontal forces in buildings (Figure 1.1). The construction practices in the building industry of different regions of the world offer different forms of RC structural walls such as in-situ concrete, tilt-up concrete or pre-cast concrete structural walls. Some engineers believe that structural walls should be only used to resist the lateral forces while the gravity loads should utilize a separate load path to the ground. Hence, some practicing engineers prefer to use gravity columns even very close to the structural walls to avoid transferring any gravity force to the structural walls. It is believed that having different load paths for the gravity loads and the lateral forces can reduce the risk of progressive/total collapse of multi-storey shear wall buildings under severe earthquakes. This concept was implemented commonly in older multi-storey shear wall buildings. The axial force

in these kinds of structural walls is quite low, typically less than $0.05f_cA_g$. However, in some design codes, the upper limit of allowable axial forces in structural walls is set and an example is the limit at $0.35f_cA_g$ according to new amendment of NZS3101:2006.

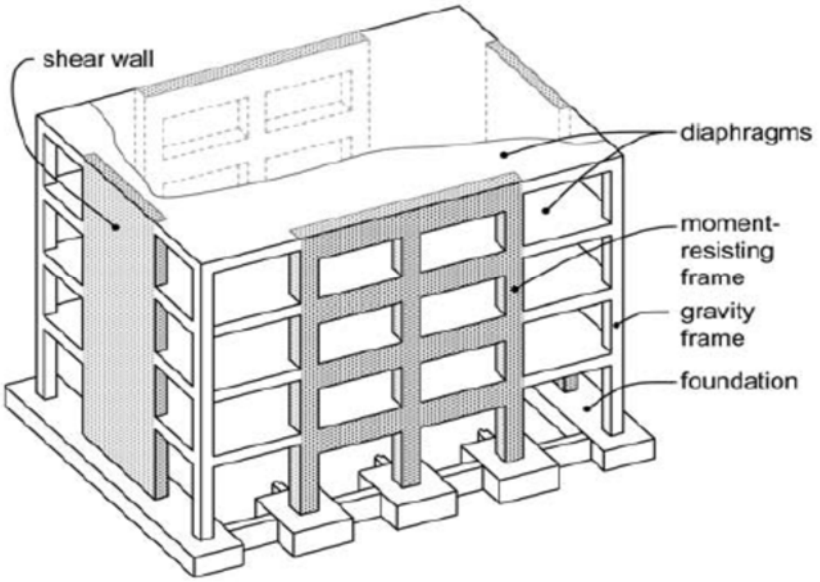

Figure 1.1: Basic building structural system comprising diaphragms (flooring system), vertical elements (walls or moment frames or gravity frames), and foundation (Moehle et al., 2010)

On the other hand, construction practices in Japan and North America utilize RC structural walls to resist not only lateral forces but also the gravity loads in multi-storey shear wall buildings. Hence, such structural walls are subjected to lateral loads and the gravity loads concurrently. These type of structural walls may be called bearing walls. Some practicing engineers feel that this class of walls may reduce the safety of the whole structure when subjected to earthquake excitations. Concern has been raised about the ability of structural walls to transfer gravity loads after suffering significant damage in their critical zones. However, with the improvement of analytical and numerical tools for conducting nonlinear pushover or response history analysis, the application of performance-based seismic design approach has become more common. Hence, structural engineers are able to conduct a detailed deformation analysis to find the likely level of damage in any structural sub-assemblage.

Performance-based design and rigorous nonlinear analysis methods boost the confidence of structural engineers to control the response of structural walls subjected to simultaneous gravity force and seismic excitation more rigorously.

Structural walls used for the resisting in-plane bending and shear type actions are called shear walls. These walls commonly resist the lateral force in the form of cantilever action unlike the moment resisting frame elements. This means that flexurally dominant shear walls rarely fail in the shear mode unlike what their names imply. The capacity design approach of structural walls intends to achieve a ductile flexural response by forming a plastic hinge near the base of structural walls and to avoid shear failure at any point over the building height. Structural walls have different categories according to their geometry which include slender walls; low-rise squat walls, coupled shear walls (Figure 1.2). They also can have a different cross sectional shapes such as I, L, T, and C depending on the architectural requirements. The lateral force resisting system for a multi-storey structural wall building is commonly concentrated in a relatively few structural walls distributed around the floor slab or within a central core (core wall) to provide the lateral strength and stiffness. A minimum stiffness is needed to limit the lateral deformations to acceptable (design standard) levels. Some typical types of multi-storey shear wall building plans are introduced in the following section.

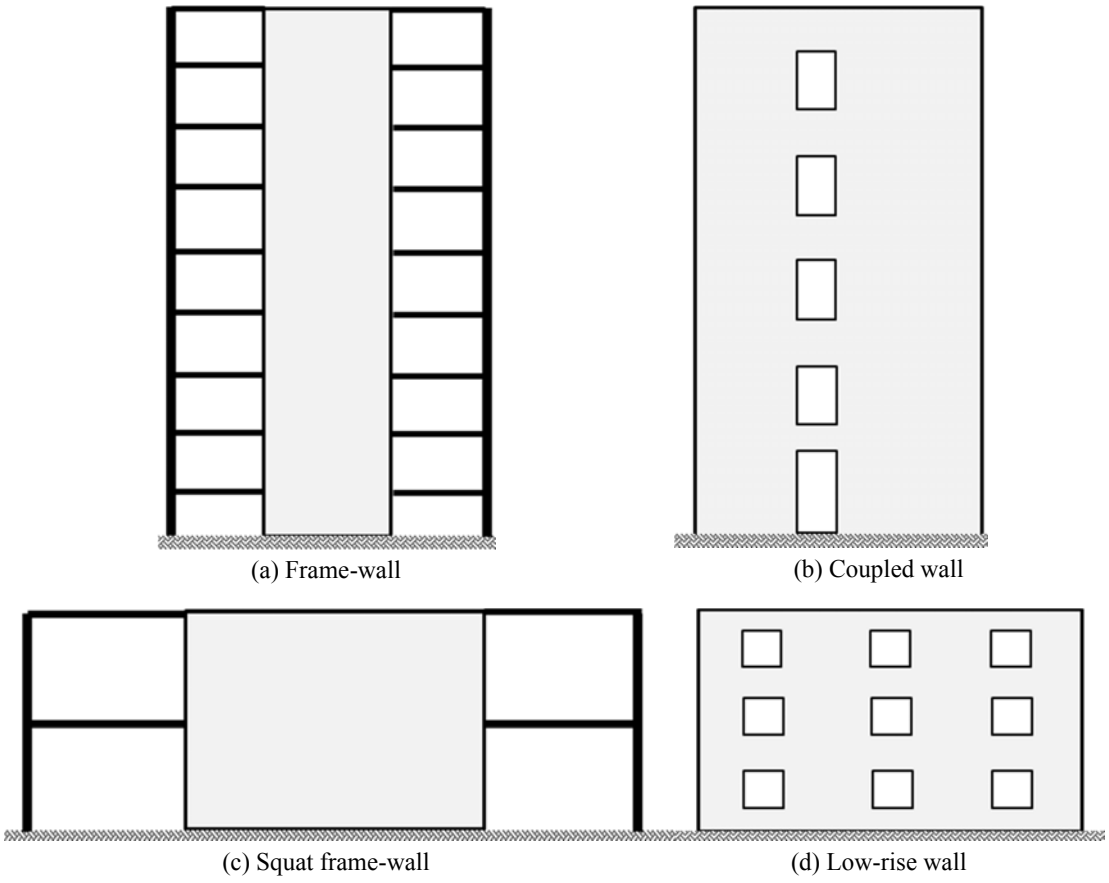

Figure 1.2: Different type of multi-storey shear wall buildings

Extensive analytical research has been carried out by employing relatively simple or crude analytical models to study the behaviour of RC structural walls and frame-wall systems under seismic ground motion excitation. However, it is essential to balance the model simplicity with the ability to predict reliably enough the inelastic responses under seismic loads both at the global and local levels. It is also important to ensure that the employed analytical or numerical model reasonably represents the hysteretic response of the primary lateral force-resisting elements (including the foundation), as well as the interaction between the wall and other structural (gravity) members. Despite, it is common practice in design offices or research community to overlook the effect of gravity system (the columns and the flooring systems) in lateral response analysis. Hence, an improved finite element method (multi-layer shell element) has been adopted in this thesis to address the structural wall-floor slab and gravity frames interaction.

The total deformation of shear walls is comprised of flexural, shear and axial deformations. Low rise shear walls are controlled commonly by the shear behaviour (shear deformation) while medium to high rise walls respond predominantly in a flexural manner (flexural deformation).

Wall behaviour under lateral loads is generally classified according to the structural wall aspect ratio (H_w/L_w) (H_w is the wall height and L_w is the wall horizontal length) or shear-span-to-depth ratio (M/VL_w) (M is the base bending moment and V is the base shear), as either shear-controlled (walls with aspect ratio less than approximately 1.0–1.5) or flexure-controlled (walls with aspect ratios greater than 2.5–3.0). For structural walls between these aspect ratios, herein referred to as moderate aspect ratio walls, nonlinear responses associated with both axial/bending and shear behaviour are likely. Although only flexural yielding is anticipated in such walls, nonlinear shear deformations may be significant which leads to decrease in the lateral stiffness, strength, and ductility.

Results from the numerous experimental tests reported in the literature (Oesteler et al., 1984; Hiraishi, 1984; Massone et al., 2004; Thomsen et al., 2004; Dazio et al., 2009; Ghorbanirenani et al., 2011; Menegon et al., 2015; and Shegay et al., 2017) and observation of damages in RC shear wall buildings after moderate to severe earthquakes (Wood et al., 1987; Wood, 1991; Kam et al., 2011; and NIST GCR12-917-18, 2012) have confirmed that the nonlinear response of shear walls is affected by many factors which include:

- The wall dimension and shear span ratio (M/VL_w)
- Axial-flexural-shear interaction (AFSI)
- Ratio and bond of longitudinal and transverse reinforcement
- Ratio of flexural capacity to shear capacity
- Boundary element dimension and detailing

- Strain penetration of vertical reinforcement in foundation connection
- Soil structure interaction

Therefore, prediction of precise inelastic local demands (such as rotation or curvature/strain) in RC shear walls needs a robust analytical or numerical modelling approach. The numerical method in a mathematical model ideally should be able to account for the material nonlinearities and local effects such as movement of neutral axis, tension stiffening of concrete, confinement, nonlinear shear behaviour and effect of shear-flexural-axial force interaction on the strength and stiffness of shear walls.

On the other hand, nonlinear response history of buildings is often highly sensitive to the selection and modification of input ground motions. Although many ground motion selection and scaling methods have been proposed in the literature (Kalkan and Chopra, 2010; NIST GCR11-917-15, 2011; and Dhakal et al., 2007), no consensus based and systematic guidelines exist to provide a reliable approach regarding appropriate ground motion selection and scaling in a particular response analysis. In this thesis, therefore, ground motions are selected randomly. The associated ground motion records were then uniformly scaled to impose a specific base rotation on the case study buildings.

1.2 Typical Configurations of Multi-Storey RC Shear Wall Buildings

Figure 1.3 to Figure 1.7 illustrate a number of typical floor plans for multi-storey shear wall buildings which are more common in the construction practice all over the world. In typical structural walls in the United States, the longitudinal reinforcement is commonly concentrated at the edge of wall sections to form well confined boundary zones and to achieve the effective lever arm for moment resistance. The structural wall-floor slab connections in these floor systems commonly behave as a rigid connection. However, in mid-rise buildings without the core RC structural walls, there are usually several RC structural walls in the building plan so

that individual RC structural walls are not heavily stressed and the boundary zones need not have a cross section wider than the web. Although using the bulged boundary elements is highly recommended to improve a wall's shear capacity as well as its buckling stability, structural wall stability is implicitly provided by the requirement that the wall thickness shall be at least 200 mm. The code provisions also impose a limit on the ratio of floor height to the thickness within a typical range of 12-16. It is quite worthy to mention that, while the ratio of RC shear wall area to the floor area is about 1-2% in the US practice as a rule of thumb, this value varies from 3% to 8% in the Chilean practice (Wood et al., 1987).

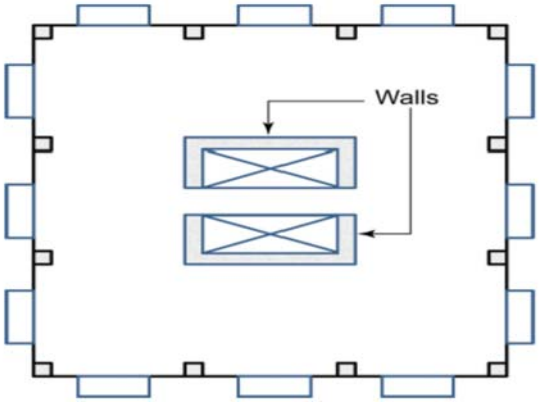

Figure 1.3: Typical building plans in high rise construction (common in U.S. (NIST GCR12-917-18))

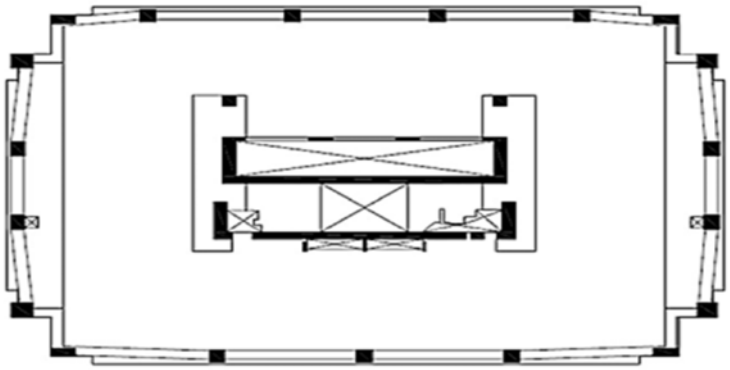

Figure 1.4: Typical building plans in high rise construction (common in Chile (NIST GCR 12-917-18))

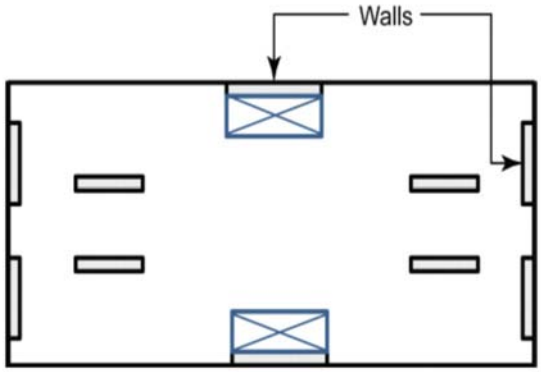

Figure 1.5: Typical building plans in mid- rise construction (common in U.S. (NIST GCR 12-917-18))

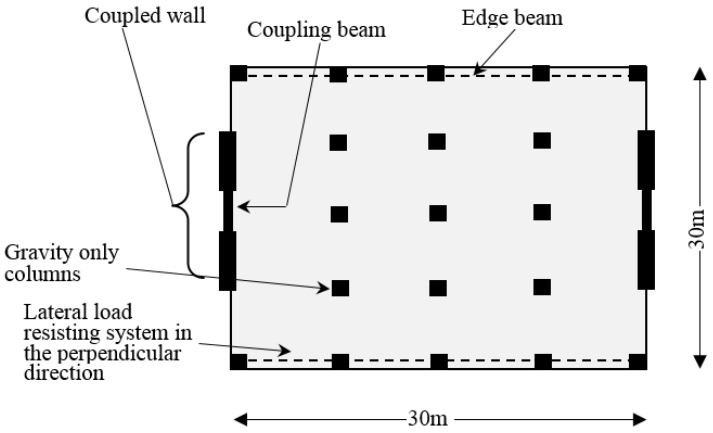

Figure 1.6: Typical building plans in mid- rise construction (common in Europe and New Zealand, (Fox et al., 2014))

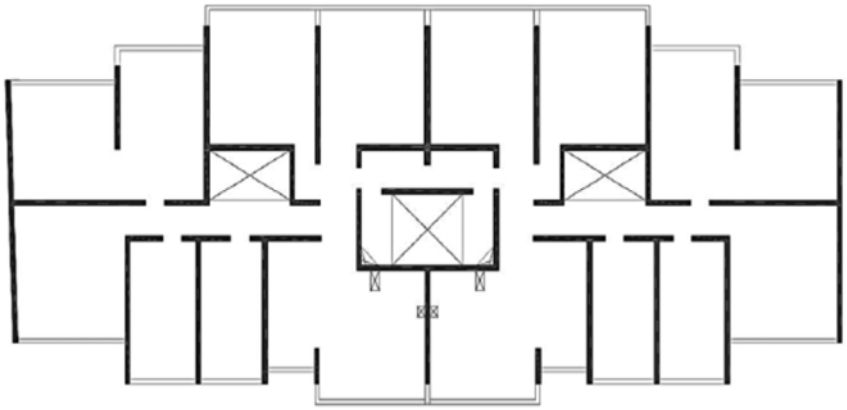

Figure 1.7: Typical building plans in mid- rise construction (common in Chile (NIST GCR 12-917-18))

The buildings selected as case studies in this project are similar to the typical multi-storey shear wall building indicated in Figure 1.5 .

1.3 Flooring Systems and their Connections to Structural Walls

Solid cast in-situ floor slabs like two-way flat RC slabs or cast in-situ slabs on the beams (shell beams) are among the common types of floors used to make a rigid diaphragm in multi-storey shear wall buildings in most countries except New Zealand. Furthermore, the structural wall-floor slab connections in these floor systems commonly behave as a rigid connection. In other words, the connections can transfer the out-of-plane moment, shear or torsion type actions. Hence, they can have considerable out-of-plane strength and stiffness. It should be emphasized that the degree of fixity/rigidity is highly dependent on detailing techniques of RC floor slab-wall connections. However, due to lack of experimental test results, it seems that engineering judgment expecting a brittle or semi-ductile behaviour for this type of connections is not uncommon.

In addition, it is quite ambiguous for design engineers to decide when and how the out-of-plane stiffness and/or strength of RC floor slabs or other equivalent floor systems should be considered in the analysis or design of RC structural wall buildings. It may need establishing some simple guidelines for practice. Moreover, capacity design guidelines need to evaluate the influence of flat RC slabs or any other floor systems on the seismic behaviour of RC structural walls. Furthermore, to the author's knowledge, no consistent guidance is available to determine the effect of floor systems on design of RC walls and gravity columns.

On the other hand, proper joint detailing of shear wall–floor slab connection is very critical to achieve a robust seismic load path. Structural responses of shear wall buildings observed during recent earthquakes have indicated a number of failures or damages in the regions of floor system to the structural wall connections. Inadequate strength or ductility capacity due to the

inappropriate connection detailing was one of the main reasons of such failures or damages. Although the connection detailing between flooring systems and structural walls has a significant effect on the building's ability to resist forces and deformations during a severe earthquake, explicit guidelines regarding the detailing of RC structural wall–floor slab joint region are not specifically included in the standard codes of practice. A limited number of experimental tests have been conducted to investigate the response of connection between RC in-situ floor slab plate and structural walls under actions perpendicular or parallel to the structural walls (Memon, 1984; Lopes et al., 2014; Surumi et al., 2015). This is shown in Figure 1.8.

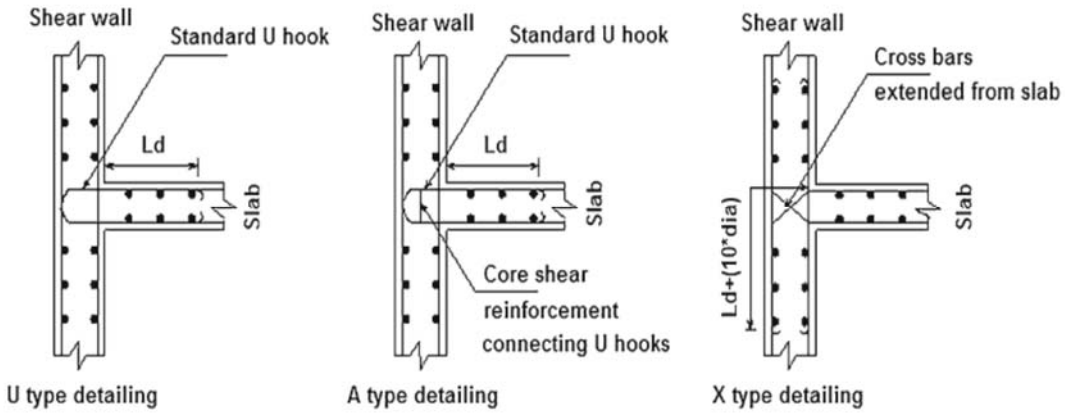

Figure 1.8: Wall to floor slab Connections (Surumi et al., 2015)

Figure 1.9 illustrates a typical recommendation from the SEAOC Blue Book (2006) for the detailing and calculation of diaphragm actions through the floor slab to the wall connections. The SEAOC Blue Book (2006) states that the building industry and structural engineers have struggled to find an appropriate detailing to connect the flooring systems to the vertical structural wall elements. However, it was commonly accepted that wet connections by using in-situ RC provide more robustness and integrity compared to pre-cast or dry joints.

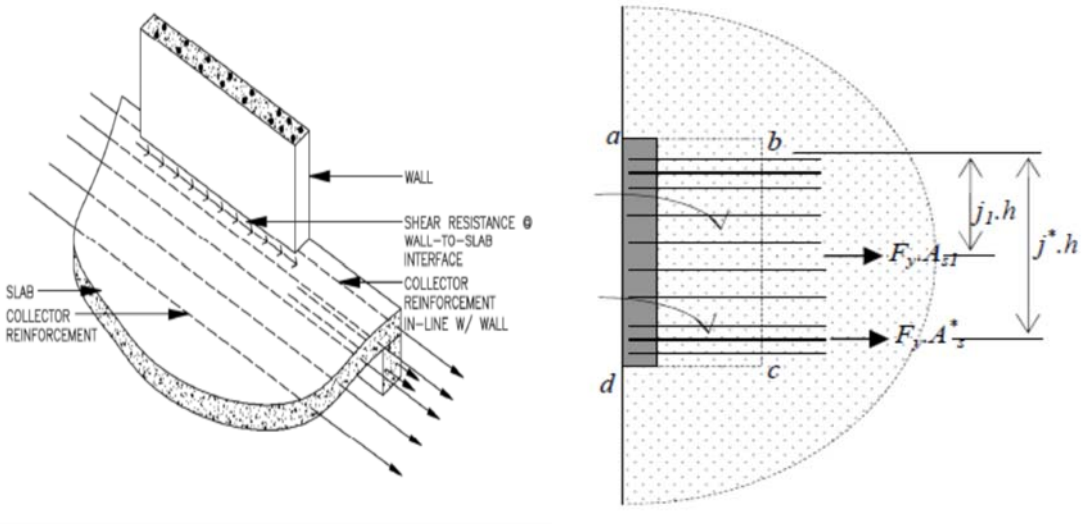

(a)

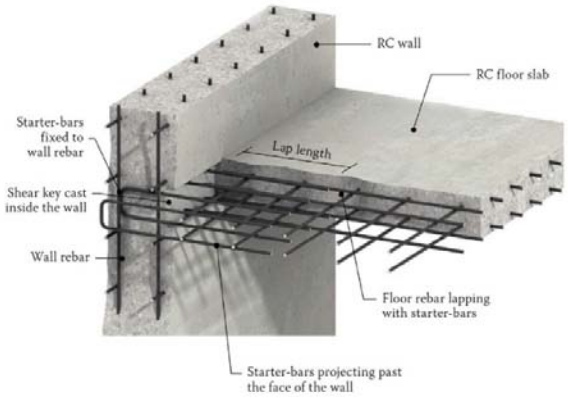

Design

- positive horizontal force transfer (shear friction)
- can develop a rigid moment connection
- allowance for variation of U bent material properties due to cold working on site

Variations

- U bent bars can be replaced with cast in anchors

(b)

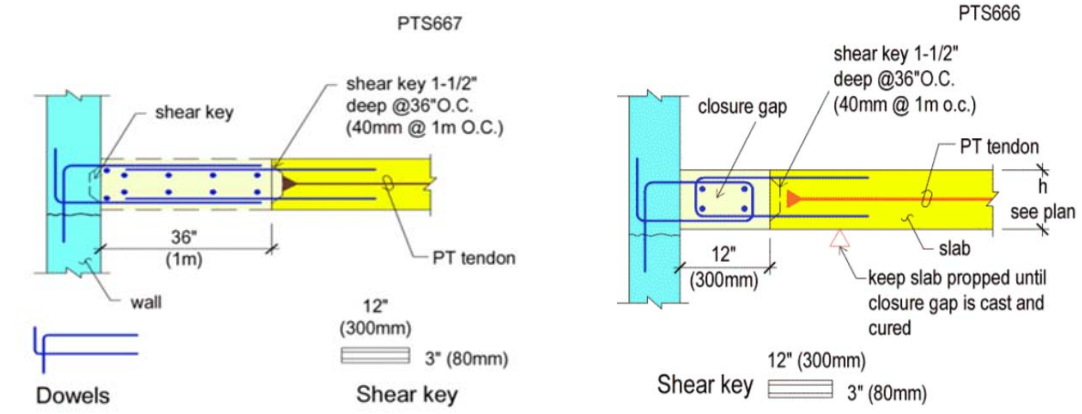

(c)

Figure 1.9: (a) In-plane actions in structural wall to slab connection (Typical) (SEAOC Blue Book, 2006) (b) Ancon building products (c) Post-tensioned floor slab-wall connection (Aalami B. O., 2014)

The structural wall to the floor slab connection may undergo severe cracking when it is subjected to earthquake excitations. However, it is expected to remain strong enough to transfer

the gravity force as well as any other actions induced due to internal redistribution of forces. In this study, the out-of-plane flexural stiffness of floor slab has been reduced significantly to account for the occurrence of extensive cracking around the floor slabs in the connection region. However, a sensitivity analysis has been conducted using different values for the flexural and torsional stiffness of floor slabs.

Another popular commercial flooring system are hollow core slabs, precast/pre-stressed concrete double tee floors and rib and in-fill floors. They are commonly used in the New Zealand construction industry which are manufactured at a pre-cast concrete plant prior to shipping to the worksite. After installation, they are typically topped with a 50 mm to 75 mm cast-in place reinforced concrete topping to level the floor surface. Structural engineers can make use of the concrete topping to increase the in-plane load-carrying capacity of the floor systems. There is a hot debate going on how one must connect these kinds of diaphragms (floor systems) to the structural walls. The drag bars embedded inside the topping concrete act as horizontal elements to transfer/resist the horizontal floor inertia forces to the vertical elements through the in-plane shear or axial actions. However, in the vertical direction, it seems only a limited stiffness or strength is introduced by the connection of only the concrete topping to the structural wall. The recent earthquakes in Christchurch has demonstrated the connection regions of these floor systems to the structural walls are deficient. The main reason has been attributed to the vertical elongation of structural walls which were critical in accelerating the collapse of the whole building (CERC Volume 1, 2012).

Figure 1.10 shows a number of typical details for some of the more commonly used connections for the load bearing pre-cast concrete walls and non-structural wall panels. The details demonstrated in these figures are just indicative. They should not be regarded as standard, but rather, as concepts on which to build. Detailed design information, such as component sizes, weld and anchorage lengths, joint sizes, and bearing pad thicknesses is purposely eliminated in

these Figures. Bearing wall connections are divided into two categories: those that mechanically connect the bearing wall and the floor or the roof slabs, and those with (non-supported) the edges of floor or the roof slab running alongside the walls without any mechanical connection. Slab to the bearing wall connections are used to join the pre-cast or cast-in-place concrete floor or roof members to the pre-cast concrete bearing walls. They can transfer any vertical load from the horizontal system and diaphragm/in-plane actions. They can also provide out-of-plane moment resistance on some cases. When the floor slab functions as a diaphragm in the building, the connections must transmit diaphragm shear forces (the floor inertia forces) and chord forces to the vertical lateral force resisting systems. Most designs result in some degree of fixity for these connections (PCI connection manual).

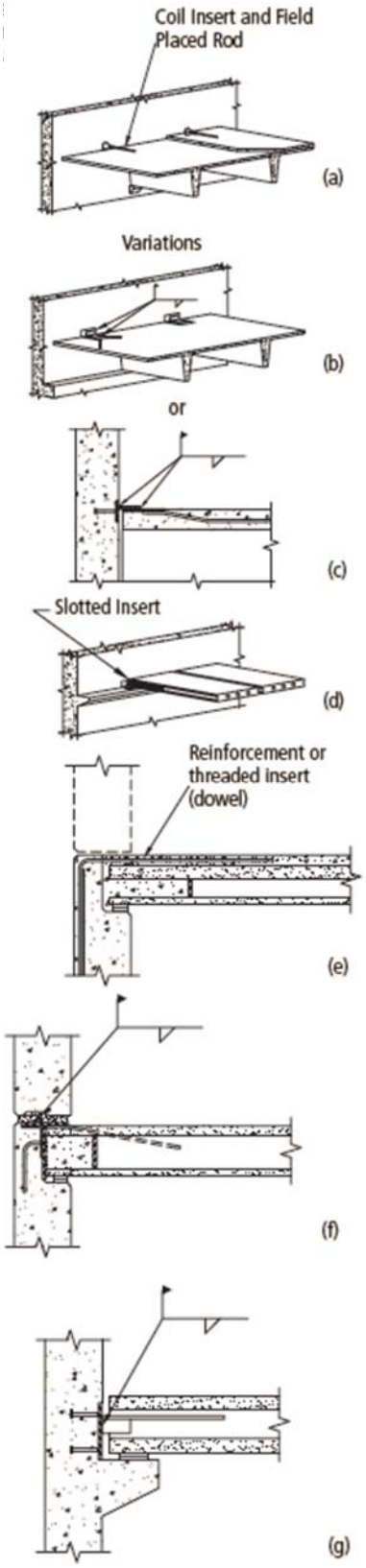

SW1

Design

- welding at bottom of slab is not recommended as excess restraint results
- no moment capacity
- must consider eccentricity of loads
- top connection transfers horizontal shear forces or provides nominal torsion restraint for spandrel

Production

- special forming required for corbel
- corbel may be precast and set in form

Variations

- variation of (d) and (g), dowel may be in topping
- steel corbel; it may use inserts in panel to position angle while welding
- flag shaped plate (g) welded to embedded plate in wall can be used in hollow-core joints

Erection

- quick and easy
- allows adequate tolerances
- temporary bracing may be necessary

Figure 1.10: Typical connections between the floor system and structural wall in pre-cast or tilt-up construction (PCI connection manual)

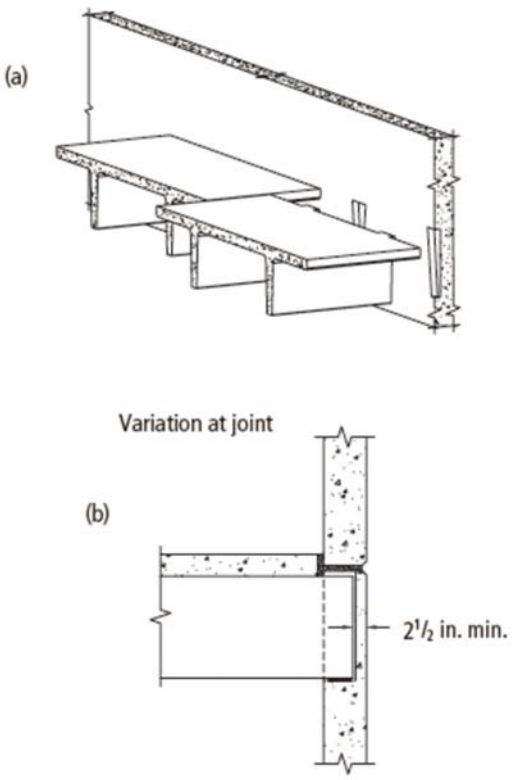

SW2

Design
- minimizes eccentricity of load on wall
- axial shortening of slab due to volume change should be considered when designing depth of recess
- pocket dimensions and tee end must be planned so that slab can swing into place; pocketed connection should not be used at both ends of slab
- top connection similar to connection SW1 (a) or (b) may be used

Production
- minimum of embedded hardware
- special forming required to allow stems to fit into pockets
- pockets in wall difficult to locate and form, usually do not follow tee taper
- pockets require adequate tolerance

Variations
- pocket may be at top of panel

Erection
- do not dry-pack pocket around tee stem to allow stem freedom to rotate
- for ease of erection, pockets should not be used at both ends of slab

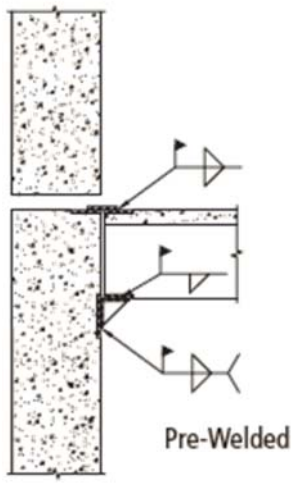

SW3

Design
- develop a rigid moment connection
- avoid use of this detail at both ends of slab to prevent excessive restraint
- rotation of wall elements and effects on bracing wall connections and volume changes must be considered
- arrangement of weld plates must allow for welding access
- avoid overhead welding, if possible

Production
- plate jigging is necessary since embed is top-in-form as cast
- steel congestion must be well thought out

Variations
- wall corbel in lieu of angle seat

Erection
- welding must be completed before setting panel above

Figure 1.10: Typical connections between the floor system and structural wall in pre-cast or tilt-up construction (Cont'd)

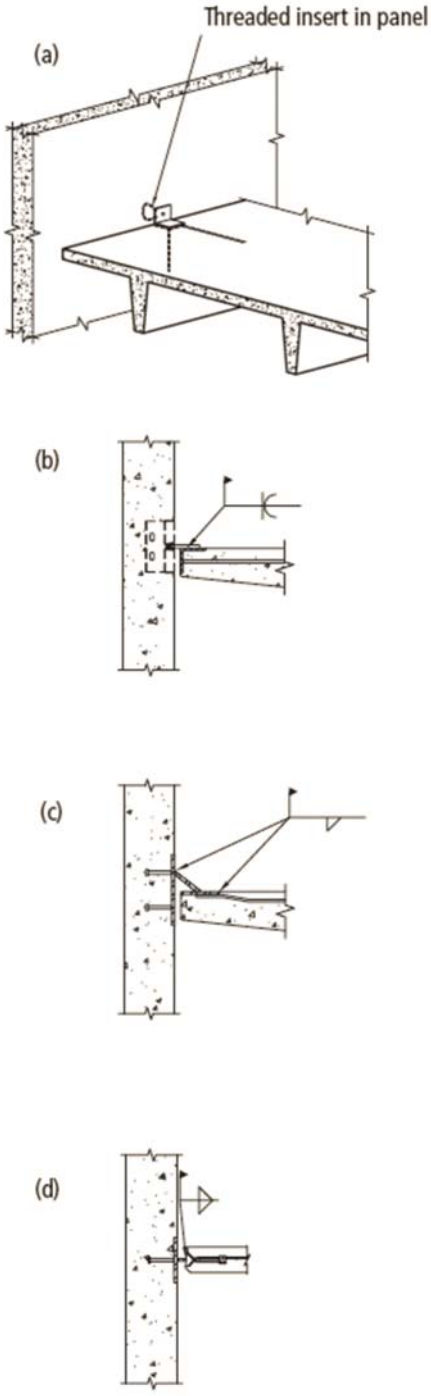

SW4

Design

- connection allows movements caused by temperature changes
- positive horizontal force transfer
- connection (c) allows vertical movement by flexing of plate and welds

Production

- insert must be plumb and true
- washer must be oversize so it does not bind in the slot connection (d) allows vertical movement through flexibility of double tee flange
- simple

Erection

- quick and easy
- tolerance problems minimized
- do not over tighten bolt in (a)

Figure 1.10: Typical connections between the floor system and structural wall in pre-cast or tilt-up construction (Cont'd)

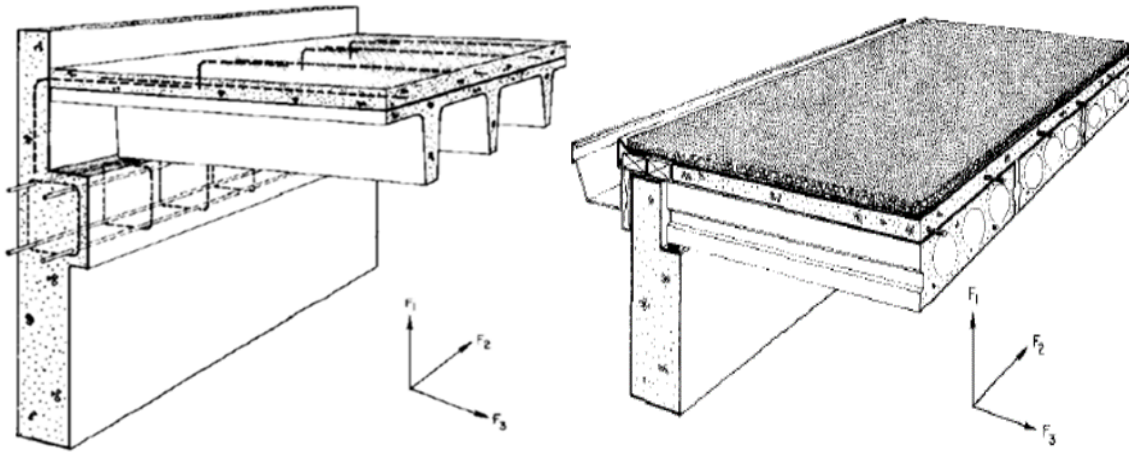

Figure 1.10: Typical connections between the floor system and structural wall in pre-cast or tilt-up construction (Cont'd)

Design practice in most of the earthquake prone countries including Japan, USA, and North America unlike Europe prefer to use in-situ reinforced concrete for the flooring systems. It is widely admitted that RC floor slabs (in-situ or post-tensioned) inherently supply significant integrity and robustness to the buildings. However, to achieve the efficient seismic behaviour in the pre-cast flooring system, proper attention should be paid to the proper detailing of their joints as well as their connections to the vertical lateral load resisting elements. Otherwise, pre-cast flooring systems can sustain significant number of failure modes when subjected to earthquake excitations. Figure 1.11 displays the deformation compatibility of flooring system with the adjacent elements under lateral loads. While the structural walls undergo the sectional rotation due to the lateral loads, the flooring system due to deformation compatibility should follow the same rotation. This type of deformation can trigger the flexural and the torsional stiffness of flooring systems. A detailed discussion of this topic is introduced in Chapter 3.

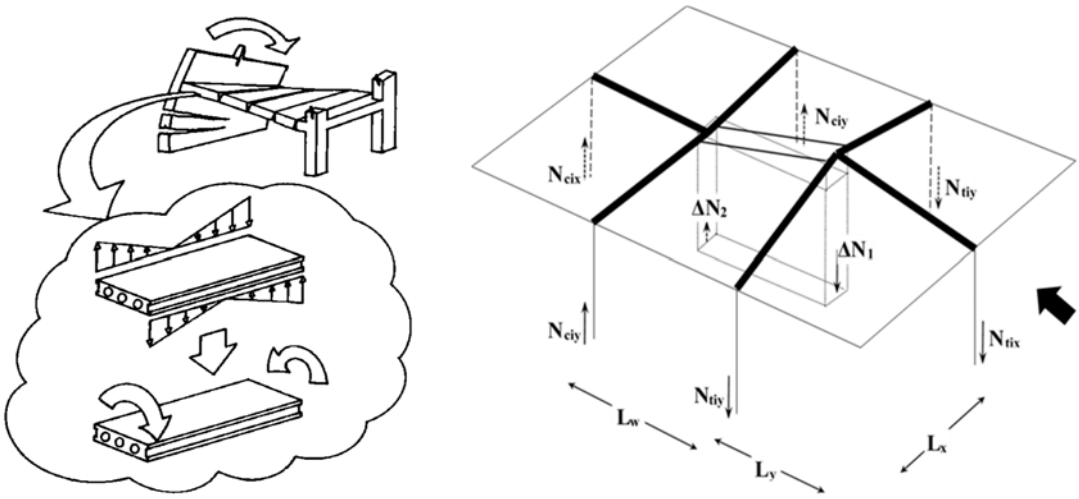

(a) (b)

Figure 1.11: a) Out-of-plane diaphragm (floor) deformation produced by dissimilar rotations of parallel walls and frames (Clough, 1982). b) Induced axial actions due to deformation compatibility

1.4 Shake Table Tests on Multi-Storey Shear Wall Buildings Including Floor Slabs

Bertero et al. (1984) performed shaking table tests on a 1/5 scale and a full scale multi-storey shear wall-frame building. Following this system-level testing, significant contribution of the flooring system (two-way slabs on beams) to the ultimate lateral strength of the building has been confirmed. They stated that axial growth and rocking of structural walls at the base (due to neutral axis movement) activate three-dimensional outrigging actions in the surrounding space frames. This phenomenon was called three-dimensional effects which were created by the axial growth and rocking of the wall which occurred mostly in the plastic hinge zone. Hence, a comprehensive capacity design of multi-storey shear wall buildings should provide a method to account for the induced outrigging action of the space frames.

Above-stated phenomenon introduces extra overstrength to the system and it is highly dependent on the level of drift which can be achieved at the ultimate limit state. Therefore, it has been called kinematic overstrength. Panagiotou et al. (2007) also conducted another experimental investigation shake table test on a slice of a multi-storey shear wall building including floor slabs and gravity columns. The authors noted that the main source of system base moment resistance in Westward direction at the DBE level shaking included three major

components: i) 55% from the web wall moment capacity; ii) 32% due to coupling of the web through the slotted slabs; and iii) 10% due to axial force in the perpendicular gravity columns. A more detailed explanation of this experiment will be presented in Chapter 3.

Gavridou et al. (2015) studied the analytical modelling of a full-scale four-storey un-bonded post-tensioned (UPT) concrete wall building tested under shake table excitation. The authors pointed out that displacement incompatibilities exist between the un-bonded post-tensioned (UPT) beams, the floor system and the structural walls. Although the bending effects of the floor slabs were neglected in the proposed analytical model, the model did consider the frame actions of UPT beams (spanning in plane of UPT concrete walls) and restraining effects due to the membrane stiffness of floor slabs. Decomposition of the base moment resistance confirmed that the frame action of UPT beams (without the floor slabs) contributed significantly to the lateral load resistance of the test building. The analytical study demonstrated that the total moment resistance of the building in the direction of the concrete walls at the instant of peak strength during the 100%-Kobe record, can be decomposed as follows: 50 % from the moment capacity at the base of the UPT walls, 35% from frame action of the UPT beams, 5 % from the column base moments and, finally 10% from the interior one-bay frame.

Hence, the results of these shake table tests along with the numerical analyses reconfirmed the importance of the system overstrength factor, induced due to the deformation compatibility between the RC structural walls and the floor slabs (or beams). Findings of these system level shake table tests clearly support the need for this research.

1.5 Importance of System Overstrength Factor in Capacity Design

A precise estimation of the overstrength factor is difficult in a multi-storey building since many factors contribute to it. However, according to FEMA-450, the basic components of structural overstrength (Ω_0) consist of material overstrength (Ω_M), system overstrength (Ω_S), and design

overstrength (Ω_D). These components of overstrength are presented schematically in Figure 1.12. This study focuses on addressing the effect of structural wall-slab-column interaction on the system overstrength (Ω_S) factor in typical multi-storey shear wall buildings.

System overstrength (Ω_S) is the ratio of the ultimate lateral force the structure is capable of resisting, F_n in Figure 1.12, to the actual force at which first significant yield occurs, F_2 in Figure 1.12. It is dependent of the amount of redundancy contained in the structure as well as any probable contribution of secondary components in resisting lateral force. Re-distribution of internal actions after ductile yielding in critical zones is another key parameter.

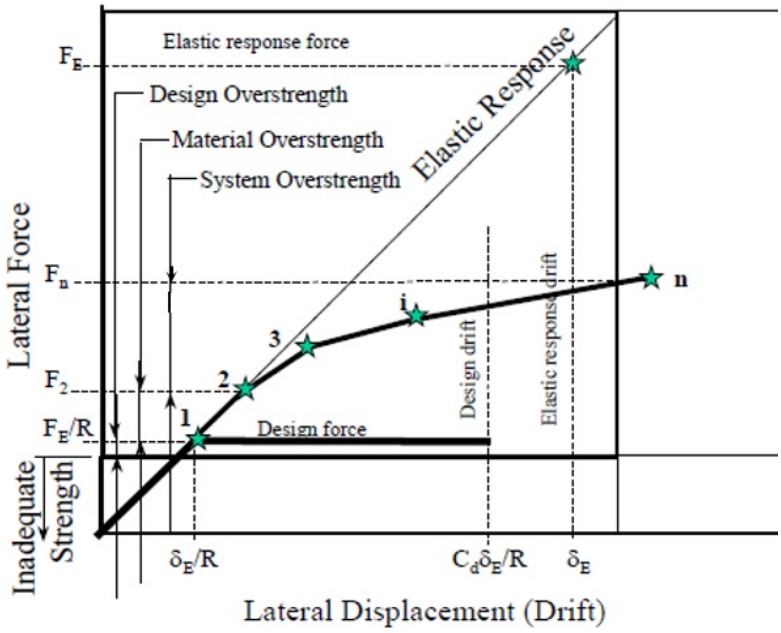

Figure 1.12: Factors affecting overstrength of a building (FEMA-450)

The fundamental objective of the current design practice and capacity design of structural wall buildings is that energy is dissipated through the formation of plastic hinges at the base of shear walls while floor diaphragms remain elastic. The flooring system is vertically supported by a combination of shear walls and gravity resisting columns. The effects of overstrength are not always beneficial in capacity design. For example, the flexural overstrength of members leads to increased shear forces when plastic hinges form which may result in non-ductile failure

(Park, 1996). Therefore, any possible source of overstrength in a building should be explicitly taken into consideration in capacity design.

In a multi-storey RC structural walls, section overstrength can be assessed by hand analysis methods by accounting for expected strength values and actual quantities of reinforcement or, alternatively, it can be determined from more rigorous moment-curvature analysis. However, overstrength of system due to three spatial interaction of walls, floor systems and frames is difficult to be parameterized.

Many researchers have endeavoured to recognize the major components of overstrength factors in different structural systems (Mitchell and Paultre, 1994; Nassar and Krawinkler, 1991). However, major parameters such as the actual strength of materials, confinement effects, the contribution of non-structural elements, and the actual participation of secondary structural elements (such as RC floor slabs or any other floor systems) lead to high uncertainties in overstrength estimation (Humar and Rahgozar, 1996). Elnashai and Mwafy (2002) studied twelve RC buildings designed and detailed in accordance with Eurocode 8, based on which a conservative overstrength factor (Rs) of 2.0 was proposed for medium and low period RC buildings designed according to Eurocode 8.

1.6 Importance of Including Slab and Gravity System in Analytical Modelling of Multi-Storey Shear Wall Buildings

The significance of spatial interaction of structural walls with adjacent frames and floor slabs was highlighted in the above mentioned shake table tests. Inclusion of wall-flooring slab-gravity columns interaction in a nonlinear model can change the overall system behaviour compared with an analytical model with only structural walls particularly when the system response is in the post-elastic range. It may also alter the seismic behaviour of structural wall itself. The effect of wall-floor slab-gravity system interaction needs to be investigated more to understand and quantify their effects on strength, stiffness and ductility of whole building.

Gravity system (in-situ RC slabs and gravity columns) inclusion into the analytical modelling of multi-storey shear wall buildings (with interaction possibility) can increase the overturning moment capacity of the whole building. This interaction leads to not only an increase in overall capacity of the whole building but also an increase in shear demand induced at the base of structural walls. As soon as the tension reinforcement at the wall base section starts yielding, the upward movement (displacement) of the wall edge in the tension side needs to keep deformation compatibility with adjacent floor slab or beams connected to the wall at the floor levels. This upward movement (displacement) triggers the out-of-plane stiffness (flexural or torsional) of the floor slabs or other flooring systems. Hence, this interaction may introduce some additional over strength to the whole system. In other words, as flexural cracks remain open in the plastic hinge region at the base of cantilever walls during the monotonic nonlinear responses, the neutral axis moves away from the centre of the wall base section because of cracking. The tension reinforcement starts yielding immediately after the flexural cracking stage, and it causes irrecoverable flexural plastic deformation. These phenomena cause a monotonic elongation of the element along its geometric axis. In cyclic analysis, the cracks close back (or partially close back) and then open again on the opposite side as the deformation cycle reverses. The reinforcement eventually undergoes cumulative inelastic deformation and does not return to its original length as the cracks close, leading to cumulative residual and maximum cyclic elongation of the structural walls (Fenwick et al., 1995; Lee and Watanbe, 2003; Peng et al., 2011). This cyclic elongation generates the maximum and residual upward and downward movement (displacement) in the wall edges vertically. However, in the dynamic sense, these phenomena excite the masses directly or indirectly (the floor systems) attached to the wall, and they will experience a cyclic vertical motion.

1.7 Overview of Common EDP (Engineering Demand Parameters) in Multi-Storey Shear Wall Buildings

In this section, an overview of important engineering demand parameters in multi-storey RC shear wall buildings is discussed.

1.7.1 Base Curvature Demands

The most critical engineering demand parameter in structural walls is the base curvature or the base rotation. Flexure dominated structural walls dissipate energy through cyclic moment-curvature or moment-rotation in the plastic hinge region located mostly at their bases. The approach, implemented in NZS3101:2006 utilizes the base curvature as a reliable index to control the base section ductility capacity. The inelastic curvature demand ϕ_p can be estimated directly from the inelastic displacement demand at the top of the wall Δ_p as follows (refer to Figure 1.13 and Figure 1.14):

$$\phi_p = \frac{\theta_p}{l_p} = \frac{\Delta_p}{l_p \times (H_w - 0.5 l_p)} \tag{1.1}$$

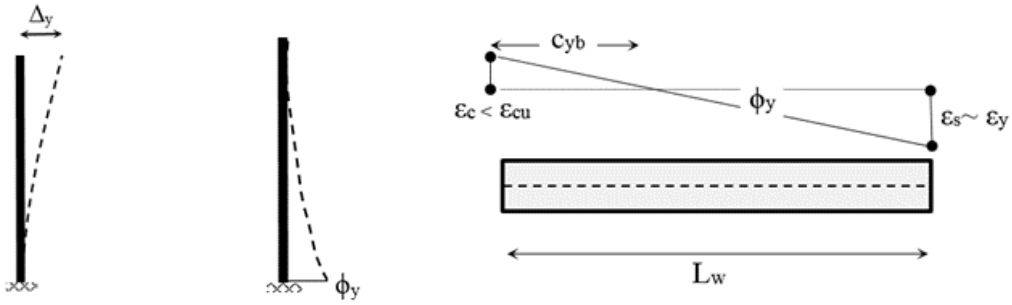

Figure 1.13: Idealized model for the curvature and deformation distribution over the height and corresponding base curvature in the yield state

Where the plastic curvature demand is equal to the plastic rotational demand Θ_p divided by the plastic hinge length l_p and the plastic rotational demand is equal to the plastic displacement demand at the roof divided by the height of wall measured above the centre of plastic hinge ($H_w - 0.5l_p$). Thus, the design requirement that the curvature capacity must be greater than or equal to the curvature demand can be demonstrated as:

$$\emptyset_c \geq \emptyset_y + \frac{\Delta_p}{l_p \times (H_w - l_p)} \quad (1.2)$$

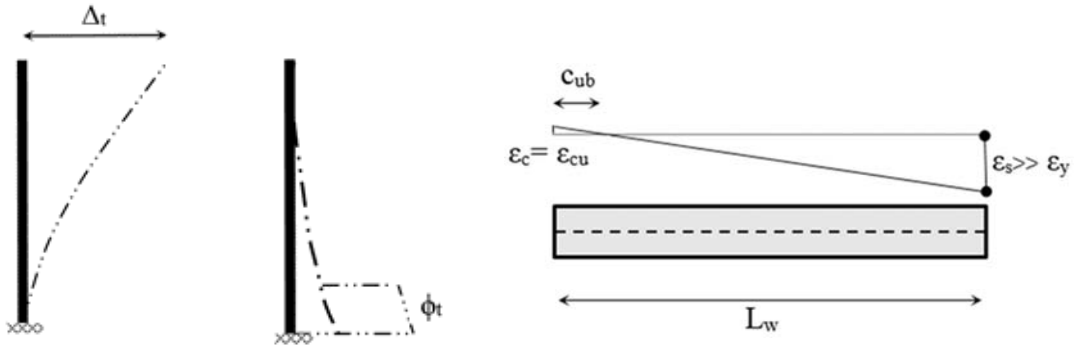

Figure 1.14: Idealized model for the curvature and deformation distribution over the height and corresponding base curvature in the total state

Hence, an accurate prediction of plastic displacement demand can increase the accuracy of plastic hinge rotation at the base. In the commonly used force base design; most engineers calculate the total displacement based on equivalent linear static analysis using the displacement coefficients proposed in the standards. The plastic displacement can simply be found from the total displacement minus elastic displacement.

The New Zealand seismic loading standard (NZS1170.5:2004) states that where the equivalent static method or modal response spectrum method of analysis is used, the horizontal deflection at each level can be obtained from modal response spectrum method multiplied by a scale factor equal to the structural ductility factor μ. NZS1170.5:2004 also prescribes an additional modification factor to adjust the deformation pattern determined from the linear methods. This value intends to account for the differences in deformation pattern of elastic structure and yielding structure obtained through equivalent static method. The recommended values for the drift modification factor, k_{dm}, are presented in Table 1-1. These modification factors are generic for all types of structural systems and even for a given structural system; the same value of modification factor is applied to all floors.

Table 1-1: Drift modification factor

Structure Height	Drift Modification Factor (DMF)
H_w<15 m	1.2
15<H_w<30 m	1.2+0.02(H_w-15)
H_w>30 m	1.5

H_w: Wall Height

However, it seems that the recommended values in Table 1-1 should be verified particularly for structural wall systems. For more exact prediction of displacement demands in shear wall building, one needs to conduct nonlinear response history analyses of such buildings to find out the roof displacement and inter-storey drifts.

1.7.2 Storey Shear Force Demands

The distribution of the lateral forces over the height of a multi-storey structure specified in building codes for the equivalent lateral force analysis is usually an inverted triangle. This loading shape is quite adequate for predicting the moment distribution, but normally, it needs some modifications to account for the maximum shear forces in flexurally dominated structural walls under dynamic earthquake loads.

Existing research on dynamic response of isolated walls have confirmed that higher modes of vibration increase the elastic shear demand of cantilever multi-storey walls. Shear distribution over the height of multi-storey shear walls exacerbate after the formation of a plastic hinge at the wall base. Consequently, the seismic design strength determined by the code requirements may underestimate the seismic shear and flexural demands over the height of multi-storey cantilever walls subjected to earthquake excitations.

The equivalent linear static analysis is commonly used in design offices to determine the global displacement and force demands of RC shear walls. However, NZ concrete standard (NZS3101:2006) was among the first codes in the world to introduce a dynamic amplification

factor to increase the storey shear force demand due to the higher modes. However, any probable interaction of structural wall elements with the flooring systems is still disregarded in the design process in most codes.

Design shear force at any level above the plastic hinge shall not be taken less than the corresponding shear force found from the equivalent static analysis multiplied by an overstrength factor (φ_o) and a dynamic shear magnification factor (ω_v) such that:

$$V^*_{wall}=\omega_v\varphi_o V^*_E \quad (1.3)$$

Where ω_v is a dynamic shear magnification factor which is given by

$$\omega_v=0.9+n_t/10 \quad \text{, for building up to 6 storey} \quad (1.4)$$

$$\omega_v=1.3+n_t/30<=1.8 \quad \text{, for building above 6 storey} \quad (1.5)$$

In this proposed modification factor, n_t is a number of stories and φ_o is the over strength factor related to sectional over strength under the flexural actions in the plastic hinge zone. In other words, assuming a typical value of $\varphi_o=1.4$ and an example eight storey building, this amplification factor is approximately equal to 2.19 which should be applied to the base shear calculated from the linear static analysis.

It is worth mentioning that, the above shear demand amplification markedly causes a reduction in the effective height of the structural walls (shear span ratio). In the author's view, it is essential to consider this huge amplification in the selection of wall specimens in experimental tests as a true representative of prototype buildings. A preliminary evaluation has illustrated that additional shear demand may be imposed on structural walls when the idealized mathematical model accounts for the spatial interaction between frames and structural walls in presence of floor slabs or adjacent beams.

1.7.3 Roof Displacement Demands

Roof displacement demand provides a good indicator of the global displacement demands on structural wall buildings. Estimating the roof displacement demand is one of the most important aspects of seismic design of RC multi-storey shear wall buildings especially when displacement based design are employed to design and detailing of boundary elements in RC structural walls (ACI-318-08). Moreover, roof displacement demand can be used to determine the inelastic rotation demands at the base of the wall. Furthermore, experimental tests (Corley et al., 1981; Oesterle et al., 1984; Biskinis et al., 2004; ATC-72-1, 2010) have confirmed that shear strength capacity of structural walls with shear span ratio less than three degrades once flexural yielding occurs at the wall base section. Hence, shear strength should be reduced based on curvature or rotational ductility demand. Therefore, the base rotation demand is employed to estimate the shear strength degradation in low to moderate height RC shear walls.

The prediction of roof displacement demand in cantilever RC walls depends on the effective sectional stiffness (flexural rigidity) EI_e used for the shear wall section in the analysis. Available recommendations on the effective linear stiffness of concrete shear walls vary significantly. ATC-72-1 (2010) recommends using an effective stiffness of 0.40Ig to 0.50Ig for structural walls with a $0.10f_c'A_g$ axial compression force level based on limited shake table results. Some researchers have used much lower effective stiffness's - in the order of 0.20Ig - to obtain a good estimate of the roof displacement demand of a seven storey shear wall building (Panagiotou et al., 2007). Deciding appropriate effective stiffness to estimate the maximum roof displacement demand in SLS and ULS is a challenging topic.

Different effective stiffness's can be used for each part of wall section through the height, depending on how much cracking under a given lateral load is expected. Some engineers, as a thumb rule, use the cracked flexural stiffness for the lowest 1/8 to 1/6 of the total building

height as a reasonable value. Table 1-2 compares the effective flexural stiffness recommended for a given wall section at ULS in different references. It is worth highlighting that most of above recommendations assume a constant (average) axial force on the wall sections over the height.

This complexity in stiffness calculations signifies effectiveness of using material based constitute models (fibre sections or filament type shell elements) for conducting nonlinear time history analysis especially when axial forces change during the analysis. The axial force in structural walls can vary due to coupling between shear walls or due to the wall's interaction with the floor systems.

1.7.4 Inter-Storey Drift Demands

Maximum inter-storey drift ratio (IDR) in multi-storey shear wall buildings includes rigid body rotation of the wall segment within a storey due the accumulated rotation of floors below the target storey, and it cannot provide a good indication of wall damage except when the IDR corresponds to the 1st storey including the base of structure. This concept is consistent with adoption of capacity design approach in structural wall design and limiting ductile behaviour in the plastic hinge zone at the base. However, IDR can be utilized as a good indicator of damage to the non-structural elements or slab-column connections in multi-storey shear wall buildings.

Table 1-2: Effective flexural stiffness of an example wall

Code (Reference)	Proposed effective stiffness	Effect of axial forces in formulation	Effect of reinforcement in formulation
ASCE/SEI41-06,uncracked	$0.80I_g$	No	No
ASCE/SEI41-06, cracked	$0.50I_g$	No	No
NZS-3101(μ=6)	$0.29I_g$	Yes	No
NZS-3101(μ=3)	$0.54I_g$	Yes	No
Paulay and Priestley (1992)	$0.25I_g$	No	Yes
ACI-318	$0.32I_g$	Yes	Yes
Moment-Curvature	$0.20I_g$	Yes	Yes

Inter-story drift demands markedly induce the deformation demands on the gravity-load system including the columns and the slab-column connections. Inter-story drifts can impose larger rotational demands on slab-column connections, and this increases the probability of a punching shear failure of the slabs. There are limited available data in the literature to form generic and versatile recommendations on how one should control the punching shear failure based on inter-storey drift demands.

In practice, inter-storey drift demands are usually determined from a linear analysis such as equivalent linear static or response spectrum analysis. Due to the concentration of inelastic rotation at the base of a cantilever wall, the inter-storey drift profile may deviate significantly from the values determined from a linear analysis.

1.7.5 Floor Acceleration Demands

Non-structural components can be categorized based on sensitivity to two different response parameters, as acceleration sensitive or drift sensitive. Hence, the prediction of floor acceleration demand in the ductile (yielding) multi-storey shear wall buildings including the floor systems play a significant role in the design of acceleration sensitive components. Some research has been carried out to estimate the peak horizontal floor acceleration distribution over

the height of buildings. However, with few exceptions (e.g., Rodriguez et al., 2002) most previous work has involved buildings remaining linear or nearly linear during an earthquake. For example, Miranda and Taghavi (2005) presented a simple but elegant method that can be used for approximating peak horizontal floor acceleration for linear or nearly linear buildings when subjected to a particular ground motion.

The following section presents a summary of different building code requirements for design of non-structural components.

- **ASCE7-10 Accelerations Demand on Components:**

Design accelerations of rigid non-structural components are given implicitly by the Equation (1.6) to calculate the horizontal seismic design force on non-structural components. The horizontal seismic design force of acceleration-sensitive components, F_p, is given by:

$$F_p = \frac{0.4 a_p S_{DS} W_p}{\frac{R_p}{I_p}} \left(1 + 2\frac{z}{H}\right) \leq 1.6 S_{DS} I_p W_p \qquad F_p \geq 0.30 S_{DS} I_p W_p \ , \tag{1.6}$$

where a_p is the component amplification factor (a_p equal to 1.0 and 2.5 for rigid and flexible components, respectively). R_p and I_p refer to the component response modification and importance factor, respectively. W_p is the weight of the component, S_{DS} is the design earthquake short period spectral acceleration, and z/H is the relative height ratio of the floor at which the component is supported. The components in design code ASCE7-10 are classified as rigid when the period of vibration is less than or equal to 0.06 seconds. They are categorized as flexible when a period of vibration is greater than 0.06 seconds. Accordingly, the numerical value for a_p is equal to one for the rigid components and 2.5 for the flexible components.

From Equation (1.6), it is evident that peak floor acceleration (PFA) is varied linearly over the height from the PGA (= 0.4 S_{DS}) at the ground level (i.e., z/H = 0) to 3 times the PGA at the roof level (i.e., z/H = 1.0).

This equation indicates that acceleration demand for those flexible components which responds elastically (i.e., $R_p = 1$) and locates at the roof level (i.e., relative height z/H = 1) is equal to 3.0 × 2.5 = 7.5 times that of PGA (a_p = 2.5 for flexible components), regardless of the characteristics of the supporting structure. For instance, according to ASCE7-10 in a site with PGA = 0.4g (design earthquake level in Wellington), the design acceleration demand on elastic, flexible components located at the roof level is equal to 0.4g × 7.5 = 3.0g, regardless of the number of stories and type of lateral force system.

From the example explained earlier, it can be seen that ASCE7-10 does not distinguish between elastic or inelastic response of the supporting structure. Further, it does not take to account various types of lateral resisting systems (i.e., moment resisting frames versus structural walls), number of stories/floor levels, and ratio of components periods to supporting structure period.

- **Eurocode 8 Accelerations Demand on Components:**

Sullivan et al. (2013) was examined the accuracy of Eurocode 8 (CEN EC8 2004) provisions for calculation of the acceleration demands imposed on the components. In Eurocode 8, acceleration demand, S_a, imposing on a component can be obtained from the following equation:

$$S_a = a_g S \left(\frac{3\left(1+\frac{z}{h}\right)}{1+\left(1-\frac{T_p}{T_1}\right)^2} - 0.5 \right) \geq a_g S \quad , \tag{1.7}$$

where a_g is the design ground acceleration (in units of g) for a rock site, S is soil modification factor, z is the height of the components above the ground level, H is the total height of the structure, T_p is the period of the component and T_1 is the natural (first-mode) elastic period of the building in the direction of excitation.

For example, Equation (1.7) suggests that the peak elastic acceleration imposed on a component at roof level, (when $T_p = T_1$) would be 5.5 times that of the peak ground acceleration (PGA) at the site. The main feature of this equation is that the ratio of components periods to supporting structure period (primary lateral force resisting system) is taken to account. However, as in ASCE7-10, the differentiation between elastic or inelastic response of supporting structure is not considered.

- **New Zealand Standard Acceleration Demand on Components:**

New Zealand standard (NZS1170.5:2004) predicts a maximum acceleration on components (or "parts") using the equations below. The horizontal design actions on a component (or part) shall be determined from Equation (1.8):

$$F_{ph} = C_p(T_p)C_{ph}R_pW_p \leq 3.6W_p \quad (1.8)$$

where $C_p(T_p)$= the horizontal design coefficient of the part determined from Equation (1.9)

C_{ph}= the part horizontal response factor (varied from 0.45 to 1 depending the ductility of component)

R_p= the part risk factor (varied from 1 to 2 depending the consequence of damage)

W_p= the weight of the part

The horizontal design coefficient for the components (or the parts) shall be determined from Equation (1.9):

$$C_p(T_p) = C(0)C_{Hi}C_i(T_p) \quad (1.9)$$

where:

C(0)= the site hazard coefficient for T=0 depending on soil type and location of site

C_{Hi}= the floor height coefficient for level i, determined from Equation (1.10)

$$C_{Hi} = \begin{Bmatrix} \left(1 + \frac{h_i}{6}\right) & for\ all\ h_i < 12\ m \\ \left(1 + 10\frac{h_i}{h_n}\right) & for\ all\ h_i < 0.2h_n \\ 3.0 & for\ all\ h_i \geq 0.2h_n \end{Bmatrix} \quad (1.10)$$

where:

h_i= height of the attachment point of the part (from the ground)

h_n= height from the base of structure to the uppermost seismic weight

$C_i(T_p)$= the part spectral shape factor at level I determined from Equation (1.11)

$$C_i(T_p) = \begin{Bmatrix} 2.0 & for\ T_p \leq 0.75\ s \\ 0.5 & for\ T_p \geq 1.5\ s \\ 2\left(1.75 - T_p\right) & for\ 0.75 < T_p < 1.5s \end{Bmatrix} \quad (1.11)$$

where:

T_p=the period of the part

New Zealand standard NZS1170.5:2004 predicts a maximum acceleration on components (or "parts") at roof level of 6.0 times the PGA, but unlike Eurocode 8, the peak floor acceleration (PFA) is independent of period of the supporting structure and it depends solely on the period of the components.

This recommendation seems to stem from the findings of Drake and Bachman (1995), Rodriguez et al. (2002), and Shelton et al. (2002), who found that acceleration demands are not necessarily dominated by the response of the building's first mode of vibration.

1.7.6 Effect of Shear and Flexure Interaction on Estimation of Displacement Demands and Shear Strength in RC Shear Wall Buildings

Although the shear force in a simple cantilever wall subjected to a point load at the top is constant over the height, but once an RC wall develops several cracks and the longitudinal reinforcement yields the shear strains are not evenly distributed over the wall height and

section. Methods used to disintegrate the total deformation into the shear and the flexural deformations in experimental tests or even analytical models are, to some extent, subjective. There are limited reliable experimental data on shear walls to obtain a reliable value for the shear stiffness and shear strength of structural walls at different drift demands.

Most macro element based analytical programs such as SAP2000, Ruaumoko, etc. the shear stiffness of beam-column elements is allocated a constant value. It cannot be updated during the loading process. State-of-the-art in the numerical modelling of structural walls are discussed in Chapter 2.

If shear transfer mechanisms in structural walls are designed to not degrade (and transverse reinforcement to not yield) during all cycles of curvature demand up to the failure, experimental results (Hines et al., 1999; Beyer et al., 2008; Beyer et al., 2011) have confirmed that the shear stiffness at the peak displacements decreases in a similar proportion to the flexural stiffness of the structural wall. This behaviour was observed even in structural walls whose behaviour was controlled by flexure. Hence, reduction in shear stiffness can add extra flexibility to the displacement profile of wall structures. To account for this flexibility, the shear stiffness of wall sections is significantly ($GA_e=0.10GA_g$) reduced after shear cracking in analytical models (ATC-72-1, 2010).

However, there is another important issue related to the reduction of shear strength of structural walls when subjected to cyclic curvature demands. Structural walls with shear span ratio below three are more likely susceptible to this type of behaviour. Wall shear strength decreases as the wall critical zone is severely damaged due to the cyclic curvature demands (degraded based on curvature or rotation ductility), as is shown in Figure 1.15 (ATC-72-1, 2010).

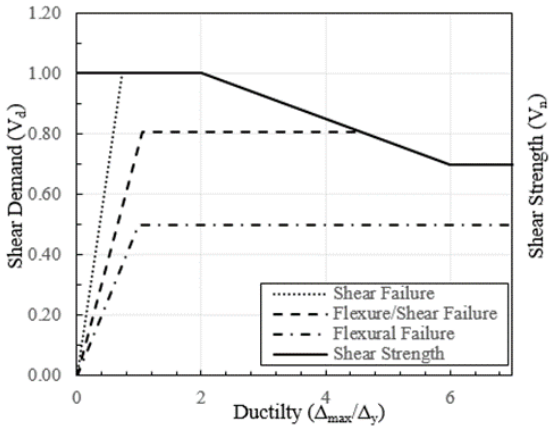

Figure 1.15: ASCE/SEI41-06 formula for the variation of column shear strength versus ductility demand (ATC-72-1, 2010)

There is no available macro model to account for this type of interaction between shear and flexural behaviours in RC structural walls. However, this can be done indirectly by calculating the ductility demand at the end of each analysis and updating the shear strength. The shear deformation capacities (γ_{cap} and γ_{cr}) and shear strength in this study are based on a limited literature review, mostly the experimental tests which include shear wall panels with aspect ratio close to 1.

1.8 Modelling of Flooring Systems

A horizontal system (roof, floor or other membrane or horizontal bracing) acting to transmit lateral forces to vertical-resisting elements can be referred as a floor diaphragm.

The floors and roof of a building, in addition to the resisting gravity loads, are also generally designed to act as diaphragms. In this respect, they are required both to distribute seismic forces to the main elements of lateral resistance, such as frames and/or shear walls and also to tie the structure together so that it acts as a single unit during an earthquake. The robustness and redundancy of a structure are highly dependent on the performance of the diaphragms. Pre-cast floor systems without an in-situ topping are not generally advised in the seismically active areas. The dried connections between the floor systems and the vertical lateral load resisting system in discrete points may act as a weak point during the seismic excitation.

In a ductile structure, diaphragms will almost always be required to remain elastic, so that they can sustain their function of transferring forces to the principal lateral-resisting structure, and tying the building together. Diaphragms should, in principle, therefore have the strength to sustain the maximum forces that may be induced in them by the chosen yielding mechanism within the rest of the structure.

Usually, seismic analysis of buildings is carried out on the assumption that deformations in the diaphragms are so small compared with those in the main lateral load-resisting structure that the diaphragms can be treated as rigid. The in-plane stiffness of the floor systems of most building structures is very high compared to the stiffness of framing members. As a result, the in-plane deformations can be neglected, assuming that it is infinitely stiff for axial deformations.

In most cases, this assumption is quite satisfactory, because usually diaphragm flexibility affects neither overall structural stiffness (nor hence natural period) nor the distribution of forces within a structure. Moreover, during a major earthquake, in ductile structures where the diaphragms are designed to remain essentially elastic, the superstructure deflections include large horizontal plastic deformations, which is very large relative to diaphragm deformations. However, in case of structural walls, large plastic deformation can occur in the vertical direction (upward and downward) which can influence the diaphragm behaviour.

A diaphragm may be considered rigid in-plane when its midpoint displacement, under lateral load, is less than twice the average displacements (inters-storey displacements) of lateral force resisting system at its ends (NZS1170.5:2004). It is based on the assumption that the diaphragm does not deform itself and will cause each vertical element to deflect the same amount. Rigid diaphragms can consist of reinforced concrete diaphragms, pre-cast concrete diaphragms, and composite steel deck.

Some engineering judgment is required when determining the properties of floor concrete slabs, composite decks or other flooring systems as the diaphragms because the cracking can affect the stiffness. ACI-318-08 lists approximate effective moment of inertias that are permitted for various structural members. Although there is not a modification factor for the diaphragms, the factors listed for the structural walls may be most appropriate for use with diaphragms. ACI-318-08 states that effective stiffness equal to 0.70Ig should be utilized for un-cracked walls and 0.35Ig should be used for the cracked RC walls.

In the rigid diaphragm assumption approach, all constrained nodal points (joints) are slaved to one another in each floor so that they undertake no in-plane deformations in the rigid plane (note that a rigid diaphragm does not affect the out-of-plane behaviour of the floor slab).

It is interesting to note that very strong and stiff floor systems (post-tensioned floors or other stiffened floor systems) can act as an outrigger system in high rise buildings with the core walls. Outrigger systems reduce the overturning demands on the slender vertical elements (core walls) of the lateral-force-resisting system. It is important to consider the impact of the outriggers on the gravity columns and structural walls when maximum demand levels occur. For example, an outrigger system supported by perimeter gravity columns may be result in an axial force (axial force demand) much greater than has traditionally been expected. Evaluating the over-strength characteristics of an outrigger system, and its potential impacts on axial and shear demands is critical to ensure that the overall building system will perform as expected. A detailed explanation of how floor systems might act as outriggers in high rise buildings can be found in the PEER, Tall Buildings Initiative (TBI), 2010 report.

1.9 Analysis Methods

Nonlinear static procedures have become one of the favourite and commonly used methods of analysis in the engineering practice. However, it is highly advisable to perform the nonlinear

static or pushover analysis along with nonlinear response history analysis for a reliable prediction of seismic demands in RC shear wall buildings.

In the simplified version of nonlinear static analysis, an idealized model of the building is subjected to the monotonically increasing invariant arbitrary distribution of lateral forces until a target displacement is attained. The target displacement is currently determined from the procedures developed according to an equivalent linear SDOF system or displacement coefficient method (ASCE/SEI41-06).

Although response history analysis is the most rigorous method to evaluate the seismic demands of buildings structures, it is relatively complex for design offices due to the fact that response history analyses require a considerable number of ground motions. On the other hand, nonlinear static or pushover analysis offers a superior advantage over response history analysis because demands can be computed directly from a design or site-specific hazard spectrum. This feature makes pushover analysis an attractive proposition for the practitioners. However, there are still several unresolved issues in identifying appropriate lateral load patterns to be used in the pushover method.

Current structural engineering practice uses invariant load distributions described in ATC-40 or FEMA-356. While those invariant load distributions (such as inverted triangle, uniform, or mass proportional) are based on the assumption that the response is primarily in its fundamental mode of vibration, it can lead to incorrect estimates for structures with significant higher mode contributions. This shortcoming urges the research community to find a better procedure for the lateral load patterns in pushover analyses. Recently, several improved pushover procedures have been proposed (e.g., Chopra et al., 2002; Jan et al., 2003; Chopra et al., 2004) to account for higher mode effects while retaining the simplicity of invariant load patterns. These newly developed procedures provide more accurate estimates of inter-story drift values compared to

the conventional pushover analysis using inverted triangular, uniform or other modal patterns. However, none of them can account for the redistribution of inertia forces due to the structural yielding and the associated changes in the modal attributes of the structure.

To overcome these limitations, force-based and displacement–based adaptive pushover methodologies have emerged to follow more closely the time-variant distributions of inertia forces (e.g., Satyarno, 1998; Gupta and Kunnath, 2000; Elnashai, 2000; Antoniou and Pinho, 2004).

1.10 Thesis Objectives

This thesis seeks to address some important issues in the seismic behaviour of multi-storey shear wall buildings. The key objectives are:

- To obtain a variation of system over strength factor in typical configuration of multi-story shear wall buildings
- To find the variation of axial force amplification in structural walls and gravity columns due to the three-dimensional spatial interaction of floor systems and frames
- To investigate the effect of out-of-plane stiffness of the floors on seismic response of multi-story shear wall buildings
- To explore the effect of different damping models in emulating the nonlinear response history of multi-story shear wall buildings under dynamic excitation
- To develop a simplified method to quantify effects of interaction between structural walls, floor systems and frames in capacity design of structural walls

The final output presents some guidelines to design engineers on how to account for system overstrength factor in the analysis of the multi-storey shear wall buildings.

1.11 Thesis Organization

This thesis divided into seven chapters. This section explains the outline of the main chapters of this thesis.

1.11.1 Challenges in Analytical Modelling of Multi-Storey Shear Wall Buildings, Modelling approach and Verification

Most researchers and practicing engineers are overwhelmed with many analytical modelling options available for the structural walls. These analytical models usually have been developed based on assumptions which can be very different from each other. For example, while the FEMA-356, USA or Canada design methods are based on plastic hinge rotation which requires modelling the wall elements with multiple vertical line element method (MVLEM) or shell elements, NZ and European codes employ the section behaviour with line elements to define plastic deformation.

One of the primary objectives of this chapter is to recognize most of the currently available mathematical models. Highlighting the pros and cons of such models along with their theoretical background will be another aim of this section. Moreover, analytical or numerical modelling of structural walls should be computationally efficient for modelling structural walls in buildings.

The multi-layered shell element used to model multi-storey shear wall buildings has been found to be computationally very efficient. This element has some promising features, but it requires some degree of verification and/or calibration of some analysis parameters. This element is capable of fully reproducing the axial-flexural interaction in structural walls. This feature is very critical in the numerical simulation of coupled walls or the structural walls with varying axial forces. Furthermore, this element can model, to some extent, axial-flexural-shear interaction. The deformational interaction between axial, flexural and shear type actions is the latest challenge faced by the research community. Different specimens under the static and

dynamic loads has been employed to display the ability of the model to capture the global strength and stiffness (Rojas et al., 2012).

1.11.2 Wall-Slab-Gravity System Interaction in Multi-Storey Shear Wall Buildings

In this chapter, a multi-storey shear wall building will be designed completely based on the New Zealand standards as a reference prototype building. This model will be used as a benchmark for the parametric studies in this thesis. Many aspects of modelling gravity system, slab and wall will be addressed. Further, after detailed introduction of interaction mechanism in this chapter, closed form equations are developed to find the variation of elastic and plastic floor rotations over the multi-storey structural walls. Extensive moment curvature analysis is also conducted to develop the effective base curvature for the structural wall sections based on wall axial force, reinforcement and section geometry. The base curvature modification factor is also introduced to account for the number of floors on displacement and floor rotation profile over the multi-storey structural walls. The overall concept will be summarized in a simple hand calculation methods.

1.11.3 Parametric Studies to Investigate the Effect of Wall-Slab-Gravity Columns Interaction on the System Overstrength

The development of practical design recommendations and prediction of realistic system overstrength due to interaction between flooring system, wall and gravity column interaction require conducting parametric studies based on primary variables of the analytical model. This chapter will investigate the effect of some parameters like span length and slab stiffness on the system response.

The interaction between gravity system including floor slabs and columns with the structural walls changes not only the system response as a whole but also the gravity columns and

structural walls itself. Hence, more investigation will be conducted in this chapter to find additional demands induced in gravity columns or structural walls.

1.11.4 Nonlinear Response History Analysis of Typical Multi-Storey Shear Wall Buildings

Pushover analysis, as one of the promising methods of analysis in performance based design, will be employed in this project. However, the robustness of results needs to be verified, to some extent, by subjecting the structure to the number of ground motions records. Hence, nonlinear response history analysis will be conducted on a number of specific case studies to demonstrate the ability of pushover analysis as an efficient method of analysis in this research.

Attention should be paid to some challenges in performing nonlinear time history analysis. Apart from the inevitable uncertainties on the selection of representative ground motions at a given site; serious concerns arise from the uncertainty on modelling of damping in nonlinear structures. To the author's knowledge, there is a limited reliable practical recommendations (Puthanpurayil et al., 2016) to model damping in nonlinear structures except numerical damping's (such as Rayleigh method) which could be useful in linear dynamic analysis. More discussion on this issue will be presented in Chapter 6.

1.11.5 Outline of Simplified Methodology and Design Recommendations

Capacity design should account for all sources of overstrength actions induced in the ultimate limit states. Moreover, it is essential to find an appropriate estimate of shear force in the non-ductile elements or essentially elastic components to avoid shear failure. Hence, quantifying any source of overstrength in the whole multi-storey shear wall system is a vital part of the routine design process. Hence, a simplified step by step procedure has been proposed to find the system overstrength factor due to the presence of the floor systems.

1.11.6 Concluding Remarks and Research Recommendations

This chapter will include a summary of findings and main contributions of thesis along with some recommendations for the future research.

1.12 References

ACI Committee (2008). Building code requirements for structural concrete (ACI 318-08) and commentary. American Concrete Institute.

Aktan, A. E., and Bertero, V. V. (1984). Seismic response of R/C frame-wall structures. *Journal of Structural Engineering*, *110*(8), 1803-1821.

Antoniou, S., and Pinho, R. (2004). Development and verification of a displacement-based adaptive pushover procedure. *Journal of Earthquake Engineering*, *8*(05), 643-661.

ASCE/SEI Seismic Rehabilitation Standards Committee. (2006). Seismic rehabilitation of existing buildings (ASCE/SEI41-06). *American Society of Civil Engineers, Reston, VA*.

ASCE/SEI (2010). *Minimum design loads for buildings* (Standard ASCE/SEI7-10). *American Society of Civil Engineers, Reston, VA*.

ATC-40 (1996). *Seismic evaluation and retrofit of concrete buildings*. Redwood City, California: Applied Technology Council, Seismic safety commission.

ATC-72-1 (2010). *NEHRP recommended provisions for seismic regulations for new buildings and other structures*. Redwood City, California: Applied Technology Council.

Aalami, B. O. (1990). Load balancing: A comprehensive solution to post-tensioning. *ACI Structural Journal*, *87*(6), 662-670.

Beyer, K., Dazio, A., and Priestley, M. J. N. (2008). Quasi-static cyclic tests of two U-shaped reinforced concrete walls. *Journal of earthquake engineering*, *12*(7), 1023-1053.

Beyer, K., Dazio, A., and Priestley, N. (2011). Shear deformations of slender reinforced concrete walls under seismic loading. *ACI Structural Journal*, *108*(EPFL-ARTICLE-162084), 167-177.

Biskinis, D. E., Roupakias, G. K., and Fardis, M. N. (2004). Degradation of shear strength of reinforced concrete members with inelastic cyclic displacements. *Structural Journal*, *101*(6), 773-783.

Canterbury Earthquakes Royal Commission, (2012). *Part 1: Volumes 1 to 3, Seismicity, Soils and the Seismic Design of Buildings* http://canterbury.royalcommission.govt.nz, June.

Canterbury Earthquakes Royal Commission, (2012). *Part 2: Volume 4, Earthquake Prone Buildings* http://canterbury.royalcommission.govt.nz, October.

Canterbury Earthquakes Royal Commission, (2012). *Part 3: Volumes 5 to 7, Canterbury Television Building (CTV); Roles and Responsibilities* http://canterbury.royalcommission.govt.nz, December.

Carr, A. J. (1980-2016). Ruaumoko–Program and manual for inelastic dynamic analysis. Department of Civil Engineering, University of Canterbury, Christchurch, New Zealand.

CEN EC8 (2004). Eurocode 8 – *Design provisions for earthquake resistant structures*. *EN-1998-1:2004.* Brussels, Belgium: Comite Europeen de Normalization.

CERC (2012). Canterbury Earthquakes Royal Commission Reports. https://canterbury.royalcommission.govt.nz/vwluResources/FinalReportVol1Print/$file/Final_Report_Volume_1_Web.pdf.

Chopra, A. K., and Goel, R. K. (2002). A modal pushover analysis procedure for estimating seismic demands for buildings. *Earthquake engineering and structural dynamics*, *31*(3), 561-582.

Chopra, A. K., Goel, R. K., and Chintanapakdee, C. (2004). Evaluation of a modified MPA procedure assuming higher modes as elastic to estimate seismic demands. *Earthquake Spectra*, *20*(3), 757-778.

Clough, D. P. (1982). Considerations in the design and construction of precast concrete diaphragms for earthquake loads. *PCI Journal*, *27*(2), 79-93.

Corley, W.G., Fiorato, A.E., and Oesterle, R.G., (1981). *Structural Walls*, American Concrete Institute, Publication SP-72, Detroit, Michigan, pp. 77-131

Dazio, A., Beyer, K., and Bachmann, H. (2009). Quasi-static cyclic tests and plastic hinge analysis of RC structural walls. *Engineering Structures*, *31*(7), 1556-1571.

Dhakal, R. P., Singh, S., and Mander, J. B. (2007). Effectiveness of earthquake selection and scaling method in New Zealand. *Bulletin of the New Zealand Society for Earthquake Engineering, 40(3), 160-171*.

Drake, R. M., and Bachman, R. E. (1995). Interpretation of instrumented building seismic data and implications for building codes. *Proceedings of the 1995 SEAOC Annual Convention*.

Elnashai, A. S. (2000). Advanced inelastic static (pushover) analysis for seismic design and assessment. *Proceedings of the G.Penelis international symposium*. Greece: Aristotele University of Thessaloniki, 23–34.

Elnashai, A. S., and Mwafy, A. M. (2002). Overstrength and force reduction factors of multistorey reinforced□concrete buildings. *The structural design of tall buildings*, *11*(5), 329-351.

FEMA 356 (2000). *Commentary for the seismic rehabilitation of buildings*. Washington, DC: Fedearl Emergency Management Agency.

FEMA 450 (2003). *NEHRP recommended provisions for seismic regulations for new buildings and other structures*. Washington, DC: Building Seismic Safety Council.

FEMA 440 (2005). *Improvement of nonlinear static seismic analysis procedures*. Washington, DC: Fedearl Emergency Management Agency.

FEMA 695 (2009). *Quantification of building seismic performance factors*. Washington, DC: Fedearl Emergency Management Agency.

Fenwick, R. C., and Davidson, B. J. (1995). Elongation in ductile seismic-resistant reinforced concrete frames. *Special Publication*, *157*, 143-170.

Fox, M. J., Sullivan, T. J., and Beyer, K. (2014). Capacity design of coupled RC walls. *Journal of Earthquake Engineering*, *18*(5), 735-758.

Gavridou, S. (2015). Shake table testing and analytical modeling of a full-scale, four-story unbonded post-tensioned concrete wall building *(Doctoral dissertation, UCLA)*.

Ghorbanirenani, I., Tremblay, R., Léger, P., and Leclerc, M. (2011). Shake table testing of slender RC shear walls subjected to eastern North America seismic ground motions. *Journal of Structural Engineering*, *138*(12), 1515-1529.

Gupta, B., and Kunnath, S. K. (2000). Adaptive spectra-based pushover procedure for seismic evaluation of structures. *Earthquake spectra*, *16*(2), 367-392.

Hamburger, R., Bonelli, P., Lagos, R., and Wyllie Jr, L., (2012). *Comparison of US and Chilean building code requirements and seismic design practice 1985-2010* (NITS GCR 12-917-18). NEHRP seismic design technical brief no.3, Washington, DC. Retrieved from https://ws680.nist.gov/publication/get_pdf.cfm?pub_id=915494.

Hines, E. M., Seible, F., and Priestley, M. J. N. (1999). *Cyclic tests of structural walls with highly-confined boundary elements* (Report No. SSRP-99/15). Dept. of Structural Engineering, University of California, San Diego.

Hiraishi, H. (1984). Evaluation of shear and flexural deformations of flexural type shear walls. *Bulletin of the New Zealand National Society for Earthquake Engineering, 17*(2), 135-144.

Humar, J. L., and Rahgozar, M. A. (1996). Concept of overstrength in seismic design. *Eleventh world conference on earthquake engineering*. 639, 1-8. Retrieved from http://www.iitk.ac.in/nicee/wcee/article/11_639.PDF.

Jan, T. S., Liu, M. W., and Kao, Y. C. (2003). An upper-bound pushover analysis procedure for estimating the seismic demands of high-rise buildings. *Eng. Struct., 26(1)*, 117–128.

Kabeyasawa, T., Shiohara, H., Otani, S., and Aoyama, H. (1983). Analysis of the full-scale seven-story reinforced concrete test structure. *Journal of the Faculty of Engineering*: *University of Tokyo, 37*(2), 431-478.

Kalkan, E., and Chopra, A. K. (2010). Practical guidelines to select and scale earthquake records for nonlinear response history analysis of structures. *US geological survey open-file report*, *1068*(2010), 126.

Kam, W. Y., Pampanin, S., and Elwood, K. (2011). Seismic performance of reinforced concrete buildings in the 22 February Christchurch (Lyttleton) earthquake. *Bulletine of the New Zealand Society for Earthquake Engineering, 44*(4), 239-278.

KSN Anchores (2018). Reinforcment continuty system in slab to wall moment connections. *Ancon Building Products.*

Lee, J. Y., and Watanabe, F. (2003). Predicting the longitudinal axial strain in the plastic hinge regions of reinforced concrete beams subjected to reversed cyclic loading. *Engineering Structures*, *25*(7), 927-939.

Lopes, A. V., Lopes, S. M., and do Carmo, R. N. (2014). Stiffness of reinforced concrete slabs subjected to torsion. *Materials and structures*, *47*(1-2), 227-238.

Malley, J. O., Dierlein, G., Krawinkler, H., Maffei, J. R., Pourzanjani, M., Wallace, J., and Heintz, J. A. (2010). *Modelling and Acceptance Criteria for Seismic Design and Analysis of Tall Buildings* (PEER/ATC-72-1). San Francisco, California: Applied Technology Council, Pacific Earthquake Engineerinf Research Center.

Mander, J. B., Priestley, M. J., and Park, R. (1988). Theoretical stress-strain model for confined concrete. *Journal of structural engineering*, *114*(8), 1804-1826.

Massone, L. M., and Wallace, J. W. (2004). Load-deformation responses of slender reinforced concrete walls. *Structural Journal*, *101*(1), 103-113.

Memon, M. (1984). *Strength and stiffness of shear wall-floor slab connections* (Doctoral thesis). University of Glasgow, UK.

Menegon, S. J., Wilson, J. L., Gad, E. F., and Lam, N. T. K. (2015). Out-of-plane buckling of limited ductile reinforced concrete walls under cyclic loads. *Proceedings of the 2015 New Zealand Society of Earthquake Engineering Technical Conference.* Rotorua, New Zealand.

Miranda, E., and Taghavi, S. (2005). Approximate floor acceleration demands in multistory buildings. I: Formulation. *Journal of structural engineering*, *131*(2), 203-211.

Mitchell, D., and Paultre, P. (1994). Ductility and overstrength in seismic design of reinforced concrete structures. *Canadian Journal of Civil Engineering*, *21*(6), 1049-1060.

Moehle, J. P., Hooper, J. D., Kelly, D. J., and Meyer, T. R. (2010). *Seismic Design of cast-in-place concrete diaphragms, chords, and collectors* (NITS GCR 16-917-42). NEHRP seismic design technical brief no.3, Washington, DC. Retrieved from https://doi.org/10.6028/NIST.GCR.16-917-42.

Nassar, A. A., and Krawinkler, H. (1991). *Seismic demands for SDOF and MDOF systems* (Report No. 95). California: Stanford University, Blume Earthquake Engineering Center, Department of Civil Engineering.

New Zealand Society for Earthquake Engineering (NZSEE), (2006). *Assessment and Improvement of the Structural Performance of Buildings in Earthquake*. The New Zealand Society for Earthquake Engineering.

NIST GCR-12-917-18 (2012). *Comparison of US and Chilean Building Code Requirements and Seismic Design Practice 1985-2010* (Report (NISTGCR)-12-917-18).

NIST GCR-11-917-15 (2011). *Selecting and scaling earthquake ground motions for performing response-history analyses* (Report (NISTGCR-12-917-15).

NZS3101 (2006). Concrete Structures Standard, NZS 3101:2006 Parts 1 and 2 Standards New Zealand.

NZS1170.5 (2004). Strcutral Deisng Actions, NZS 1170.5:2004 Parts 1 and 2 Standards New Zealand.

Oesterle, R. G., Fiorato, A. E., Johal, L. S., Carpenter, J. E., Russell, H. G., and Corley, W. G. (1976). *Earthquake resistant structural walls-tests of isolated walls* (PCA-R/D-SER-1571). National Science Foundation, Washington, D.C.

Oesterle, R. G., Aristizabal-Ochoa, J. D., Shiu, K. N., and Corley, W. G. (1984). Web crushing of reinforced concrete structural walls. *ACI Journal Proceedings*, *81*(3), 231-241.

Panagiotou, M., Restrepo, J. I., and Conte, J. P. (2007). *Shake Table Test of a 7-story Full Scale Reinforced Concrete Structural Wall Building Slice, Phase I: Rectangular Section* (Report No. SSRP-07/07). San Diego, CA: Department of Structural Engineering, University of California,.

Panagiotou, M., Restrepo, J. I., and Conte, J. P. (2010). Shake-table test of a full-scale 7-story building slice. Phase I: Rectangular wall. *Journal of Structural Engineering*, 137(6), 691-704.

Park, R. (1996). Explicit incorporation of element and structure overstrength in the design process. *Proceedings of the 11th WCEE. IAEE.* Acapulco, Mexico.

Paulay, T., and Priestley, M. N. (1992). *Seismic design of reinforced concrete and masonry buildings*. New York: John Wiley and Sons.

PEER(TBI). (2010). Guidelines for Performance-Based Seismic Design of Tall Buildings. PEER 2010/05. Pacific Earthquake Engineering Research Center, Berkeley, CA.

Peng, B. H., Dhakal, R. P., Fenwick, R. C., and Carr, A. J. (2011). Elongation of plastic hinges in ductile RC members: model development. *Journal of Advanced Concrete Technology*, *9*(3), 315-326.

Precast/Prestressed Concrete Institude (2007). Architectural precast concrete. Retrived from http://www.enterpriseprecast.com/uploads/Image/PCI_Architectural_Precast_Concrete_Manual.pdf.

Priestley, M. J. N. (1997). Displacement-based seismic assessment of reinforced concrete buildings. *Journal of earthquake engineering*, *1*(01), 157-192.

Priestley, M. J. N., Calvi G. M., and Kowalsky M. J. (2007). *Displacement-based seismic design of structures*. Pavia, Italy: IUSS Press.

Puthanpurayil, A. M., Lavan, O., Carr, A. J., and Dhakal, R. P. (2016). Elemental damping formulation: an alternative modelling of inherent damping in nonlinear dynamic analysis. *Bulletin of Earthquake Engineering*, *14*(8), 2405-2434.

Rodriguez, M. E., Restrepo, J. I., and Carr, A. J. (2002). Earthquake induced floor horizontal accelerations in buildings. *Earthquake engineering and structural dynamics*, *31*(3), 693-718.

Rojas, F. (2012). Development of a nonlinear quadrilateral layered membrane element with drilling degrees of freedom and a nonlinear quadrilateral thin flat layered shell element for the modeling of reinforced concrete walls. *Los Angeles, California: University of Southern California*.

SAP2000, CSI, S. (2016): Ver. 17.1.1, integrated finite element analysis and design of structures basic analysis reference manual. Berkeley (CA, USA), Computers and Structures INC.

Satyarno, I., Carr, A. J., and Restrepo, J. (1998). Refined pushover analysis for the assessment of older reinforced concrete buildings. *Proceedings of the New Zealand Society for Earthquake Engineering Technology Conference*, 75-82.

SEAOC Seismology Committee. (2006). SEAOC Blue Book: Seismic Design Recommendations. *Structural Engineers Association of California, Sacramento, CA*.

Shegay, A. S., Motter, C. J., Henry, R. S., and Elwood, K. J. (2017). Modelling of RC walls with ductile detailing subjected to high axial loads. *16th World Conference on Earthquake Engineering, Santiago,* 9-13.

Shelton, R.H., Park, S.G. and King, A.B. (2002). Earthquake response of building parts. *Proceedings of NZ Society for Earthquake Engineering Annual Conference.*

Sullivan, T. J., Calvi, P. M., and Nascimbene, R. (2013). Towards improved floor spectra estimates for seismic design. *Earthquakes and Structures, 4(1),* 109-132.

Surumi, R. S., Jaya, K. P., and Greeshma, S. (2015). Modelling and Assessment of Shear Wall–Flat Slab Joint Region in Tall Structures. *Arabian Journal for Science and Engineering*, *40*(8), 2201-2217.

Thomsen IV, J. H., and Wallace, J. W. (2004). Displacement-based design of slender reinforced concrete structural walls - experimental verification. *Journal of Structural Engineering*, *130*(4), 618-630.

Wood, S. L. (1991). Performance of reinforced concrete buildings during the 1985 Chile earthquake: implications for the design of structural walls. *Earthquake Spectra*, *7*(4), 607-638.

Wood, S. L., Wight, J. K., and Moehle, J. P. (1987). *The 1985 Chile earthquake: observations on earthquake-resistant construction in Viña del Mar*. University of Illinois Engineering Experiment Station. College of Engineering. University of Illinois at Urbana-Champaign.

2 Challenges in Analytical Modelling of Multi-storey Shear Wall Buildings, Modelling Approach and Verification

2.1 Introduction

Shear walls are commonly used as a main lateral force resisting system in low, medium and high rise reinforced concrete (RC) buildings in seismically active countries. With development of performance based design or assessment, engineers require to conduct nonlinear static or dynamic analysis to accurately estimate local and global seismic demands in terms of inter storey drift ratios, element rotations, section curvatures or strains. While material strain or curvature demands seems to be more robust in seismic design or assessment, available commercially used software and assessment guidelines give acceptance criteria for ductile components in different limit states (or performances) in terms of rotations in beams, columns and slender walls (ASCE/SEI41-06). The New Zealand standard (NZS3101:2006) evaluates the curvature and strain ductility demand in different limit states in RC building components.

A robust analytical shear wall model for nonlinear analysis of multi-storey buildings is essential for reliable seismic performance assessment. These models must be capable of estimating the global seismic demands with an acceptable accuracy and within a reasonable computational time. Moreover, they must be applicable in three-dimensional analyses of multi storey buildings. There are many variables such as shear span ratio, interacting nonlinear axial, shear and flexural behaviour, boundary elements, connections to slabs and transverse girders, which affect the seismic behaviour of shear walls in buildings. Hence, accuracy of a model in the simulation of isolated wall specimen is not necessarily sufficient to employ in real multi-storey shear wall building analyses. In the authors' knowledge, there is no current reliable macro element capable of capturing all the different failure patterns in multi-storey shear wall buildings.

In this chapter, attention is focused on relatively simple and reasonably accurate wall analytical models based on a macroscopic approach. The main features of these models are discussed and

an attempt is made to offer a practical model that is capable of predicting the behaviour of shear walls in three-dimensional reinforced concrete structures.

2.2 Review of Available Nonlinear Models

Different analytical models of reinforced concrete (RC) structural walls along with their applications to the simulation of multi-storey RC structural walls are reviewed and discussed in the following sections.

2.2.1 Wide Column Analogy

Treating a shear wall as a wide column is a common approach. In this model (Figure 2.1), rotation occurs around the wall centroidal axis and movement of the neutral axis and rocking (upward and downward movement of boundary elements) cannot be captured. However, when the vertical deformation of wall edges is of great importance, especially in the case of considering wall interaction with adjacent frames, this effect can be accounted for by adding horizontal rigid beams on either side of the vertical columns (Bertero et al., 1984). However, this approach cannot realistically model movement of the wall edges, especially with large axial tension, and the elongation of a wall under horizontal reversed cyclic demands.

In the one component model (Giberson, 1967), the line elements aligned at the wall centroidal axis require the elastic flexural stiffness and strength (based on section moment curvature analysis or code recommendations) in the middle segment and also the post-elastic stiffness for nonlinear rotational spring at the ends (Figure 2.1). The end springs have an infinite stiffness before the occurrence of flexural yielding and all plastic deformation is lumped in these springs. The one component model has been modified to include inelastic shear springs at its end in series with the flexural springs (Satyarno et al., 1998). This can be seen in Figure 2.1(b). The most commonly used moment rotation hysteresis rule for the end rotational springs are the Takeda or modified Takeda hysteresis (Otani, 1974 and Saiidi and Sozen, 1979) having a tri-

linear backbone curve to account for cracking, yielding and strain hardening of the concrete elements and with stiffness degradation. In a linear analysis, design codes commonly recommend a constant flexural stiffness reduction factor over the entire height of multi-storey buildings to account for concrete cracking, reinforcement yielding and axial forces. However, a wide range of recommendations is found for these flexural stiffness values in different codes. This model may not be appropriate in shear wall buildings with high axial gravity forces, high shear force demand or walls with varying axial forces during the analysis. Moreover, shear wall buildings with high axial forces and a light longitudinal reinforcement restrict cracking only to a small portion of the walls; and the significant un-cracked part is commonly neglected in the moment curvature idealization or equivalent stiffness method.

The wide column analogy adopts the Bernoulli Hypothesis and it uses the *plane section remains plane* assumption in its formulation by enforcing a linear distribution of strain at the section level. Moreover, the shear strength and stiffness properties of the walls are commonly derived independently. The shear spring properties are assumed constant during the structural analysis. In other words, this model commonly overlooks shear-flexure interaction. This implies that shear strength and stiffness do not degrade by increasing flexural rotational or displacement ductility demands. Satyarno et al. (1998) implemented a shear spring in the finite element analysis program Rauamoko using the curvature ductility demands to reduce the shear strength of shear springs.

The advantage of this beam analytical model is its computational efficiency in a nonlinear response history analysis of large multi-storey shear wall buildings. It is also easy to calculate capacity in terms of rotation or inter storey drifts and to compare with available performance acceptance criteria in guidelines. Hence, this model is commonly used in exploring dynamic response of multi-storey shear wall buildings (Goodsir et al., 1983 and Roudriguez et al., 2002).

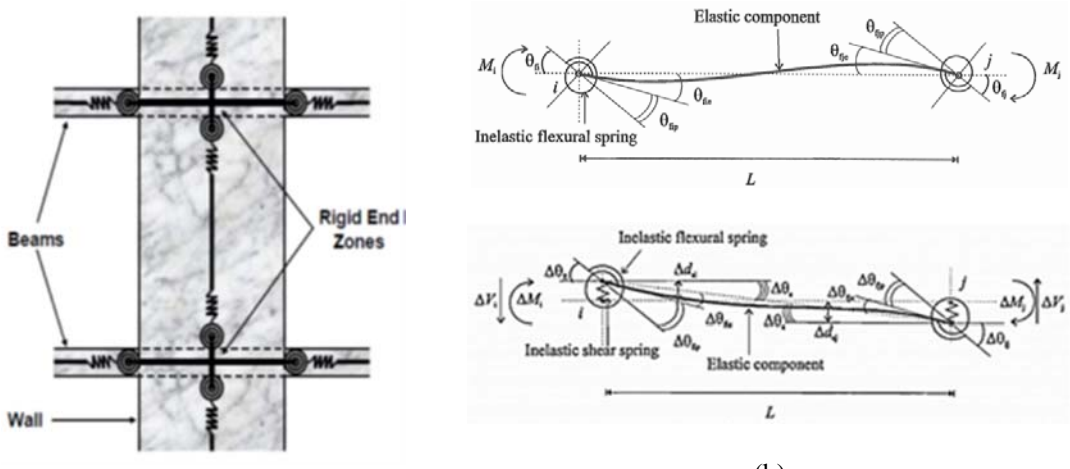

(a) (b)

Figure 2.1: Wide column analogy (a) and one component Giberson (1967) beam (with and without shear springs (b))

2.2.2 Line Elements with Fibre Section

In this approach, sections are discretized into many uniaxial steel and concrete fibres with their own mechanical and geometric properties (Figure 2.2). The basic idea was introduced by Park et al. (1972) to capture flexural cyclic behaviour of beams. Based on this concept, Taylor (1977) proposed a wall element using uniaxial cyclic behaviour of concrete and reinforcement at each fibre at each integration section over the length of the wall. This model, which was incorporated in Ruaumoko, allows for the shift in neutral axis which is very important in coupled shear walls.

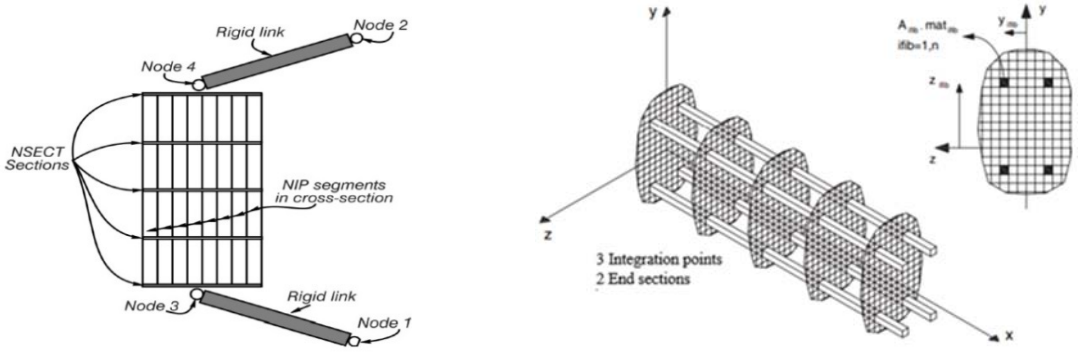

(a) (b)

Figure 2.2: Wall element in Rauamoko2D (a) and a fibre section line element in OpenSees (b)

The Bernoulli' hypothesis is commonly used in fibre section formulation. This type of beam assumes that the cross-sections remain plane and normal to the reference axis during the deformation history. This assumption implies a perfect bond between reinforcement and concrete. The force based fibre beam column element assumes linear moment and axial force distribution over the length of element. Based on the flexibility approach, the section forces are determined (moment and axial forces) from interpolation of element end forces. Nonlinear behaviour of the materials is tracked in three cross sections along the length of the elements. In these models distribution of plasticity is induced through the member cross section and along the member length by numerical integration. The fibre elements report the seismic demands as strains in reinforcement and concrete. Calculation of plastic hinge rotations in these models requires the user to post process outputs (strains). The strain demands in this approach are quite sensitive to moment gradient, element length, integration method and strain hardening. Likewise, displacement based elements enforce linear curvature along the member. Therefore, more elements are required in regions of high curvature variations (like plastic hinge zones). These two elements are implemented in OpenSees.

Martinelli and Filippou (2009) employed this approach to simulate the shaking table test of a seven storey shear wall building. He recommended application of this model for walls of medium to high slenderness undergoing primarily flexural response with negligible shear effects. More recently, Pugh (2012) demonstrated the incapability of force based fibre element in capturing ductility demands even with increasing the number of integration points. A material regularization method was proposed to adjust the uniaxial behaviour of concrete and steel based on the number of integration points (mesh dependent behaviour) in force based fibre elements.

The big advantage of this approach is that axial flexural interaction can be explicitly captured and there is no need to define controversial values of effective elastic stiffness for members.

This flexural stiffness is a serious concern for engineers especially in coupled walls when the axial forces can significantly change the flexural stiffness during the analysis. On the other hand, this approach has some unanswered questions about their robustness to predict nonlinear shear strains and their degradation with axial strains.

2.2.3 Truss Analogy

An equivalent truss model was employed to predict monotonic strength capacity of walls in the experimental tests carried out by Hiraishi (1984) and Oesteler et al. (1984). Truss members are used in this macro model which consists of two vertical and one diagonal truss member connected to each other by a rigid horizontal beam or tie. The diagonal truss is used to represent the diagonal compression strut in the web providing shear resistance. The assumption in this analogy is that the truss elements are statically determinate. Non-prismatic truss elements can be employed in plastic hinge regions to avoid the *plane section remains plane* assumption.

The applicability of this approach is usually limited only to monotonic loading mainly because assigning appropriate properties of the truss members under cyclic loading is very challenging (Vallenas et al., 1979). Moreover, it is not easy to decide a suitable number of truss members for whole shear wall, and realistic prediction of deformation due to gravity load and lateral force is not easy to achieve in this analogy. However, if carefully calibrated, this model may give useful results under small gravity load and static monotonic force (Linde and Bachmann, 1994).

Recently, some researchers attempted to improve the truss analogy of Hrennikoff (1941) to simulate the cyclic response of shear wall specimens (Panagiotou et al., 2012). In the enhanced lattice models, implemented into Ruaumoko, longitudinal, transverse and diagonal truss elements in a finite element type mesh were used to represent concrete and reinforcement steel. This model captures stiffness and strength degradation, the strain histories in the reinforcement

and concrete, and accounts for the dependency of the concrete stress-strain relationship in compression on the transverse strains.

2.2.4 Multi Spring Elements

The multi spring element concept (Figure 2.3) was initially introduced for analytical modelling of columns (Lai et al., 1984), and it was used to simulate column sections under biaxial bending. A similar concept was employed to simulate a three-dimensional shear wall building by Fu et al. (1992). This model has been further enhanced by Li (2010) to account for cracking, tension stiffening and confinement effect in compression and nonlinearity in shear.

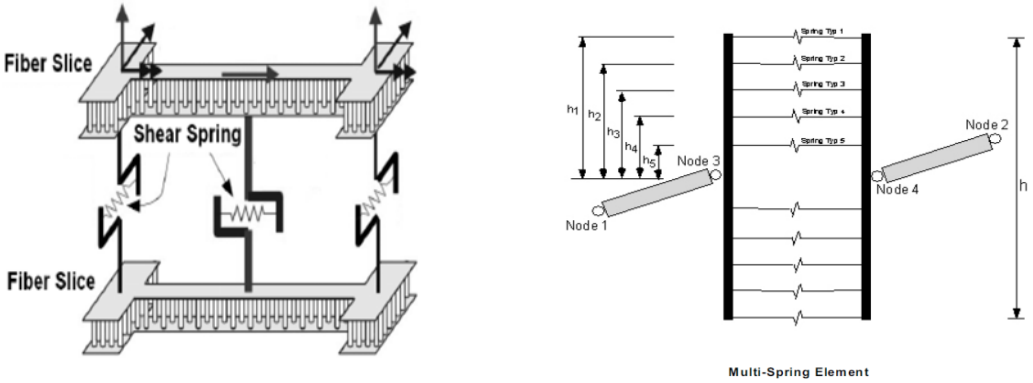

Figure 2.3: Multi spring model for wall in Finite Element Programs Canny and Ruaumoko

Another version of multi-spring element was developed by Speith et al. (2004). This is shown in Figure 2.3. This element comprises of 10 concrete and 10 steel springs with cyclic behaviour which can be employed to simulate behaviour of critical sections in shear walls. It has been implemented in Ruaumoko and has been used to capture seismic performance and modelling of post-tensioned precast reinforced concrete frame structures with rocking beam-column connections and also shear wall structures.

One of the main turning points in understanding hysteresis behaviour of shear wall buildings was when Kabeyasawa et al. (1983) conducted shaking table test of a seven storey RC building with shear wall and frames. Three vertical line element model (TVLEM) was proposed as a

reliable tool to predict the shear wall response by Kabeyasawa et al. (1983). TVLEM approach idealized a wall member under uniform bending (constant curvature in each storey) as three vertical springs with infinitely rigid beams at the top and bottom (Figure 2.4). Two outside truss like elements represented the axial stiffness of the boundary columns and their axial stiffness varied with the sign and level of axial stress, and degraded with tensile stress history. This was modelled using the Axial-Stiffness Hysteresis Model (ASHM) shown in Figure 2.4. The central vertical element was a one component model in which vertical, horizontal and rotational springs were concentrated at the base. The effect of strain gradient across the wall section was represented by the rotational spring in the centre and shear deformation was controlled by the deformation of horizontal spring with Origin Oriented Hysteresis Model (OOHM) (Figure 2.5). Most of the important aspects of nonlinear global behaviour of a wall could be simulated by this model quite well except for the shear deformations. However, this mode was developed based on specific test data and it requires many empirical parameters for calibration.

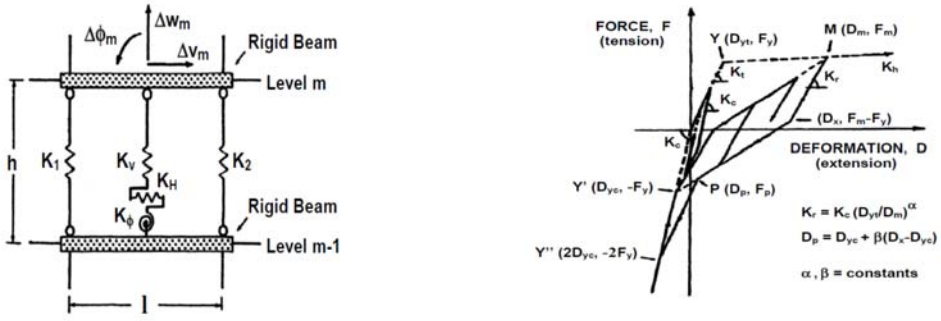

Figure 2.4: TVLEM model and hysteresis rule for axial springs (ASHM)

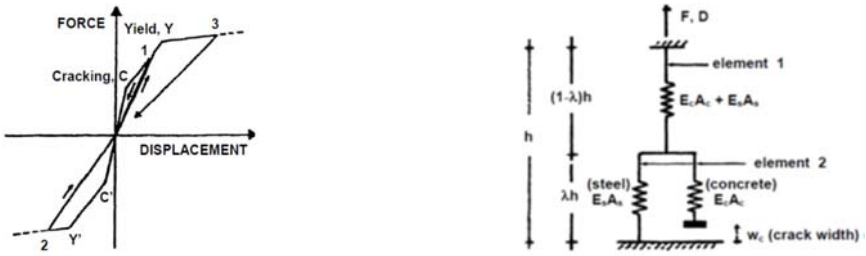

Figure 2.5: OOHM model for shear and parallel springs to capture tension stiffening in TVLEM

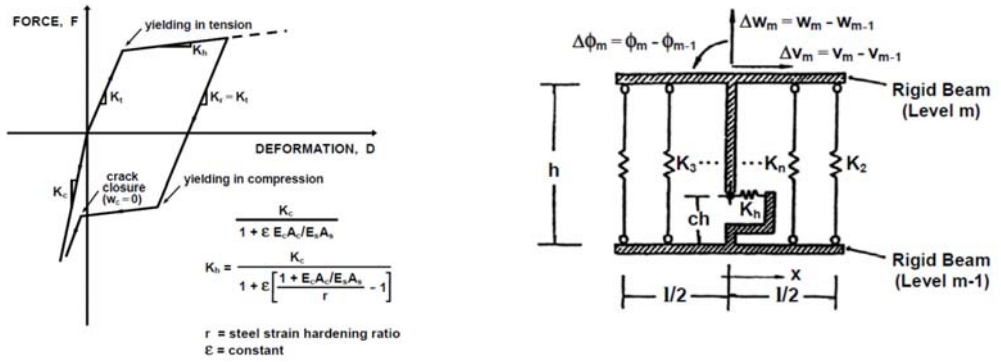

Figure 2.6: MVLEM model based on material law

Many researchers tried to reduce empirical assumptions in the TVLEM model and increase the reliability of the model by employing material based hysteresis rules. Vulcano et al. (1988) improved the TVLEM by replacing the rotational spring with a number of longitudinal springs (Figure 2.6). In their multiple vertical line element model (MVLEM), a structural wall is represented as a stack of springs which are placed on top of each other. While the two outside springs model the axial stiffness of the boundary columns, the interior springs with axial stiffness, represent globally the axial and flexural stiffness values of the central panel. They introduced the centre of rotation for a wall panel based on the assumption of constant or linear curvature distribution in each wall panel. However, suitable values for centre of rotation in each wall need calibration. Furthermore, they attempted to use hysteresis response of steel springs and concrete springs in parallel and in series to account for the tension stiffening effect (Figure 2.5).

The main limitations of such multi spring models are the adoption of *plane section remains plane* in their formulation which is poor assumption in deep beams and shear walls. Moreover, nonlinear shear flexure interaction cannot be reproduced by these models and under high shear stress demands the shear response cannot be realistically predicted. Colotti (1993) modified the above model to enable it to capture shear flexure interaction in monotonic loading, especially when shear span ratios are less than 2.5. He employed the modified compression field theory to account for shear flexure interaction in each panel of a wall.

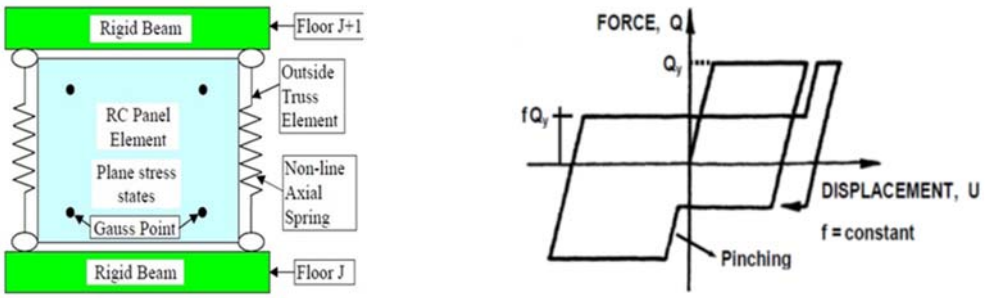

Figure 2.7: Improved models for shear behaviour

Linde and Bachmann (1994) modified the basic TVLEM by adding additional degrees of freedom at each node of the infinite rigid beam to eliminate the middle rotational spring. They attempted to generate the wall stiffness matrix based on elastic section properties and wall kinematic behaviour. However, in the proposed element, like initial element, an origin oriented hysteresis model (OOHM) was employed for shear behaviour to capture the dynamic curvature ductility demands in multi-storey shear wall buildings. Ghobarrah and Youssef (1999) attempted to enhance the TVLEM model to capture shear flexure interaction in cyclic analysis. They adopted modified compression field theory to consider the axial and shear strain interaction in each wall panel element. Chen and Kabeyasawa (2000) improved the TVLEM shear model by replacing the shear spring with an isoparameteric panel element with biaxial behaviour in the middle of the wall (Figure 2.7).

The MVLEM model was recently improved by implementing refined hysteretic uniaxial, cyclic material constitutive models instead of simplified force-deformation rules to predict the inelastic response of slender RC walls (Orakcal et al., 200; Massone et al., 2006; Kolozvari et al., 2012; Kolozvari et al., 2014a; Kolozvari et al., 2014b). They attempted to reproduce monotonic and cyclic nonlinear shear flexure interaction in this element by adopting modified compression field theory and this element has been implemented in the nonlinear finite element analysis program OpenSees. However, experimental verification for some specimens with high shear stress demands was not convincing.

2.2.5 Shell Elements with Fibre Section

In order to model bending, shear and diagonal compression behaviour, a wall element consisting of five layers acting in parallel was developed and implemented in Perform3D (Figure 2.8(a)). In the vertical and horizontal directions, axial and bending modes of wall behaviour were reproduced by some layers or springs based on vertical and horizontal fibre cross section properties including steel and concrete fibres. One shear layer assumes constant shear stress uniformly distributed over the wall length and its properties are defined from the shear resistance of concrete. Diagonal strut layers assume constant diagonal compression stress over the wall length. Through interaction with the axial-bending deformation in horizontal and vertical layers (springs), the diagonal compression layer can transfer the shear and account for the contribution of horizontal reinforcement in the shear resistance of the wall. However, the stiffness matrix derivation for this element is not clear in the manual and the model does not appear to predict the behaviour accurately in case of high shear force demands in squat walls. Moreover, no experimental verification is available to assess the robustness of the proposed element. This element has been used in analytical investigation of shear walls by several researchers (Kim and Wallace, 2014 and Tuna, 2012).

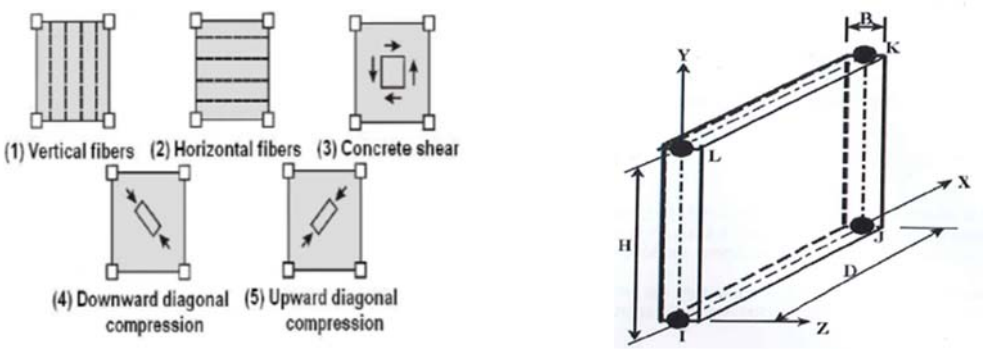

(a) Shell element (b) Wall element

Figure 2.8: Shell element (a) and Wall element (b)

2.2.6 Wall Macro Element in Ruaumoko3D

A new macro element based on uniaxial behaviour of many filaments has been incorporated in the nonlinear analysis program Ruaumoko3D (Figure 2.8(b)). The two dimensional Taylor Wall element which previously introduced in (Figure 2.2(a)) has been developed in Ruaumoko2D. This element was fine in a two dimensional model as the shear-centre is always in the plane of the wall. In three dimensions this is not possible as locating the shear-centre when parts of the concrete section are cracked or the steel is yielding is difficult. As an alternative approach, taking a near-rectangular finite element, the wall geometry with flanges and closed cells is built up and the shear centre is dealt with automatically. The element has 24 degrees of freedom including the drilling degrees of freedom (or a rotational degree of freedom perpendicular to element) at the nodes which make it easy to connect with beam and slab elements. The wall cross-section element includes 10 concrete and 10 steel filaments in the vertical direction, 4 concrete and 4 steel filaments in the horizontal direction and either 2 diagonal springs representing the shear action similar to that proposed by Peng et al. (2013) or as a single shear spring similar to that shown for the MVLEM model. The diagonal shear spring model introduces an axial-flexure-shear interaction whereas the single shear spring model has only the axial-flexure interaction. Many hysteresis options are available for the concrete and reinforcement. One of the main features of this element which makes it distinct from others is the use of cubic functions for in-plane edge displacements avoiding the *plane section remains plane* constraint. The out-of-plane behaviour is modelled with a hybrid-stress plate bending finite element though a full two-dimensional cross section is under development. Initial results are promising but the element needs extensive verification and further research to enhance the shear-flexure interaction.

2.3 Global Challenges

2.3.1 Effect of Shear Force and Shear Deformation

Flexural stresses are distributed in wider lengths in walls compared to columns and beams. The simultaneous presence of shear force and moment results in shear cracking before yielding of transverse reinforcement over the length of a wall. These shear flexure cracks can affect the overall behaviour of walls in plastic hinge regions even in slender walls with flexure dominant behaviour (Vallenas et al., 1979; Hiraishi 1984; Beyer et al., 2011).

Most engineers use the shear modulus of concrete based on elastic theory while using a wide column analogy for shear walls in low and mid-rise buildings. The elastic shear modulus of concrete is calculated as $0.4E_c$ and keeping it constant during nonlinear response history analysis gives very small shear deformations in plastic hinge regions. Thus, its effect is commonly assumed negligible in the overall response of walls.

Many experimental tests (Oesteler et al., 1976 and Hines et al., 1999) demonstrated that in most walls designed for yielding in flexure, shear cracking induces considerable shear deformation in plastic hinge regions and consequently it affects the overall deflection of walls. This implies that shear cracking decreases the elastic shear modulus of concrete even in flexure dominant walls which is often overlooked in nonlinear response history. Lack of reliable experimental data for nonlinear behaviour of shear spring (shear force versus shear strains) in slender walls and appropriate analytical tools are some of the main issues. Shear deformation is more pronounced in slender walls when shear transfer mechanisms start to deteriorate because of high shear stress in plastic hinge regions. This phenomenon decreases the shear strength and shear stiffness of a wall which is called shear-flexure interaction (Beyer et al., 2011).

Krolicki et al. (2011) enhanced the shear strength and stiffness prediction equations for shear walls originally proposed by Kowalsky and Priestley (2000). The shear strength formula was improved to reliably estimate the cyclic shear capacity of walls considering the effect of axial force and displacement ductility. Shear failure is one of the major concerns even in capacity designed walls because of the inherent large uncertainty in shear strength and its deterioration mechanism. However, it is not uncommon for researchers to keep the shear strength constant during analysis and to assume that shear strength degradation or failure is controlled solely by curvature ductility demands.

Mergos and Beyer (2014) introduced a beam element to include shear stiffness degradation during analysis. Based on some experimental results, they assumed that flexural to shear displacement ratio remains more or less constant during the whole range of inelastic cycles. The equation below was proposed to calculate the shear deformation based on wall geometry (H_n is the wall shear span) and assuming constant neutral axis depth (c) after yielding. The above analytical method is implemented in the IDARC program.

$$\frac{\Delta_s}{\Delta_f} = \frac{(\frac{L_w}{2} - c)}{H_n.tan\beta} \tag{2.1}$$

Kolozvari et al. (2016) demonstrated that the modelling parameters associated with wall shear behaviour have a significant effect on the computed responses for models in which shear behaviour is not coupled with axial-flexural behaviour. The authors suggested that using the commonly recommended effective shear stiffness of $0.2E_cA_w$ to account for the effects of concrete cracking provides a reasonable estimate of roof displacement response. However, wall shear demands, and inter-story drift at stories where wall yielding occurs, tend to be overestimated and underestimated respectively, in comparison with results obtained using models in which shear behaviour is coupled with axial-flexural behaviour.

The shear backbone curve displayed in Figure 2.9 was proposed by Kelly (2007) using experimental data available in the literature. Another model proposed in ASCE/SEI41-06 for shear behaviour of slender walls, where flexural yielding limits the wall shear demand, is shown in Figure 2.10. The shear force in this model is calculated based on $V=M/H_{eff}$, where H_{eff} is the effective height of the lateral resultant forces, and the shear strain at yield is taken as 0.0015.

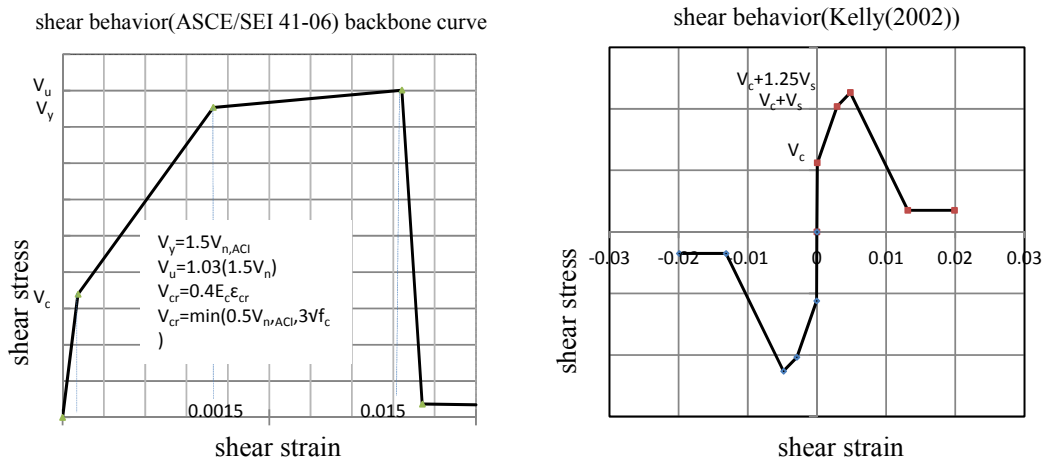

Figure 2.9: Recommendations for shear behaviour of walls

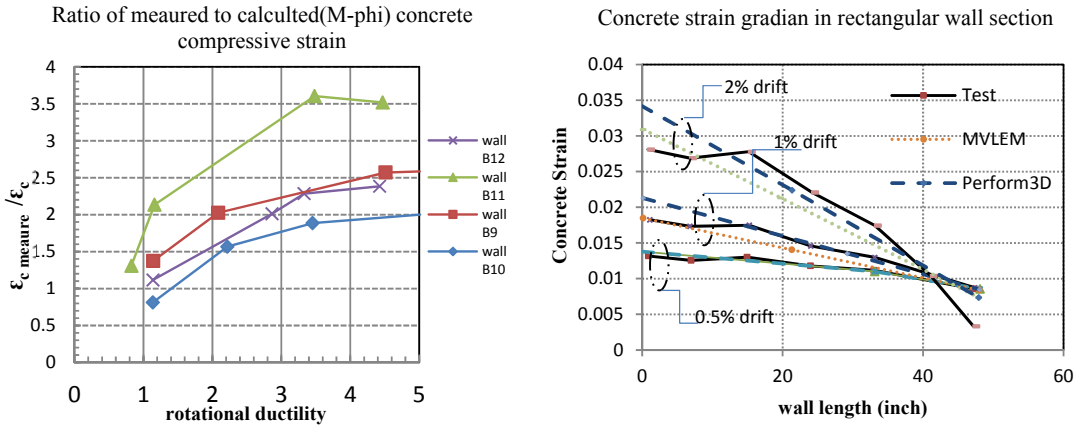

Figure 2.10: Concrete compressive strain variation in wall section (and with ductility)

2.3.2 Three-dimensional Effects

Practicing engineers need a computationally efficient wall model to use in seismic performance assessment/prediction of multi-storey shear wall buildings with different configurations. Such

models must be three-dimensional and be able to interact with beams and slabs which can induce additional actions on walls and it can result in considerable change in the assumed shear span ratio and the shear demands on the wall.

To explore more on this issue, one of the specimens from the PCA test program (R2 specimen) was selected to conduct nonlinear pushover analysis to understand the effect of slab in the predicted wall response. This specimen was modelled based on the material properties specified in the test report. The new wall element based on concrete and steel filaments in a wall section was employed in analysis. Results indicate that the yielding moment and moment capacity of the wall agrees well with experimental results. In the next step, a slab of dimensions 2000×1905×60 mm was assumed in each transverse direction. Gravity columns at slab corners were defined to remain elastic, which constrained vertical movement of slab corner nodes. The out-of-plane stiffness of the slabs was activated assuming infinite in-plane stiffness (rigid diaphragm).

The author conducted analysis on a RC structural wall with and without floor slabs and the preliminary results (Figure 2.11) demonstrated that before yielding of the wall in flexure, the effect of slabs on walls was negligible. However, as soon as the wall yielded, the contribution of stiffness from the slabs and the axial stiffness of columns increased the post yield stiffness of the wall by up to 30 percent. The restrained slabs (even without transverse girders common in monolithic construction) intensify the seismic base shear demand in multi–storey shear walls. However, results show that the slab out-of-plane stiffness does not change the flexural capacity of the wall itself as much.

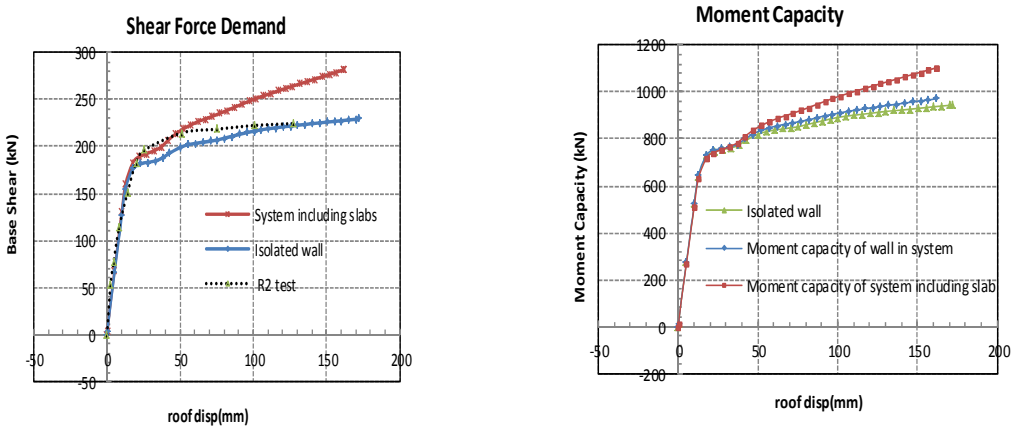

Figure 2.11: Contribution of out-of-plane stiffness of slab and gravity columns

2.4 Finite Element Modelling Approach and Numerical Analysis Package

Nowadays several finite element analysis software packages are used by engineering practices to develop simple and complex analytical and numerical models of multi-storey RC structural walls. Since the formulation of each of these models is based on different assumptions and theories, the accuracy, computational time, and applicability of each may vary. SAP2000, one of the commonly used programs in engineering practice, was used in this research to perform linear and nonlinear (including material and geometric nonlinearity) analyses. Hence, the verified and validated results of this study provides an opportunity to develop a set of recommendations for practical modelling of multi-storey structural walls. Furthermore, the results of analyses allow a better understanding of the limitations of this commercially available program, helping its user to choose the best approach to performing nonlinear dynamic and static analyses. A summary of the results and the relevant limitations of the research performed are presented in Chapters 4 and 5.

Table 2-1 provides a summary of the different modelling approaches used by finite element analysis software programs, along with their strength and weakness in the nonlinear modelling of multi-storey RC structural wall buildings. The key feature of employed element for modelling RC structural walls is to have the compatible degrees of freedoms with the element

used for the floor systems in the mathematical model. This study used the multi-layer shell element in SAP2000 for the finite element analysis of all prototype case study buildings. Although Ruaumoko3D was computationally efficient compared with SAP2000 and Perform-3D, at the time of this research, the new wall element in this program was still under the development. It is also important to note that a general nonlinear layered shell object has been introduced in SAP2000 and it has modelling features similar to the wall objects in Perform-3D.

Table 2-1: Features of different modelling approaches

Element type		Program	Cyclic model of concrete	Cyclic model of bar	AFI	AFSI	PS	3D effect
Line elements	Multi-spring	Ruaumoko2D	Bilinear	Bilinear	yes	no	yes	no
	2D wall element	Ruaumoko2D	Kent et al. 1969	Bilinear	yes	no	yes	no
	Wide column	Ruaumoko2D, OpenSees, SAP2000	Various models	Various models	yes	no	yes	no
	MVLEM	OpenSees	Mander et al. 1988	Menegotto and Pinto 1973	yes	yes	yes	no
	Fiber section	OpenSees	Mander et al. 1988	Menegotto and Pinto 1973	yes	no	yes	no
Wall element	Wall element	Perform-3D	Multi-linear	Bilinear	yes	no	yes	yes
	Wall with diagonal spring	Ruaumoko3D	Peng et al. 2013	Bilinear	yes	no	no	yes
	Wall with horizontal spring	Ruaumoko3D	Peng et al. 2013	Bilinear	yes	no	no	yes
	Multi-layered shell	SAP2000	Otani et al.1974	Multi-linear	yes	yes	no	yes

AFI: Axial-flexural interaction, AFSI: Axial-flexural-shear interaction PS: Plain section

Three-dimensional nonlinear finite element models are built using SAP2000 for the prototype buildings to calculate the engineering demand parameters. The advanced features of this element are described in the following section. The seismic mass at all floors was assigned as distributed mass on walls. While the floor system can act in out-of-plane in prototype buildings, the in-plane stiffness of floor system set to infinite. Hence, a rigid diaphragm is incorporated

by slaving the translational degrees of freedom at each floor level. The foundation of the building was assumed as rigid, and P-Delta effects are taken into account.

2.4.1 Multi-Layer Shell Element

In SAP2000 the shell element is a three or four node element that combines membrane and plate bending behaviour. The shell element can be of two types:

i) Homogeneous is the most commonly used type of shell. It combines membrane and plate behaviour (Figure 2.12). The membrane behaviour uses an isoparametric formulation that includes translational in-plane stiffness components and a "drilling" rotational stiffness component in the direction normal to the plane of the element. Plate bending behaviour includes two-way, out-of-plane, plate rotational stiffness components and a translational stiffness component in the direction normal to the plane of the element.

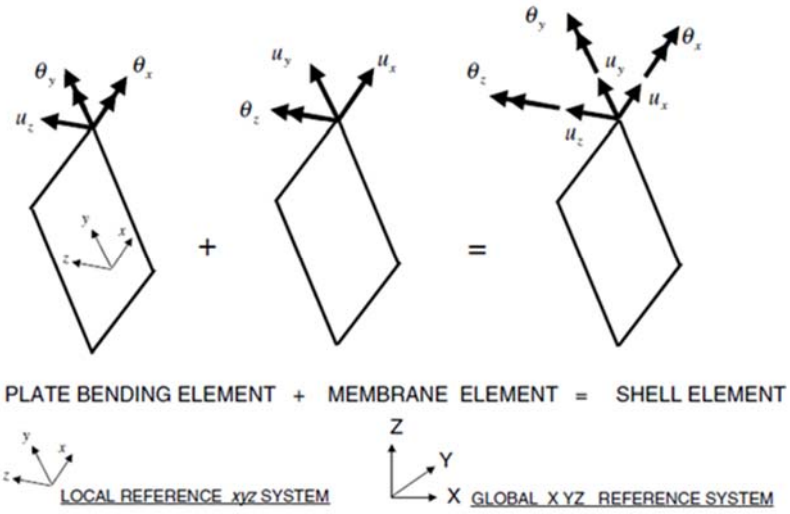

Figure 2.12: Plate bending element, membrane element and shell element degrees of freedom

ii) The layered shell allows any number of layers to be defined in the thickness direction, each with an independent location, thickness, behaviour, and material (Figure 2.13). Material behaviour may be nonlinear in each single layer. Out-of-plane displacements are quadratic and are consistent with the in-plane displacements. The layered shell usually represents full-shell behaviour, although this can be controlled on a layer-by-layer basis.

The shell element is made up of many layers with different thickness and different material properties are assigned to various layers. This means that the rebars are smeared into one layer or more in either direction. During the finite element calculation, the axial strain and curvature of the middle layer can be obtained in one element. Then according to the assumption that plane section remains plane, the strains and the curvatures of the other layers can be calculated.

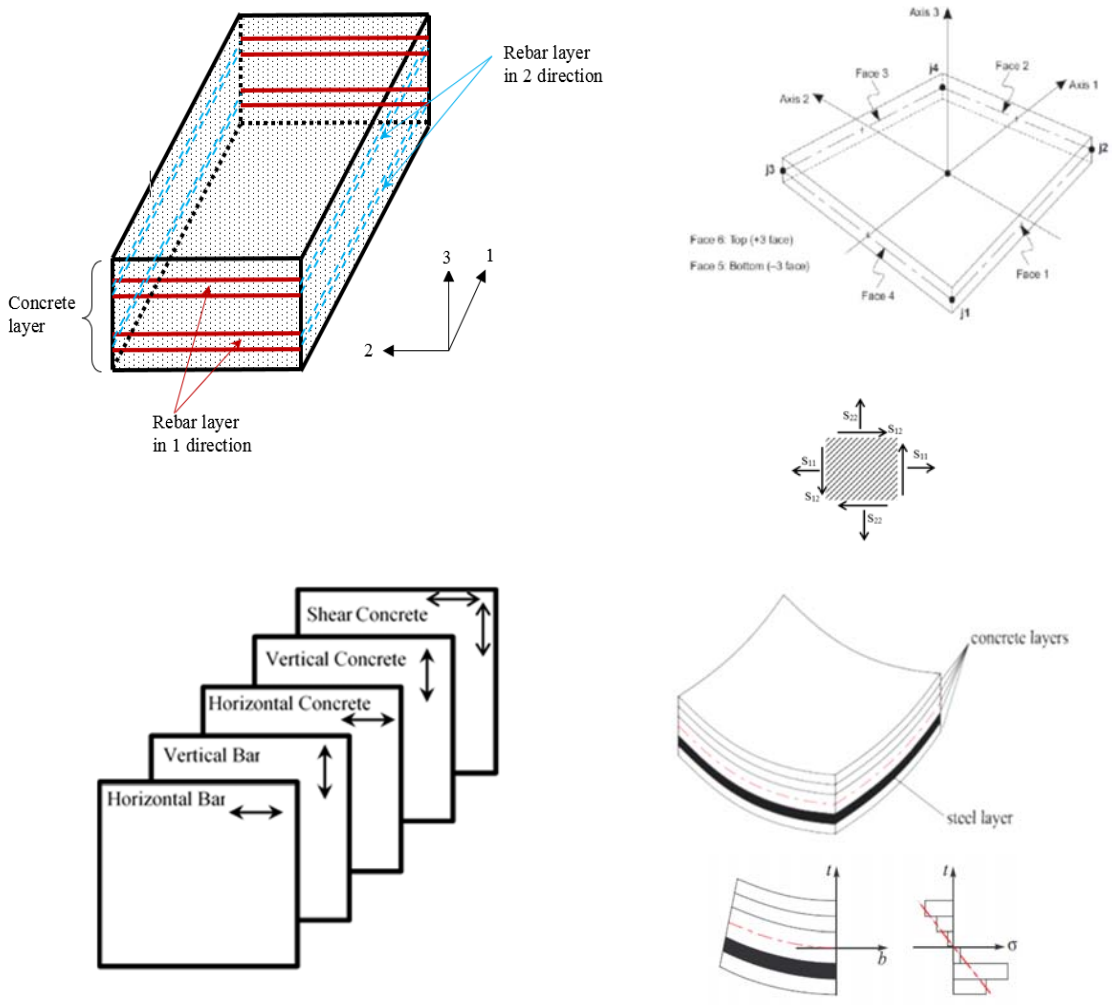

Figure 2.13: a) Multi-layer shell element b) A four node shell element and in plane stress

Then, the corresponding stress will be calculated through the constitutive relations of the material assigned to the layer. From the above principles, it is seen that the structural performance of the shear wall can be directly connected with the material constitutive law. Material behaviour is integrated (sampled) at a finite number of points in the thickness direction

of each layer. We may choose one to five points for each layer. The location of these points fallows standard Gauss integration procedures. Nonlinear behaviour may require more integration points or more layers in order to capture yielding near the top and bottom surfaces. Using an excessive number of integration points can increase the analysis time. We may need to experiment to find a balance between accuracy and computational efficiency. Force deformation behaviour is computed by integrating the stress-strain behaviour through the thickness and over the surface plane of the element. We can specify the number of integration points in the thickness direction of each layer as described above.

For each of these layers in the thickness direction, integration in the plane is performed at the standard 2×2 Gauss points (coordinates ± 0.577 on a square of size ± 1.0). Nonlinear behaviour is sampled only at these points. This is equivalent to having two fibres, located approximately at the 1/4 and 3/4 points, in each of the local 1 and 2 (on the surface) directions. Plotted or tabulated stresses at locations other than the four Gauss points are interpolated or extrapolated, and do not necessarily represent the sampled nonlinear stresses. For this reason, stresses at the joints may sometimes appear to exceed failure stresses. Layers are kinematically connected by the Mindlin/Reissner assumption that normal to the reference surfaces remain straight after deformation. This is the shell equivalent to the beam as it is assumed that plane sections remain plane in each single element of meshed area.

Hence, multi-layer shell elements may take the in-plane bending, in-plane shear and out-of-plane bending actions coupling together in RC shear wall components into account. Thus, it may reflect the main mechanical characteristics of RC shear walls fully.

Nonlinearity of RC shear walls is commonly reproduced indirectly by employing equivalent wide column analogy in practical applications. The significant shortcoming of this model is that it is unable to reproduce the effect of neutral axis migration explicitly in the model. Hence,

it cannot include 3D spatial effect of the whole system in inelastic range. The realistic neutral axis migration capability of the analytical model makes possible to evaluate the effect of wall edge upward (or downward) movement on beams or slabs connected to walls in each story. In that, yielding of reinforcement at the base of wall tends to move the extreme tension edge of the wall upward.

While yielding of beams and columns in a frame causes nonlinear shear type deformation in each storey (inter-storey drift), yielding at the base of structural walls cause not only horizontal displacement but also vertical displacement along the wall (say it vertical yielding). The framing interaction between walls and adjacent elements can highly affect the response of the overall building. Thus, one can adopt fiber shell elements to investigate the effect of wall edge upward or downward movement when reinforcing bars in RC walls yielded. This element is more realistic, reasonable and easier to simulate the nonlinear mechanical characteristics of RC shear walls. Multi-layer shell elements simulate the nonlinear behavior of RC shear walls by material constitutive models of concrete and rebar directly. Thus, the material constitutive models of concrete and reinforced are critical in appropriate evaluation of wall elements in a building. Therefore, careful attention should be paid to employ reliable constitute laws for rebars and concrete in structural walls to reproduce the more realistic behavior in each layer.

Unlike what is common in practice to simplify the analytical modelling of beam, columns, walls and connections (joints) by offering individual springs in each degree of freedom to simulate the nonlinear cyclic response, material based elements such as fiber sections or multilayer shell elements require careful attention in material models to do cyclic nonlinear analysis. This chapter seeks to demonstrate the capability of a commercially available software (SAP2000) in the modelling of structural walls.

2.4.1.1 Vertical and Horizontal Concrete Layers

The compressive backbone curve for concrete in both vertical and horizontal directions is based on the proposed model by Mander et al. (1988) for confined and confined concrete. The default ultimate strain capacity in confined concrete is estimated based on equality of area between confined and unconfined concrete stress strain curves to the area under the confinement steel stress-strain curve through iteration process in the program. However, one can calculate the confinement of section and ultimate strain capacity of concrete by other methods or packages available in the literature (for example Xtract, COMBIA) and it can be used in the program.

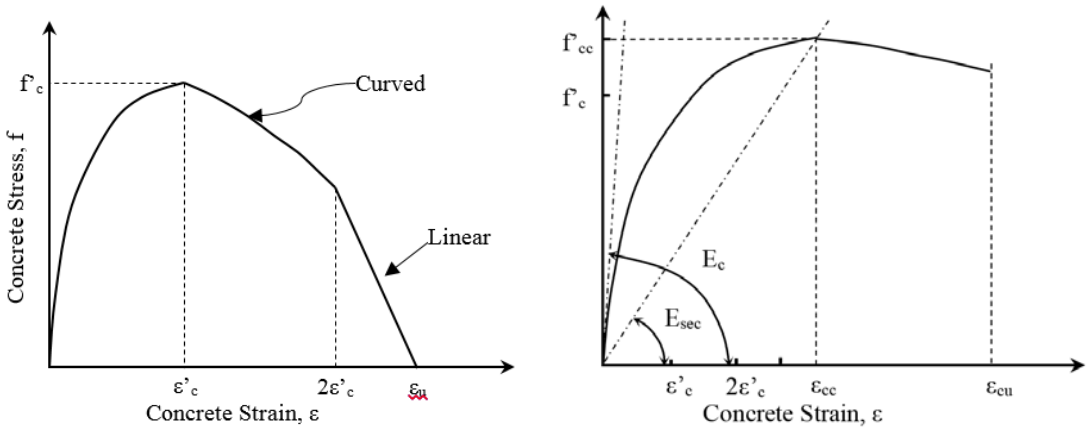

Figure 2.14: Unconfined and confined concrete layer stress-strain curve (Mander et al., 1988)

The effect of tensile strength of concrete neglected in axial and flexural layers since the contribution of the tensile strength of concrete is very small in the ultimate flexural strength of elements. However, effect of tension stiffening (mainly because in cracked RC, the concrete material between cracks in vertical concrete layers are intact and they can carry some average stress due to a bond with the embedded reinforcement) is implicitly included in the model by modifying the bare rebar specification to a new material as an embedded rebar in cracked concrete (Figure 2.15).

2.4.1.2 Horizontal and vertical reinforcement rebar layers

The embedded bar in concrete has lower average yield strength compared with the yield stress of a bare rebar. Belarbi and Hsu (1994) examined some RC panels to propose a simplified equation to estimate the embedded bar specification based on a known bare rebar specification for a given reinforcement steel ratio and concrete stress-strain curve in tension (Figure 2.15). Although the cyclic behavior of embedded rebar in the proposed model is very sophisticated to precisely capture the physical response of RC panels, the simple Takeda rule is adopted here for the cyclic behavior of embedded rebar in concrete. Available hysteresis rules available at the material level are very limited in the software employed in the analysis. Experimental study of the structural walls under cyclic loads has confirmed that opening and closing of the horizontal and/or vertical cracks cause reduction of the stiffness in each cycle of applied loading. Simulation of experimental tests by the proposed numerical technic demonstrated that modifying the bare rebar properties according to the above procedure and adopting the Takeda formulation for the hysteresis (path dependent) rule can reproduce the cyclic response of specimens reasonably well (Belarbi and Hsu, (1994)).

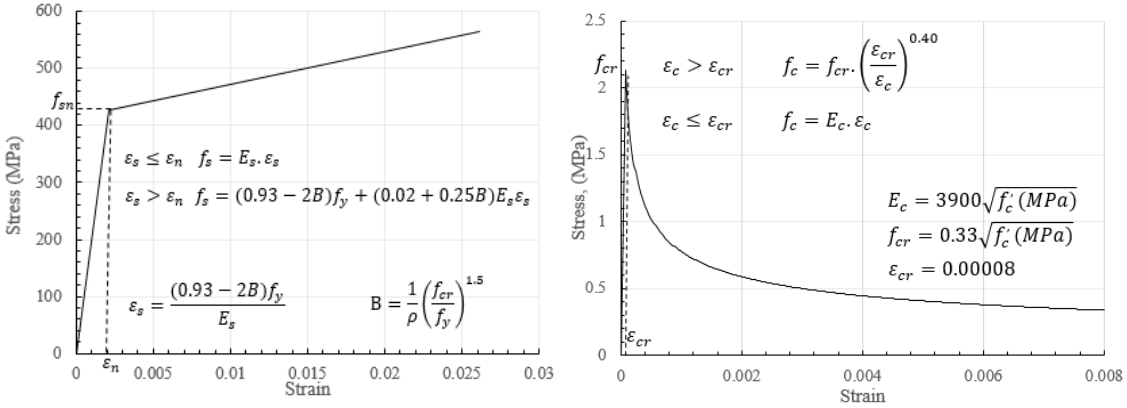

(a) (b)

Figure 2.15: a) Average tensile stress strain relation for rebar embedded in concrete (Belarbi and Hsu, 1994) b) Average stress strain relation for concrete in tension (Belarbi and Hsu, 1994)

2.4.1.3 Shear Layer

The precise finite element modelling of the shear transfer mechanism in reinforced concrete panels is very complex. Extensive research has been done to capture the behavior of concrete, and the steel bars inside concrete. The main characteristic of concrete is the formation of cracks, when it experiences different states of stress. This characteristic makes it difficult to develop rational constitutive material models for cracked reinforced concrete because the formation of cracks produces a new orthogonal material, which causes redistribution of stresses and changes its stiffness. Furthermore, the nonlinear behavior of concrete (mainly in shear wall structures) not only depends on the stress (tension or compression) in the direction of loading but also on the stresses in other directions (multi-axial effects). Stiffness and strength of concrete also deteriorate by unloading and reloading in cyclic loadings. The modelling of reinforced concrete in biaxial stress state has been under investigation for a long time. Mainly, two different research groups, one from the University of Toronto (Modified Compression Field Theory) and the other from the University of Houston (Softened Truss Model), have been constantly conducting analytical and experimental studies to develop the reinforced concrete constitutive models.

In an actual wall, especially in a "squat" wall, there can be substantial coupling between axial-bending and shear. In particular, the shear strength of a wall may depend substantially on the axial forces and bending moments. The employed multi-layered shell element adopts the modified Darwin and Darwin and Pecknold (1974) reinforced concrete material model, a two-dimensional concrete material model that can explicitly account for the interaction between bending and shear strength in shear wall structures. It considers cracking and crushing of concrete, and when it is combined with a steel material it considers yielding of the reinforcement. Compressive strength reduction based on perpendicular tensile strain is accounted for as described in Vecchio and Collins (1986) but the effect of biaxial compression

stresses on the compression strength of the concrete (i.e. confinement) is not accounted for in this model. Hence, the effect of confinement are calculated separately and the calculated stress strain curve of confined concrete was introduced to the program by definition of separate layers in the confined zone. Figure 2.16 (a) shows a wall element, and the stresses at a point in the wall. The initial material axes are fixed relative to the wall element. In general, there can be normal and shear stresses in these axes, as shown in Figure 2.16 (b). There are also principal material axes, as shown in Figure 2.16 (c). Note that although the shear stress is zero in the principal material axes, the shear modulus is not zero. Hence, when a strain increment is applied, the change in shear stress generally will not be zero. During an analysis, the principal stress directions, and hence the principal material axes, can rotate progressively.

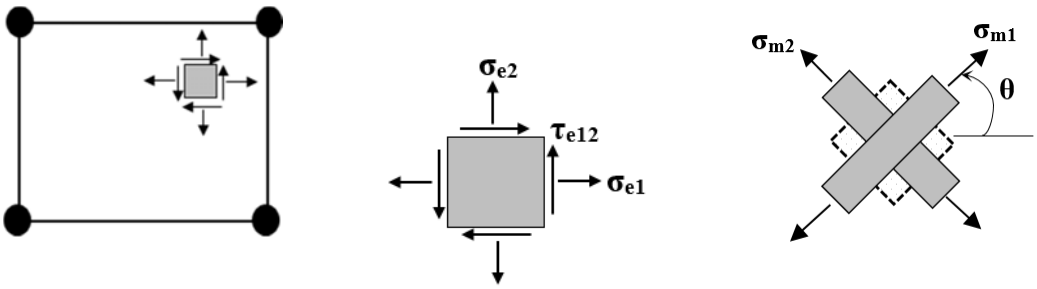

(a) Wall finite element, Stress at a point

(b) Element axes

(c) Material axes

Figure 2.16: Initial and principal material axes

2.4.1.4 Initial Elastic Stress-Strain Relationship and Yield Surface for Biaxial Stress

If a material has not yet yielded or cracked, it has a linear elastic relationship with the initial value of Young's modulus, as shown below:

$$\begin{Bmatrix} d\sigma_1 \\ d\sigma_2 \\ d\tau_{12} \end{Bmatrix} = \frac{1}{1-\nu^2} \begin{bmatrix} \mathrm{E}_0 & \nu\mathrm{E}_0 & 0 \\ \nu\mathrm{E}_0 & \mathrm{E}_0 & 0 \\ 0 & 0 & \mathrm{E}_0 \frac{1-\nu}{2} \end{bmatrix} \begin{Bmatrix} d\varepsilon_1 \\ d\varepsilon_2 \\ d\gamma_{12} \end{Bmatrix} \quad (2.2)$$

where:

$d\sigma_1$ *and* $d\varepsilon_1$:incremental linear change in stress/strain in prinicpal stress direction 1

$d\sigma_2$ and $d\varepsilon_2$: incremental linear change in stress/strain in prinicpal stress direction 2

$d\tau_{12}$ and $d\gamma_1$: incremental linear change in shear stress/strain in prinicpal stress axes

E_0: stress dependent material property (material modulus)

ν: poisson's ratio

This equation is independent of the stress and strain directions, and hence it applies in both the initial and principal material axes.

2.4.1.5 Post-yield or Cracked Material Behavior

After yield or cracking, the material modulus changes and the Poisson's ratio is neglected. In general, the stresses, strains and moduli will be different along the two principal directions. Equation 2.2 can be modified for the material nonlinearity as follows:

$$\begin{Bmatrix} d\sigma_{m1} \\ d\sigma_{m2} \\ d\tau_{m12} \end{Bmatrix} = \frac{1}{1-\nu^2} \begin{bmatrix} \mathrm{E}_1 & \nu\sqrt{\mathrm{E}_1\mathrm{E}_2} & 0 \\ \nu\sqrt{\mathrm{E}_1\mathrm{E}_2} & \mathrm{E}_2 & 0 \\ 0 & 0 & \mathrm{G}_m \end{bmatrix} \begin{Bmatrix} d\varepsilon_{m1} \\ d\varepsilon_{m2} \\ d\gamma_{m12} \end{Bmatrix} \tag{2.3}$$

where :

$d\sigma_{m1}$ and $d\varepsilon_{m1}$:incremental linear change in stress/strain in material axis 1 (coincsides with the current principal stress direction 1)

$d\sigma_{m2}$ and $d\varepsilon_{m2}$: incremental linear change in stress/strain in material axis 2 (coincsides with the current principal stress direction 2)

$d\tau_{m12}$ and $d\gamma_{m1}$: incremental linear change in shear stress/strain in material axes (coincsides with the current principal stress axes)

E_1 and E_2 : stress dependent material properties (material modulus) in materail axes (coinside with the current principal stress directions)

ν: poisson's ratio

The shear modulus in the principle material axes, is specified to maintain coaxiality between the principal stresses and strains. Hence, the shear stiffness is not related to shear strain directly. The corresponding relationship in the initial material axes is obtained by applying the rotation between the initial and principal material axes, θ, as shown in Figure 2.16 (c). A detailed description of the model can be found in Darwin and Pecknold (1974).

2.4.1.6 Strength Reduction under Perpendicular Tensile Strain

When concrete is subjected to shear stresses, it often cracks in one direction and is in compression in the other direction. Failure in shear may occur when the concrete crushes in compression. Vecchio and Collins (1986) showed that the compression strength of concrete depends on the magnitude of the tensile strain in the perpendicular direction. The effective compression strength of concrete in such situations can be substantially smaller than the original f'_c. Figure 2.17 shows the relationship between the compression strength and perpendicular tensile strain developed in Vecchio and Collins (1986), which is implemented in material model, adopted for this research.

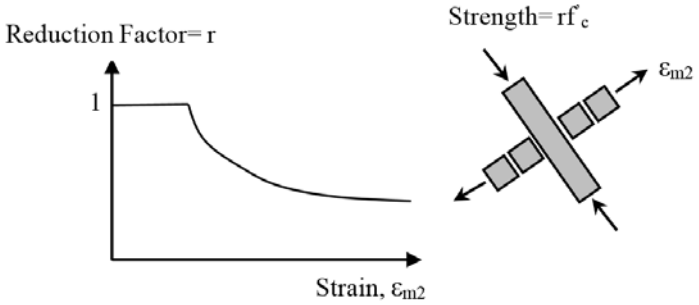

Figure 2.17: Reduction in compression strength due to tensile strain in the perpendicular direction

The following equation from Vecchio and Collins (1986) is used for the compression strength reduction factor r:

$$r = \frac{1}{0.8 - 0.34\frac{\varepsilon_{m2}}{\varepsilon'_c}} \leq 1 \qquad (2.4)$$

where ε_{m2} is the instantaneous tension strain (positive) in the perpendicular direction and ε_c' is the specified uniaxial crushing strain in compression (negative). Hence, the uniaxial stress-strain relationship of concrete in compression is modified as indicated. However, the moduli of uniaxial concrete do not change when the strength of concrete is modified.

2.5 Verification and Validation of the Mathematical Model of Multi-storey Shear Wall Building

To evaluate the credibility of the multilayered shell element in reproducing the behavior of structural walls under the combined actions, two types of experimental specimens are employed. The first series of tests include the experimental specimens subjected to static loads. At the second stage, the results of a shake table test conducted on a full-scale multi-storey shear wall building (including floor slabs and columns) are used to verify the finite element analysis.

2.5.1 Monotonic and Cyclic Laboratory Static Tests

Results of seven experimental tests are employed to validate the proposed finite element approach for the numerical modelling of walls using multi-layered shell elements. These test units include specimens which dominantly failed in compression zone at the base section of structural the tested walls due to a combination of axial, bending and shear actions. While specimens WSH3, WSH4, and RW2 failed in flexural mode accompanied by concrete crushing and/or rebar buckling, specimens SW11, SW12, SW22, and SW23 failed in compression zone under in a combination of shear and axial compression modes. It should be noted that we only seek to verify the capability of the numerical model to reproduce the overall shape of the force displacement curve under the monotonic and cyclic loads. While four specimens (SW11, SW12, SW22 and SW23) were tested under monotonic loads, specimens WSH3, WSH4 and RW1 were subjected to cyclic displacement reversals.

2.5.1.1 Specification of Specimens

Table 2-2 shows the main specification and properties of all seven test specimens used for the verification reported herein. The specimens SW11 and SW12 (Lefas et al. 1990) are the squat walls (aspect ratio of 1) having similar cross sections but different amount of axial forces. Experimental observation demonstrated that a significant shear cracking occurred during the loading process before the failure of these specimens in shear compression mode. On the other hand, specimens SW22 and SW23 (Lefas et al. 1990) are flexural type shear walls (aspect ratio of 2) which developed extensive flexural cracking before final failure in compression shear mode specimens. SW22 and SW23 had the same cross section but the applied axial forces were equal to 0.1fcAg and 0.2fcAg, respectively. Hence, the higher axial force plus the moment induced axial force had a more pronounced effect on the final failure mechanism than in the latter specimen. Due to space limitation, no further explanation is presented here about the behaviour of these specimens and the reader can refer to the original research papers. It should be mention that the top four specimens were tested under monotonic loading.

The test unit WSH3 (Dazio et al. 2009) represented a ductile wall in terms of the reinforcement amount properties, and detailing. The longitudinal reinforcement layout and the ductility properties of the reinforcing bars of the two test units were very similar but unlike WSH3, WSH4 (Dazio et al. 2009) had no confining or stabilizing reinforcement and it was not specifically designed for a ductile behavior. Failure mechanism of both specimens was due to the bending induced actions near the wall boundary zones. While the specimen WSH3 failed due to the reinforcement rebar fracture and buckling of previously yielded reinforcement rebar in tension, WSH4 failed by crushing of the unconfined concrete in the compression zone.

The specimen RW1 (Thomsen and Wallace, 1995) was tested under reversed cyclic lateral loading with increasing displacement amplitudes. The specimen RW1 failed in flexural mode

accompanied by rebar buckling, which cannot be captured by the adopted numerical model because bar buckling effect is not included in the material models.

It is worth mentioning that this chapter mainly seeks to represent the overall ability of the numerical model to recover the general shape of the test results that is, the initial secant stiffness to the first yield and the ultimate (peak) strength. Moreover, the ultimate displacement predicted by the numerical model is also compared to the experimental values (failure point as defined in the original research paper) for demonstration and validation of the numerical model.

Table 2-2: Specification and reinforcement of the wall specimens used for verification

Specimen	L_w	H_w	t_w	b_w	ρ_{ver}	ρ_{hor}	ρ_{flex}	f_{yver}	f_{yhor}	P_{axial}
SW11 (Lefas et al. 1990)	750	750	70	140	2.4%	1.1%	3.1%	470	520	0
SW12 (Lefas et al. 1990)	750	750	70	140	2.4%	1.1%	3.1%	470	520	0.10 f_cA_g
SW22 (Lefas et al. 1990)	650	1300	65	140	2.5%	0.8%	3.3%	470	520	0.10 f_cA_g
SW23 (Lefas et al. 1990)	650	1300	65	140	2.5%	0.8%	3.3%	470	520	0.20 f_cA_g
WSH3 (Dazio et al. 2009) (with confinement)	2000	4560	150	150	0.54%	0.25%	1.54%	601 (569.2)	489	0.058 f_cA_g
WSH4 (Dazio et al. 2009) (without confinement)	2000	4560	150	150	0.54%	0.25%	1.54%	576 (584)	519	0.057 f_cA_g
RW1(Thamsen and Wallace 1995)	1219	3658	102	172	1.12%	0.33%	2.9%	414	448	0.10 f_cA_g

*All dimension in N, mm, MPa

Numerical models of all specimens with the appropriate boundary conditions were built in the finite element package and the monotonic and cyclic displacement (similar to those applied in the tests) were applied to conduct the static nonlinear analysis. It needs to be highlighted that a robust and detailed physical modelling of the specimens using sophisticated finite element packages especially developed for the numerical modelling of cracked reinforced concrete panel elements is very complicated. These packages can include the effect of cracking, damage evolution, softening of compression concrete struts under variable perpendicular concrete tensile strains, tension stiffening and softening of concrete explicitly. Most of these finite

element packages adopt the fundamental notions such as MCFT (Modified Compression Field Theory), SCTM (Softened Concrete Truss Model) or concrete damage plasticity models.

Table 2-3 presents the modified reinforcement properties of the specimens according to Belarbi and Hsu (1994). The embedded reinforcement has a different yield strength and yield strain in tension as explained in the previous section. The compression strength of concrete also shown in this table. Mathematical definition of the stress-strain curves for the materials follows the rules described in the preceding sections.

Table 2-3: Embedded reinforcement properties and concrete strength of specimens

Specimen	Bare bar	f_y	f'_y(embedded rebar in tension)	ε_y	ε'_y(embedded rebar in tension)	f'_c
SW11(Lefas et al. 1990)	8mm	470	427.8	2.35e-3	2.139e-3	52.3(0.9)**
	6mm	520	472.2	2.6e-3	2.3618e-3	
SW12(Lefas et al. 1990)	8mm	470	427.7	2.35e-3	2.138e-3	53.6(0.9)**
	6mm	520	472.0	2.6e-3	2.360e-3	
SW22(Lefas et al. 1990)	8mm	470	428.6	2.35e-3	2.143e-3	50.6(0.9)**
	6mm	520	472.9	2.60e-3	2.365e-3	
SW23(Lefas et al. 1990)	8mm	470	429.0	2.35e-3	2.145e-3	47.8(0.9)**
	6mm	520	473.4	2.60e-3	2.367e-3	
WSH3 (Dazio et al. 2009) (with confinement)	12mm	601	544.6	3.0e-3	2.72e-3	39.2
	8mm	569.2	487.4	2.85e-3	2.44e-3	
WSH4 (Dazio et al. 2009) (without confinement)	12mm	576	520.6	2.88e-3	2.60e-3	40.9
	8mm	583.7	500.0	2.9e-3	2.50e-3	
RW1(Thomsen and Wallace 1995)	No.3	414	377.0	2.07e-3	1.886e-3	32.8
	No.2	448	330.0	2.24e-3	1.65e-3	

*All dimension in N, mm, MPa
** Cubic strength to cylindrical strength

2.5.1.2 Verification of Results

The aim of this study is not to display the capability of the numerical model in simulating the evolution of cracks during the loading, failure mechanism or the value of failure displacement (or point of significant strength degradation in the force displacement curve) of the analysed specimens. Moreover, the available approach to solve the numerical equations in the analysis

platform was not able to easily converge in some cases. The numerical convergence problem mostly would occur when the vertical concrete layer strongly interacted (coupled) with the shear layer. The degree of interaction (coupling) between the concrete layers could be more critical when the high shear force demand combined with direct or indirect axial forces was applied to the confined boundary zone of the structural walls. It is worthy to mention that rebar buckling (one of the failures in the flexural mode) is a complicated phenomenon which could not be considered in this model explicitly.

The force displacement curves obtained by the numerical analysis are compared to the experimental force displacement curves in Figure 2.18 to Figure 2.21. Moreover, the von Mises stresses of the concrete layer at the final step of analysis are also presented in these figures. The predicted values agreed reasonably well with the experimental results.

Although, one can employ this numerical approach to determine the failure displacement capacity of multi-storey shear wall buildings approximately (most of the cases, the numerical prediction is quite conservative), Tables 10.19 and 10.20 in ASCE/SEI41-06 (which were produced by the averaging the results of experimental tests) can be adapted to verify the reliability of failure displacements predicted by the numerical analysis. This approach is required when one needs to assess or design a structural wall based on its displacement capacity.

Comparisons between the experimental results and the numerically predicted values of peak strength, the displacement at which the reinforcement rebar yielded in tension and the failure displacement are reported in Table 2-4.

The measured and calculated peak strength of different specimens are shown in Table 2-4. The differences could be acceptable for practical application, especially when an axial force on a wall is not very high. It is evident that the peak strength is under predicted in most specimens.

Although the initial stiffness of all specimens indicated a good agreement with the experimental results, a significant difference was observed between the post cracking stiffness of the models and experimental results.

Table 2-4: Prediction of model versus test results

Specimens	Peak strength			Yield displacement			Ultimate displacement		
	Test	Model	Difference	Test	Model	Difference	Test	Model	Difference
SW11	254.51	235.0	-7.6	3.59	2.78	-22.5	8.6	10.0	+16.28
SW12	330.51	280.7	-15	2.90	3.16	+8.9	9.6	6.6	-31.25
SW22	151.14	126.4	-16.3	4.91	6.0	+22.1	15.97	9.6	-39.89
SW23	180.7	129.2	-28.5	5.20	6.82	+31.0	14.2	8.50	-40.14
WSH3	450.0	394.0	-12.4	11.3	14.25	+26.0	92.0	109.2	+18.70
WSH4	440.0	432.13	-1.8	11.4	12.1	+6.1	72.0	77.0	+6.94
RW1	147.6	165.1	+11.8	12.60	12.0	-5.0	92.0	110	+19.57

*Units: kN, mm
*Yield displacement when first bars in boundary yielded in the positive direction
*Difference in percent

Figure 2.18 demonstrates the numerical and experimental force displacement responses of specimens SW11 and SW12. The von Mises stress of concrete layers are also presented in this figure.

The results show that the numerical model could not reproduce the evolution of stiffness in specimen SW11 very well. However, the model could capture the peak strength and the failure displacement with reasonable accuracy in this specimen. The shear stiffness of this test unit (zero axial force) governs the response and extensive shear cracking occurred during the loading. It seems that the numerical model could not simulate the degradation of shear stiffness with the evolution of shear cracking properly. Unlike the specimen SW11, imposing the axial force on specimen SW12 reduced the extent of shear cracking and the slope of the numerical curve follows the experimental curve reasonably well. However, the prediction of peak strength

and the failure displacements is under predicted 15% and 31.25% respectively compared to the specimen SW11 (corresponding values of 7.6% and 16.28% for specimen SW11).

The specimens SW22 and SW23 both acted predominantly in a flexural manner with extensive flexural cracks during the loading. These test units both failed in high concrete compression strain under the monotonic horizontal loads in the experimental program. The axial force on SW22 is two times larger than SW23 ($0.1f_cA_g$ compared to $0.2f_cA_g$). The numerical results show that the prediction of yield displacement and secant stiffness to the first yield are reasonable in both cases. However, the model under predicts the peak strength in specimen SW23 by 28.5%. The ultimate strength prediction in SW22 is more precise than specimen SW23, which has twice more axial force than SW22. Failure displacement in both cases is under predicted by approximately 40 percent. It is worth mentioning that no additional effort was made to find the best match between the numerical models and experimental results by using different material models for the concrete or manipulating the post-peak slope of the concrete material models.

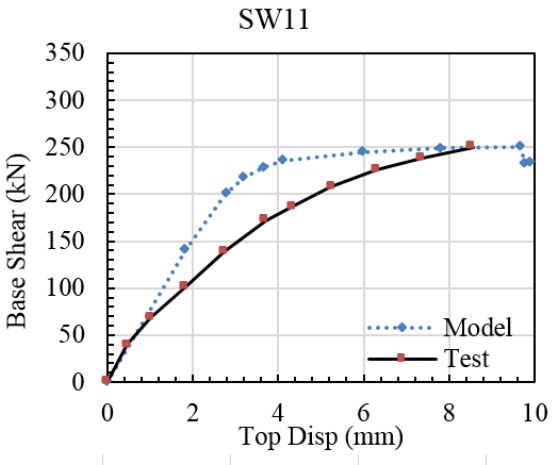

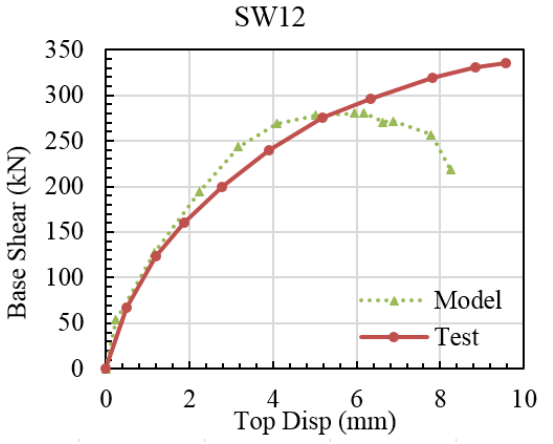

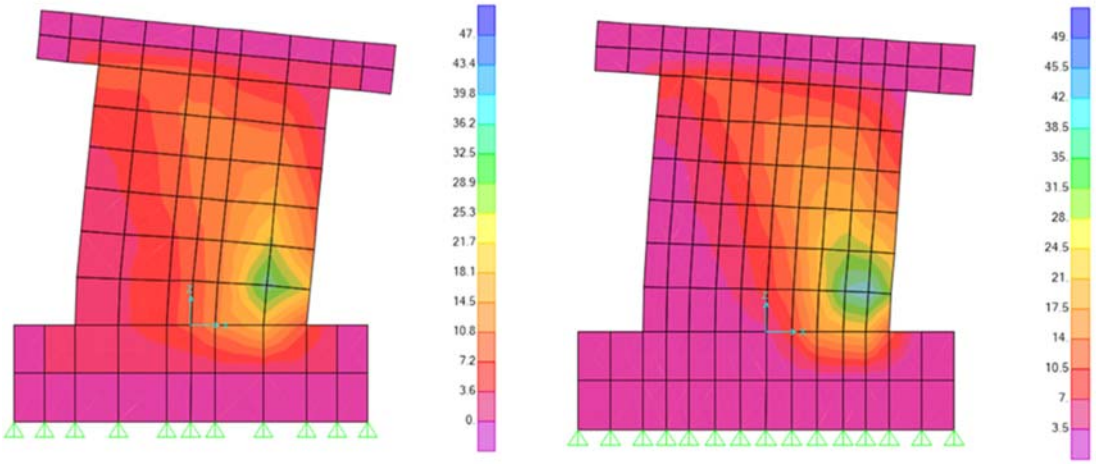

(a) (b)

Figure 2.18: (a) Force versus displacement for SW11 and von Mises stress (b) Force versus displacement for SW12 and von Mises stress

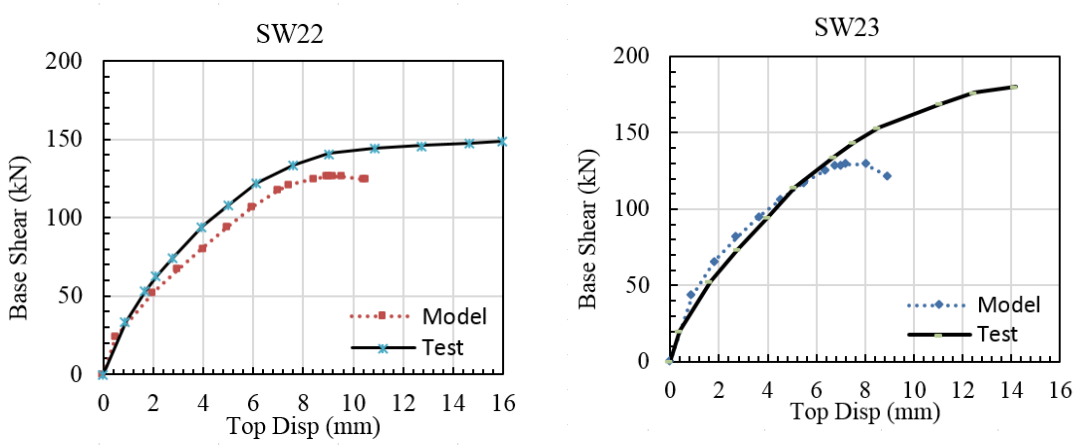

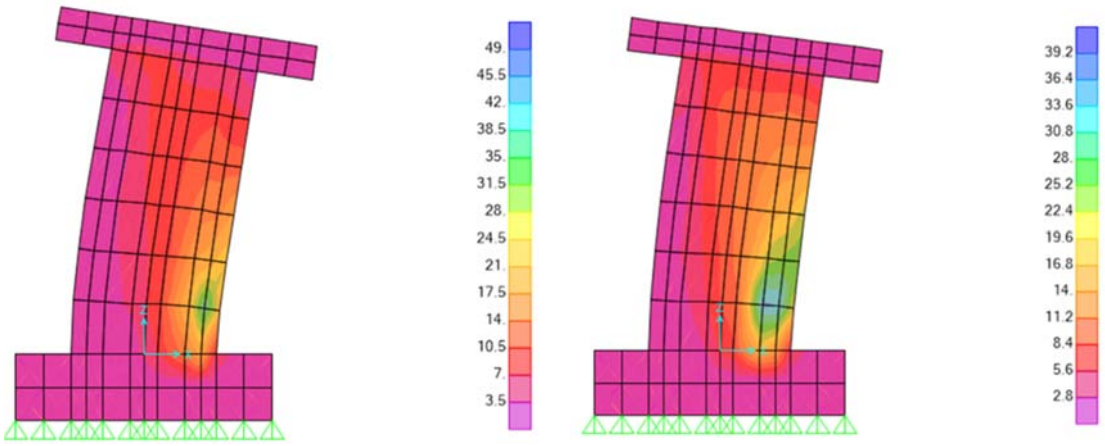

(a) (b)

Figure 2.19: (a) Force versus displacement for SW22 and von Mises stress (b) Force versus displacement for SW23 and von Mises stress

Three additional specimens were used to verify the ability of the model in simulating force displacement curve of structural walls under static cyclic loads. Figure 2.20 shows the results obtained for the specimens WSH3 and WSH4. It is evident that the numerical force displacement curve does not match with experimental results precisely. However, considering the numerous uncertainty involved in seismic response of multi storey shear wall buildings, its application for the building analysis seems quite reasonable. Due to space limitation no further details are presented about the numerical results.

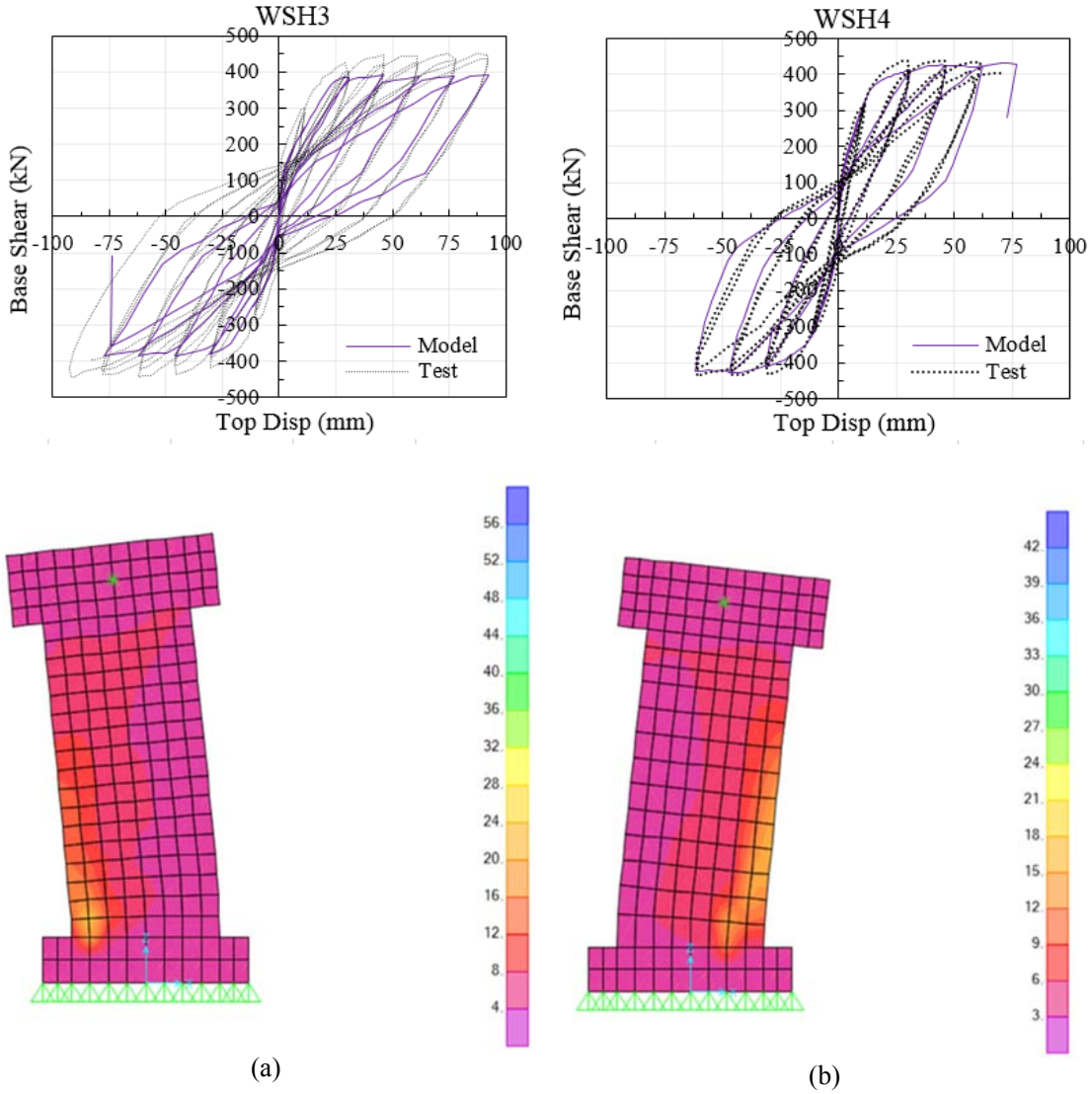

Figure 2.20: (a) Force versus displacement for WSH3 and von Mises stress (b) Force versus displacement for WSH4 and von Mises stress

Figure 2.21 shows the results of numerical simulation for specimen RW1. The employed model with simple material laws predicts the peak strength, and the yield and failure displacement of the specimen with reasonable accuracy.

In general, although the prediction of the failure displacements in specimens tested under the monotonic loading is lower than the experimental results, the employed model slightly overpredicts the failure displacement of specimens tested under cyclic loading.

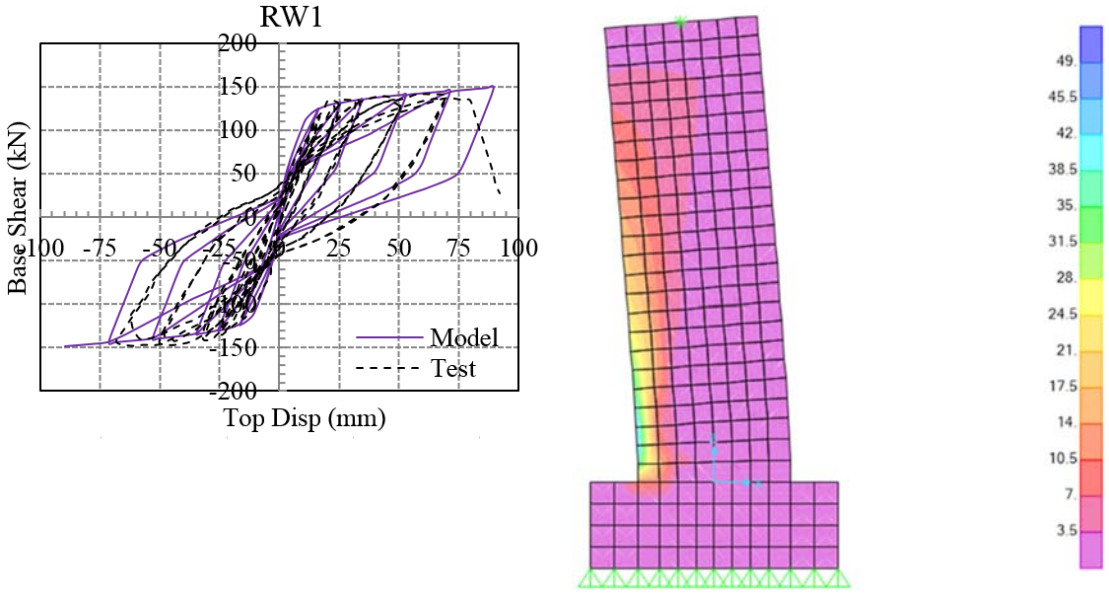

Figure 2.21 : Force versus displacement for RW1 and von Mises stress

In summary, the ability of the numerical model to reproduce the energy dissipation characteristic of structural walls due to material nonlinearity and the peak strength capacity appears reasonable/acceptable for practical purpose. It seems that for practical modelling of structural walls in a system (multi-storey shear wall), this approach could be considered as an alternative compared to more refined finite element analysis.

2.5.2 Shake Table Test

Accurate prediction of nonlinear response history of RC multi-storey shear wall buildings under ground motion excitations plays a critical role in performance based design method. Although numerical or analytical models of RC shear wall buildings can be useful for comparative studies, realistic and accurate prediction of response of RC shear wall buildings under the dynamic excitation remains a significant challenge within the earthquake engineering community. One of the promising methods to validate the numerical models is to use field data obtained from the response of instrumented or damaged real buildings. Unfortunately, this type of data currently is not available. Hence, only the results of shake table tests on a slice of multi-storey shear wall building was used for validation and verification process. This chapter outlines the validation and verification of multi-layered shell element and material constitute laws employed in the numerical simulation of multi-storey RC shear wall buildings.

The nonlinear response histories which were obtained from the mathematical model are compared with the results of experimental test data. The slice of the multi-storey shear wall was used to perform a shake table test in US. The building geometry, dimension, and reinforcement detailing are explained in detail in the following sections. The material specification and mass information used in this chapter are consistent with the data provided in the test report (Panagiotou, 2007). Some of the dynamic analysis input variables such as damping value and slab equivalent stiffness properties have also been calibrated based on the test results.

Different response measures (engineering demand parameters) have been presented in the experimental report. To the author's knowledge, the latest state of knowledge in earthquake engineering is not capable of predicting simultaneously all engineering demand parameters accurately enough. In other words, while some mathematical models can predict the

displacement response with enough accuracy, they are not able to predict the acceleration or residual responses with the same accuracy. Hence, in this chapter, only a number of specific engineering demand parameters are considered through the verification process.

Although the test specimen has been subjected to four different consecutive ground motion records with increasing amplitudes, the verification process has been conducted only based on the final results. The final test results were obtained once the previously cracked specimen was subjected to the final ground motion record. This ground motion (named EQ4 in the test report) record was representative of the design based earthquake (DBE) level representative of 500 year return period hazard in the specific site at Los Angeles. Hence, in the evaluation of errors involved in the numerical simulation results, the difference between cracked and un-cracked concrete should be taken into account.

The measured response of the test specimen was used to assess the capability of the mathematical model, which was built in SAP2000, to simulate the seismic response of RC shear walls. The experiment report provides full-scale shake table test data that can be used to validate the ability of the mathematical model to accurately simulate the specific engineering demand parameters.

2.5.2.1 Geometry and Specification of the Test Structure

Shake table tests were conducted on a full-scale 7-story slice of an RC structural wall building at UC San Diego in 2005. The building system was subjected to four uniaxial earthquake ground motions named EQ1, EQ2, EQ3, and EQ4. The peak acceleration amplitudes of the records ranged from 0.11g to 0.91 g. Details of the building construction have also been explained in detail in Panagiotou (2007). An overall view of the building structure is shown in Figure 2.22. This section only presents the summary of main input parameters necessary to conduct the nonlinear time history analysis.

The test structure is composed of two main perpendicular walls: the web wall and the flange wall linked with slotted slabs (Figure 2.22). A precast pier along with horizontal pin braces were provided to prevent the torsional movement. Gravity columns were also employed to support the floor slabs in the building. The building slice, which was designed using a displacement- based and capacity approach for a site in Los Angeles, resulted in design lateral forces that are significantly smaller than those currently specified in building codes used in the United States.

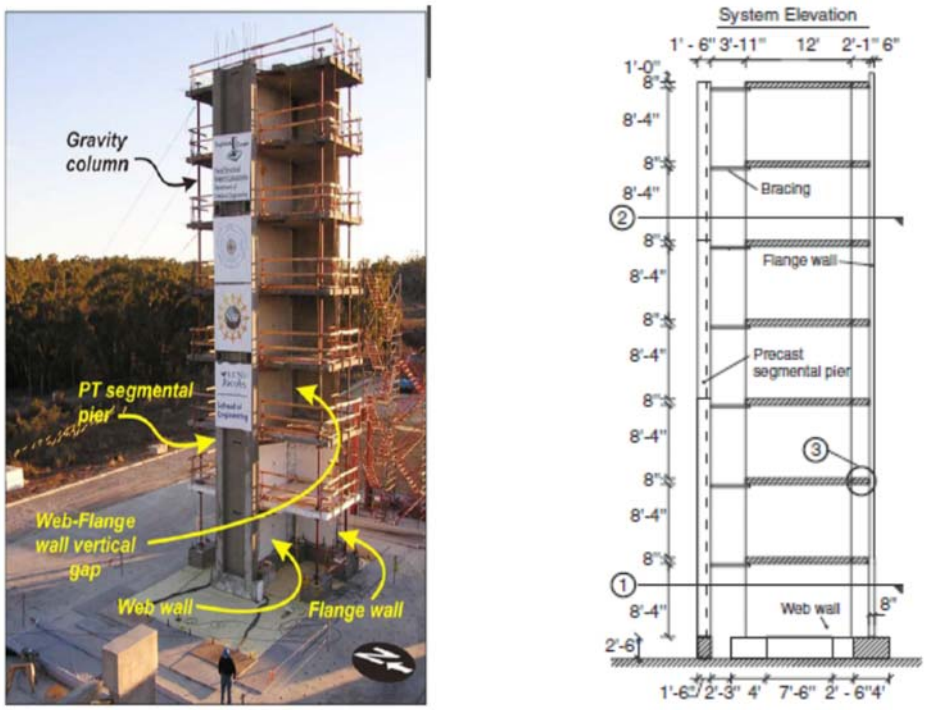

Figure 2.22: Building overall overview and geometry (Panagiotou et al., 2010)

Figure 2.22 illustrates the photo of the building slice, floor heights and wall length. The tested structural wall which is called the web wall has dimensions of 3657.6 mm length, 203.2 mm thicknesses in the first storey and 152.4 mm in the remaining above six stories. Each floor has an RC slab on each side of the web wall which was supported by a pair of pin ended gravity columns. The gravity columns were made of strong steel pipes and filled with high performance

grout. These columns were meant to resist some of the gravity load from the reinforced concrete floor slabs. They remained fully elastic during the experimental test.

Figure 2.23 shows the plan views at the building of the foundation and floor levels. The building slice (web wall including the floor slabs) was subjected to ground motions at the base in the West-East direction. The mathematical model excluded the modelling of base foundation and hence it neglected any probable flexibility due to foundation movement.

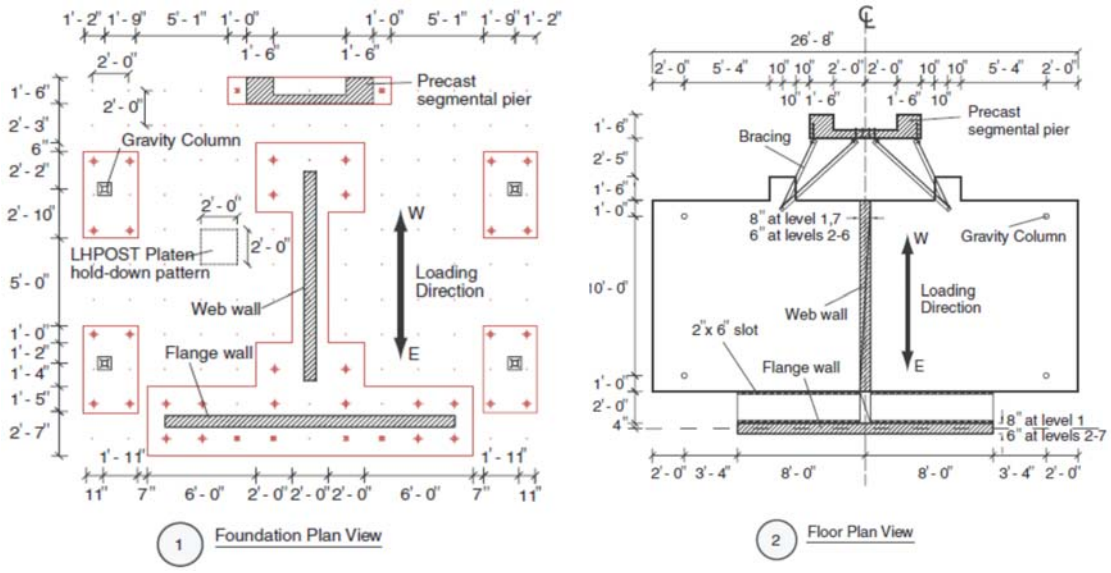

Figure 2.23: Plan view of prototype building slice (Martinelli and Filippou, 2009)

The horizontal movement of the web wall in North-South direction was suppressed by providing horizontal support in the North-South direction. The North-South horizontal movement or any corresponding torsional displacements were suppressed by the pair of horizontal pinned truss elements. These bracings were used to fix the web wall to the strong precast segment pier. The horizontal bracings only restricted the torsional movement of the web wall in the horizontal direction.

Figure 2.24 shows the reinforcement detailing of flooring slabs. Slabs have two layers of reinforcement in either direction. The connection between the floor slab and the wall was

expected to behave as a rigid connection. This detailing enabled the wall to slab connection to transfer the bending moment or torsional type actions to the structural walls. However, the estimation of realistic values of flexural or torsional stiffness of slabs is very complicated and it is still a significant challenge.

Figure 2.25 also shows the cross sectional view of the flooring slabs as well as the slotted slabs. Detail 3 in Figure 2.22 illustrates the location of the web wall to the flange wall connection through the linking slabs (slotted slabs). The slotted slabs were expected to transfer only the storey shear forces through their axial actions. However, it will be shown that the small moment capacity of the slotted slabs may induce additional vertical axial force in the web wall in the nonlinear state. These vertical axial forces may significantly change the system response (Panagiotou et al. 2010).

The moment capacity of the slotted slab connection on the either side (West and East) has been calculated by the moment curvature analysis. Hence, the slotted slab was modelled by a beam element with a lumped plastic hinges at their both ends. The moment rotation curves of the slotted slabs are presented in the following section.

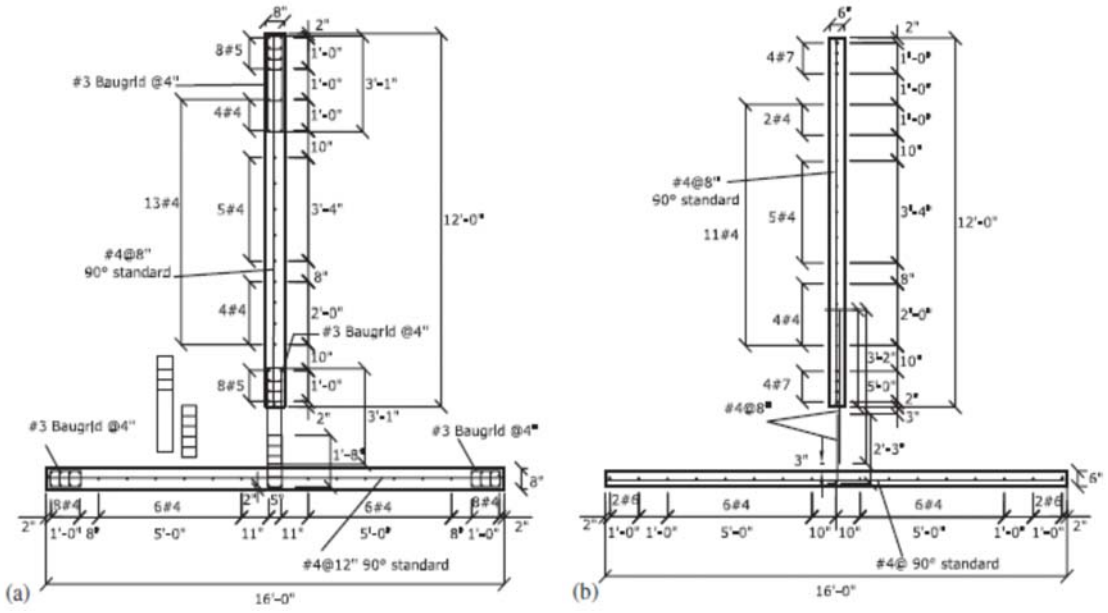

Figure 2.24: Reinforcement details of web wall a) first storey b) upper stories (Panagiotou et al., 2007)

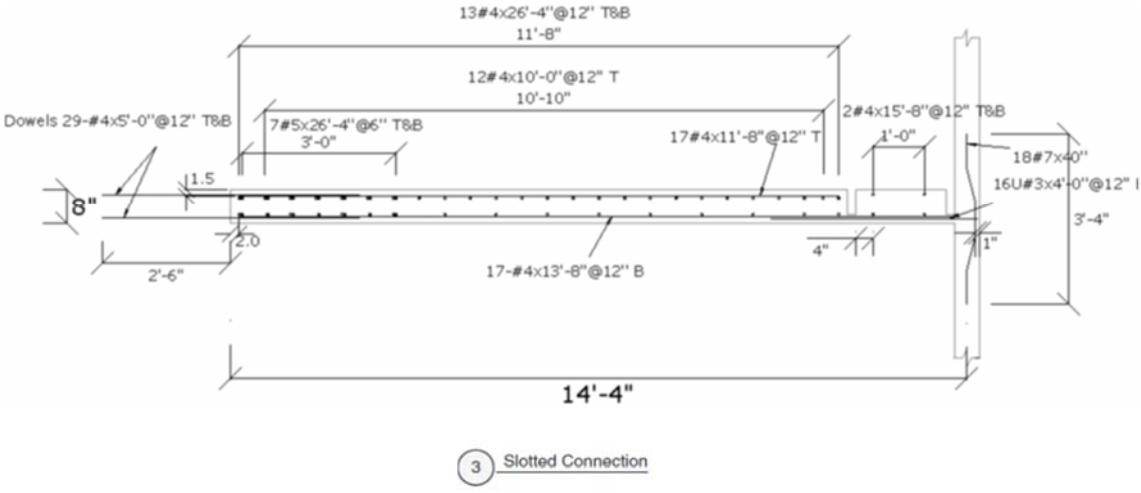

Figure 2.25: Reinforcement details of floor slabs and linking slabs (slotted slab) (Panagiotou et al., 2007)

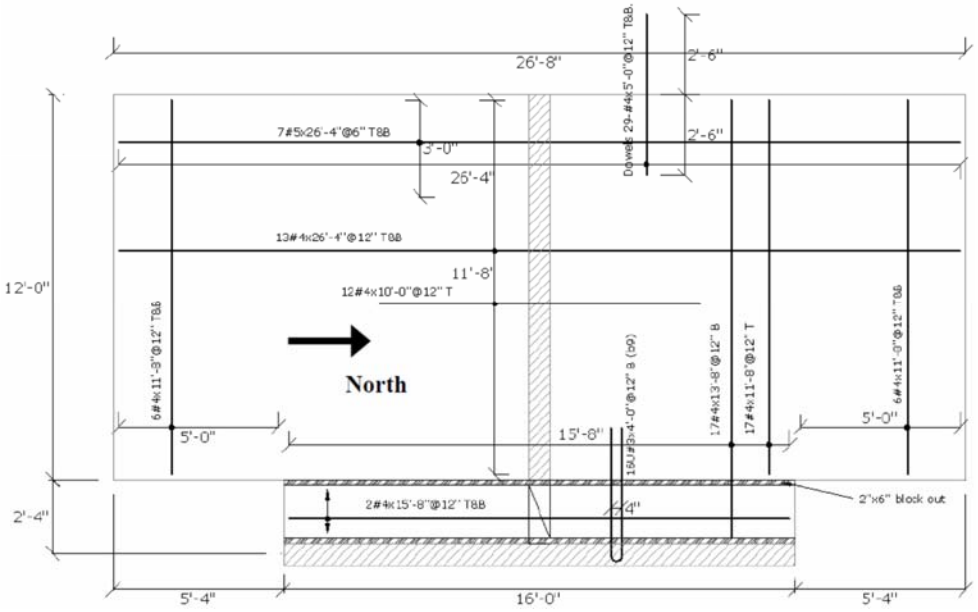

Figure 2.26: Reinforcement details of floor slabs and linking slabs (slotted slab) (Panagiotou et al., 2007) (Cont'd)

2.5.2.2 Input Accelerations and Response Spectra

As mentioned earlier, four ground motion records were applied to the building foundation in the East-West direction. The final ground motion record time series (named EQ4) and its acceleration response spectrum are presented in Figure 2.27. It should be emphasized that EQ4 ground motion record was corresponding to the Sylmar Olive View Med 360 station recorded during the 1994 Northridge earthquake (M_w=6.7). The data obtained from the PEER ground motion data base shows the peak ground acceleration equal to 0.84g. However, Panagiotou et al. (2010) specified the peak ground acceleration equal to 0.91g on the base of the test structure. Hence, the mathematical model was exposed to the EQ4 record with the peak base acceleration equal to 0.91g. The initial un-cracked fundamental period of the building prior to any high amplitude dynamic excitation was equal to 0.51 sec according to the experimental results. The numerical initial period based on un-cracked properties of concrete was equal to 0.45 sec. It is evident that the experimentally measured value of the initial period of vibration agreed reasonably well with the numerical value obtained by Eigen value analysis. The EQ4 ground

motion record has the maximum acceleration equal to 0.91g at t= 4.2 sec. This ground motion record was selected to match closely with the US design response spectrum at periods of 0.5 sec to 1.0 sec. This record pushed the test specimen well beyond the yielding point in force displacement curve.

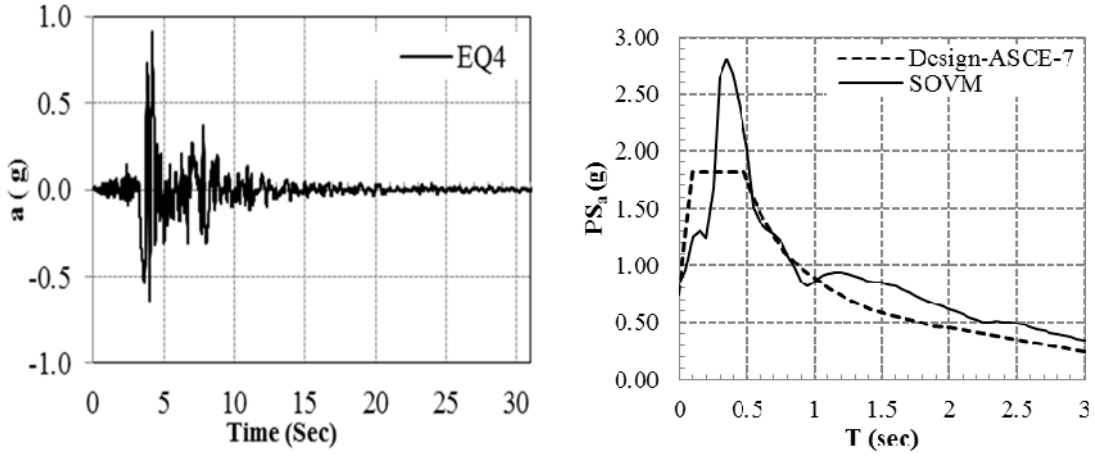

Figure 2.27: EQ4 record time series and pseudo acceleration response spectrum (ζ=5%)

2.5.2.3 Mathematical Model of the Structure

The web wall in the building slice was modelled by multi-layered shell elements including rebar and concrete material laws. The nonlinear shell element is composed of different layers of material lumped at specified integration points. Elastic shell elements were used to simulate the response of flooring slabs in each floor. The stiffness properties of the flooring slabs were calibrated according to test results. The effect of gravity columns was simulated by employing vertical elastic truss elements.

2.5.2.4 Distribution of Masses

The mass of the floors and self-weight of other elements was lumped at the middle node of the web wall at each floor level. The mass of each floor was calculated by estimating the mass of the floor slab and one-half floor height of the web wall, pier and gravity columns above and

below the floor. The values of mass on each floor (see Table 2-5) were consistent with the information provided in the test report. The vertical mass is assumed to be zero. The numerical values of the gravity load are also presented in Table 2-5. The maximum normalized axial force on the steel column at the base is approximately equal to $0.075f_cA_g$.

Table 2-5: Mass and gravity force on web wall

Floor level	Mass(kN*s^2/m)	Gravity force on web wall (kN)
1	31.52	115.60
2	28.89	115.60
3	28.85	115.60
4	28.81	115.60
5	28.81	115.60
6	29.53	115.60
7	23.68	115.60

2.5.2.5 Material Constitutive Laws

The multi-layered shell element is made of different layers of materials lumped at two integration points over the element surfaces and/or thickness. Hence, the definition of material equivalent thickness and properties in each layer can be assigned separately. Hence, different input variables are necessary to define the rebar and concrete properties in each layer over the height of the building. Concrete and reinforcement material specification in each layer differ from one storey to another storey according to as-built drawings provided in the test report.

The typical stress strain curves for rebars and concrete are shown in Figure 2.28 and Figure 2.29. The material properties are consistent with the materials used in the experiment test. The average tensile yield strength of the rebar #5 and #7 is equal to 434.4 MPa and 461.9 MPa respectively. The ultimate strain of rebars at the ultimate point on the stress strain curve, which is also the beginning of strength degradation part of the curve, was set to equal to 0.06. The strain hardening ratio of steel rebars was approximately equal to 0.022.

The unconfined and confined concrete average compression strength in the first floor was equal to 37.4 MPa and 45.8 MPa respectively. Confined concrete compression strength and post-peak slope have been derived based on Mander et al. (1988) mathematical model.

The cyclic behaviour of rebars and concrete are assumed to follow the Takeda hypothesis rule. The tensile strength of concrete was neglected during the analysis. Hence, the cracking and tension stiffening effect are excluded from the mathematical model.

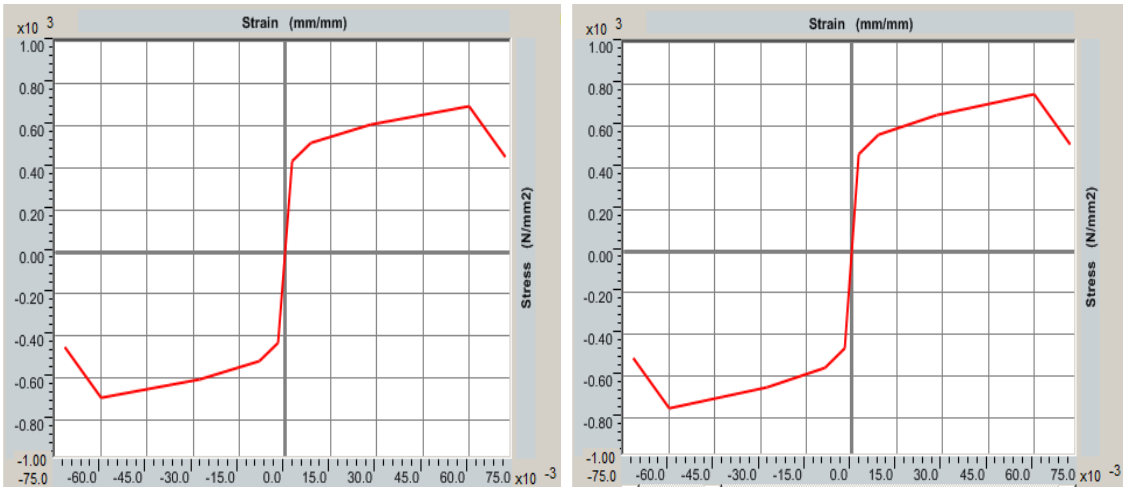

Rebar #5 **Rebar #7**

Figure 2.28: Definition of reinforcement material properties

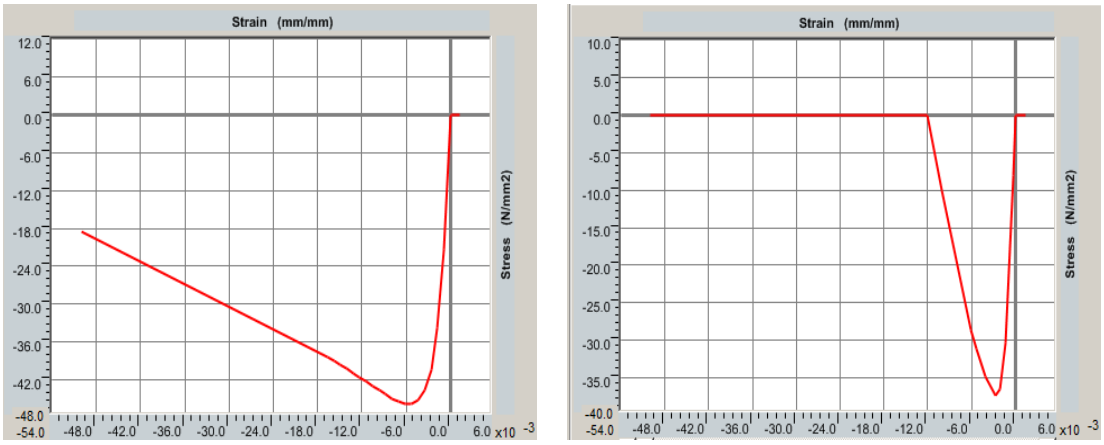

Figure 2.29: Definition of confined and unconfined concrete material properties

One of the valuable lessons learnt from this experimental test was that the slotted slabs and the flooring slabs had significant impact on the whole system response. Hence, to capture the real response, the mathematical model should account for the effect of the slotted slabs and the flooring slabs. The equivalent beam element with nonlinear rotational springs (hinges) at their ends were used in the mathematical model to capture the effect of slotted slabs. Figure 2.30 and Figure 2.31 shows the nonlinear moment rotation definition of the hinges (springs) at the end of equivalent beams which was employed to model the slotted slabs.

Another challenge in the simulation process was that how one should model the effect of flooring slabs on the system response. The deformation compatibility between the flooring slab and vertical movement of the structural wall caused flexural and torsional deformation in RC floor plates. It was a quite complicated problem to find the appropriate level of cracking over the floor plate in each floor separately. It is quite obvious that the degree of interaction highly depends on the flexural and torsional stiffness of slabs. Hence, in this specific example, trial and error was used to find the best value for the flexural and torsional stiffness of slabs which produce the best prediction compared to the experimental outputs.

Extensive parametric dynamic analysis was conducted to find the best flexural and torsional stiffness properties for the flooring slab. The effective flexural stiffness equal to 0.2 EI_g and torsional stiffness equal to 0.1GJ_g has been found appropriate. Hence, the pushover analysis and nonlinear time history analysis results are presented only for the above final case. Although the effective stiffness values for the floor slabs (at ultimate limit state) were selected to match the results of numerical analysis with the experiment, it is quite challenging to generalize the broad application of these values to all cases. It is believed that several full scale system level shake table tests are still needed to confirm the proposed values. However, the selected values agrees reasonably well with the recommended values in the PEER, Tall Buildings Initiative (TBI), 2010 report for the effective stiffness of floor slabs at two limit states (see Table 2-6).

Table 2-6: Floor effective stiffness values

Floor system*	Service-Level Linear Models			MCE-Level Nonlinear Models		
	Axial	Flexure	Shear	Axial	Flexure	Shear
Floor slabs(diaphragms)	$0.5E_cA_g$	$0.5EcI_g$	$0.4E_cA_g$	$0.25E_cI_g$	$0.25E_cI_g$	$0.1E_cA_g$
Post-tensioned floor slabs(diaphragms)	0.8EcAg	0.8EcIg	0.4EcAg	0.50EcIg	0.50EcIg	0.2EcAg

*Specified stiffness values for diaphragms are intended to represent expected values. Alternative values may be suitable where bounding analyses are used to estimate bounds of forces. For diaphragms that are not associated with major force transfers, common practice is to model the diaphragm as being rigid in its plane. Flexural rigidity of diaphragms out of plane is usually relatively low and is commonly ignored. The exception is where the diaphragm acts as a framing element to engage gravity columns as outrigger elements, in which case out-of-plane modelling may be required.

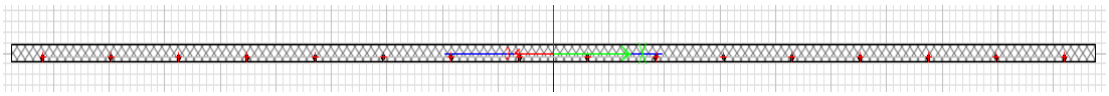

(a)

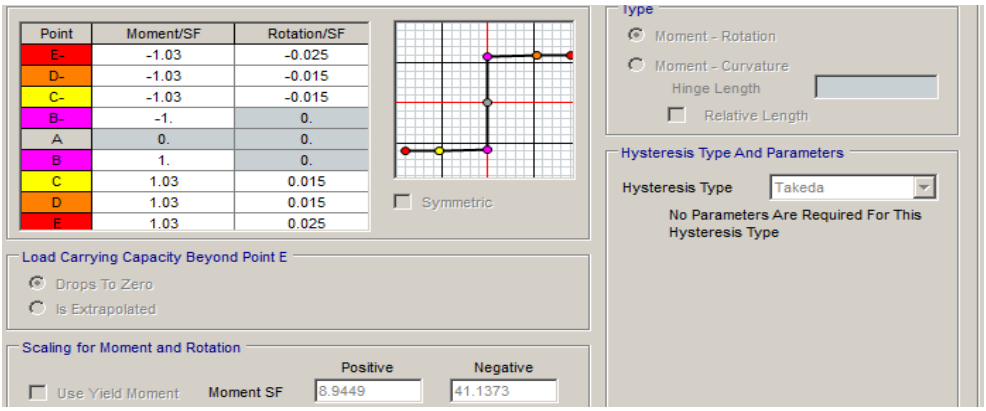

(b)

Figure 2.30: (a) Slotted slab section in Westward direction (b) Definition of slotted slab moment rotation curve

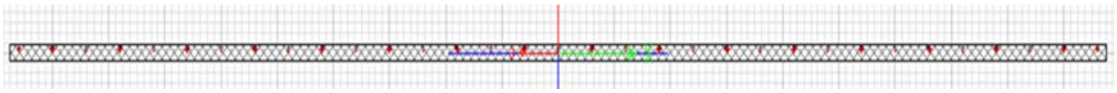

(a)

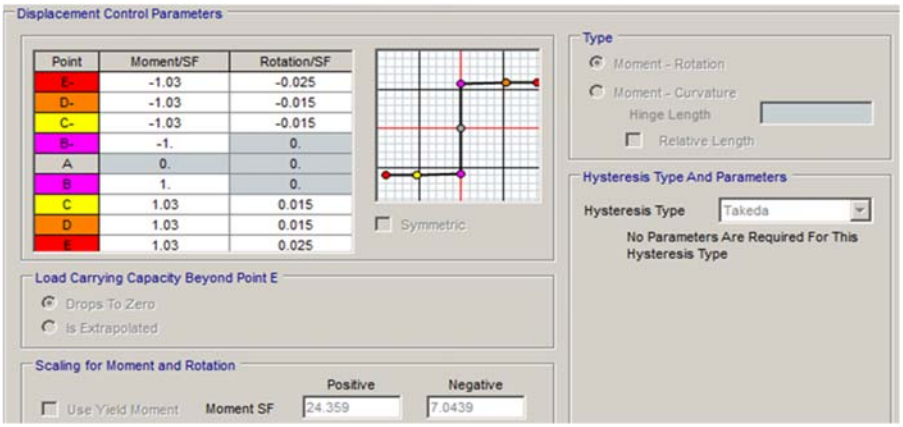

(b)

Figure 2.31: (a) Slotted slab section in Eastward direction (b) Definition of slotted slab moment rotation curve

Figure **2.32** illustrates the three-dimension view of the specimen including the slotted slab and the flooring slabs. A mesh sensitivity analysis was conducted, which confirmed that three meshes over the floor height could produce sensible results.

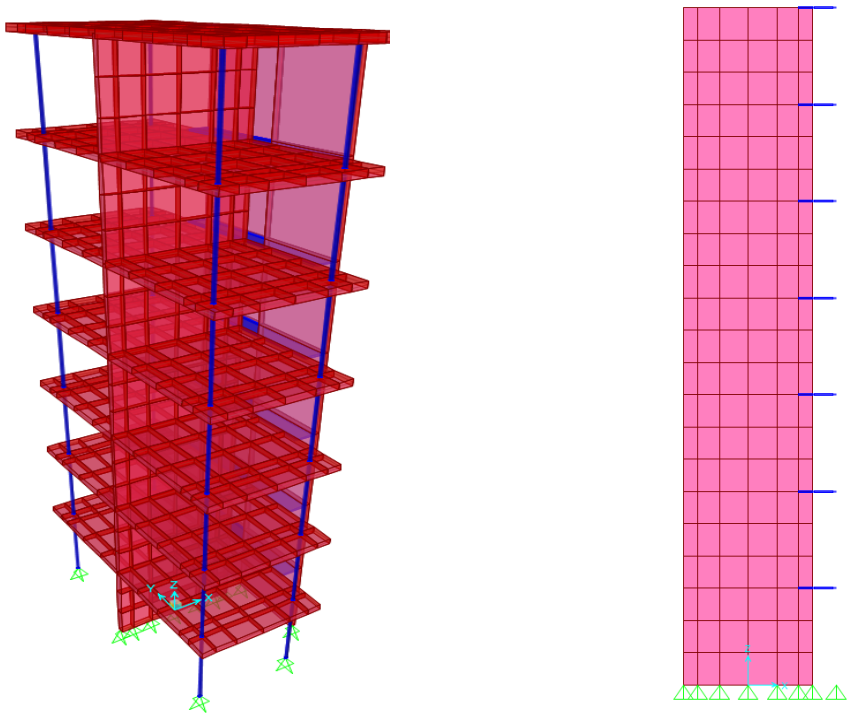

Figure 2.32: Three-dimensional view of mathematical model of test structure

2.5.2.6 Damping Model

Material damping was accounted for by calibrating the parameters of Rayleigh damping coefficients. Different equivalent viscous damping parameters were specified to the materials. The stiffness coefficient of damping in the elements which are likely to yield under the excitation is set to zero to avoid spurious damping forces during the analysis. Hence, different values of damping coefficients were assigned to rebar and concrete in the first and second floor compared to the remaining floors. Table 2-7 shows the numerical values of damping coefficients specified with respect to the rebar and concrete characteristics. It should be emphasized that the damping is a very complicated phenomenon and it is not easy to quantify even in experimental tests. Moaveni et al. (2006) showed that the test building demonstrated approximately 3% damping on the first horizontal mode when it was exposed to the white noise excitation. However, in numerical predictions damping equal to 0.025 of critical damping in

the first and second modes produced better results. The first and second modes of the building was obtained based on cracked section properties.

Table 2-7: Mass and stiffness proportion damping parameters

Material	Rebar and concrete (yielding)	Rebar and concrete (non-yielding)
α (sec^{-1}) (mass proportional)	0.1885	0.1885
β (sec) (stiffness proportional)	0	4.297e-4

2.5.2.7 Verification of Results

Numerical prediction of the test results has been predicted only for the EQ4 excitation to validate and verify the capability of the mathematical model to predict the experimental results. Moreover, some of the critical parameters including the numerical damping values and the floor slab flexural and torsional stiffness were calibrated with respect to the test results. It is worth mentioning that it is almost impossible to find a perfect mathematical model to capture all engineering demand parameters with high accuracy using the current state of knowledge in earthquake engineering. However, an extensive analytical investigation was conducted to find the best model which can predict most of the engineering demand parameters close enough to the experimental results.

Although an extensive parametric analysis was conducted to obtain the best numerical values for the damping and stiffness parameters of the floor slabs, results are presented here only for the final values of these parameters, which provide a good correlation with the experimental results.

Figure 2.33 (a) shows the East-West direction pushover curves of the test specimen. Figure 2.33 (a) also includes the base moment versus the roof displacement curve obtained during the test under the EQ4 record. As the specimen was previously subjected to a couple of low to medium

amplitude ground motion records, the web wall had extensive cracking or even minor rebar yielding before applying the EQ4 record.

It is evident from Figure 2.33 (a) that the maximum base moment at maximum roof displacement matched very well with the experiment in both directions. However, pushover analysis results show stiffer response compared to the experimental test as expected in the initial loading stage.

Figure 2.33 (b) illustrates the results of numerical simulation for the base moment versus base rotation for the specimen under EQ4 record. Corresponding pushover analysis results are also presented on this graph to confirm that no spurious damping was generated in the mathematical model through dynamic analysis.

Figure 2.34 (a) presents the results of dynamic analysis and the experimental base moment versus base rotation response. It seems that the numerical model is capable of predicting the overall global response of the building. Given a wide range of other approximations accepted in earthquake engineering, although the shape of the base moment versus roof displacement does not match exactly with the experimental results, the numerical results of the mathematical model are deemed acceptable. Figure 2.34 (b) also demonstrates the base moment versus base rotation response obtained from the analysis. There is no data for this engineering demand parameter in the test report.

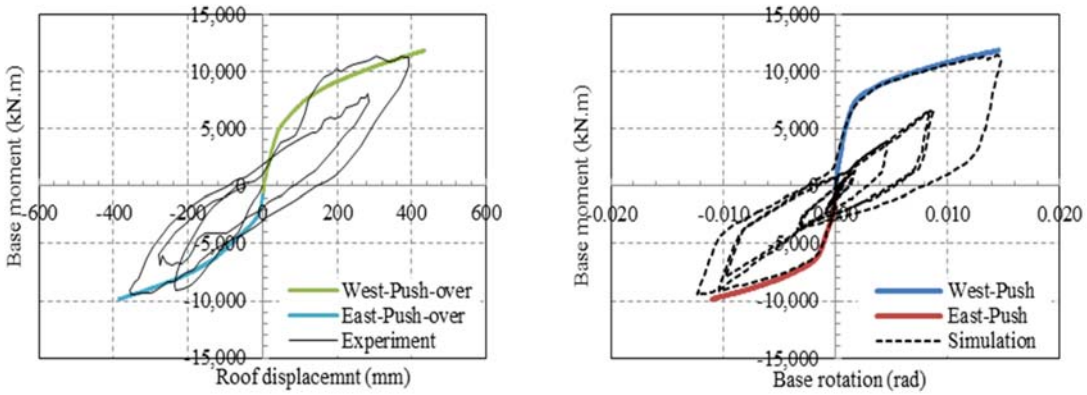

(a) (b)

Figure 2.33: (a) Experimental base moment versus roof displacement and pushover analysis, (b) Numerical base moment versus base rotation curve and pushover results

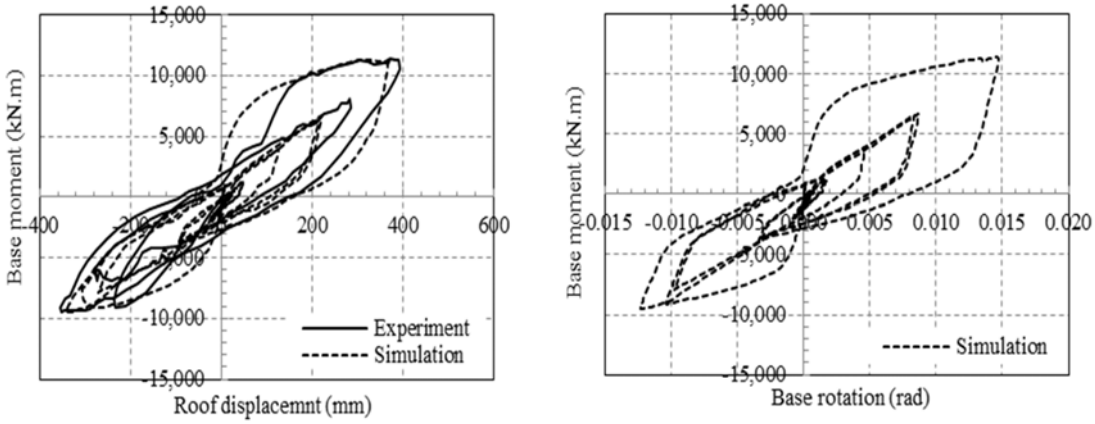

(a) (b)

Figure 2.34: (a) Experimental and numerical base moment versus roof displacement, (b) Numerical base moment versus roof displacement

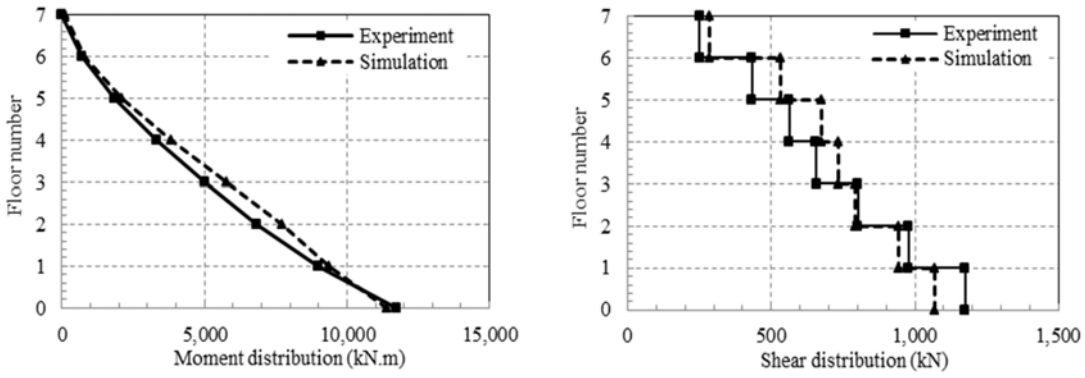

(a) (b)

Figure 2.35: (a) Moment distribution comparison, (b) Shear distribution comparison

Figure 2.35 (a) displays the moment distribution over the height of the building obtained from the test and analysis. The numerical values were obtained from the absolute maximum values of the response histories. It shows that the peak base moment found from the analysis is equal to 11381 kN.m compared to 11733 kN.m in the test, giving a difference of about 3 percent in the prediction of peak base moment. The model predicts the distribution of moment in the remaining stories, on average, 12 percent higher than the experiment.

Figure 2.35 (b) shows the distribution of storey shear forces over the building height found from the analysis and test results. It is evident that the model under predicts the first storey shear (base shear) and second storey shear response by approximately 8.8 percent and 3.5 percent respectively. The results of the analysis for the third storey shear force is equal to 880.1 KN compared to the experimental value of 793.8 KN. However, the calculated storey shear forces for the remaining upper stories was overestimated by an average of 17.1 percent. It should be highlighted that the maximum moment and shear did not happen concurrently. It is evident that the model predicts the moment envelop much better than the shear envelope for this case.

One of most important engineering demand parameters is the displacement profile and its tangent as an inter-storey drift ratio.

Figure 2.36 (a) illustrates the comparison of displacement profile obtained from the simulation and test results. While the numerical model predicts the first storey displacement with 21.9 percent error (the analysis value is 30.52 mm compared to the experimental value of 39.1 mm) the displacement of upper stories was underestimated by an average error value of 5.76 percent. Part of the difference between the model and the experiment can be attributed to the flexibility of the experimental specimen due to any prior damage foundation rotation, loss of reinforcement bond and other none modelled physical phenomena. Hence, this mathematical model not only cannot reproduce these effects but also cannot capture the lap splice failure of the specimen during EQ4 event.

On the other hand, Figure 2.36 (b) shows the maximum inter-storey drift profiles estimated from simulation and experimental results. The model predictions for the first, second and third storey inter-storey drifts are equal to 0.011, 0.019, and 0.021 respectively. The corresponding values obtained from the test results are equal to 0.015, 0.018, and 0.022. The model under predicts the inter-storey drift of the upper floors by an average of 6.23 percent.

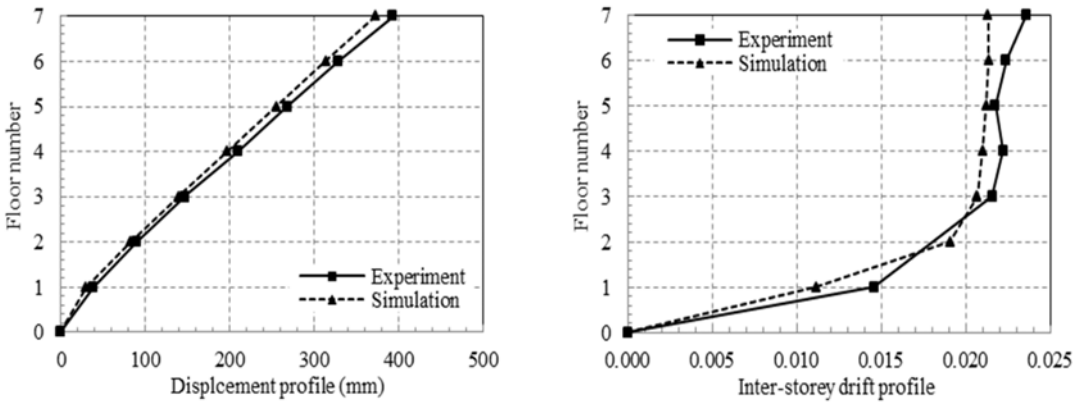

(a) (b)

Figure 2.36: (a) Displacement profile, (b) Inter storey drift ratio

The peak floor acceleration profile is another important response index which represent the demand on acceleration sensitive components of the building. Total acceleration of each floor

was calculated by summation of relative acceleration of a node on each floor and input base acceleration of the test structure obtained from the analysis outputs. The total acceleration of each floor was normalized to the peak base acceleration to get the amplification or de-amplification coefficients. Figure 2.37 presents the experimental and simulation results of total acceleration profile of the test structure. The error in the prediction of the maximum acceleration profile was within 20% more in floor 6 and floor 3 than in other floors. Both experimental and numerical curves confirm that the maximum ground acceleration is de-amplified in all floors except at the top floor.

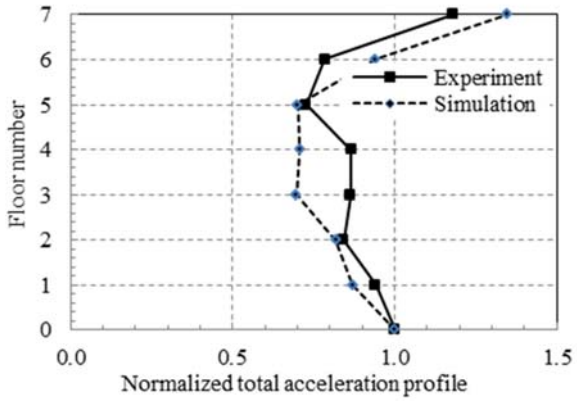

Figure 2.37: Peak acceleration profile

In summary, to judge the credibility of the numerical simulation in the prediction of the most essential engineering demand parameters, the error has been defined as a difference between the prediction and experimental results. The peak roof displacement, peak base moment, peak base shear and peak vertical displacement of the wall edges are some of the fundamental engineering demand parameters considered in the design practice. Table 2-8 displays the error involved in the prediction of these parameters.

Table 2-8: Errors in the prediction of important engineering demand parameters

EDP	Experiment	Numerical	Percentage Error
Peak roof displacement (mm)	394	373	-5.4
Peak base moment (kN.m)	11733.1	11381.3	-3.0
Peak base shear (kN)	1174.3	1070.6	-8.8
Wall edge vertical deformation (max) (mm) (Roof level)	64.8	63.9	-1.4
Wall edge vertical deformation (min) (mm) (Roof level)	-10.4	-14.8	42.3

As can be seen in Table 2-8 the percentage error in the estimation of above engineering demand parameters are less than 10 percent except for the error in estimation of vertical contraction of the wall edges at the roof level. This range of error is typically acceptable in the engineering practice given the uncertainties involved in the calculation. The large error in the prediction of the wall edge vertical contraction may have occurred due to neglecting the tensile strength of concrete in the numerical analysis.

The error values for the different engineering demand parameters are plotted against the floor level in Figure 2.38. It seems that the numerical predictions of displacement, inter-storey drift, and bending moment values are more favourable than the predictions of the storey shear and the acceleration profile.

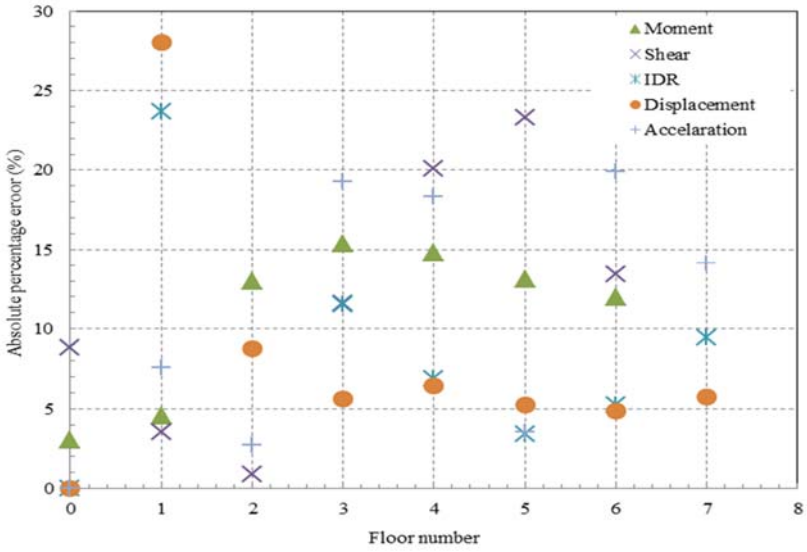

Figure 2.38: Error in estimation of different engineering demand parameters

2.6 Conclusion

Common approaches to modelling RC shear walls available in literature are scrutinised in this chapter. The advantages and drawbacks of available models/elements for analytical modelling of multi-storey shear wall buildings are discussed. Although a wide variety of analytical modelling approaches have been proposed/developed/employed by different researchers; most of these are aimed to simulate the experimental response of isolated walls and are not easily/readily applicable in practice where engineers have to deal with 3D response of shear wall buildings in which walls invariably interact with other elements of the building. Three main drawbacks of several existing models are: (1) inability to capture the nonlinear strain profile due to the plane section remains plane assumption; (2) inability to convincingly account of shear-axial-flexural interaction; and (3) inability to allow consideration of the effect of slabs on the wall response. To facilitate a realistic performance assessment of shear wall buildings by practicing engineers, a macro wall element is needed which offers a reliable approach to modelling nonlinear behaviour of shear wall buildings without the abovementioned drawbacks. Currently, an attempt is being made at University of Canterbury to develop a new macro wall element comprising of a number of filaments analysed based on material behaviour. Although

the multi-layered shell element appears promising and lacks any major obvious limitations, this is still under development and more research is needed to verify the model for different applications.

As numerical model for real scale structural walls using multi-layered shell element has been developed in this chapter. This model can predict the bending moment and overall acceleration as well as displacement profiles of the specimen under dynamic excitation with reasonable accuracy. The effective flexural and torsional stiffness of the slabs equivalent to 0.20 and 0.10 of their gross stiffness were found to yield prediction matching well with test results. Similarly, numerical damping value of 0.025 in the first and second mode based on cracked section properties was formed to predict reasonable results.

2.7 References

ASCE/SEI Seismic Rehabilitation Standards Committee. (2006). Seismic rehabilitation of existing buildings (ASCE/SEI41-06). *American Society of Civil Engineers, Reston, VA*.

Bertero, V., Aktan, A. E., Charney, F., and Sause, R. (1984). Earthquake simulator tests and associated experimental, analytical, and correlation studies of one-fifth scale model. ACI Special Publication, 84. 375-424

Beyer, K., Dazio, A., and Priestley, N. (2011). Shear deformations of slender reinforced concrete walls under seismic loading. *ACI Structural Journal*,108(2), 167-177.

Belarbi, A., and Hsu, T. T. (1994). Constitutive laws of concrete in tension and reinforcing bars stiffened by concrete. *Structural Journal*, *91*(4), 465-474.

Carr, A. J. 1980-2015. Ruaumoko–Program for inelastic dynamic analysis. Department of Civil Engineering, University of Canterbury, Christchurch, New Zealand.

Chen, S., and Kabeyasawa, T. (2000). Modelling of reinforced concrete shear wall for nonlinear analysis. *Proceedings of the 12th WCEE, New Zealand Society of Earthquake Engineering*. Auckland, New Zealand.

Colotti, V. (1993). Shear behaviour of RC structural walls. *Journal of Structural Engineering*, *119*(3), 728-746.

Darwin, D., and Pecknold, D. A. (1974). *Inelastic model for cyclic biaxial loading of reinforced concrete*. University of Illinois Engineering Experiment Station. College of Engineering. University of Illinois at Urbana-Champaign.

Dazio, A., Beyer, K., and Bachmann, H. (2009). Quasi-static cyclic tests and plastic hinge analysis of RC structural walls. *Engineering Structures*, *31*(7), 1556-1571.

Fu, J., Shibata, A., Shibuya, J. I., and Saito, T. (1992). 3-D inelastic earthquake response of RC frames with shear walls. *Proceeding of 10th World Conference on Earthquake Engineering* (pp. 4303-4308). Madrid, Spain.

Ghobarah, A., and Youssef, M. (1999). Modelling of reinforced concrete structural walls. *Engineering Structures*, *21*(10), 912-923.

Giberson, M. F. (1967). *The response of nonlinear multi-story structures subjected to earthquake excitation* (Doctoral thesis, California Institute of Technology, Pasadena, California). Retrieved from https://thesis.library.caltech.edu/3604/1/Giberson_m_f_1967.pdf.

Goodsir, W. J., Paulay, T., and Carr, A. J. (1983). A study of the inelastic seismic response of reinforced concrete coupled frame-shear wall structures. *Bulletin New Zealand National Society for Earthquake Engineering*, *16*(3).

Hines, E. M., Seible, F., and Priestley, M. J. N. (1999). *Cyclic tests of structural walls with highly-confined boundary elements*. (Doctoral dissertation, Dept. of Structural Engineering, University of California, San Diego).

Hiraishi, H. (1984). Evaluation of shear and flexural deformations of flexural type shear walls. Bulletin New Zealand National Society for Earthquake Engineering. Vol 17(2) Wellington.

Hrennikoff, A. (1941). Solution of problems of elasticity by the framework method. *Journal of applied mechanics*, *8*(4), 169-175.

Kabeyasawa, T., Shiohara, H., Otani, S., and Aoyama, H. (1983). Analysis of the full-scale seven-story reinforced concrete test structure. *Journal of the Faculty of Engineering*: *University of Tokyo, 37*(2), 431-478.

Kelly, T. (2007). A blind prediction test of nonlinear analysis procedures for reinforced concrete shear walls. *Bulletin of the New Zealand Society for Earthquake Engineering*, *40*(3), 142-159.

Kent, D. C., and Park, R. (1969). Inelastic behaviour of reinforced concrete members with cyclic loading (Doctoral dissertation, University of Canterbury).

Kim, S., and Wallace, J. W. (2014). Shear Demands of Structural Walls. In *Tenth US National Conference on Earthquake Engineering Frontiers of Earthquake Engineering*. Alaska, USA.

Kolozvari, K., Tran, T., Wallace, J. W., and Orakcal, K. (2012). Modelling of cyclic shear–flexure interaction in reinforced concrete structural walls. *Proceedings of the 15th world conference on earthquake engineering.* Lisbon, Portugal. Retrieved from https://www.iitk.ac.in/nicee/wcee/article/WCEE2012_2471.pdf.

Kolozvari, K., Orakcal, K., and Wallace, J. W. (2014a). Modeling of cyclic shear-flexure interaction in reinforced concrete structural walls. I: Theory. *Journal of Structural Engineering*, *141*(5), 04014135.

Kolozvari, K., Tran, T. A., Orakcal, K., and Wallace, J. W. (2014b). Modeling of cyclic shear-flexure interaction in reinforced concrete structural walls. II: experimental validation. *Journal of Structural Engineering*, *141*(5), 04014136.

Kolozvari, K., and Wallace, J. W. (2016). Practical nonlinear modeling of reinforced concrete structural walls. *Journal of Structural Engineering*, *142*(12), G4016001.

Kowalsky, M. J., and Priestley, M. N. (2000). Improved analytical model for shear strength of circular reinforced concrete columns in seismic regions. *ACI Structural Journal*, 97(3).

Krolicki, J., Maffei, J., and Calvi, G. M. (2011). Shear strength of reinforced concrete walls subjected to cyclic loading. *Journal of Earthquake Engineering*,15(S1), 30-71.

Lai, S. S., Will, G. T., and Otani, S. (1984). Model for inelastic biaxial bending of concrete members. *Journal of structural engineering*, *110*(11), 2563-2584.

Lefas, I. D., Kotsovos, M. D., and Ambraseys, N. N. (1990). Behavior of reinforced concrete structural walls: strength, deformation characteristics, and failure mechanism. *Structural Journal*, *87*(1), 23-31.

Li, K. N. 2010. Three-dimensional nonlinear static/dynamic structural analysis computer program-users. manual and data-input manual of CANNY.

Linde, P., and Bachmann, H. (1994). Dynamic modelling and design of earthquake resistant walls. *Earthquake engineering and structural dynamics*, *23*(12), 1331-1350.

Mander, J. B., Priestley, M. J., and Park, R. (1988). Theoretical stress-strain model for confined concrete. *Journal of structural engineering*, *114*(8), 1804-1826.

Martinelli, P., and Filippou, F. C. (2009). Simulation of the shaking table test of a seven-story shear wall building. *Earthquake Engineering and Structural Dynamics*, *38*(5), 587-607.

Massone, L. M., Orakcal, K., and Wallace, J. W. (2006). Shear-flexure interaction for structural walls. SP-236. *ACI special publication—Deformation capacity and shear strength of reinforced concrete members under cyclic loading*, 127–50.

Mazzoni, S., McKenna, F., Scott, M. H., and Fenves, G. L. (2006). OpenSees command language manual. *Pacific Earthquake Engineering Research (PEER) Center*, *264*.

Menegotto, M. and Pinto, P. (1973). Method of analysis for cyclically loaded RC plane frames including changes in geometry and non-elastic behavior of elements under combined normal force and bending. In *Proc. of IABSE symposium on resistance and ultimate deformability of structures acted on by well-defined repeated loads, IABSE Reports Vol. 13, Lisbon, 1973*.

Mergos, P. E., and Beyer, K. (2014). Modelling shear–flexure interaction in equivalent frame models of slender reinforced concrete walls. *The Structural Design of Tall and Special Buildings*, *23*(15), 1171-1189.

Moaveni, B., He, X., Conte, J. P., and Restrepo, J. I. (2010). Damage identification study of a seven-story full-scale building slice tested on the UCSD-NEES shake table. *Structural Safety*, *32*(5), 347-356.

NZS3101 (2006): Concrete Structures Standard, NZS 3101:2006 Parts 1 and 2 Standards New Zealand.

Oesterle, R. G., Fiorato, A. E., Johal, L. S., Carpenter, J. E., Russell, H. G., and Corley, W. G. (1976). *Earthquake resistant structural walls-tests of isolated walls* (PCA-R/D-SER-1571). National Science Foundation, Washington, D.C.

Oesterle, R. G., Aristizabal-Ochoa, J. D., Shiu, K. N., and Corley, W. G. (1984). Web crushing of reinforced concrete structural walls. *ACI Journal Proceedings*, *81*(3), 231-241.

Orakcal, K., and Wallace, J. W. (2006). Flexural modeling of reinforced concrete walls-experimental verification. *ACI Materials Journal*, *103*(2), 196.

Otani, S. (1974). Inelastic analysis of R/C frame structures. *Journal of the Structural Division*, *100*(7), 1433-1449.

Park, R., Kent, D. C., and Sampson, R. A. 1972. Reinforced concrete members with cyclic loading. *Journal of the Structural Division*, *98*(7), 1341-1359.

Panagiotou, M., Restrepo, J. I., and Conte, J. P. (2007). *Shake Table Test of a 7-story Full Scale Reinforced Concrete Structural Wall Building Slice, Phase I: Rectangular Section* (Report No. SSRP-07/07). San Diego, CA: Department of Structural Engineering, University of California.

Panagiotou, M., Restrepo, J. I., and Conte, J. P. (2010). Shake-table test of a full-scale 7-story building slice. Phase I: Rectangular wall. *Journal of Structural Engineering*, 137(6), 691-704.

Panagiotou, M., Restrepo, J. I., Schoettler, M., and Kim, G. (2012). Nonlinear cyclic truss model for reinforced concrete walls. *ACI Structural Journal*, *109*(2), 205.

Peng, B. H., Dhakal, R. P., Fenwick, R. C., Carr, A. J., and Bull, D. K. (2013). Multispring hinge element for reinforced concrete frame analysis. *Journal of structural engineering*, *139*(4), 595-606.

PEER(TBI). (2010). Guidelines for Performance-Based Seismic Design of Tall Buildings. PEER 2010/05. Pacific Earthquake Engineering Research Center, Berkeley, CA.

PERFORM 3D, CSI. (2006). Nonlinear Analysis and Performance Assessment for 3D Structures, Version 4. Computers and Structures, Inc., Berkeley, California.

Pugh, J. S. 2012. *Numerical simulation of walls and seismic design recommendations for walled buildings* (Doctoral thesis, University of Washington). Retrieved from http://hdl.handle.net/1773/22579.

Reinhorn, A. M., Roh, H., Sivaselvan, M., Kunnath, S. K., Valles, R. E., Madan, A., and Park, Y. (2009). IDARC 2D version 7.0: A program for the inelastic damage analysis of buildings. *Buffalo, New York*.

Rodriguez, M. E., Restrepo, J. I., and Carr, A. J. (2002). Earthquake induced floor horizontal accelerations in buildings. *Earthquake engineering and structural dynamics*, *31*(3), 693-718.

Saiidi, M., and Sozen, M. A. (1979). Simple and complex models for nonlinear seismic response of reinforced concrete structures. University of Illinois Engineering Experiment Station. College of Engineering. University of Illinois at Urbana-Champaign.

SAP2000, CSI, S. (2016): Ver. 17.1.1, integrated finite element analysis and design of structures basic analysis reference manual. Berkeley (CA, USA), Computers and Structures INC.

Satyarno, I., Carr, A. J., and Restrepo, J. (1998). Refined pushover analysis for the assessment of older reinforced concrete buildings. *Proceedings of the New Zealand Society for Earthquake Engineering Technology Conference* (pp. 75-82).

Spieth, H. A., Carr, A. J., Murahidy, A. G., Arnolds, D., Davies, M., and Mander, J. B. (2004). Modelling of post-tensioned precast reinforced concrete frame structures with rocking beam-column connections. *Proceedings of the 2004 New Zealand Society of Earthquake Engineering Technical Conference.* Rotorua, New Zealand.

Speith, H.A., Arnold, D., Davies, M., Mander, J.B. and Carr. A.J. (2004). Seismic Performance of Post-tensioned Precast Concrete beam to Column Connections with Supplementary Energy Dissipation. *Proceedings of the 2004 New Zealand Society of Earthquake Engineering Technical Conference.* Rotorua, New Zealand.

Taylor, R. G. (1977). *The nonlinear seismic response of tall shear wall structures*. (Doctoral thesis). University of Canterbury, Christchurch, New Zealand.

Thomsen IV, J. H., and Wallace, J. W. (1995). *Displacement-based design of reinforced concrete structural walls: An experimental investigation of walls with rectangular and T-shaped cross sections* (Rep. No. CU/CEE-95-06), Deaprtment of Civil and Environmental Engineering, Clarkson University, Postdam, N.Y.

Tuna, Z. (2012). *Seismic performance, modelling, and failure assessment of reinforced concrete shear wall buildings* (Doctoral thesis, University of California, Los Angeles). Retrieved from https://escholarship.org/uc/item/3c96x2gn.

Vallenas, J. M., V. V. Bertero and E. P. Popov (1979). Hysteretic behaviour of reinforced concrete structural walls. Report no. UCB/EERC-79/20, *Earthquake Engineering Research Center*, University of California, Berkeley.

Vecchio, F. J., and Collins, M. P. (1986). The modified compression-field theory for reinforced concrete elements subjected to shear. *ACI J.*, *83*(2), 219-231.

Vulcano, A., Bertero, V. V., and Colotti, V. (1988). Analytical modelling of RC structural walls. *Proceedings of 9th world conference on earthquake engineering* (pp. 41-46). Tokyo-Kyoto, Japan, Science Council of Japan.

Wallace, J. W. (2007). Modelling issues for tall reinforced concrete core wall buildings. *The structural design of tall and special buildings*, *16*(5), 615-632.

Waugh, J. D., and Sritharan, S. (2010). Lessons learned from seismic analysis of a seven-story concrete test building. *Journal of Earthquake Engineering*, *14*(3), 448-469.

3 Three-dimensional Interaction between Structural Walls, Gravity Frames and Floor Slabs

3.1 Introduction

Reinforced concrete (RC) structural walls with two-way concrete flat slabs (in-situ or post-tensioned) are one of the common lateral-load-resisting systems that are built in many countries nowadays, and also many existing buildings were constructed with this system. In typical structural design practice, because the performance of lateral-load-resisting systems is the main focus of (nonlinear) lateral analysis, floor systems are considered only as a source of mass and gravity loads. Therefore, the contribution of the floor systems (such as two-way flat slabs) to the overall stiffness or strength of the building is often neglected.

Bertero et al. (1984) performed shaking table tests on a 1/5 scale and a full scale multi-storey shear wall-frame building. Following these system-level testing, the significant contribution of the flooring system (two-way slabs) to the ultimate lateral strength of the building has confirmed. They stated that the axial growth and rocking of the structural wall at its base (due to neutral axis movement) caused activation of a three-dimensional outrigging action in the surrounding space frames. This phenomenon was called three-dimensional effects which were created by the axial growth and rocking of the wall. The induced outrigging action of the space frames should be accounted for in the design process. This phenomenon introduced extra overstrength to the system and it is highly dependent on the level of drift which can be achieved at the ultimate limit state. Therefore, it has been called kinematic overstrength. Panagiotou et al. (2007) also conducted another experimental investigation with the shake table test on a slice of a multi-storey shear wall building including floor slabs and gravity columns. The authors noted that the main source of system base moment resistance in Westward direction at the DBE level shaking included three major components: (i) 55% from the web wall moment capacity (ii) 32% due to coupling of the web through the slotted slabs (iii) 10% due to axial force in the perpendicular gravity columns.

A precise estimation of the system overstrength factor is difficult to determine in multi-storey buildings since many factors are contributing to it. However, according to FEMA-450, the basic components of structural overstrength (Ω_0) consists of material overstrength (Ω_M), system overstrength (Ω_S), and design overstrength (Ω_D). These components of overstrength are presented schematically in Figure 3.1. This study focuses on addressing the effect of structural wall-slab-column interaction on the system overstrength (Ω_S) factor in typical multi-storey shear wall buildings. System overstrength (Ω_S) is the ratio of the ultimate lateral force the structure is capable of resisting, F_n in Figure 3.1, to the actual force at which first significant yield occurs, F_2 in Figure 3.1. It is dependent on the amount of redundancy contained in the structure as well as any probable contribution of secondary components in resisting lateral force. Re-distribution of internal actions after ductile yielding in critical zones is another key parameter.

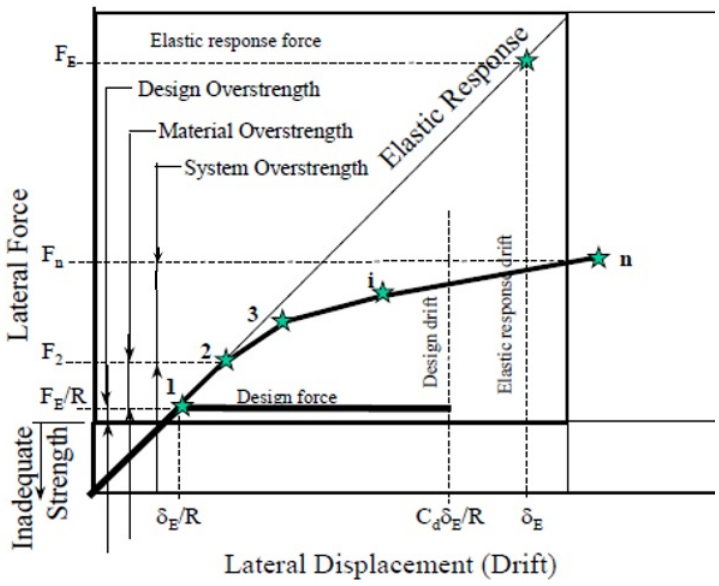

Figure 3.1: Factors affecting overstrength of a building (FEMA-450)

The fundamental objective of the current design practice and capacity design of structural wall buildings is that energy is dissipated through the formation of plastic hinges at the base of shear walls while the floor diaphragms remain fully elastic (or in specific cases a certain degree of

cracking is allowed without yielding). The flooring system is vertically supported by a combination of shear walls and gravity resisting columns. The effects of overstrength are not always beneficial in capacity design. For example, the flexural overstrength of members leads to increased shear forces when plastic hinges forms which may result in non-ductile failure (Park, 1996). Therefore, any possible source of overstrength in a building should be taken into consideration in capacity design.

Many researchers have endeavoured to recognize the major components of overstrength factor in different structural systems (Mitchell and Paultre, 1994; Nassar and Krawinkler, 1991). However, major parameters such as the actual strength of materials, confinement effects, the contribution of non-structural elements, and the actual participation of secondary structural elements (such as RC floor slabs) lead to high uncertainties in overstrength estimation (Humar and Rahgozar, 1996). Elnashai and Mwafy (2002) studied twelve RC buildings designed and detailed in accordance with Eurocode 8, based on which a conservative overstrength factor (R_s) of 2.0 for medium and low period RC buildings designed according to Eurocode 8.

The first part of this chapter introduces the mechanism of three-dimensional (spatial) interaction between the floor systems, structural walls and frames and the most significant parameters being identified.

Then, chapter attempts to investigate the system overstrength in multi-storey RC wall buildings with floor slabs in five cases of lateral-load-resisting systems: (i) case 1-1 has concrete structural walls only (zero out-of-plane flexural stiffness of slabs); and (ii) the remaining four cases have rectangular shear walls with floor slabs having different section flexural stiffness and/or varying lengths. This chapter intends to investigate the preliminary effects of length (or bay length) and out-of-plane sectional stiffness of slabs on the system overstrength factor of shear wall buildings in the direction of walls in-plane. This chapter also aims to propose a

simplified method to account for the system overstrength factor in design. It also presents the results from a finite element analysis and discusses the influence of modelling RC floor slab systems on the predicted performance of shear wall buildings. Hence, this chapter questions can be summarized as:

(1) Which variables/parameters play a significant role in spatial interaction between the floor systems, structural walls and frames?

(2) How much does the out-of-plane flexural stiffness of two-way slabs affect the system overstrength factor in multi-storey shear wall buildings?

(3) Is the system overstrength factor sensitive to flexural stiffness of slabs more than the bay length?

(4) Can we predict the system overstrength due to presence of floor slabs in multi-storey shear wall buildings with the gravity columns by employing a simplified analysis and assumptions?

However, the following section highlights several key assumptions and limitations of this research:

- Nonlinearity is limited to the base plastic hinge of RC structural walls, and all other failure mechanisms (such as wall-slab or columns-slab connections) are suppressed across the analysis.
- The effective floor stiffness (cracked) is uniform across the floor plate and is distributed equally in both directions.
- Flexural behavior of gravity columns is neglected in the analysis of multi-storey structural wall buildings to isolate the effect of floor systems.
- Conclusions and recommendations are limited to those typical multi-storey buildings with similar configuration to the case studies.

3.2 Mechanism Related to Wall-Frame-Slab Interaction

This section explains the mechanism related to the wall-frame-slab interaction in the post-elastic (yield) phase. Typical floor plan of the multi-storey shear wall building, the wall section and the design information are illustrated in Figure 3.2 and Table 3-1. An eight-story building with a floor plan of 30 m by 18 m is used as the reference building. The gravity system of the building consists of 200 mm thick RC slabs and circular (500 mm diameter) RC columns. Five cases are used in this study; the same structural wall thickness is used in all cases. Typical story height is assumed to be 3.20 meter. The building is designed based on the design provisions defined in the NZ concrete structures standard (NZS3101:2006) and the NZ loading standard (NZS1170.5:2004). Prototype buildings are assumed to be located in Christchurch on Soil type C. The seismic mass of each floor is calculated as 4542.3 KN (Table 3-1). The effective design period of the buildings is estimated via Eigenvalue analysis with stiffness values for all elements as recommended in NZS3101:2006. Three-dimensional, nonlinear finite element models are developed in SAP2000 for all prototype buildings (building with and without interaction) using consistent modelling approaches.

The deformation patterns of the whole system in the linear and nonlinear phase are demonstrated in Figure 3.3.

These figures illustrate only the system behaviour in Y direction indicated in the building floor plan. Figure 3.4 also shows a schematic deformation of representative flooring system due to rocking of structural wall sectional deformation. The connection between the flooring system and the structural walls significantly differs in construction practice due to variability in the flooring types. However, in this study typical rigid connection is assumed in both directions.

For a given applied force pattern over the building height, tensile edge elongation or compression edge shortening of structural walls in the post-elastic response (due to the

movement of neutral axis in monotonic loading and elongation (axial growth) of the wall in cyclic loading) trigger out-of-plane stiffness of slabs (or other roofing/flooring systems). This interaction induces significant additional axial forces in the gravity columns, which can develop extra moment capacity in the system. As there is no shear resistant element in the different stories of the whole system except the wall sections, any additional shear force is required to be resisted by the structural walls themselves. The implication is that, shear force demand on the structural wall in different stories will be increased. However, the amount of induced axial forces in gravity columns are more pronounced when wall elements start yielding (post-elastic range). In a ductile structure, the roofing system (or flat floor slabs in this case study) will almost always be required to remain elastic, so that they can sustain their function of transferring forces to the main lateral load resisting elements, and tying the building together. Therefore, diaphragms (floor slabs) should in principle have the strength to sustain the maximum forces that may be induced in them for a chosen yielding mechanism within the rest of the structure.

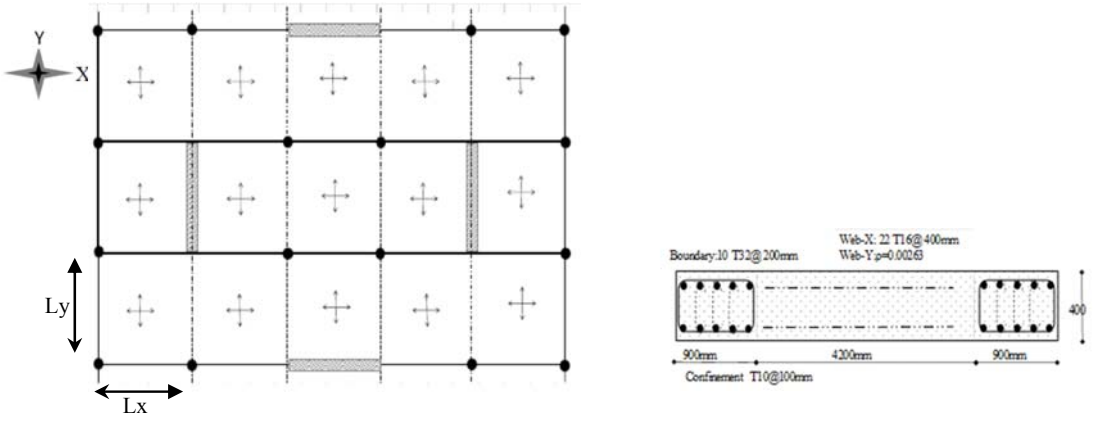

Building floor plan Wall base section

Figure 3.2: Building plan and the wall section

Table 3-1: Building design information

Rectangular wall section	6000 x 400 mm	Near fault factor	1
Typical floor height	3.20 m	Seismic weight on each wall	4542.3 kN
f_c	30 MPa	Soil type	C
f_{yl} , f_{yh}	430 MPa , 300 MPa	Near fault factor	1.0
Gravity columns dimension	D500 mm	Zone factor	0.4
Slab thickness	200 mm	Return period factor	1.0
Gravity load on each wall(base)	$0.08f_cA_g$	Structural ductility	5

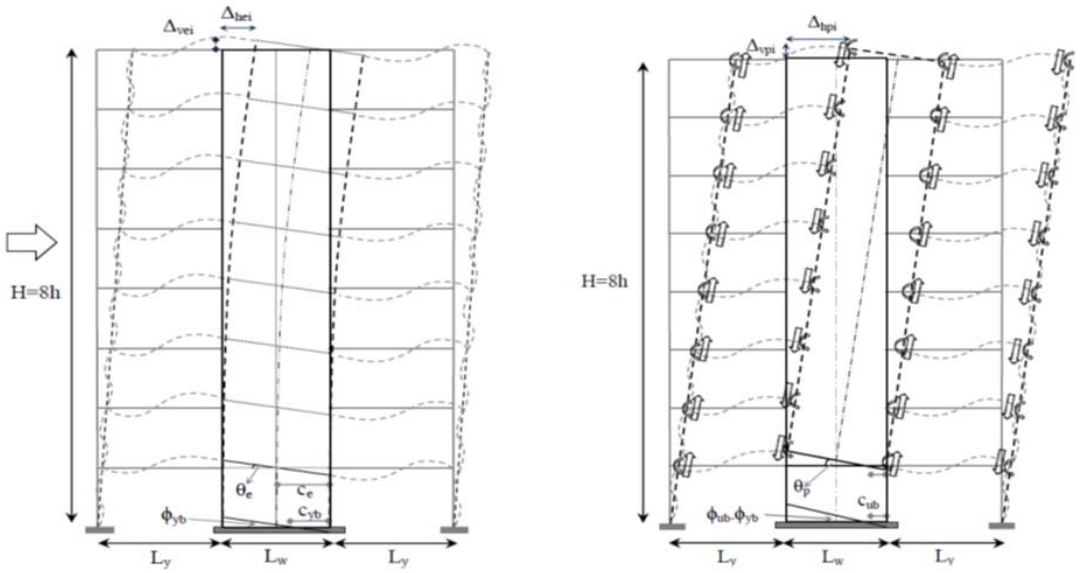

(a) (b)

H: Building Height
h: Storey Height
L_w: Wall Length
L_y: Column Distance to Wall Edge in Y direction

c_e : Neutral Axis Depth (Elastic)
c_{by} : Base Section Neutral Axis Depth at Effective Yield
c_{bu} : Base Section Neutral Axis Depth at Ultimate
θ_{ei}: Rotation of Storey Level at Effective Yield
θ_p: Plastic Rotation of Storey Level

Δ_{ei}: Vertical Displacement of Tension Edge at Effective Yield
Δ_{pi}: Plastic Vertical Displacement of Tension Edge
ϕ_{yb}: Base Effective Yield Curvature
ϕ_{ub}: Base Ultimate Curvature

Figure 3.3: a) Elastic deformation due to elastic curvature b) Plastic deformation due to plastic hinge rotation

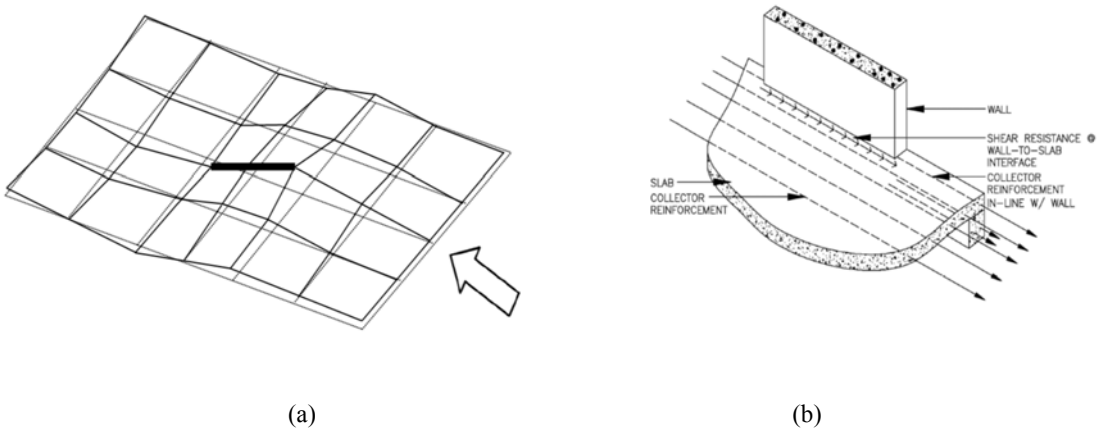

(a) (b)

Figure 3.4: a) Deformation compatibility of wall and surrounding slabs in a typical floor system b) slab to wall connection

3.2.1 Distribution of Curvature over the Height

When the wall base section curvature reaches to effective yielding curvature (equivalent to yielding of all reinforcement in the boundary element of the wall base section), the distribution of curvature over the height of the structural wall can be found at each story level (Figure 3.5). Although the distribution of lateral load over the building height could be obtained from NZ1170.5:2004 provisions approximately a rigorous method was used for the force distribution. However, assumption has been made on deformation pattern rather than the force pattern to estimate distribution of the deformation and curvature over the height of building. The adopted method is independent of lateral load pattern. A continuous lateral load pattern with zero intensity at the base has been assumed over the building height. The deformation pattern of a prismatic rectangular cantilever with constant flexural stiffness and mass can be obtained satisfying the geometric and force boundary conditions under the continuous applied load pattern. The polynomial shape function has been assumed for the deformation pattern as below:

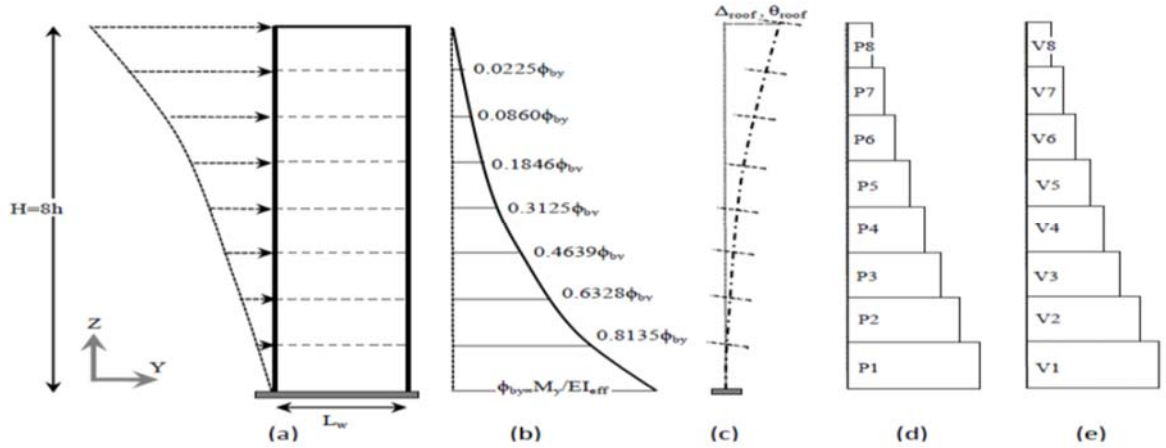

Figure 3.5: a) Force distribution b) Curvature distribution c) Flexural deformation and rotation d) Storey axial force e) Storey shear force

$$Y(Z = h_i) = aZ^5 + bZ^4 + cZ^3 + dZ^2 + eZ + f \tag{3.1}$$

Equation 3.1 shows a polynomial degree of five having the 6 unknown coefficients. $Z=h_i$ represents the height of floor i from the base of building. The current objective is to find the interrelation between the roof displacement and base curvature. Additionally, obtaining the interrelation between the floor rotations and base curvature is also another goal.

The obvious boundary conditions are:

$$Y(0) = Y'(0) = 0\,, EI.Y''(H) = 0\,, EI.Y'''(H) = 0\,, EI.Y''''(0) = 0\,, Y(H) = \Delta_{roof}$$

These boundary conditions imply the moment, shear force and lateral force intensity are equal to zero at the roof level. Rotation and deformation are also equal to zero at the base. The deformation equation is estimated based on the roof displacement which results in:

$$Y(Z) = \frac{\Delta_{roof}}{11H^5}Z^5 - \frac{10\Delta_{roof}}{11H^3}Z^3 + \frac{20\Delta_{roof}}{11H^2}Z^2 \tag{3.2a}$$

$$Y'(Z) = \frac{5\Delta_{roof}}{11H^5}Z^4 - \frac{30\Delta_{roof}}{11H^3}Z^2 + \frac{40\Delta_{roof}}{11H^2}Z \tag{3.2b}$$

$$Y''(Z) = \frac{20\Delta_{roof}}{11H^5}Z^3 - \frac{60\Delta_{roof}}{11H^3}Z + \frac{40\Delta_{roof}}{11H^2} \tag{3.2c}$$

$$Y''(0) = \emptyset_{base} = \frac{40\Delta_{roof}}{11H^2} \rightarrow\rightarrow\rightarrow \Delta_{roof} = \frac{11H^2}{40}\emptyset_{base} \quad (3.2d)$$

Substituting for Δ_{roof} in Equation (3.2c), we obtain the generic equation for the curvature distribution in terms of base curvature:

$$Y''(Z) = \emptyset(Z) = \frac{M(Z)}{EI(Z)} = \frac{\emptyset_{base}}{2H^3}Z^3 - \frac{3\emptyset_{base}}{2H}Z + \emptyset_{base} \quad (3.3)$$

Therefore, the distribution of curvature over the wall height (in each storey level) can be estimated by employing Equation (3.3) when the curvature at base section reaches the effective yield curvature. Similarly, the distribution of rotation in each storey level can be estimated as:

$$Y'(Z) = \theta(Z) = \frac{\emptyset_{base}}{8H^3}Z^4 - \frac{3\emptyset_{base}}{4H}Z^2 + \emptyset_{base}Z \quad (3.4)$$

This is important to highlight that in a real multi-storey shear wall building the lateral load distribution is a discreet function over the building height depending on number of floors. Hence, The Equation (3.2d) may introduce some errors when it has been used to find a relation between the base curvature and roof displacement in a cantilever structural wall. For a given height and the base shear, different distributions of forces can be applied over the height of building depending on distribution of mass (number of floors). Figure 3.6 displays the 5 different cases for the discrete distribution of lateral force over the height of building for a given base shear. Although we can distribute the base shear linearly over the height of building according to code, distribution of lateral forces here are assumed to be proportional to the square of the height of a given floor from the base. This can be expressed with the Equation (3.5) as:

$$F_i = \frac{h_i^2}{\sum_{i=1}^{n} h_i^2} \quad (3.5)$$

which h_i is the height of floor i from the base. In the above equation mass of all floors are assumed to be equal.

Table 3-2 indicates the relation between base curvature and roof displacement as well as estimation error compare to discrete load distribution. It is apparent that the error which is involved in employing Equation (3.2d) is reduced when the number of floors (n) has been increased. Hence, the correction factor are defined to adjust the Equation (3.2d) based on number of stories (n). The regression analysis is performed to find the best fit curve. Figure 3.7 illustrates the correction factor (λ) starts with the value of 0.8258 for the one storey and it reaches to the approximately 1 with increasing the number of stories. Thus, the modified form of Equation (3.2d) is proposed to include the effects of number of stories with multiplying the Equation (3.2d) by the correction factor (λ) as:

$$\Delta_{roof} = \frac{11H^2}{40} \emptyset_{base} \times \lambda \qquad (3.6)$$

$$\lambda = 0.835n^{0.0465} \qquad (3.7)$$

Given the fact that most of multi-storey shear wall buildings commonly have 5 or more storeys, the application of Equation (3.2d) has the maximum 10% error in our calculation. It seems application of Equation (3.2d) is justifiable for the practical purpose.

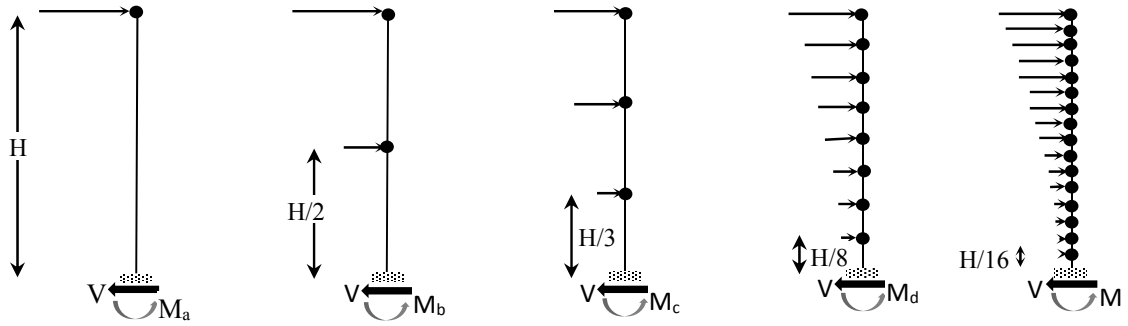

Figure 3.6: Different distribution of forces over the height

It is interesting to note that the proposed simplified method relies on base section effective yield curvature and more significantly on the base plastic rotation. The proposed method is independent of force applied to the system.

Table 3-2: Inter-Relation between base curvature and roof displacement (continues load versus discreet load)

Case	Δ_{roof}	Eq.(3-2d) $\Delta_{roof}=\frac{11H^2}{40}\phi_{base}$	Error (%)	Correction factor (λ)
a (n=1)	$0.333\phi_{base}.L^2$	$0.275\phi_{base}.L^2$	21%	0.8258
b (n=2)	$0.316\phi_{base}.L^2$	$0.275\phi_{base}.L^2$	14.9%	0.8700
c (n=3)	$0.308\phi_{base}.L^2$	$0.275\phi_{base}.L^2$	12%	0.8930
d (n=8)	$0.295\phi_{base}.L^2$	$0.275\phi_{base}.L^2$	7.3%	0.9320
e (n=16)	$0.290\phi_{base}.L^2$	$0.275\phi_{base}.L^2$	5.4%	0.95

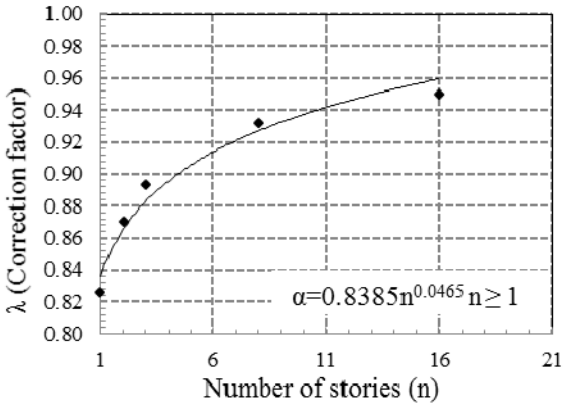

Figure 3.7: Different distribution of forces over the height

Another important variable is the neutral axis location in each storey level. Due to inelastic behaviour of RC and negligible strength of concrete in tension, the section neutral axis is shifted to satisfy the equilibrium in the section level. However, when the wall base section has the effective yield curvature, it is obvious that the section curvatures at upper storey levels are less than the effective yield curvature.

3.2.2 Estimation of Effective Yield Curvature and Neutral Axis Depth

An extensive parametric section-analysis is conducted to find the variation of effective yield curvature (and equivalent neutral axis depth) in the moment- curvature diagram. Moreover, the parametric study also investigates the variation of neutral axis depth when the section reaches its ultimate flexural strength. The effective yield curvature is determined using standard moment-curvature analyses satisfying strain compatibility (linear across the section with plain

section remains plane assumption), material stress-strain relationships, and equilibrium. Although the realistic effective yield curvature of a section can change slightly due to tension stiffening of RC concrete, diagonal cracks and reinforcement bar slip, this study neglects them. The longitudinal boundary reinforcement was assumed to be distributed uniformly with 200 mm spacing, and the longitudinal web reinforcement was assumed to be uniformly distributed with 400 mm spacing (Figure 3.8 (a)). The stress-strain curve for concrete in compression is assumed based on the model proposed by Mander et al. (1988). For reinforcement bars, elasto-plastic relationship with no strain hardening is employed (Figure 3.8 (b), (c)).

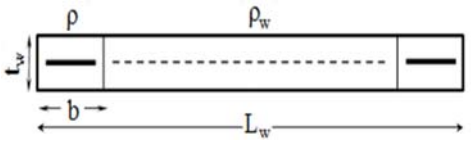

a) Section parameters

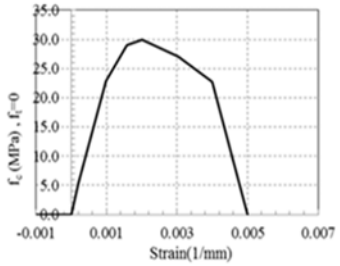

b) Concrete

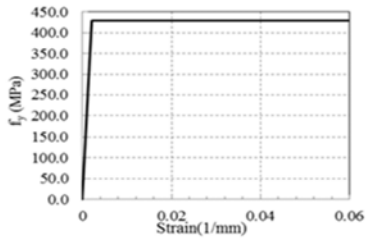

c) Rebar

Parameters	Definition
L_w	Wall length
	4 m , 6 m , 8 m , 10 m
t_w	Wall thickness
	400 mm
b	Boundary length
	$0.1L_w$, $0.2L_w$
ρ	Boundary reinforcement ratio
	0.005-0.01-0.02-0.03
ρ_w	Web reinforcement ratio
	0.0025
$N/(A_g.f_c)$	Axial force ratio
	0.025-0.05-0.075-0.1
f_c	Concrete compressive stress
E_c	Concrete young's modulus
ε_c	Concrete peak strain
	30 MPa
	$Ec=5000\sqrt{f_c}=27386$ MPa
	0.002
f_y	Rebar yield strength
E_s	Rebar young's modulus
	430 MPa
	200000 MPa
cover	Distance to center of first rebar
	50 mm

d) Section analysis variables

Figure 3.8: Moment-curvature analysis and variables definition

The effective yield curvature, ϕ_{yeff}, is obtained from extrapolating the first-yield curvature, ϕ_y to a point where the moment reaches ultimate strength, M_u, assuming elasto-plastic response, or

$$\phi_{yeff}=(M_u/M_y)*\phi_y \quad (3.8)$$

where M_y = moment resistance when first longitudinal rebar located in the boundary zone (lumped at single point in the middle of boundary zone) reaches ε_y (this condition holds true when the applied axial force on wall sections are relatively low) and ultimate (nominal) flexural strength, M_u, is defined as the moment resistance corresponding to a concrete strain of 0.003 at the extreme compression fibre.

Charts are generated to allow rapid estimation of the effective yield curvature of rectangular wall cross sections for a given axial force and section geometry. However, due to space limitation, a few numbers of cases are presented in this study. Each chart plots the effective yield curvature as a function of the axial load level for a number of longitudinal boundary reinforcement ratios, a specified longitudinal web reinforcement ratio, specified concrete compressive strength, and steel reinforcement yield strength. Typical charts are given in Figure 3.9 and Figure 3.10 for a rectangular cross section. For a given axial load level, wall length, longitudinal boundary reinforcement ratio, and longitudinal web reinforcement ratio, the effective yield curvature coefficient can be interpolated between the curves. The bilinear idealization method that is adopted here according to Equation (3.8) may introduce some errors in sections with low percentage of boundary reinforcement and low axial force. For example, while the first yield curvature should increase with increase in axial force ratio, Figure 3.9 and Figure 3.10 show a reduction in effective yield curvature between axial force ratio 0.0 to 0.025 for most cases with 0.5 and 1 percent boundary reinforcement ratio.

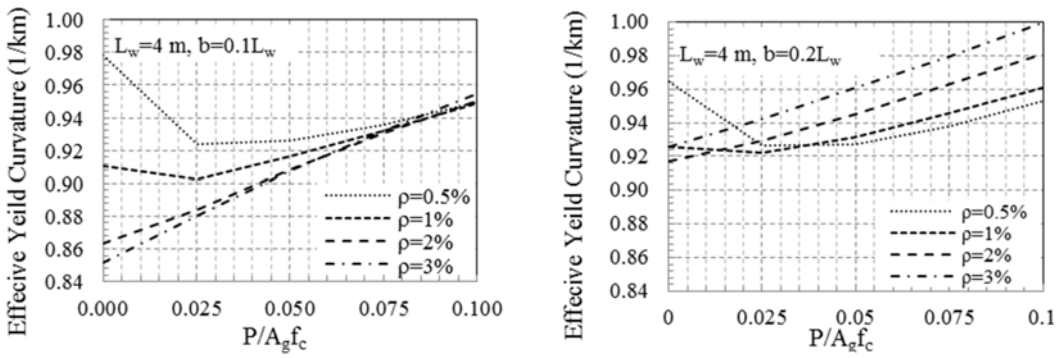

Figure 3.9: Variation of effective yield curvature with different parameters (L_w=4 m and b=0.1-0.2L_w)

From the moment-curvature analyses, it is observed that effective yield curvature is nearly significantly sensitive to the wall length for a given concrete and rebar strength. It is also observed that the rectangular sections with different boundary zone length exhibit similar results for the range of values covered in this study. Figure 3.11 (b) displays the normalized neutral axis depth (measured from extreme compression fibre to zero strain axis) when the section reaches its ultimate strength. It is evident that the value of c_{ub}/L_w varies between 0.08 to 0.2 depending on boundary zone reinforcement and wall length. However, it is insensitive to wall length. Due to minor difference in the value of neutral axis depth for various wall lengths, the differences are not visible in Figure 3.11 (b).

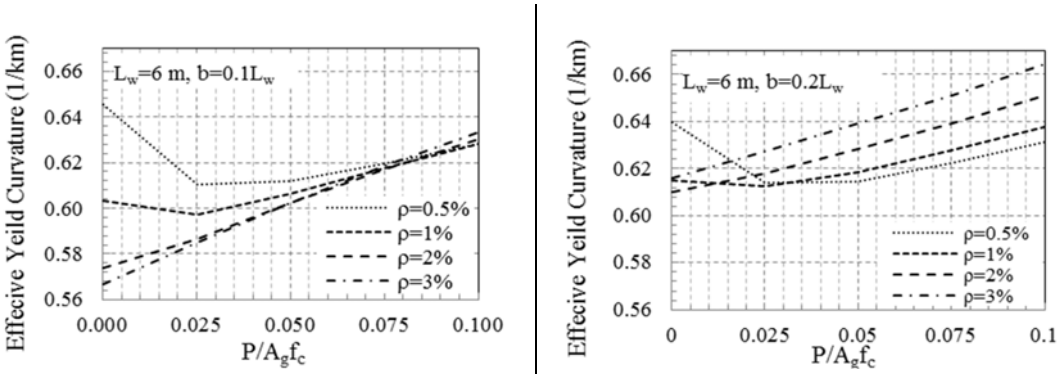

Figure 3.10: Variation of effective yield curvature with different parameters

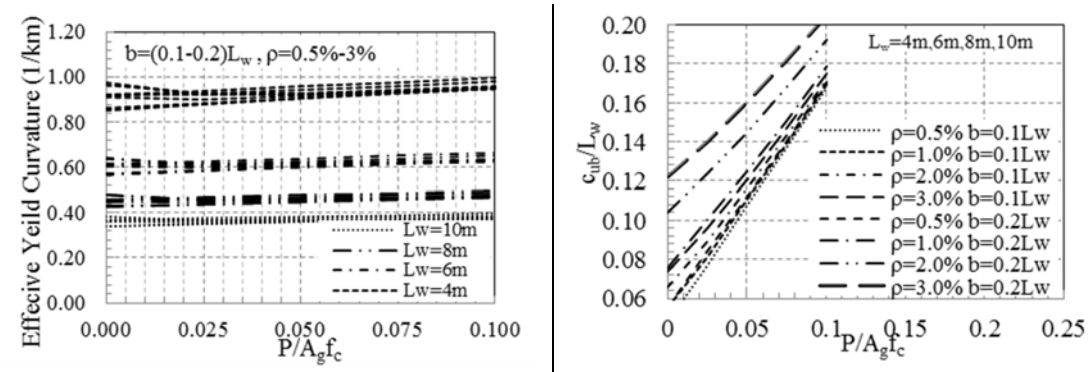

(a) (b)

Figure 3.11: a) Effect of wall length on effective yield curvature b) Variation of neutral axis depth with different parameters at maximum flexural strength

3.2.3 Estimation of Vertical Deformation of Wall Edges

Figure 3.12 demonstrates the detailed procedure to estimate the wall edge deformations in elastic and plastic states. When the base section reaches the effective yield curvature the geometry of the displaced wall is presented in Figure 3.12 (a). The vertical deformation of wall at left (tension) and right (compression) side edges are determined in each story level. Plastic deformation of wall edges due to plastic hinge rotation at the base section presents in Figure 3.12 (b). The total upward or downward deformation of wall edges is equal to:

$$\delta_{ti}=\Delta_{vei}+\Delta_{vpi} \tag{3.9}$$

which δ_{ti} is the total vertical deformation of wall edge at the storey i, Δ_{vei} represents the elastic vertical deformation of wall edge at the storey i and Δ_{vpi} represents the plastic vertical deformation of wall edge at the storey i.

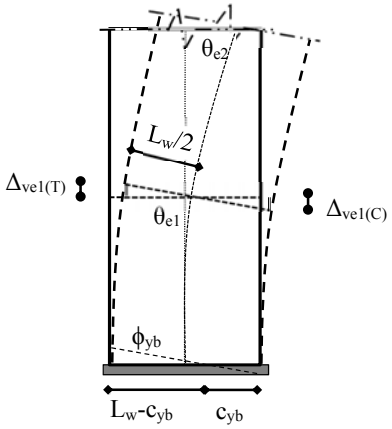

a) Edge deformation when the base curvature reaches the effective yield

Steps to estimate the deformation of wall edges at effective yielding

1) Calculate the effective yield curvature at the base section by Equation 3-8 (or chart)

2) Calculate the rotation distribution at storey level by Equation 3-4

3) Calculate the wall edge deformation as:

$\Delta_{ve1(T)}= \Delta_{ve1(C)}=(L_w/2).\theta_{e1}$ storey 1

$\Delta_{vei\ (T)}= \Delta_{vei\ (C)}=(L_w/2).\theta_{ei}$ storey i

$\Delta_{vei(T)}$, $\Delta_{vei(C)}$: Tension and Compression edge upward and downward deformation

θ_{ei} :Rotation at storey level i

L_w:Wall length

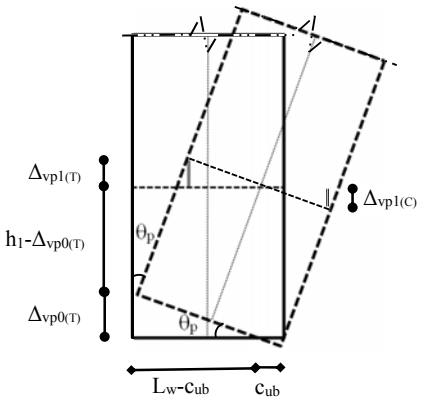

b) Edge plastic deformation

Steps to estimate the plastic deformation of wall edges

1) Calculate the effective yield curvature at the base section by Equation 3-8 (or chart)

2) Calculate ultimate usable curvature by moment-curvature analysis or use NZS1170.5:2004 recommendation and plastic hinge length equal to $0.33L_w$

3) Calculate neutral axis depth (C_{ub}) at maximum flexural strength by moment-curvature analysis or use proposed charts in Figure 3.11 (b).

4) Calculate the wall edge plastic deformation

$\Delta_{vp0(T)}=(L_w-c_{ub}).\theta_p$ $\Delta_{vp0(T)}=(c_{ub}).\theta_p$ base

$\Delta_{vpi(T)}=\Delta_{vp0(T)}-h_i.(1-\cos\theta_p)$ storey i

$\Delta_{vpi(C)}=\Delta_{vp0(C)}-h_i.(1+\cos\theta_p)$ storey i

$\Delta_{vpi(T)}$, $\Delta_{vpi(C)}$: Tension and Compression edge upward and downward plastic deformation

θ_p: Plastic hinge rotation

C_{ub}: Neutral axis depth at maximum flexural strength

h_i: Storey i distance from the base

Figure 3.12: Steps to estimate the elastic and plastic deformation of wall edges

It is important to highlight that storey rotations (and consequently the wall edges deformation) in Figure 3.12 (a) are cumulative summation of curvature below the given storey level, while plastic deformation of wall edges in each storey level is only controlled with base plastic hinge rotation as well as storey distance from the base.

In the proposed procedure the wall edge vertical plastic deformations (denoted as Δ_{vpi}) are estimated based on value of base plastic rotation (θ_p), neutral axis depth (c_{ub}) and floor height (h_i). The challenging part is how to find the plastic rotation of wall base section. The appropriate value of base plastic rotation highly depends on appropriate selection of plastic hinge length and ultimate curvature. It will be discussed in the next section.

3.2.4 Floor Slabs Contribution

To simplify the hand calculation method, two-way slabs in each floor should be replaced with an equivalent elastic beams. In a real structure, slabs subject to out-of-plane deformation due to defamation compatibility in their boundaries in which are connected to the structural walls. Hence, the floor slabs bend not only like beams (they have curvature in both direction) but also subject to torsional warping. However, we assume zero torsional stiffness for slabs to find a simple hand calculation method.

Figure 3.13 shows a representative floor plan in the prototype multi-storey shear wall building. We only consider the system behaviour in Y direction. The equivalent slab width in X and Y direction are assumed quale to half of the bay length. Results of hand calculation method confirms that this is a reasonable assumption. Although various formulations have been proposed in the literature to calculate the effective with of floor slabs, they mostly are proposed to find a good match between the strength obtained from the experimental results and theoretical calculation. Here, the effective widths of floor slabs are required to find the best estimate of shear force transfer to gravity columns via slabs deformation.

Hence, we assume the equivalent width of floor slabs equal to the bay length (half of bay length in each direction). This makes it easy to replace them with an equivalent beam type element. Moreover, it is obvious the deformation of slabs out of their horizontal plane may induce some additional axial forces in the corner columns. Neglecting the contribution of axial force in the corner columns is another assumption which has been adapted in this study.

By assuming the low flexural stiffness for gravity columns, the sub-assemblage which is representing the floor slabs with effective width can be replaced with a beam with a pin on the far end from the wall.

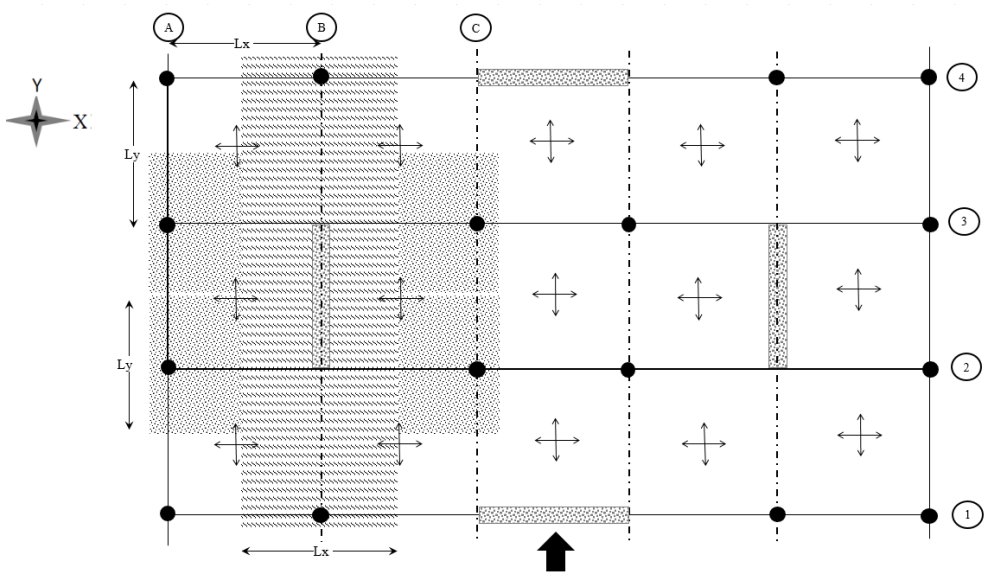

Figure 3.13: Equivalent slab length in a typical floor plan in X and Y direction

The other end of equivalent beam should follow the deformation of wall edges. Hence, the enforced boundary conditions stem from the vertical deformation of wall edges as well as sectional rotation at each floor level. Thus, these vertical and rotational deformations are prescribed as a boundary condition on the equivalent beam where it is connected to the wall. The equivalent width of slabs is chosen equal to centre of the bay length since the gravity columns spanned in equal distance (Figure 3.13).

3.2.5 Maximum Moment Capacity of the System

The additional moment capacity due to axial force in columns in the ultimate limit states can be summarized as in the following formulation. We need to find the wall edges vertical deformation in each storey at effective yield and ultimate limit state.

We rewrite the Equation (3.4) by replacing the $\phi_{base}=\phi_{yeff}$ and z with the variable h_i. Thus, the elastic rotation of each storey obtains by Equation (3.10).

$$\theta_{ei}(z=h_i)=\left(\frac{\phi_{yeff}}{8H^3}h_i^4-\frac{3\phi_{yeff}}{4H}h_i^2+\phi_{yeff}h_i\right) \tag{3.10}$$

The total rotation of each storey is the summation of elastic rotation and plastic rotation in each floor level. Plastic rotation of the base can obtain from Equation (3.11) by employing ultimate usable curvature of base section and plastic hinge length. This formulation is based on simple plastic hinge analysis. In this method, realistic plastic curvature distribution in the critical zone is replaced with an equivalent rectangular plastic curvature. Hence, the Equation (3.11) is employed to estimate the plastic hinge rotation. The effective yield curvature formulation has been already established.

$$\theta_p=(\phi_u-\phi_{yeff})\times l_p \tag{3.11}$$

$$\theta_i=\theta_{ei}+\theta_p \tag{3.12}$$

To find the sectional rotation of structural wall in each floor and the corresponding vertical deformation of wall edges due to arbitrary lateral force, we can use Equation (3.10) and Equation (3.12) along with the procedure are presented in Figure 3.12 which result in wall edges vertical deformation in tension and compression side:

$$\delta_{ti}=\left(\frac{\phi_{eff}}{8H^3}h_i^4-\frac{3\phi_{eff}}{4H}h_i^2+\phi_{yeff}h_i\right)\times\left(\frac{L_w}{2}\right)+(L_w-c_{ub})\times\theta_p-h_i(1-cos\theta_p) \tag{3.13}$$

$$\delta_{ci}=\left(\frac{\phi_{yeff}}{8H^3}h_i^4-\frac{3\phi_{yeff}}{4H}h_i^2+\phi_{yeff}h_i\right)\times\left(\frac{L_w}{2}\right)+(c_{ub})\times\theta_p-h_i(1+cos\theta_p) \tag{3.14}$$

δ_{ti} and δ_{ci} are the total wall edge vertical deformation due to total sectional rotation of structural walls in each floor in tension and compression side respectively. This vertical deformation along with total sectional rotation has been applied as a boundary condition to the adjacent floor slabs or equivalent beams. Figure 3.14 illustrate the application of those deformations as an enforced boundary condition on the equivalent beams in Y and X direction. The boundary conditions in the beam to the gravity columns connections are treated as a pin end without any vertical flexibility. It implies that axial deformation due to induced axial force in gravity columns is overlooked.

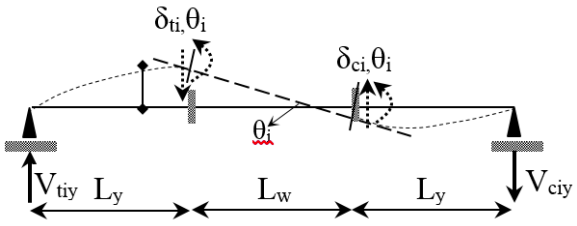

Equivalent beam in Y direction (storey i)

(a)

$V_{tiy}=3EI_{eff}*\delta_{ti}/L_y^3+3EI_{eff}*\theta_i/L_y^2$

V_{tiy}: Left edge (Tension side) shear force in strorey i

$V_{ciy}=3EI_{eff}*\delta_{ci}/L_y^3+3EI_{eff}*\theta_i/L_y^2$

V_{ciy}: Right edge (Compression side) shear force in strorey i

$\delta_{ti}=\Delta_{vei}+\Delta_{vpi}$ $\delta_{ci}=\Delta_{vei}+\Delta_{vpi}$ $\theta_i=\theta_{ei}+\theta_p$

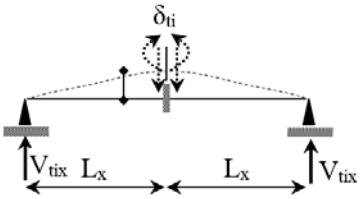

equivalent slab in X direction
(Tension side)
(b)

$V_{tix}=3EI_{eff}*\delta_{ti}/L_x^3$

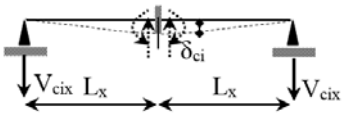

equivalent slab in X direction
(Compression side)
(c)

$V_{cix}=3EI_{eff}*\delta_{ci}/L_x^3$

Figure 3.14: Equivalent beams in X and Y direction and enforced boundary condition due to deformation compatibility

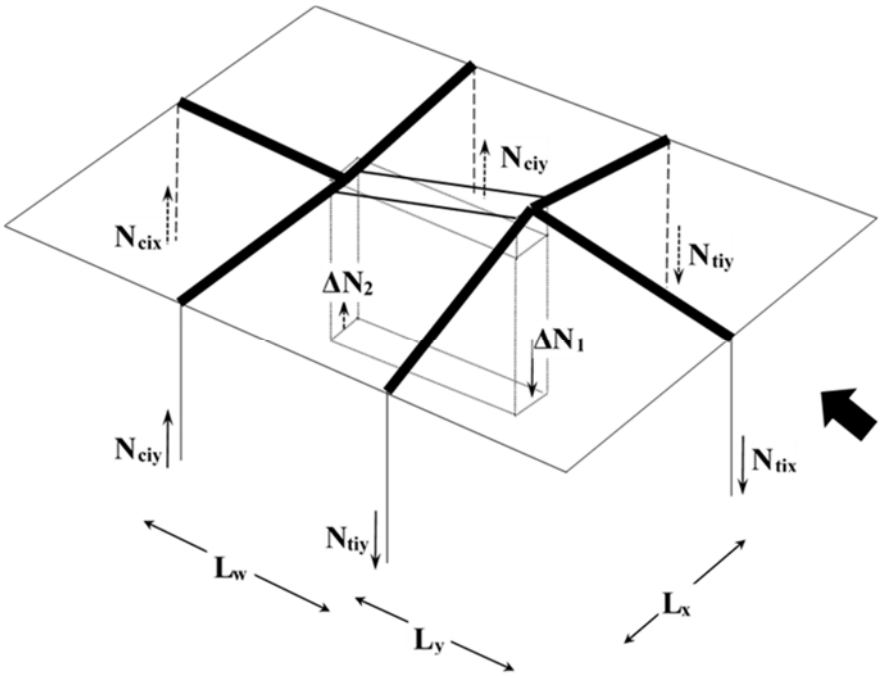

Figure 3.15: Induced axial forces in gravity columns/walls due to structural wall sectional deformation compatibility

Figure 3.15 illustrate a deformed shape of wall cross section in a typical floor of a multi-storey shear wall building. Extra moment capacity due to induced axial force in gravity columns can be estimated in each storey. Figure 3.15 demonstrates the schematic spatial representation of induced actions in the gravity columns. They generate additional storey moments in the each storey. This extra moment capacity is obtained by multiplying the axial force in the columns by their distance from centre of wall section. Figure 3.16 present step by step procedure to find the induced actions in gravity columns due to enforced boundary conditions on the equivalent beams. The proposed procedure accounts for the differences in the value of boundary conditions in the each storey level. The induced actions in tension and compression side of structural walls are estimated separately. The summation of all storey moments gives the total base moment resistant of the system as indicated in Equation (3.15).

$$\sum_{i=1}^{n} M_{col} = \sum_{i=1}^{n}\left(\frac{3EI_{eff}\delta_{ti}}{L_y^3} + \frac{3EI_{eff}\theta_i}{L_y^2}\right)(L_y + L_w/2) + \sum_{i=1}^{n}\left(\frac{3EI_{eff}\delta_{ti}}{L_x^3}\right)\left(\frac{L_w}{2}\right) \times 2 +$$

$$\sum_{i=1}^{n}\left(\frac{3EI_{eff}\delta_{ci}}{L_y^3} + \frac{3EI_{eff}\theta_i}{L_y^2}\right)(L_y + L_w/2) + \sum_{i=1}^{n}\left(\frac{3EI_{eff}\delta_{ci}}{L_x^3}\right)\left(\frac{L_w}{2}\right) \times 2 \qquad (3.15)$$

This additional moment capacity of system at ultimate limit state can be normalized to the nominal wall flexural strength in order to establish the system overstrength as below:

1) Calculate effective width of slabs in X and Y direction respectively : L_x and L_y

2) Calculate shear force induced in the equivalent slab element in X direction at storey i:

$V_{tix}= (3EI_{eff}* \delta_{ti}/L_x^3)$, $V_{tix}= (3EI_{eff}* \delta_{ci}/L_x^3)$

3) Calculate shear force induced in the equivalent slab element in Y direction at storey i:

$V_{tiy}=(3EI_{eff}*\delta_{ti}/L_y^3+3EI_{eff}*\theta_i/L_y^2)$, $V_{ciy}=(3EI_{eff}*\delta_{ci}/L_y^3+3EI_{eff}*\theta_i/L_y^2)$

4) Calculate total axial force in the storey columns in X direction:

$N_{tix}=\sum V_{tix}$, $N_{tix}=\sum V_{tix}$

5) Calculate total axial force in the storey columns in Y direction:

$N_{tiy}=\sum V_{tiy}$, $N_{ciy}=\sum V_{ciy}$

6) Calculate the storey moment of system due to axial force in the storey columns in X direction:

$M_{tix}= N_{tix} *(L_w/2)$ and $M_{cix}= N_{cix}*(L_w/2)$

7) Calculate the storey moment of system due to axial force in the storey columns in Y direction:

$M_{tiy}= N_{tiy} *(L_y+L_w/2)$

$M_{ciy}= N_{ciy} *(L_y+L_w/2)$

8) Calculate the total storey moment of system due to axial force in the storey columns:

$M_{tit}(T)= M_{tix} + M_{tiy}$

$M_{cit}(C)=M_{cix} + M_{ciy}$

$M_i = M_{tit}(T) + M_{cit}(C)$

9) Calculate additional shear demand introduced to the structural walls due to axial force in the storey columns $V_i= M_i/h$

Figure 3.16: Proposed steps to calculate the induced actions due to deformation compatibility of slabs in each storey

$$\Omega_s = \frac{M_{wall-nominal}+M_{wall-hardening}+\sum_{i=1}^{m} M_{col}}{M_{wall-nominal}} \tag{3.16}$$

$$\Omega_s = 1 + \frac{M_{wall-hardening}}{M_{wall-nominal}} + \frac{\sum_{i=1}^{n} M_{col}}{M_{wall-nominal}} = 1.25 + \frac{\sum_{i=1}^{n} M_{col}}{M_{wall-nominal}} \tag{3.17}$$

This normalization is adopted only in the hand calculation method. However, in the finite element analysis, hardening flexural strength automatically included in the model by employing material laws for strain hardening of rebar and confinement effect of concrete. To comparison in a consistent manner, the value of material overstrength in hand calculation is assumed 25% higher than nominal flexural strength of walls. This procedure implies a consistent comparison between finite element method and simplified method. The reliable value of Ω_s (additional moment capacity due to wall and floor slab interaction) should be quantified for different typical simple and complex configuration of multi-storey shear wall buildings. This could be a critical value when capacity design against the shear failure is desired in the structural walls.

3.3 Hand Calculation Approach

The proposed simplified formulation are applied to a building prototype with the same slab length in two directions equal to 6 m and effective flexural stiffness equal to 0.25EIg which later has been named case 2.

3.3.1 Estimation of the Wall Edges Vertical Deformation and Sectional Rotation

For the designed wall sections in the prototype buildings the effective yield curvature, the yield moment and the effective flexural stiffness are obtained ($\phi_{yb}= \phi_{yeff}$ =0.63 1/km, M_{yb}=35780 kN.m , I_{eff}=1.902 m^4 , I_{eff}/I_g=0.265) respectively. Thus, the curvatures and the elastic rotations of the wall in each story level are calculated by employing the proposed method. The calculated values are shown in Table 3-3. When the nonlinear behaviour of the structural walls is of interest, due to movement of neutral axis as well as base plastic rotation, relatively large vertical displacement occurred at the wall edges in each story. It is very important to consider that the vertical displacement of wall edges increases with the height of the floor from the base. For

example, the total vertical deformation in the tension side is equal to 113.511mm at roof level this value for first storey is equal to 103.35 mm.

It is apparently evident from the values in Table 3-3 that the most significant wall edges deformation is occurred in nonlinear stage. For example, the elastic and plastic vertical deformation in the tension side and compression side in roof level is equal to 93.063 mm and 20.448 mm respectively. Hence, it is very critical to assess the effect of this behaviour in the design or assessment at ultimate limit state. In the following section, five prototype buildings are analysed to scrutinize the effect of explained three-dimensional spatial effects of slabs on the system behaviour.

3.3.2 Calculation of Induced Actions

In this section, based on the values calculated for the vertical deformation of wall edges in tension and compression side as well as sectional rotation (Table 3-3), the induced actions are calculated in each storey by employing proposed method. Table 3-3 presented the value of axial force and their corresponding moments in each storey level. We sum up all the storey moments to obtain the extra base moment capacity. Table 3-6 summarizes the total base moment in each storey level and it is shown that the system-over strength is equal to 1.7 in this particular system.

Table 3-3: Elastic and plastic vertical displacement of wall edges for case 2

Storey section	**0 (Base)**	**1**	**2**	**3**	**4**	**5**	**6**	**7**	**8 (Roof)**
Curvature(φ_i) (1/km)	0.71	0.7105	0.7151	0.7281	0.7536	0.7957	0.8585	0.9464	1.064
Θ_{ei} (rad)	0	0.0020	0.0037	0.0049	0.0058	0.0064	0.0067	0.0068	0.0068
Δ_{vei}(T) (mm)	0	6.1787	11.102	14.831	17.466	19.145	20.048	20.396	20.448
Δ_{vei}(C) (mm)	0	6.1787	11.102	14.831	17.466	19.145	20.048	20.396	20.448
Θ_p(rad)	0.0192	-	-	-	-	-	-	-	-
Δ_{vpi} (T) (mm)	-	97.767	97.179	96.592	96.003	95.415	94.827	93.651	93.063
Δ_{vpi}(C) (mm)	-	16.665	16.077	15.489	14.901	14.313	13.725	13.137	12.550
δ_{ti} (mm)	-	103.35	107.69	110.83	112.88	113.97	114.28	114.04	113.51
δ_{ci} (mm)	-	22.844	27.179	30.320	32.367	33.458	33.774	33.534	32.997

Table 3-4: Extra moment due to induced actions in gravity columns in each storey for case 2

Tension Edge / Storey	$\delta_{i(T)}=\Delta_{vei}+\Delta_{vpi}$ (m)	θ_i (rad)	V_{tiy} (kN)	V_{tix} (kN)	$N_{tiy}=\sum(V_{tiy})$ (kN)	$N_{tix}=\sum(V_{tix})$ (kN)	M_{tiy} (kN.m)	M_{tix} (kN.m)	$M_{tit(T)}$ (kN.m)
8	0.11350	0.026	113.81	47.93	-113.81	-47.93	1024.33	287.61	371.09
7	0.11405	0.026	114.00	48.16	-227.82	-96.10	2050.34	576.60	744.95
6	0.11429	0.026	113.81	48.27	-341.63	-144.37	3074.65	866.21	1120.07
5	0.11397	0.025	112.92	48.14	-454.55	-192.51	4090.92	1155.05	1493.62
4	0.11288	0.025	111.04	47.68	-565.59	-240.19	5090.30	1441.15	1861.69
3	0.11083	0.024	107.96	46.82	-673.54	-287.01	6061.89	1722.07	2219.42
2	0.10769	0.023	103.48	45.50	-777.02	-332.51	6993.21	1995.06	2561.27
1(Total)	0.10335	0.021	97.49	43.67	-874.51	-376.18	7870.62	2257.07	2881.18

Table 3-5: Extra moment due to induced actions in gravity columns in each storey for case 2 (Cont'd)

Compression Edge / Storey	$\delta_{i(C)}=\Delta_{vei}+\Delta_{vpi}$ (m)	θ_i (rad)	V_{ciy} (kN)	V_{cix} (kN)	$N_{ciy}=\sum(V_{ciy})$ (kN)	$N_{cix}=\sum(V_{cix})$ (kN)	M_{ciy} (kN.m)	M_{cix} (kN.m)	$M_{cit(C)}$ (kN.m)
8	0.0330	0.026	79.79	13.91	79.79	13.91	718.15	83.49	371.09
7	0.0335	0.026	79.98	14.14	159.78	28.06	1437.98	168.36	744.95
6	0.0338	0.026	79.79	14.25	239.57	42.31	2156.11	253.85	1120.07
5	0.0335	0.026	78.90	14.12	318.47	56.43	2866.20	338.57	1493.62
4	0.0324	0.025	77.02	13.66	395.49	70.09	3559.40	420.55	1861.69
3	0.0303	0.024	73.94	12.80	469.42	82.89	4224.81	497.35	2219.42
2	0.0272	0.023	69.46	11.48	538.88	94.37	4849.95	566.22	2561.27
1(Total)	0.0228	0.021	63.47	9.65	602.35	104.02	5421.18	624.11	2881.18

Table 3-6: System overstrength due to interaction for case 2

Storey	M_i (total moment) (kN.m)	Ω_{si}
8	2113.58	
7	4233.27	
6	6350.83	
5	8450.74	
4	10511.39	
3	12506.13	
2	14404.44	
1(Total)	16172.99	1.45+0.25=1.70

3.4 Finite Element Modelling

Three-dimensional nonlinear finite element models are built using SAP2000 (CSI, 2014) for the prototype buildings to obtain their capacity curves. The seismic mass at all floors was

assigned as distributed mass on walls. A rigid diaphragm is incorporated by slaving the translational degrees of freedom at each floor level. The foundation of the building was assumed as rigid, and P-delta effects are taken into account.

Nonlinear shell elements representing the in-plane behaviour of RC panels were used to model the rectangular walls. The confined and unconfined concretes were modelled differently, but the tensile strength of concrete was neglected. Concrete stress-strain relationship was based on Mander model (Mander et al., 1988) as shown in Figure 3.17 (a). The steel reinforcement stress-strain was as shown in Figure 3.17 (b). Shear behaviour was modelled using the automated inelastic shear layer in SAP2000 for nonlinear shell element.

Slabs are modelled as elastic shell elements with stiffness values of $EI_{eff} = 0.25EI_g$ (flexural) and $GA = 0.5GA_g$ (shear). All slabs are assigned a specified concrete strength of $f'_c = 30$ MPa. Shear modulus (G) is calculated using a Poisson's ratio $\nu = 0.2$.

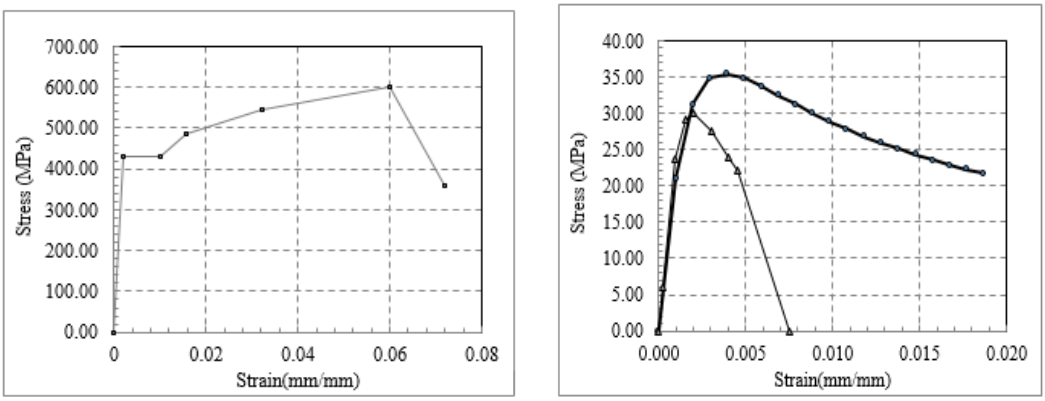

(a) (b)

Figure 3.17: Material stress-strain backbone curves; a) Reinforcement b) Concrete

The columns are modelled as elastic beam elements with very low flexural stiffness. The elastic properties of the columns are calculated using the cross-section dimensions and the stiffness modification factors; i.e. $EI_{eff} = 0.01EI_g$ (flexural), $GA = 1.0GA_g$ (shear). This approach can give us a transparent comparison between the models without interaction (case 1) and those with interactions (case 2 to case 5).

3.5 Analysis Method and Results

Generally, the accuracy of pushover analysis in representing the structural seismic performance is debatable. Although distribution of load pattern in the pushover analysis should be updated instantaneously due to stiffness variation during the analysis (due to cracking, yielding and force redistribution) of system, this study has adopted the constant load pattern up to end of analysis. However, this simple method provides a useful understanding of the expected behaviour of the structures. Therefore, this study is based on the pushover analysis results. Primarily, lateral forces are applied to a group of selected prototype buildings in line with FEMA-450 guideline. As per FEMA-450 recommendations the lateral force are proportion to the product of the mass and height considering the effects of the higher modes. Later, the pushover curves obtained from the analysis are idealized according to FEMA-695 approach. All analyses are performed with a gravity load of P=1.0D+0.25L.

The simplified hand calculation method which is proposed to account for system overstrength is verified for the five different cases. The slab flexural stiffness and geometrical dimensions of these cases are listed in Table 3-7. Typical floor plan and geometry of prototype buildings have been already defined in the previous section, Figure 3.2 and Table 3-1. In all case studies, the structural wall properties keep the same while the floor slab bay length and/or their flexural stiffness are varied.

Table 3-7: Variables for different case studies

Case	slab flexural stiffness	slab length in X direction(Lx)(m)	slab length in Y direction(Ly)(m)
1	0	6	6
2	$0.25EI_g$	6	6
3	$0.25EI_g$	6	8
4	$0.25EI_g$	8	6
5	$0.50EI_g$	6	6

To scrutinize the application of the proposed simplified formula for overstrength estimation, the overstrength of above case studies is calculated by employing the simplified hand calculation method as well as finite element approach. Cases 3 and 4 are selected to represent the effect of change in length of slabs (bay) in x and y directions, respectively. The out-of-plane stiffness of these two cases is the same as case 2. In case 5, the length of slabs is equal to case 1 while the flexural out-of-plane stiffness of slab is doubled.

From the above mentioned case studies two examples (case 1 and case 2) are selected and their response parameters are investigated in the specific drift levels including their yielding points. The results of displacement control pushover analysis for the first two cases are compared in Figure 3.18. To find the effective period of building, the estimated capacity curve should be idealized to obtain the equivalent single degree of freedom. Detailed description of converting the multiple degrees of freedom capacity curve to the equivalent single degree of freedom capacity curve can be found in ATC-40. It is evident from Figure 3.18 that case 2 demonstrates considerable overstrength due to contribution of slabs in the system response. It is also obvious that the system overstrength is drift-dependent. The difference between the two pushover curves demonstrates that the slab out-of-plane stiffness starts contributing to the overall strength of the system significantly when the structural walls gradually enter the inelastic range due to reinforcement yielding at boundary elements.

At the roof displacement of 495 mm (equal to 1.95% drift ratio), the ratio of base shear in case 2 (6058 kN) to case 1 (4225 kN) is equal to 1.44. Various methods have been proposed in the literature to obtain the significant yielding point on the capacity curve. In this chapter, significant yield point is established when all reinforcement in the boundary element yield in tension or when the first boundary element in the mathematical model reached yielding state The contribution of slab on base shear resistance at yielding point is approximately 23% larger in case 2 than in case 1 with no interaction. Case 1 obtains the maximum system overstrength

equal to 1.24 at 2.7% drift. However, maximum overstrength in case 2 is found to be 1.52 at 2.3% drift. While overstrength of case 1 is attributed mainly to strain hardening and confinement of concrete in the critical section, case 2 benefits much more from the contribution of slab in resisting the lateral force.

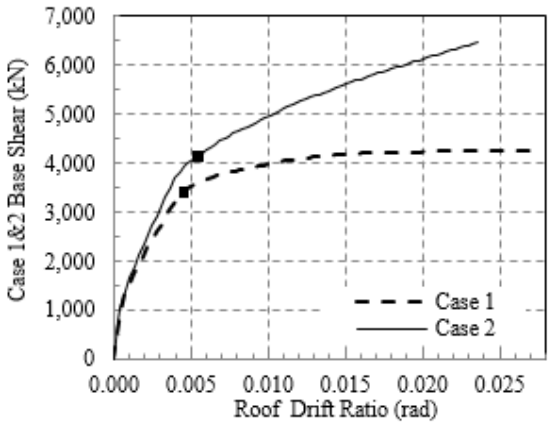

Equivalent SDOF

Case 1:	**Case 2:**
▪ Significant yielding point (0.118 m , 3450.3kN) ▪ First mode mass participation factor=0.67 ▪ Total seismic mass=3703.68 kN.s^2/m ▪ S_a/g=0.1349 ▪ S_d=0.080 m ▪ Effective fundamental period=1.52 s ▪ Ultimate strength=4258.78 kN ▪ Ultimate strength /yield strength =1.24	▪ Significant yielding point (0.153 m , 4254.3kN) ▪ First mode mass participation factor=0.67 ▪ Total seismic mass=3703.68 kN.s^2/m ▪ S_a/g=0.1444 ▪ S_d=0.10 m ▪ Effective fundamental period=1.56 s ▪ Ultimate strength=6457.5 kN ▪ Ultimate strength /yield strength =1.52

Figure 3.18: Case 1 and 2 pushover analysis

While system including slabs should be stiffer than without slabs the estimated period of building without slabs (case 2) are slightly less than case 1. It demonstrates a shortcoming in the simple idealization method employed in the study.

More investigation has been conducted on the remaining cases to verify the application of simplified hand calculation method. The numerical analyses result also is employed to address the importance of bay length as well as the flexural stiffness of slabs on the system-over strength factor.

The error and calculate values for all cases presented in Table 3-8. It demonstrates that in a few case studies were examined in this chapter; the overall error in estimation of overstrength values is approximately on average 12 percent.

Table 3-8: Comparison of simplified and finite element method

Case	$\Omega_{\text{Finite element}}$	Ω_{simple}	Error
1	0	0	0
2	1.91	1.70	11.5%
3	1.836	1.565	14.7%
4	1.843	1.655	10.2%
5	2.420	2.154	11.2%

Three main assumptions may alter the predicted values: First, the simplified method overlooks the presence of corner columns as one of the boundary conditions around the slabs. Second, the effective width of slabs is assumed equal to bay length in proposed equations. Third, any variation in amount of axial force on the structural wall itself neglected in hand calculation method. It seems that both assumptions are crude and they require further investigation. The equivalent slab length can be changed to find the best agreement with the finite element calculation. However, to achieve robust values for the system overstrength the different arrangement of structural walls and floor slabs should be represented in the model.

3.6 Conclusions

This chapter has explored the effect of wall-slab-gravity system interaction on the overall behaviour of shear wall building systems. It has been re-confirmed through analytical and numerical investigation that the out-of-plane stiffness of slabs can induce some additional axial forces in gravity columns and this interaction can increase the system moment capacity and the corresponding overstrength of the whole structure. In the all case study buildings the system-overstrength varied from 1.9 to 2.5 due to presence of slabs. However, it was also demonstrated that the doubling the out-of-plane stiffness of slabs can increase the system overstrength by 27%. Changing the bay length from 6 m to 8 m in the any direction would reduce the system-over strength only 5 %. It seems that value of Ω_s mostly depends on the flexural stiffening of slabs to a large extent and bay length to a smaller extent. In capacity design philosophy, this overstrength may affect the strength hierarchy of different failure modes of the structural walls mainly due to additional shear force demand induced in the different storeys of the structural walls. This system interaction effect requires additional allowance in base shear demand calculation and shear force envelope proposed for the structural walls.

3.7 References

Aktan, A. E., and Bertero, V. V. (1984). Seismic response of R/C frame-wall structures. *Journal of Structural Engineering*, *110*(8), 1803-1821.

ATC-40 (1996). *Seismic evaluation and retrofit of concrete buildings*. Redwood City, California: Applied Technology Council, Seismic safety commission.

Bertero, V., Aktan, A. E., Charney, F., and Sause, R. (1984). Earthquake simulator tests and associated experimental, analytical, and correlation studies of one-fifth scale model. ACI Special Publication, 84. 375-424

Building Seismic Safety Council (2004). *NEHRP recommended provisions for seismic regulations for new buildings and other structures* (FEMA 450). Retrieved from https://www.nehrp.gov/pdf/fema450provisions.pdf.

Elnashai, A. S., and Mwafy, A. M. (2002). Overstrength and force reduction factors of multistorey reinforced□concrete buildings. *The structural design of tall buildings*, *11*(5), 329-351.

FEMA 695 (2009). *Quantification of building seismic performance factors*. Washington, DC: Fedearl Emergency Management Agency.

Humar, J. L., and Rahgozar, M. A. (1996). Concept of overstrength in seismic design. *Eleventh world conference on earthquake engineering*. 639, 1-8. Retrieved from http://www.iitk.ac.in/nicee/wcee/article/11_639.PDF .

Kabeyasawa, T., Shiohara, H., Otani, S., and Aoyama, H. (1983). Analysis of the full-scale seven-story reinforced concrete test structure. *Journal of the Faculty of Engineering*: *University of Tokyo, 37*(2), 431-478.

Mander, J. B., Priestley, M. J., and Park, R. (1988). Theoretical stress-strain model for confined concrete. *Journal of structural engineering*, *114*(8), 1804-1826.

Mitchell, D., and Paultre, P. (1994). Ductility and overstrength in seismic design of reinforced concrete structures. *Canadian Journal of Civil Engineering*, *21*(6), 1049-1060.

Nassar, A. A., and Krawinkler, H. (1991). *Seismic demands for SDOF and MDOF systems* (Report No. 95). California: Stanford University, Blume Earthquake Engineering Center, Department of Civil Engineering.

New Zealand Society for Earthquake Engineering (NZSEE), (2006). *Assessment and Improvement of the Structural Performance of Buildings in Earthquake*. The New Zealand Society for Earthquake Engineering.

NZS1170.5 (2004). Concrete Structures Standard, NZS 1170.5:2004 Parts 1 and 2 Standards New Zealand.

NZS3101 (2006). Concrete Structures Standard, NZS 3101:2006 Parts 1 and 2 Standards New Zealand.

Panagiotou, M., Restrepo, J. I., and Conte, J. P. (2010). Shake-table test of a full-scale 7-story building slice. Phase I: Rectangular wall. *Journal of Structural Engineering*, 137(6), 691-704.

Park, R. (1996). Explicit incorporation of element and structure overstrength in the design process. *Proceedings of the 11th WCEE. IAEE.* Acapulco, Mexico.

Priestley, M. J. N. (1997). Displacement-based seismic assessment of reinforced concrete buildings. *Journal of earthquake engineering*, *1*(01), 157-192.

Priestley, M. J. N., Calvi G. M., and Kowalsky M. J. (2007). *Displacement-based seismic design of structures*. Pavia, Italy: IUSS Press.

SAP2000, CSI, S. (2014): Ver. 17.1.1, integrated finite element analysis and design of structures basic analysis reference manual. Berkeley (CA, USA), Computers and Structures INC.

4 Parametric Study to Investigate the Effect of Wall-Slab and Gravity Columns Interaction

4.1 Introduction

This chapter attempts to investigate system overstrength in multi-storey reinforced concrete (RC) wall buildings with the floor slabs in twenty-two different cases of lateral-load-resisting systems: (i) case 1-1 (wall only) has concrete structural walls only (zero out-of-plane flexural stiffness of slabs); and (ii) the remaining cases have concrete rectangular shear walls with slabs having different section flexural stiffness and/or varying bay lengths. This study intends to investigate effects of bay length and out-of-plane sectional stiffness of slabs on the system overstrength factor of shear wall buildings in the in-plane direction of walls as well as structural wall overstrength factor. It also presents the results from a finite element analysis and discusses the influence of modelling RC floor slab elements on the predicted performance of shear wall buildings. To understand the effect of building height on the system overstrength factor the geometry and specification of above case studies extended to the buildings with 5 and 10 storeys to explore the effect of height on the system overstrength factor.

4.2 Variables Related to Wall-Frame-Slab Interaction

In the previous chapter, a detailed description of the spatial interaction between the floor system, structural walls and frames were presented. Since a large number of variables are involved in this mechanism, this chapter seeks to explore and to quantify the contribution of different parameters involved in system interaction mechanism. Then, the result of different case studies compared with the base case building (Case1-1) to determine the contribution of each parameter on the system overstrength factor as well as amount of induced axial force in structural walls and gravity columns.

While the floor slabs running in parallel to the structural walls act more like an equivalent flexural beam, the floor slabs running perpendicular to the structural walls act more like

equivalent flexural/torsional beams each with different boundary condition. Hence, the bay length in either direction varied to investigate the effect of the length factor.

Furthermore, very stiff floor systems can induce more vertical forces in their boundary condition (gravity frames). Thus, different values are assigned as an out-of-plane stiffness of floor systems to find the variation of system overstrength factor and induced axial forces in columns and walls.

Another key variable in the spatial system interaction is attributed to the building height. Effect of building height can be seen from two different viewpoints. First, the induced axial force in frames due to system interaction is accumulated from the top to the bottom of the building. Second, the vertical plastic deformation at the wall edges being increased with the height. Therefore, the first group of case studies was re-analysed with two different heights.

4.3 Description of Case Studies

An eight-story building with a floor plan of 30 m by 18 m is used as the reference building. Typical floor plans, sections and design parameters are illustrated in Figure 4.1. The gravity system of the building consists of 200 mm thick RC slabs and circular (500 mm diameter) RC columns. Twenty-two cases are used in this study; the same structural wall thickness is used in all cases. Typical story height is assumed to be 3.20 meter. The building is designed based on the design provisions which were defined in the NZ concrete structures standard (NZS3101:2006) and the NZ loading standard (NZS1170.5:2004). Prototype buildings are assumed to be located in Christchurch on Soil type C. The Seismic mass of each floor is calculated as 4542.3 KN (Figure 4.1). The effective design period (for the ultimate limit state, ULS) of the buildings is estimated via eigenvalue analysis with stiffness values for all elements as recommended in NZS3101:2006. Three-dimensional, nonlinear finite element models are

developed in SAP2000 for all prototype buildings (building with and without interaction) using consistent modelling approaches.

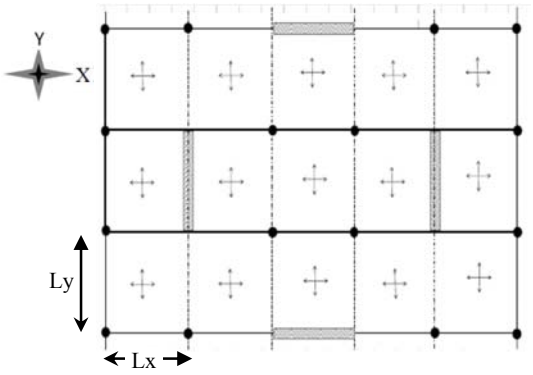

Building Floor Plan

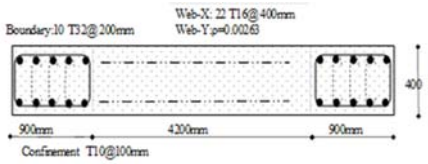

Wall Base Section

Rectangular wall section	6000 x 400 mm	Near fault factor	1
Typical floor height	3.20 m	Seismic weight on each wall	4542.3 kN
f_c	30 MPa	Soil type	C
f_{yl} , f_{yh}	430 MPa , 300 MPa	Near fault factor	1.0
Gravity columns dimension	D500 mm	Zone factor	0.4
Slab thickness	200 mm	Return period factor	1.0
Gravity load on each wall(base)	$0.08f_cA_g$	Structural ductility	5

Figure 4.1: Building plan and design information

Table 4-1, Table 4-2 and Table 4-3 provide the properties of three groups of case study buildings in this chapter.

Table 4-1: Variables in the first group case studies

Case	Slab flexural stiffness	Slab length in X direction(L_x)(m)	Slab length in Y direction(L_y)(m)
1-1/wall only	0	6	6
2-1	$0.25EI_g$	6	6
3-1	$0.25EI_g$	6	4
4-1	$0.25EI_g$	6	8
5-1	$0.25EI_g$	4	6
6-1	$0.25EI_g$	8	6
7-1	$0.25EI_g$	4	4
8-1	$0.25EI_g$	8	8

Table 4-2: Variables in the second group case studies

Case	Slab flexural stiffness	Slab length in X direction(L_x)(m)	Slab length in Y direction(L_y)(m)
2-2	$0.50EI_g$	6	6
3-2	$0.50EI_g$	6	4
4-2	$0.50EI_g$	6	8
5-2	$0.50EI_g$	4	6
6-2	$0.50EI_g$	8	6
7-2	$0.50EI_g$	4	4
8-2	$0.50EI_g$	8	8

Table 4-3: Variables in the third group case studies

Case	Slab flexural stiffness	Slab length in X direction(L_x)(m)	Slab length in Y direction(L_y)(m)
2-3	$0.10EI_g$	6	6
3-3	$0.10EI_g$	6	4
4-3	$0.10EI_g$	6	8
5-3	$0.10EI_g$	4	6
6-3	$0.10EI_g$	8	6
7-3	$0.10EI_g$	4	4
8-3	$0.10EI_g$	8	8

4.3.1 Definition and Parameters

The floor slab-wall-gravity column interaction can change not only the system overstrength significantly but also can alter the structural wall behaviour itself. In this section, the effect of bay (or slab) lengths as well as sectional flexural stiffness of slabs on the system response and the structural walls will be addressed. The first step is how to define the main variables in the force-displacement response of the whole system and the structural wall itself. Thus, we need to find the resistance of system in terms of base moment (representative of the force resistance) versus wall base rotation (representative the controlled displacement) for the whole system as well as the structural wall itself. Hence, the base moment versus the base rotation curves for the whole system and the structural wall are investigated separately. Firstly, it is essential to establish the different source of moment resistant in the whole system. Figure 4.2 illustrates the four different components which are contributing to the moment resistance of the whole system. The curve 1 in Figure 4.2 displays the moment resistance of system due to presence of structural wall with zero hardening in the post-elastic range. Curve 2 illustrates the additional strength of system due to the post-elastic hardening. Hardening part of resistance stems from difference between first yielding strength (it is highly dependent on the idealizing procedure adopted in the model) and full yielding strength of the wall critical section. Hence, enhancement of section flexural strength due to the strain hardening of reinforcement rebars and confined concrete is very important to find the slope of this curve. Curve 3 is the representative of resistance originated from remaining secondary elements available in the system including gravity columns and slabs. It is important to highlight that contribution of slabs and gravity columns in the moment resistance starts from beginning of analysis even in the linear stage. However, we will observe that their contribution to the global response increases significantly after yielding of reinforcement rebars in the structural walls. The last component of moment in the system attributed to the destabilization effect of P-Δ actions in

the system response (curve 4). In other words, to obtain the true moment resistance of the system one should reduce the moment generated in the system due to P-Δ effects. When a system enters to nonlinear stage, gravity force (any axial loads) can induce larger moment demand on the system compared to the linear stage.

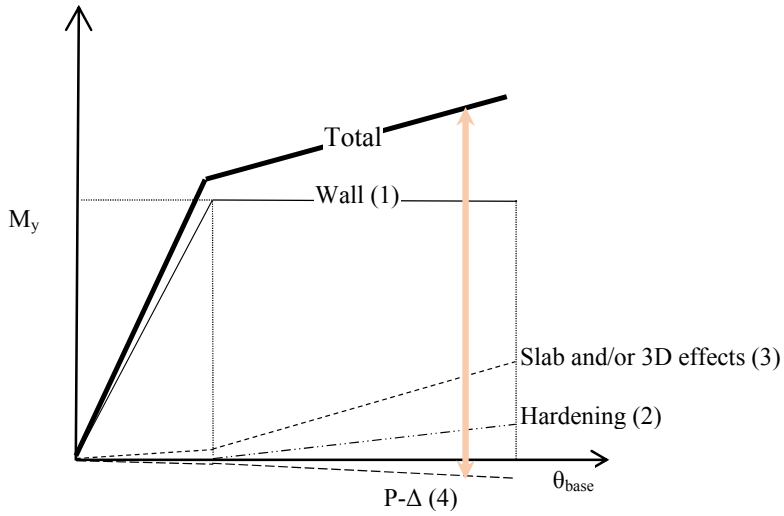

Figure 4.2: Different components of system moment resistance

Figure 4.3 (a) and (b) illustrate the base moment versus base rotation for the whole system and the structural wall in the two different cases. For a given out-of-plane stiffness of slabs and bay (slab) length, the yielding point of whole system and structural wall itself may change due to the system interaction. Moreover, the interaction also increases the post-elastic stiffness (slope) of the whole system after the yielding point. The importance of this interaction has been addressed quantitatively in the next section. Various methods have been proposed in the literature to obtain the significant yielding point on the capacity curve. In this chapter, significant yield point is established when all reinforcement in the boundary element yield in tension or when the first boundary element in the mathematical model reached the yielding state.

The whole system-over strength of Case2-1 (as an example case) (Ω_{sa2}) is expressed as:

$$\Omega_{sa2\text{-}1}=M_{us2\text{-}1\text{-}base}/M_{ys2\text{-}1\text{-}base} \quad (4.1)$$

where $M_{us2\text{-}1\text{-}base}$ is the ultimate moment strength of the whole system for Case2-1, $M_{ys2\text{-}1\text{-}base}$ is the effective yielding moment strength of the whole system for Case2-1.

In the similar way, the net contribution of slabs (through the gravity columns) to the moment resistance of the whole system in Case2-1 can be quantified as:

$$\Omega_{sr2\text{-}1}= (M_{us2\text{-}1\text{-}base} - M_{uw2\text{-}1\text{-}base})/M_{ys2\text{-}1\text{-}base} \quad (4.2)$$

where $M_{us2\text{-}1\text{-}base}$ and $M_{ys2\text{-}1\text{-}base}$ have the same definition as in Equation (4.1) and $M_{uw2\text{-}base}$ is the ultimate strength of the structural wall for Case2-1.

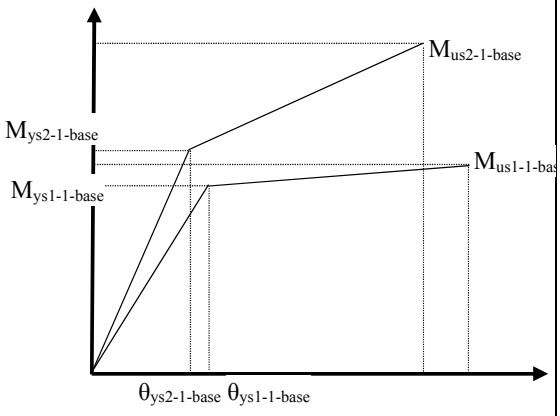

Whole system behavior for the two different cases (Case2-1 and Case1-1)

$\Omega_{sa2}=M_{us2\text{-}base}/M_{ys2\text{-}base}$

$\Omega_{sr2}=(M_{us2\text{-}base} - M_{uw2\text{-}base})/M_{ys2\text{-}1\text{-}base}$

(a)

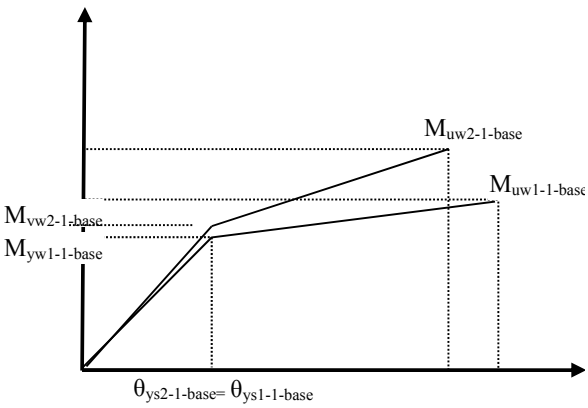

Structural wall behavior in the system for the two different cases (Case2-1 and Case1-1)

$\Omega_{w2\text{-}1}=M_{uw2\text{-}1\text{-}base}/M_{yw2\text{-}1\text{-}base}$

(b)

Figure 4.3: a) Response of two different systems b) Response of a structural wall in the two different systems

To investigate the effect of interaction between the slab-wall and gravity columns on the structural wall response, the structural wall overstrength factor is defined by Equation (4.3) as:

$$\Omega_{w2}=M_{uw2\text{-}1\text{-}base}/M_{yw2\text{-}1\text{-}base} \quad (4.3)$$

where $M_{uw2\text{-}base}$ and $M_{yw2\text{-}base}$ is the ultimate moment strength of the structural wall for the Case2-1, $M_{ys2\text{-}base}$ is the effective yielding moment strength of the structural wall for Case2-1.

In Figure 4.3, Ω_{sa2} has been defined as a ratio of base moment strength at a target drift (or ultimate drift) to the base moment at the yielding point for the whole system in the Case2-1. Base rotation as a controlled displacement can be estimated from the vertical displacement of wall elements in the finite element model. In this study, the first storey is discretized to three nonlinear shell elements over the wall height. Base rotation is obtained based on the calculation which is presented in Figure 4.4 in each step of analysis. This calculation assumes averaging the curvature over the gauge length equal to the two shell elements height at the first floor. The wall first storey height divided by 3 gives the each shell element height as 3.2/3=1.067. Hence, the gauge length or equivalent plastic hinge length is equal to 3.2*2/3=2.13 m. The equivalent plastic hinge length which is estimated here is found equivalent to $0.355L_w$.

The equivalent plastic hinge length has been studied by several authors, including Uzumeri and Paulay (1975), who adapted an equation that was proposed for beams and walls. Other expressions have incorporated effects such as shear, strain penetration (Hines et al., 2004) or the level of axial load (Bohl and Adebar, 2011). To capture the realistic values of stress and strain of material in the finite element model the number of elements at the wall base should be selected carefully to make the element length approximately equal to the expected plastic hinge length. When we use the equivalent plastic hinge length to estimate the ultimate displacement of RC elements, we should bear in mind that this equivalent plastic hinge length should be consistent with the material models used in the original study to propose the

equivalent plastic hinge length. In other words, a set of equivalent plastic hinge length and the concrete and steel material models (specially the limit on ultimate strain in the concrete model) are able to best simulate the ultimate drifts of experimental specimens. A number of different equivalent plastic hinge lengths which are proposed by different researchers are demonstrated in Table 4-4 for the comparison.

Table 4-4: Equations to compute the equivalent plastic hinge length (derived based on cyclic loading tests)

Researcher	Equation
Pauly and Priestley (1992)	$0.044L_s+0.20L_w$
Panagioraks and Fardis (2001)	$0.12\ L_s+0.014d_bf_y$
Thomsen and Wallace (2004)	$0.33\ L_w$ to $0.5L_w$
Bohl and Adebar (2011)	$(0.05L_s+0.2L_w)(1-1.5P/(f'_cA_g))<0.8L_w$
Takahashi (2013)	$4t_w$

L_s: shear span ratio, L_w: length of wall, f_y: yield strength of longitudinal rebar (MPa), d_b: diameter of longitudinal rebar (mm), P: axial load, f'_c: concrete compressive strength, A_g: wall gross section

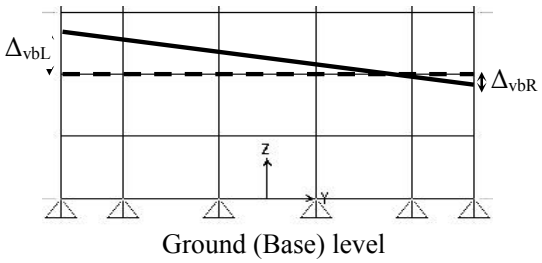

$$\theta_{base} = \frac{\Delta_{VbL} - \Delta_{VbR}}{L_w}$$

θ_{base}: Base rotation

Δ_{vL}: Left side vertical displacement

Δ_{vR}: Right side vertical displacement

L_w: Wall length

Figure 4.4: Definition of base rotation (plastic rotation and yielding rotation)

Another important variable in this study is the vertical displacement of wall edges in the tension and compression sides of the structural walls. Neutral axis movement causes large differences in the tension and compression side vertical displacements. These displacements are the main

source of system interaction due to deformation compatibility. In Chapter 3, it has been confirmed that large amount of vertical edge displacement occurs in the post-elastic stage. Although the vertical edge displacements in each storey are different the roof vertical edge displacements are selected to be representative of wall edge displacements conservatively. Hence, the wall edges displacements in tension and compression sides are normalized with respect to the wall length (Figure 4.5) and their values are estimated during the analysis.

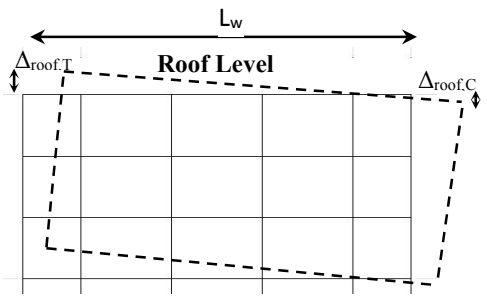

$\Delta_{roof,T}/L_w$: Normalized vertical displacement at tension side of roof (sometime refer as Left side)

$\Delta_{roof,C}/L_w$: Normalized vertical displacement at compression side of roof (sometime refer as Right side)

Figure 4.5: Definition of normalized wall edges vertical displacement at the roof level

4.3.2 Structural Wall Modelling

Nonlinear shell elements representing the in-plane behaviour of RC panels were used to model the rectangular wall. The confined and unconfined concrete were modelled differently, but the tension strength of concrete was neglected. Concrete stress-strain relationship was based on the Mander model (Mander et al., 1988); Figure 4.6 (a) shows the stress-strain relationship of the concrete material. The steel stress-strain relationship was based on the material specifications for the reinforcement rebars shown in Figure 4.6 (b). The typical value for the strain hardening is around ε_{sh}=0.0088, the ultimate strain is about ε_{su}=0.1-0.12 and the ratio of ultimate to yield stress f_u/f_y=1.35-1.50. The ratio of f_u/f_s in these case studies has been selected as 600/430=1.39. To account for the effects due to cyclic loading such as bar buckling or low cycle fatigue, the

analysis is based on the ultimate strain limit of $\varepsilon_s=0.6\varepsilon_{su}$ as recommended by Priestley et al. (2007). The shear behaviour was modelled using the automated inelastic shear layer in SAP2000 for nonlinear shell elements. The pushover analysis in all case studies is conducted until a maximum base rotation equal to 0.015 rad is applied. The post-processing of material strains confirm that in all case studies the strain demands are below the limits at this base rotation. The base flexural moment resistance of the wall and the system at each step is calculated by summing the forces which act on joints within the shell or frame elements. During the summation, the forces and moments at different joints are transformed into equivalent actions at a point located at the middle of structural walls.

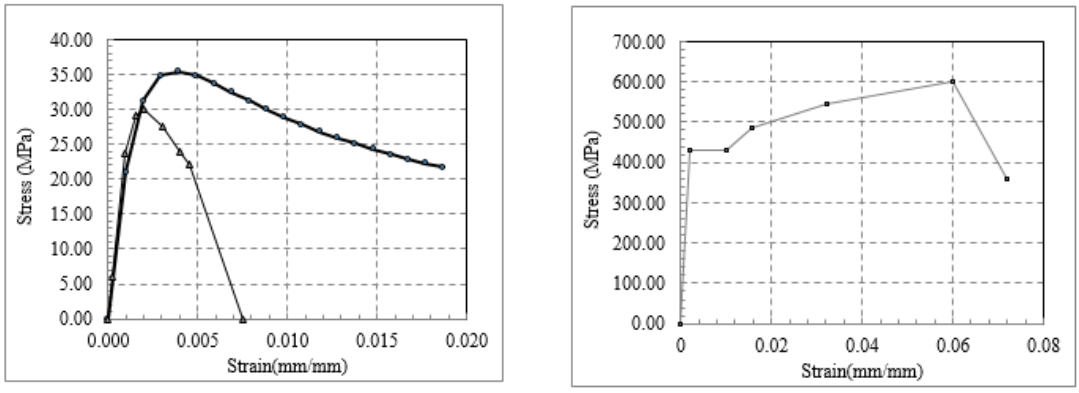

(a) (b)

Figure 4.6: Material Stress-Strain Backbone Curves; a) Concrete b) Rebar

4.3.3 Floor Slab and Frame Modelling

Floor slabs are modeled as elastic shell elements with stiffness values of $EI_{eff} = 0.25EI_g$ (flexural) and $GA = 0.5GA_g$ (shear). All floor slabs are assigned a specified concrete strength of $f'_c = 30$ MPa. Shear modulus (G) is calculated using a Poisson's ratio $\nu = 0.2$. The columns are modelled as elastic beam elements with very low flexural stiffness. The elastic properties of the columns are calculated using the cross-section dimensions and the stiffness modification factors; i.e. $EI_{eff} = 0.01EI_g$ (flexural), $GA = 1.0GA_g$ (shear). This approach can give us a

transparent comparison between models without interaction (Case1-1) and with interaction (remaining cases).

4.4 Analysis Method

The static pushover analysis is conducted mainly based on the assumption that the response of the structure is controlled by the shape of its first elastic mode of vibration. The assumed load distribution pattern remains unchanged throughout the elastic and inelastic response of the structure. This assumption provides the basis for transforming response of a MDOF structure to the response of an equivalent SDOF system. This concept is illustrated in Figure 4.7. The deflected shape of a MDOF structure is assumed to have a constant shape function represented by the vector $\{\phi\}$ that characterizes the response of structure from the beginning to the end of analysis. The deformation pattern of MDOF structure can be expressed by the relative roof displacement as $Z=\{\Phi\}z_{roof}$ (z_{roof} is the roof relative displacement). Hence, the earthquake induced motion of an elastic or inelastic MDOF system can be derived from its governing differential equation:

$$[M]\{\Phi\}\ddot{z}_{roof} + [C]\{\Phi\}\dot{z}_{roof} + \{F\} = -[M]\{1\}\ddot{z}_g \tag{4.4}$$

where [M] is the mass matrix, [C] is the damping matrix, {F} is the storey force vector, and $\ddot{z}_g$ is the ground acceleration history.

If we define the equivalent SDOF displacement z* as:

$$z^* = \frac{\{\Phi\}^T[M]\{\Phi\}}{\{\Phi\}^T[M]\{1\}} z_{roof} \tag{4.5}$$

If we multiply the Equation (4.4) by $\{\Phi\}^T$ and replace the variable z_{roof} with z* the Equation (4.4) can represent the equation of motion of equivalent SDOF system as:

$$M^*\ddot{z}^* + C^*\dot{z}^* + F^* = -M^*\ddot{z}_g \tag{4.6}$$

where M*,C* and F* represent the properties of the equivalent SDOF system and they are calculated by :

$$M^{*}=\{\Phi\}^{T}[M]\{1\} \quad (4.7)$$

$$F^{*}=\{\Phi\}^{T}[F] \quad (4.8)$$

$$C^{*}=\{\Phi\}^{T}[C]\{\Phi\}\frac{\{\Phi\}^{T}[M]\{1\}}{\{\Phi\}^{T}[M]\{\Phi\}} \quad (4.9)$$

Hence, equivalent SDOF specification can be obtained if we assume that the displacement pattern $\{\Phi\}$ is known for the MDOF structure. Then, by conducting the pushover (incremental static) analysis of MDOF structure the force-deformation properties of equivalent SDOF can be obtained. The equivalent SDOF represents the MDOF system with the same effective stiffness (secant to effective yield) and effective mass. Pushover analysis results commonly are represented by the base shear (or base moment) of structure versus the roof displacement (or base rotation). The global force deformation diagram of MDOF structure demonstrates the capacity curve of structure under a constant shape of inertia forces. However, the stiffness of MDOF structures gradually reduces with increasing load intensity (this is equivalent to period elongation) after cracking and yielding. This phenomenon implies the ideal pushover analysis should be able to account for the instantaneous change in the distribution of internal forces and displacement shape during the analysis. The numerical tool to conduct such pushover analysis is not commercially available.

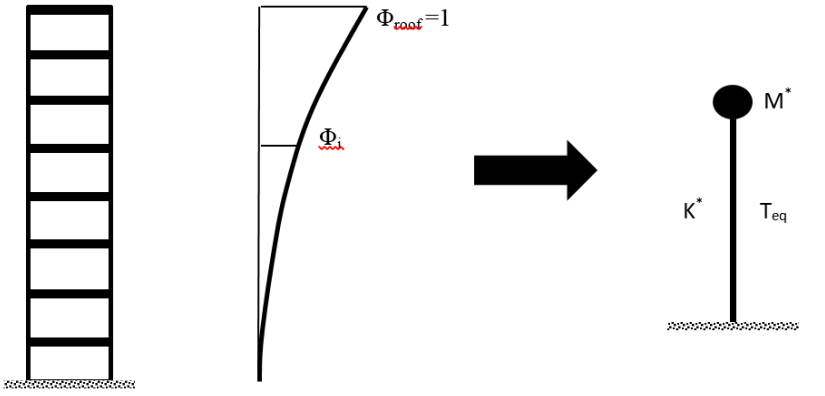

Figure 4.7: Transformation of MDOF capacity curve to equivalent SDOF

To find the nominal global strength and displacement of equivalent SDOF, the capacity curve of MDOF (Figure 4.8) is idealized to bilinear form. The bilinear format can express the yield strength V_{by}, corresponding effective stiffness K_{eff}, and the hardening stiffness of MDOF structure. The bi-linearization method is very subjective and various methods are available in literature. The strain-hardening ratio, α, of the base shear versus roof displacement relationship of the equivalent SDOF system is taken as the same as for the MDOF structure.

The yield base shear and yield roof displacement are employed to calculate the force displacement curve for the equivalent SDOF as below:

$$z_y^* = \frac{\{\Phi\}^T[M]\{\Phi\}}{\{\Phi\}^T[M]\{1\}} z_{roof,y} \tag{4.10}$$

$$F_y^* = \{\Phi\}^T F_y = \{\Phi\}^T V_{by} \tag{4.11}$$

Hence, the effective period of the equivalent SDOF system as a key variable in dynamic analysis of structures is found as:

$$T_{eq} = 2\pi\sqrt{\frac{z_y^* M^*}{F_y^*}} \tag{4.12}$$

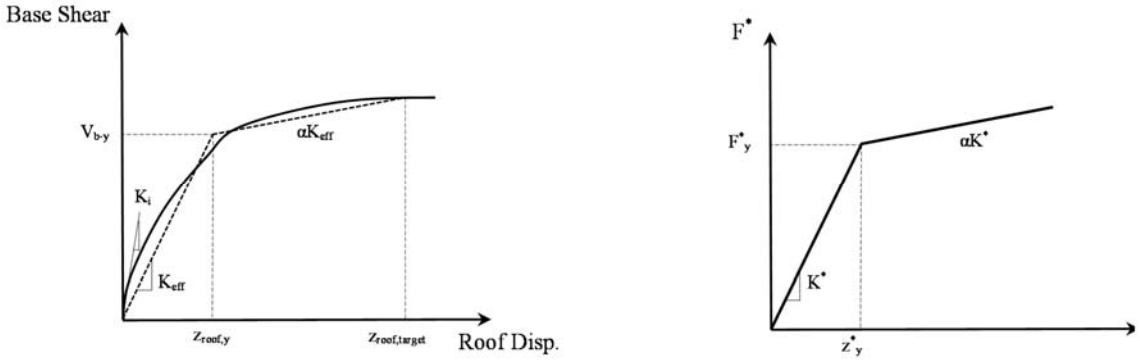

Figure 4.8: (a) Capacity curve of MDOF (b) Bilinear idealization to find equivalent SDOF

If one is interested in finding the maximum displacement demand of MDOF structure under a given ground motion, first one should find the maximum displacement of the equivalent SDOF system. The maximum displacement demand of SDOF system subjected to a given ground motion can be found from either elastic or inelastic spectra or a time-history analysis. Then the corresponding displacement of the MDOF system can be estimated by Equation (4.13):

$$z_{roof,target} = \frac{\{\Phi\}^T[M]\{1\}}{\{\Phi\}^T[M]\{\Phi\}} z^* \tag{4.13}$$

Hence, the estimated displacement demand of the equivalent SDOF may not agree well with initial assumption on the slope of the post-elastic part in the MDOF capacity curve. Iteration may be needed to obtain a target displacement on MDOF capacity curve.

The formulation of the equivalent SDOF system may not introduce much sensitivity in the results (Krawinkler et al., 1998) unless the design spectrum is sensitive to small period variations. It is also common in the pushover method that the deflected shape of the MDOF system can be represented by a single and constant shape vector regardless of the level of deformation (Krawinkler et al., 1998).

Previous studies of pushover analysis have shown that the first mode shape can provide accurate predictions of the target displacement if the response of the structure is dominated by its fundamental mode (Fajfar et al., 1996,; Krawinkler et al., 1998; and Antoniou, 2002).

4.4.1 Lateral Load Patterns

In order to perform a pushover analysis on a MDOF system, a pattern of increasing lateral forces needs to be applied to the mass points of the system. This force pattern represents all forces which are produced when the system is subjected to a ground motion. This force pattern is applied incrementally on the structure to push it the beyond the elastic limits. During the inelastic stage the system will experience a loss of stiffness and a change in its vibration period and modal characteristics of the structure. Instantaneous changes in the modal characteristics of the structure affect the loading attracted during the ground motion excitation. In other words, a separation between the supply and the demand implicitly exists in this type of pushover analysis method. This is clearly incorrect, as the inelastic structural response is load-path dependent and the structural capacity is always associated to the earthquake demand. This can be seen in the force deformation relationship of the system.

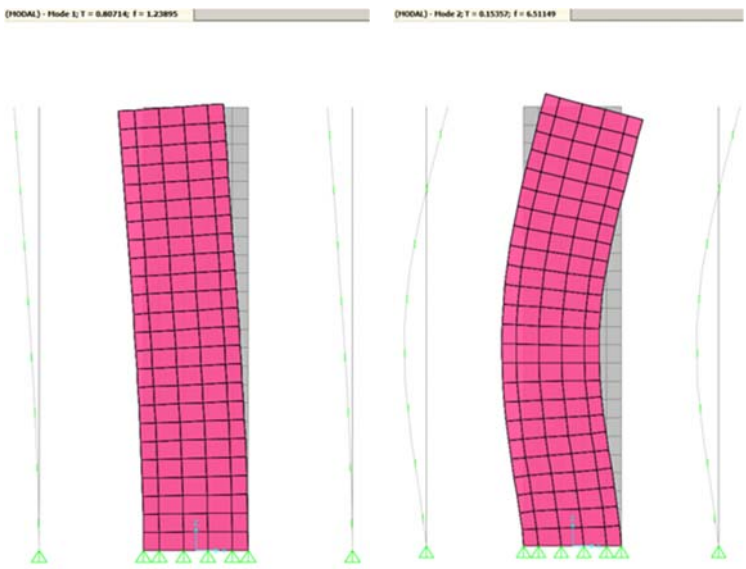

T_1=0.81 sec T_2=0.15 sec

(a)

Storey	force distributions
8	32.10
7	26.71
6	21.35
5	16.15
4	11.28
3	6.94
2	3.40
1	1.00

Lateral load distribution

(b)

Figure 4.9: First and second mode shape of case 2-1 b) distribution of force proportional to the first elastic mode shape

Figure 4.9 (a) depicts the first and second elastic mode shapes of the Case2-1. These are the main elastic mode shapes of the system. As soon as the system enters the post-elastic range due to cracking and yielding of reinforcement, the deformation pattern tends to be transformed to a linear shape. However, at this step of project, we assume that the distribution of forces is proportional to the first elastic mode shape. In other words, the mathematical form of force over the height of building is:

$$F_i=W_i\Phi_{ij} \tag{4.14}$$

where W_i is the weight of the i^{th} storey and Φ_{ij} is the i^{th} components of the elastic mode shape vector corresponding to the i^{th} storey for the j^{th} mode. This is equivalent to FEMA-356 load distribution using:

$$F_i = \frac{W_i h_i^k}{\sum_{i=1}^{n} W_i h_i^k} V_b \tag{4.15}$$

where k is a coefficient which can be assumed to be dependent on the fundamental period T_1 of the structure.

Generally, the accuracy of the pushover analysis when predicting the structural performance is a matter of controversy. However, this simple method provides a useful understanding of the expected behaviour of the structures. Therefore, this study is based on the pushover analysis results. Primarily, lateral forces are applied to a group of selected prototype buildings in the form of the recommended patterns of FEMA-450 guideline with distributions relative to mass and height considering the effects of the higher modes. Later, the pushover curves are idealized according to the FEMA-695 recommendations. All analysis are performed with gravity load of P=1.0D+0.25L.

4.5 Analysis Results

In this section, the results of monotonic pushover analysis for different case studies are presented. The analyses account for the effect of slabs flexural stiffness and bay lengths on the whole system behaviour as well as the structural walls in all cases separately.

As already has been stated, the force distribution over the height of the prototype buildings is assumed to be proportional to the first elastic mode shape. However, this force pattern is assumed to remain constant during the whole analysis. The numerical values of the force distribution for the eight storey building are presented in Figure 4.9 (b). It is worth mentioning that as soon as the base section reinforcement starts yielding the deformed shape of the structural wall may change from the assumed polynomial function (first elastic mode) to a near straight line. Thus, it would be a good advice to conduct the pushover analysis with two different force distributions. The initial force pattern may distribute proportional to the first elastic mode shape up to the nominal yield point. From the yield point up to the target (maximum) displacement a force distribution can be assumed to give a linear deformation

shape for the yielding system. However, in this chapter, we only conduct the pushover analysis by a force distribution proportional to the first elastic mode shape.

4.5.1 Effect of Bay (Slab) Length on the Yielding Base Rotation and Corresponding Yielding Base Moment of the Systems and Structural Walls

Pushover analysis results have been used to define the system behaviour in terms of base moment versus base rotation (Figure 4.3 (a)). However, the base rotation versus base moment diagram for an identical structural wall depends on the wall-slab-column interaction in the system. In other words, the structural wall in Case1-1 may have a different yielding base rotation and/or yielding base moment compared to the identical structural wall which is located in Case2-1 (Figure 4.3 (b)). Hence, the yielding point values (including yielding base moment and its corresponding yielding base rotation) may change due to the presence of adjacent slabs and/or beams and/or gravity columns. The variation of yielding base moment and yielding base rotation in each case (system level) and each wall in the system will be discussed in the next section.

Table 4-5 presents the numerical values of yielding base rotation and corresponding yielding base moment for the system ($M_{ys\text{-}base}$) and yielding base moment for the structural walls ($M_{yw\text{-}base}$) for the Case1-1 to the Case8-1. As it has been already stated, the flexural moment of the structural walls and the whole system at a specified base rotation were calculated by summing the forces which act on joints within the shell or frame elements. During the summation, the forces and moments at different joints are transformed into equivalent actions at a point located at middle of structural walls excluding the P-delta effect.

It is interesting to find that how much yielding base rotation may change due to the presence of slabs and gravity columns in a multi-storey shear wall building. This is a critical value when we use the displacement based design. The yield curvature/rotation in the displacement based design method commonly relies on a formulation which is derived from the section analysis of

isolated walls. It should be clarified that the yielding base rotation of an isolated wall without interaction (Case1-1) and yielding base rotation of identical wall acting in a system are distinctly different. Hence, Figure 4.10 (a) shows the variation of the ratio of yielding base rotations calculated for the all cases to Case1-1 (wall only). The ratio of average yielding base rotations for all cases (with the same out-of-plane flexural stiffness) to the yielding base rotation of the Case1-1 (wall only) is equal to 0.88. In other words, the presence of slabs and the gravity columns can slightly reduce the yielding base rotation of all cases compared to the yielding base rotation of an isolated wall.

Table 4-5: Values of yielding points for the Case1-1 to Case8-1

Case	yielding points (system)		
	θ_y (rad)	$M_{ys\text{-}base}$ (MN.m)	$M_{ys\text{-}wall}$ (MN.m)
Case 1-1/wall only	0.00123	67.37	67.37
Case2-1	0.00123	74.70	68.41
Case3-1	0.00126	76.70	68.90
Case4-1	0.00123	74.10	68.30
Case5-1	0.00127	78.00	69.91
Case6-1	0.00122	73.90	68.00
Case7-1	0.00129	79.50	70.20
Case8-1	0.00121	72.90	67.80

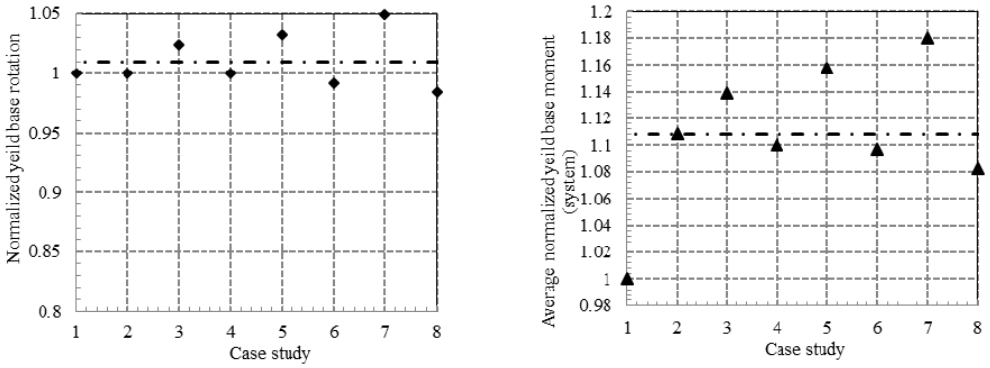

(a) (b)

Figure 4.10: a) Ratio of yielding base rotation of different cases to the yielding base rotation of wall only (Case1-1); b) Ratio of yielding base moment of different cases to the yielding base moment of wall only (Case1-1).

Figure 4.10 (b) represents the average normalized yield base moment (system level) in different cases. The system base moment was divided by the system base moment of Case1-1 (wall only) to obtain the normalized base moment for each case. It is interesting to highlight that the normalized system base moment in the case studies with the bay length equal to 4 m (in either direction) is less than cases with 8 m bay length (in either direction). The maximum ratio between the system yield base moments of these case studies to the base case (Case1-1) is equal to 1.18 for Case7-1.

4.5.2 Effect of Bay (Slab) Length on the Vertical Extension and the Vertical Shortening of Wall Edges at the Roof Level

Figure 4.11 (a) and (b) provides a graphical representation of stress contours in the longitudinal rebars in Case1-1 and Case2-1 respectively at the base rotation equal to their significant yielding points. Figure 4.11 also shows the deformed shape of two cases (at yielding stage) under the lateral forces proportional to the first mode. The significant yield point has been already established as a base rotation equivalent to the yielding of rebars in the boundary element of the mathematical model. Although this definition seems subjective, due to comparative nature of this study, it is not the key parameter in the interpretation of results throughout the whole project. Pushover analysis results are post-processed to find the significant yielding point.

It is evident form Figure 4.11 that stress in the reinforcing bars in the boundary element of structural wall at the base (the boundary element of structural wall has modelled with one element across the wall length) exceeds the yield stress equal to 430 MPa. The stress state in this element is manually monitored to find that when all integration points inside this element reaches the yielding value. This step is assumed to be equivalent to the numerical yield state of the system.

Figure 4.12 also depicts the wall vertical edge displacement contours across the wall height at the base rotation equal to 0.015 rad. It is evident from the pictures in Figure 4.12 that big differences exist in the tension and compression side vertical displacement of structural walls not only at the roof level but also in all other stories. Unlike the concept of elastic theory which one expect the same vertical displacement at the two edges of same level, the neutral axis movement across the section and height cause the big difference in the sides vertical displacements. Table 4-6 presents the numerical values of the normalized wall edge extension at four distinctive values of base rotation for the Case1-1 to Case8-1.

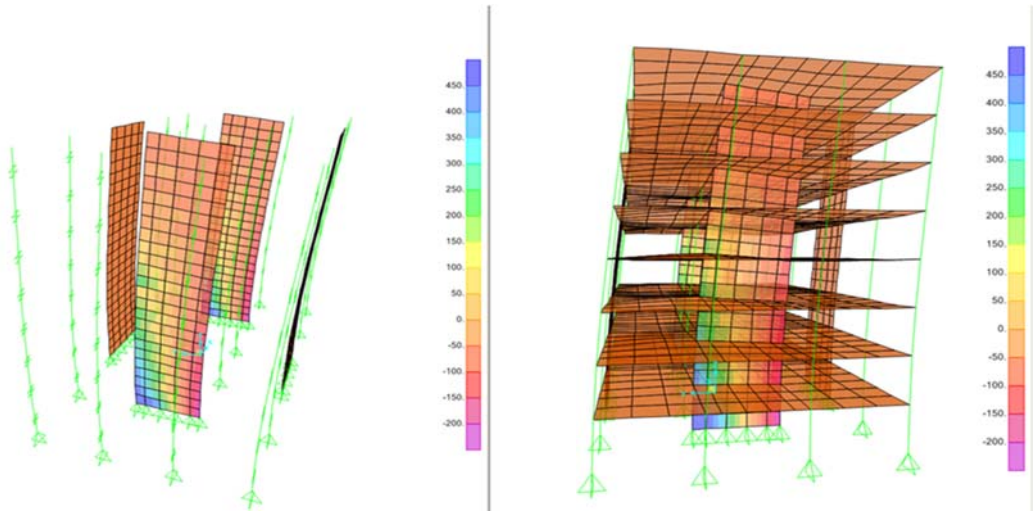

(a) (b)

Figure 4.11: a) Stress in vertical rebars at first yield in Case1-1 b) Stress in vertical rebars at first yield in Case2-1 ((N/mm^2))

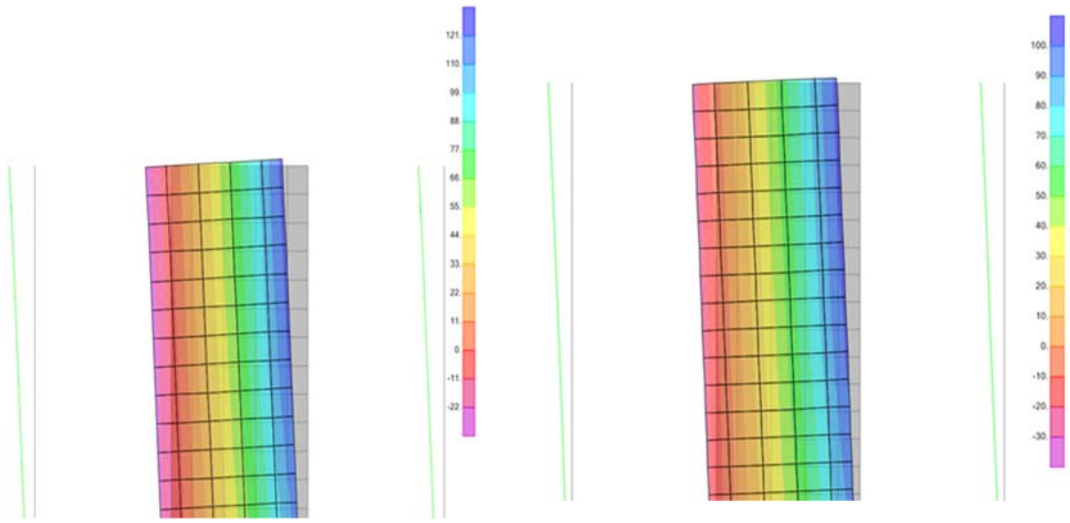

(a) (b)

Figure 4.12: a) Vertical edge displacement at θ_b=0.015 rad in Case1-1 b) Vertical edge displacement at θ_b=0.015 rad in Case2-1 (mm)

Figure 4.13 (a) illustrates the normalized wall edge extension and wall edge shortening versus the base rotation for the varying length of slabs (bays) in the eight cases. The normalized wall edge extension and shortening at the roof level has been already defined as the ratio of the wall edge extension/shortening over the wall length. The corresponding values for the wall only (Case1-1) are also shown on the graphs. The results indicate the normalized wall edge extension at yielding point (on the average base rotation equal to 0.0012 rad) is approximately equal to 0.0036 rad for the different lengths of slabs. However, the normalized wall extension is equal to 0.0127 rad for the base rotation equal to 0.01 rad in the Case2-1. In other words, while up to the yield point the ratio of base rotation to the normalized wall edge extension is equal to 0.0012/0.0036=0.33, this ratio for the base rotation equal to 0.01 reaches 0.01/0.0127=0.79. These two results demonstrate that the contribution of base rotation at base rotation of 0.01 rad to the wall vertical edge extension increases rapidly after yielding; i.e. it becomes 2.39 times larger compared to the yielding states.

Table 4-6: Values of the normalized wall edge extension for the Case1-1 to Case8-1

Wall edge Extension	θ_b @ yielding point		θ_b=0.005	θ_b=0.01	θ_b=0.015
Case 1-1/wall only	θ_y= 0.00123	0.0040	0.00834	0.01450	0.0209
Case2-1	θ_y= 0.00123	0.00363	0.00764	0.01279	0.0174
Case3-1	θ_y= 0.00126	0.00360	0.00755	0.01249	0.0171
Case4-1	θ_y= 0.00123	0.00364	0.00768	0.01284	0.0175
Case5-1	θ_y= 0.00127	0.00356	0.00746	0.01231	0.0169
Case6-1	θ_y= 0.00122	0.00365	0.00787	0.01287	0.0176
Case7-1	θ_y= 0.00129	0.00354	0.00742	0.01217	0.0167
Case8-1	θ_y= 0.00121	0.00367	0.00779	0.01299	0.0177

Figure 4.13 (a) demonstrates that normalized wall extension for the varying length of slabs reduces very slightly when the bay length is reduced either in x or y direction. The maximum difference in terms of the edge extensions between the Case1-1 (wall only) and the Case7-1 (the case with the bay length L_x=L_y=4 m) reaches 23% (difference = (0.0209-0.0167)/0.017*100) at the typical base rotation equal to 0.015 rad.

However, in these two specific examples, the value of the wall edge extensions at their corresponding yielding points is equal to 0.00432 and 0.003538 for Case1-1 (wall only) and Case7-1 (with L_x=L_y=4 m bay length) respectively. These values give the difference of 18.1% for the prediction of wall edge extensions.

Variations of the average (normalized to numerical values of Case1-1 in each drift level and then averaged in all three distinctive drift levels) normalized wall edge vertical extension also are presented in Figure 4.13 (b). It is apparent that the average normalized wall edge vertical extension for all cases (due to the presence of slabs and gravity columns) are reduced 14% compared to Case1-1.

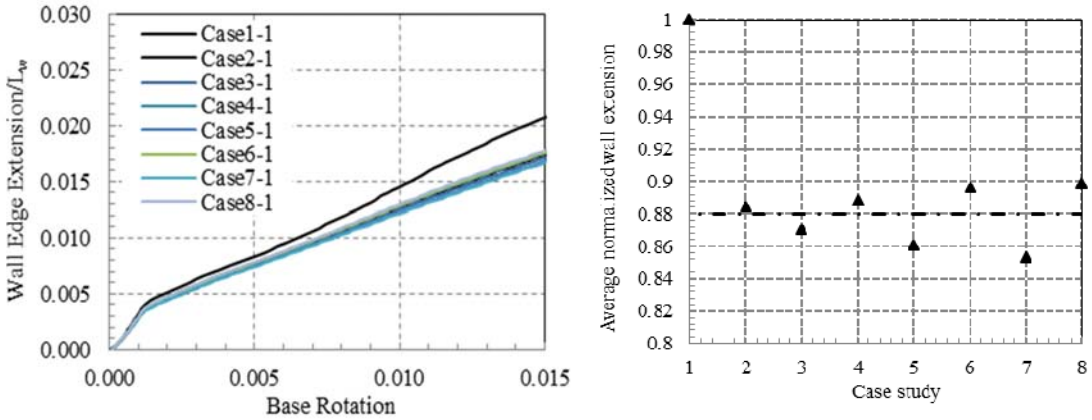

(a) (b)

Figure 4.13: a) Normalized wall edge extension for the different cases; b) Ratio of average normalized wall extension for the different cases

In a similar way, a tabular data is generated to show the normalized wall edge shortening for a given base rotation for all cases. The results of finite element analysis for the value of normalized wall edge shortening are presented in Table 4-7. It seems that slabs with varying bay length have less effect on the wall edge vertical shortening. Figure 4.14 (a) also indicates the variation of normalized wall edge shortening for all cases at different base rotation levels. Although the normalized wall edge shortening for a given base rotation slightly reduces with increasing the bay length either in x and y direction, the effect of bay (slab) length is quantified here by averaging the outputs at the different base rotation levels. Figure 4.14 (b) compares the average (normalized to numerical values of Case1-1 in each drift level and then averaged in all three distinctive drift levels) values for the wall edge shortening in the four different base rotation levels.

Table 4-7: Values of the normalized wall edge shortening for Case1-1 to Case8-1

Wall edge shortening	θ_b @ yielding point		θ_b=0.005	θ_b=0.01	θ_b=0.015
Case 1-1/wall only	θ_y= 0.00123	-0.00181	-0.00260	-0.00360	-0.00453
Case2-1	θ_y= 0.00123	-0.00174	-0.00249	-0.00336	-0.00417
Case3-1	θ_y= 0.00126	-0.00173	-0.00248	-0.00331	-0.00414
Case4-1	θ_y= 0.00123	-0.00174	-0.00250	-0.00337	-0.00418
Case5-1	θ_y= 0.00127	-0.00175	-0.00254	-0.00343	-0.00430
Case6-1	θ_y= 0.00122	-0.00173	-0.00251	-0.00332	-0.00409
Case7-1	θ_y= 0.00129	-0.00174	-0.00252	-0.00340	-0.00430
Case8-1	θ_y= 0.00121	-0.00173	-0.00250	-0.00334	-0.00411

The ratio of the average wall vertical shortening for all cases to Case1-1 (wall only) is equal to 0.94. It is evident from Figure 4.13 (b) and Figure 4.14 (b) that the presence of slabs and gravity columns has more effect on the wall edge extension than the wall edge shortening. A part of this difference may be attributed to the assumption which was adopted in the analysis. The employed finite element analysis assumes zero tensile strength for the concrete material. It means that the contribution of concrete tensile strength disregarded from the beginning of the analysis. This implies that the employed finite element analysis should demonstrate the flexible behaviour compared to a model including tensile strength of concrete. Zero tensile strength of concrete in the mathematical model overlooks not only the contribution of concrete in the tension before the cracking but also effect of tension stiffening after the cracking. The difference between the wall edge extension and shortening can be attributed to this assumption.

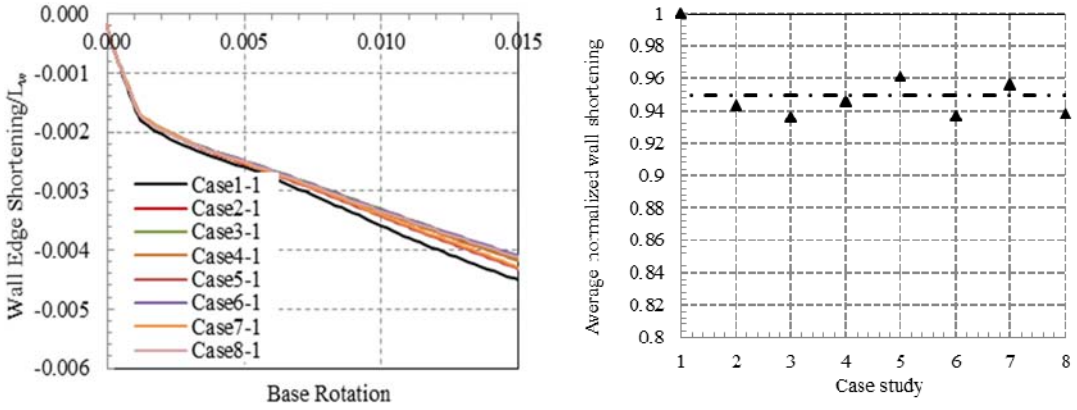

(a) (b)

Figure 4.14: a) Normalized wall edge shortening for the Case1-1 to Case8-1; b) Ratio of average normalized wall shortening for the Case1-1 to Case8-1.

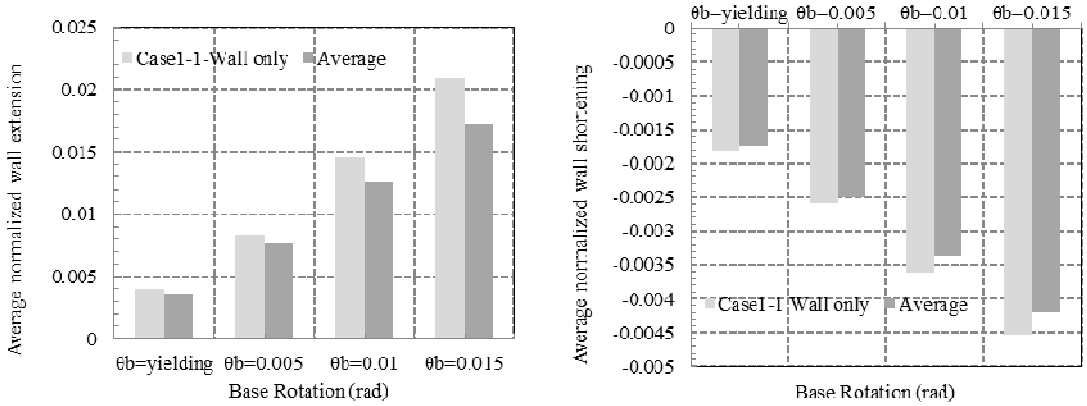

(a) (b)

Figure 4.15: a) Average normalized wall edge extension for the Case1-1 to Case8-1; b) Average normalized wall edge shortening for the Case1-1 to Case8-1.

4.5.3 Effect of Bay (Slab) Length on the System-Over Strength Factor

One of the key objectives of this chapter is to determine a typical value of system-overstrength factor due to the presence of slabs and gravity columns in multi-storey shear wall buildings. Moreover, it is intended to provide an in-depth understanding about the effect of bay (slab) length as well as out-of-plane stiffness of slabs on the system response. The overstrength of system which is defined in Figure 4.3 (a) (named as Ω_{sa}) also accounts for the overstrength due to material hardening of reinforcement as well as the confinement of concrete. The overstrength factor also allows for the strength variation that occurs in steel and concrete from their design

values. For design, a lower characteristic strength is used but to get an appropriate overstrength factor the upper characteristic strength must be considered. As the focus of this study is to estimate the overstrength factor of a system due to wall-slab and gravity columns interaction, the difference between the lower and upper characteristics of materials is not considered herein.

To obtain the contribution of slabs and/or columns on the system overstrength factor, the value of Ω_{sr} has been introduced. The value of Ω_{sr} indicates only the contribution of slabs (and/or columns) to the system overstrength factor.

Figure 4.6 (a) illustrates the variation of Ω_{sa} (the system overstrength factor) for Case1-1 to Case1-8. It is evident that the system overstrength factor is well correlated with the base rotation as it was expected.

Table 4-8 illustrates system overstrength factor calculated at the four different base rotation levels for Cases1-1 to Case8-1. For example, in Case1-1(wall only), the total base moment is equal to 7771 kN at the base rotation equal to 0.005. The yielding base moment for this case has already been found as 6737 kN.m. Hence, the overstrength factor of Case1-1 (wall only) at the base rotation equal to 0.005 rad is established as 1.153. The system overstrength factor of other cases is found by the similar method at each drift level.

Table 4-8: Values of system overstrength for the Case1-1 to Case8-1 (Ω_{sa}) (Excluding the P-Δ effects)

Ω_{sa}	θ_b @ yielding point		θ_b=0.005	θ_b=0.01	θ_b=0.015
Case 1-1, wall only	θ_y= 0.00123	1.0	1.153	1.241	1.259
Case2-1	θ_y= 0.00123	1.0	1.252	1.465	1.612
Case3-1	θ_y= 0.00126	1.0	1.268	1.498	1.672
Case4-1	θ_y= 0.00123	1.0	1.248	1.452	1.592
Case5-1	θ_y= 0.00127	1.0	1.283	1.532	1.725
Case6-1	θ_y= 0.00122	1.0	1.25	1.443	1.580
Case7-1	θ_y= 0.00129	1.0	1.294	1.554	1.764
Case8-1	θ_y= 0.00121	1.0	1.237	1.425	1.549

Figure 4.16 (b) displays the system overstrength factor of three different cases which are named Case2-1, Case7-1, and Case8-1. The bay (slab) lengths of these three cases are equal to $L_x=L_y=6$, $L_x=L_y=4$ and $L_x=L_y=8$ respectively. The reduction or increase in the bay (slab) length of Case7-1 and Case8-1 is the same amount for both directions. It is clear from Figure 4.16 (b) that for a given base rotation, the system overstrength factor of Case7-1 is higher than Case2-1. On the other hand, the system overstrength factor of Case8-1 is smaller than Case2-1. However, the amount of increase in the system overstrength factor in Case7-1 is larger than the reduction in the system overstrength factor in the Case8-1 for a given base rotation. For example, while the system overstrength factor at base rotations equal to 0.01 rad and 0.015 rad is equal to 1.425 and 1.549, the corresponding values for the Case7-1 is equal to 1.554 and 1.764. It is implied that systems with the small bay (slab) length (bays around the structural walls) may induce more system overstrength than large bay (slab) length.

Figure 4.16 (c) also indicates the system overstrength factor for Case4-2 and the Case6-2 in the second group of case studies. This graph intends to clarify the effect of bay length on the system overstrength factor. It shows that the bay length perpendicular to the structural walls has slightly more effect on the system overstrength factor than the bay length parallel to the structural walls. At base rotation of 0.015 rad, the system overstrength factor for Case 4-2 and Case 6-2 is 1.85 and 1.80 respectively, and this effect is reduced in lower base rotation levels.

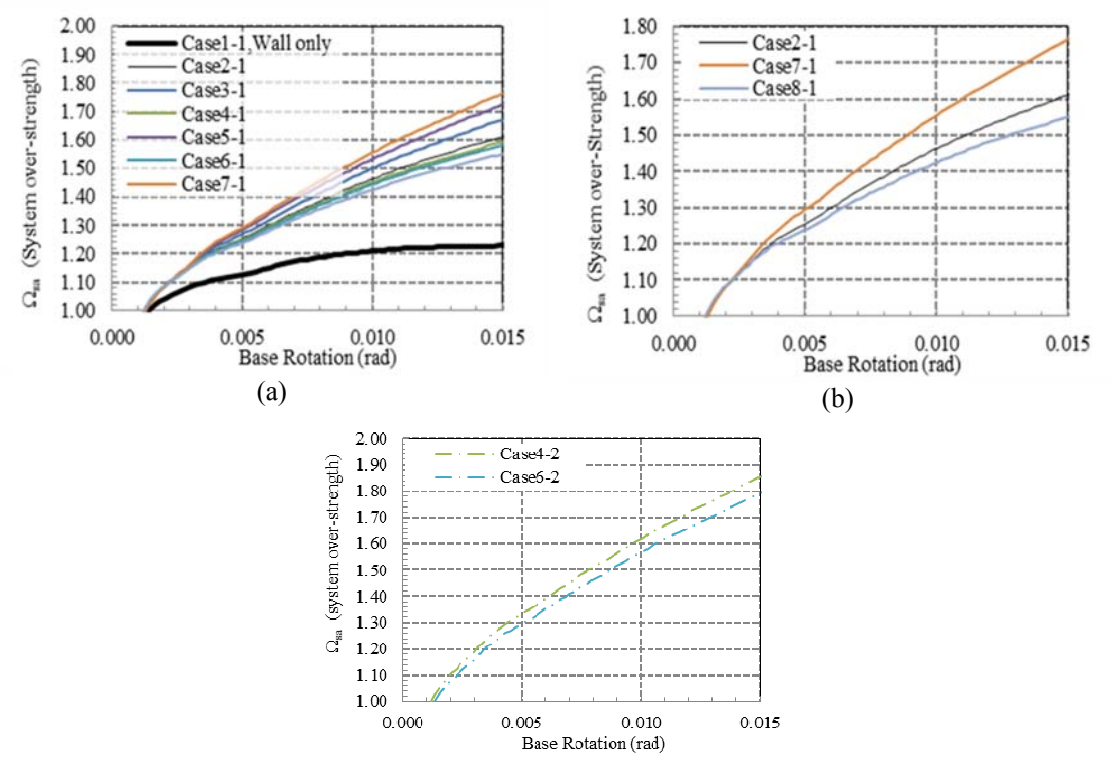

Figure 4.16: a) System overstrength factor for Case1-1 to Ccase1-8 b) System overstrength factor for the Case 2-1, Case7-1 and Case8-1 c) System overstrength factor for the Case 4-2, Case6-2

Figure 4.17 shows the average overstrength factor for Case2-1 to Case8-1 at four different base rotation levels. The comparison has been made between the Case1-1(wall only) and average overstrength factor of remaining cases due to the presence of slabs and gravity columns. While the overstrength factor of Case1-1(wall only) at the base rotation equal to 0.015 is 1.229 the average overstrength factor of Case2-1 to Case8-1 is equal to 1.549. It is obvious that the post-elastic stiffness of Case1-1 (wall only) stems from just material hardening of rebars and confinement of concrete excluding the effect of P-Delta moments.

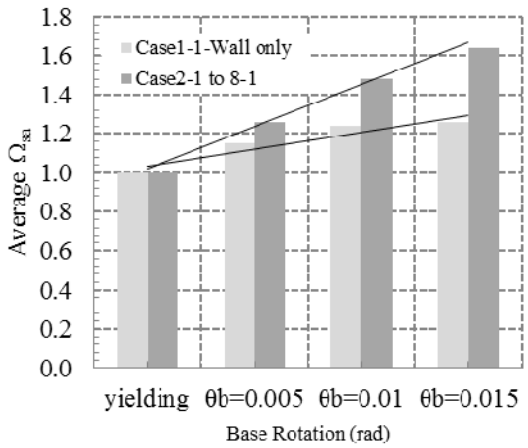

Figure 4.17: Average of system-over strength for Case1-1 to Case8-1

4.5.4 Effect of Bay (Slab) Length on the Structural Wall

In this section, we intend to investigate the effect of slabs and gravity columns on the structural wall itself. As stated before, the presence of wall-slab-gravity columns interaction can change the behaviour of structural wall itself. Figure 4.18 (a) demonstrates the variation of overstrength factors which have been calculated for the structural walls in the Case1-1 to Case8-1. Table 4-9 also shows the numerical value of structural wall overstrength factor (Ω_{sw}) at four different base rotation levels for the eight cases.

Table 4-9: Values of structural wall overstrength factor for Case1-1 to Case8-1 (Ω_{sw}) (Excluding the P-Δ effects)

Ω_{sw}	θ_b @ yielding point		θ_b=0.005	θ_b=0.01	θ_b=0.015
Case 1-1, wall only	θ_y= 0.00123	1.0	1.153	1.241	1.259
Case2-1	θ_y= 0.00123	1.0	1.184	1.301	1.360
Case3-1	θ_y= 0.00126	1.0	1.186	1.304	1.370
Case4-1	θ_y= 0.00123	1.0	1.184	1.300	1.357
Case5-1	θ_y= 0.00127	1.0	1.200	1.336	1.419
Case6-1	θ_y= 0.00122	1.0	1.181	1.288	1.340
Case7-1	θ_y= 0.00129	1.0	1.201	1.338	1.424
Case8-1	θ_y= 0.00121	1.0	1.179	1.285	1.334

Figure 4.19 (a) shows the trend of variation of average overstrength factor only in the structural walls compared to Case1-1. It can be found that increase in average wall overstrength factor due to interaction of wall-slab and gravity columns at the base rotation equal to 0.015 is equal to 1.379 while the wall overstrength factor for the Case1-1 (wall only) is 1.229. It implies the increase in the wall flexural strength is approximately equal to 12%. However, Figure 4.19 (b) shows that increase in the normalized axial force in the structural walls is 21% at the base rotation equal to 0.015. The normalized axial force of structural walls can be estimated by dividing the axial force of structural walls in each step of pushover analysis to the axial force of structural walls at the beginning of the analysis.

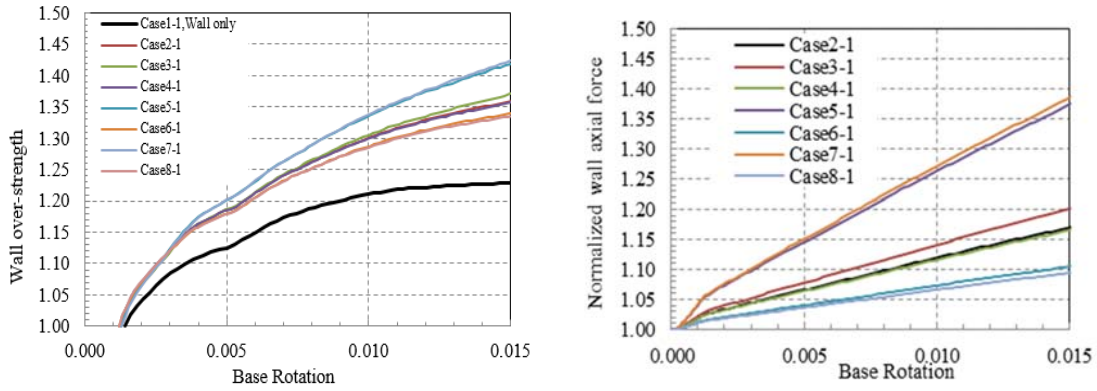

(a) (b)

Figure 4.18: a) Normalized wall overstrength factor for Case1-1 to Case8-1 b) Normalized wall axial force for Case1-1 to Case8-1.

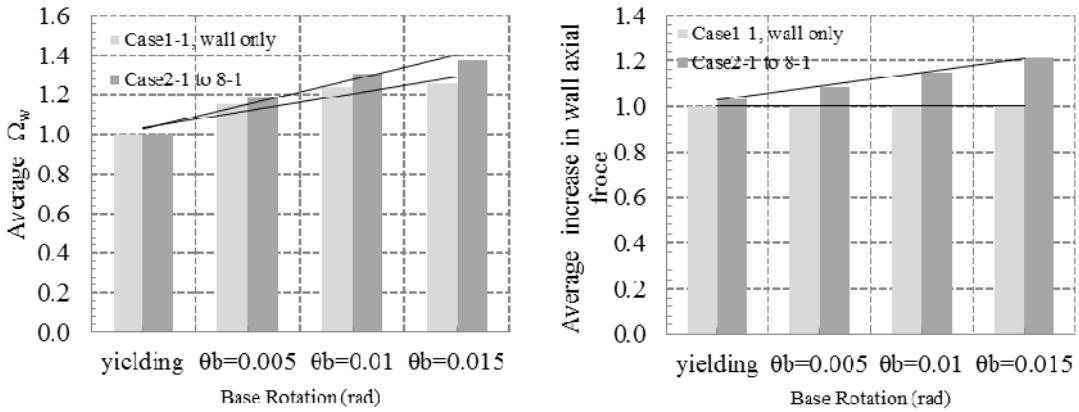

(a) (b)

Figure 4.19: a) Average overstrength factor of structural walls in Case1-1 to Case8-1 b) Average increase in the normalized wall axial force in Case1-1 to Case8-1.

4.5.5 Effect of Slab Flexural Stiffness on the Vertical Extension and Vertical Shortening of Wall Edges at the Roof Level

One of the key variables in addressing the wall-slab-gravity columns interaction is the selection of realistic value for the out-of-plane flexural stiffness of slabs. It is quite difficult to find a realistic stiffness of various flooring systems (such as slabs) in a multi-story shear wall building under the earthquake excitations. In the first group case studies, the flexural out-of-plane stiffness of slabs was assumed equal to 0.25EIg for all cases. It is important to highlight that this value has been used equally over the whole area of the floors. However, the significant reduction of flexural stiffness of slabs is attributed to the occurrence of extensive cracking around the wall-slab and/or slab-gravity columns junctions. An attempt has not been made to assign the different value of flexural stiffness to the slabs in the different region of floors. There are no reliable recommendations to find the appropriate value for the flexural stiffness of slabs under ground motion excitations. Hence, in the second and third group case studies, we changed the out-of-plane flexural stiffness of slabs to $0.5EI_g$ and $0.10EI_g$ respectively.

Table 4-10 and Table 4-11 demonstrate the wall edge extension in the different case studies with the similar geometry but having different values for the out-of-plane flexural stiffness of slabs. The numerical values in Table 4-10 show that the maximum wall edge extension in

Case2-3 and Case2-2 are 0.01882 and 0.01667 respectively. In other words, multiplying the flexural stiffness of slabs by five times ($0.5EI_g/0.10EI_g$) can reduce the wall edge extension by only 12%. Figure 4.20 (a) presents the variation of wall edge extension with increasing the out-of-plane flexural stiffness of slabs from zero (Case1-1) to $0.5EI_g$ (Case2-2). Similarly, Figure 4.20 (b) shows the variation of wall edge extension and the wall edge shortening at the four base rotation levels for the four different cases. It is evident that increase in the out-of-plane stiffness of slabs has more effect on the extension of wall edges than shortening of the wall edges.

Table 4-10: Effect of slab flexural stiffness on the normalized wall edge extension

Wall edge extension (L_x=6 L_y=6)	θ_b @ yielding point		θ_b=0.005	θ_b=0.01	θ_b=0.015
Case1-1, wall only	θ_y= 0.00123	0.00410	0.00834	0.01450	0.02087
Case2-3, EI_e=0.10 EI_g	θ_y= 0.00127	0.00392	0.00799	0.01364	0.01882
Case2-1, EI_e=0.25 EI_g	θ_y= 0.00123	0.00363	0.00764	0.01278	0.01740
Case2-2, EI_e=0.50 EI_g	θ_y= 0.00122	0.00356	0.00749	0.01225	0.01667

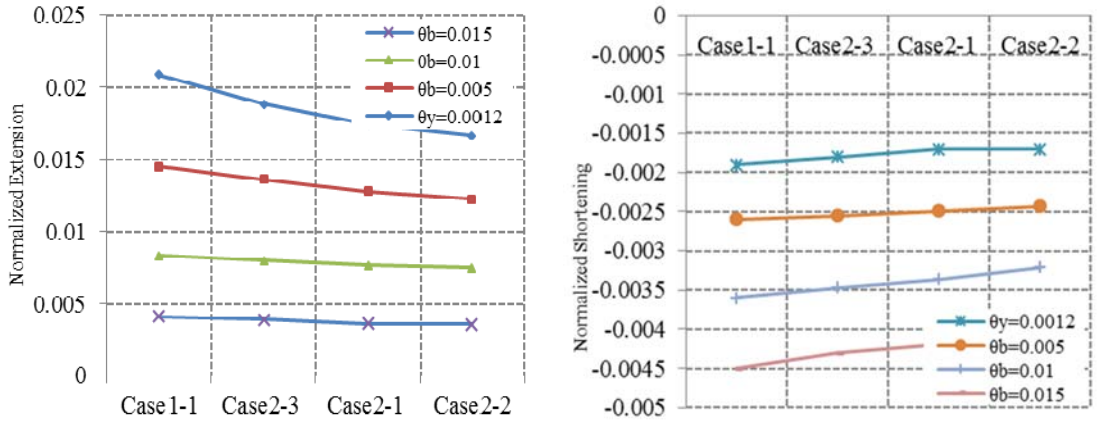

Figure 4.20: a) Normalized wall edge extension at the four base rotation levels b) Normalized wall edge shortening at the four base rotation levels.

Table 4-11: Effect of slab flexural stiffness on the normalized wall edge shortening

Wall edge shortening (L_x=6 L_y=6)	θ_b @ yielding point		θ_b=0.005	θ_b=0.01	θ_b=0.015
case1-1, wall only	θ_y= 0.00123	-0.0019	-0.00260	-0.00360	-0.0045
case2-3, EI_g=0.10	θ_y= 0.00127	-0.0018	-0.00255	-0.00347	-0.0043
case2-1, EI_g=0.25	θ_y= 0.00123	-0.0017	-0.00249	-0.00336	-0.0042
case2-2, EI_g=0.50	θ_y= 0.00122	-0.0017	-0.00243	-0.00321	-0.0040

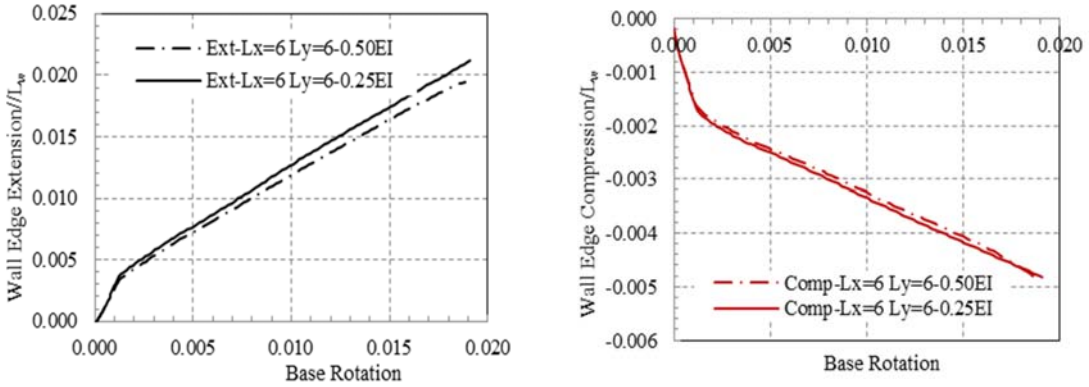

(a) (b)

Figure 4.21: a) Normalized wall edge extension in two different cases b) Normalized wall edge shortening in two different cases

4.5.6 Effect of Slab Flexural Stiffness on the System Overstrength Factor

This section intends to address the effect of out-of-plane stiffness of slabs on the system overstrength factor. The out-of-plane stiffness of slabs plays a crucial role in the wall-slab-gravity columns interaction. In other words, the system overstrength is highly dependent on the out-of-plane flexural stiffness of slabs. Figure 4.22 (a) shows the variation of the system overstrength factor for the Case2-2 to Case8-2. The out-of-plane stiffness of slabs for the second series (Case2-2 to 8-2) is equal to 0.50EI_g which is double compared to the first series (Case1-1 to 8-1). Figure 4.22 (b) also compares the three case studies with the same geometry having different out-of-plane stiffness for the slabs. The ratio of overstrength factor in Case2-2 to the Case2-1 at the base rotations of 0.005 rad and 0.010 rad is equivalent to

(1.34/1.26=1.06) and (1.64/1.46=1.13) respectively. The former ratio is equal to (1.88/1.61=1.17) at the base rotation equal to 0.015 rad.

Table 4-12: Values of the system overstrength for the Case2-2 to Case8-2 (Ω_{sa})

Ω_{sa}	θ_b @ yielding point		θ_b=0.005	θ_b=0.01	θ_b=0.015
Case2-2	θ_y=0.00122	1.0	1.336	1.643	1.884
Case3-2	θ_y=0.00125	1.0	1.363	1.695	1.985
Case4-2	θ_y=0.00121	1.0	1.338	1.623	1.861
Case5-2	θ_y=0.00127	1.0	1.388	1.746	2.012
Case6-2	θ_y=0.00132	1.0	1.301	1.563	1.790
Case7-2	θ_y=0.00130	1.0	1.405	1.785	2.071
Case8-2	θ_y=0.00130	1.0	1.286	1.541	1.739

To obtain the average values of the system overstrength factor for a given base rotation in the cases with the same out-of-plane stiffness of slabs (obviously with the varying bay length), the system overstrength factor of all cases with the same out-of-plane stiffness of slabs are averaged at a given base rotation. Table 4-13 presents the average values at the four different base rotations. Figure 4.23 also compares the variation of the average system overstrength factor for the cases with the same out-of-plane stiffness of slabs. However, the base rotation equal at the yielding state for all cases is very slightly different. For simplicity, the yield base rotation of all cases with the same out-of-plane stiffness of slabs is also represented by their average value.

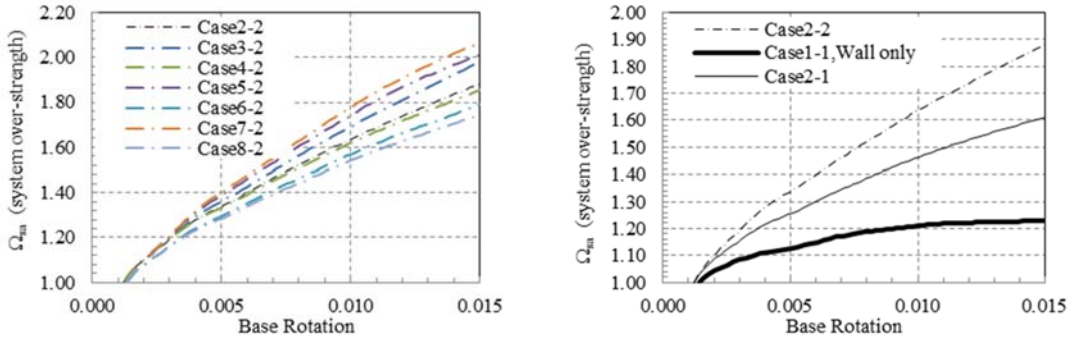

Figure 4.22: a) System overstrength factor in the second group case studies b) System over strength in Case1-1, Case2-2 and Case2-1

Table 4-13: Average system overstrength factor in the all cases with the same out-of-plane stiffness of slabs

System overstrength factor	θ_b @ yielding point		θ_b=0.005	θ_b=0.01	θ_b=0.015
Case1-1, wall only	0.00123	1.0	1.153	1.241	1.259
Cases with, EI_e=0.25 EI_g	0.00124	1.0	1.262	1.481	1.642
Cases with, EI_e=0.50 EI_g	0.00128	1.0	1.345	1.657	1.906

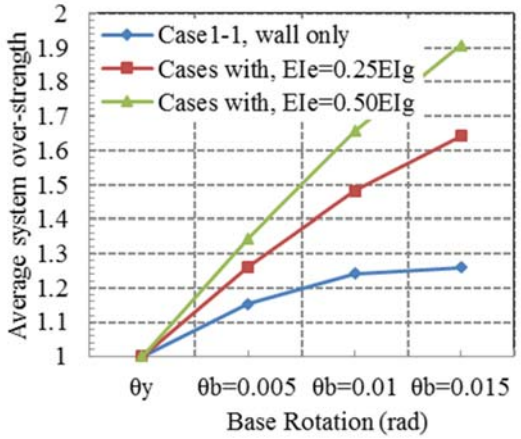

Figure 4.23: Average system overstrength factor of the all cases with same out-of-plane stiffness of slabs

4.5.7 Effect of Flexural Stiffness of Slabs on the Overstrength of Structural Wall

Figure 4.24 (a) displays the variation of wall overstrength factor for Case2-2 to Case8-2. The flexural stiffness of slab in these cases is equal to 0.50EIg. Table 4-14 provides the values of wall overstrength factor in the four different case studies with the same flexural stiffness. The numerical values in Table 4-14 confirm that wall overstrength factor follows the same trend as the system overstrength factor with changes in the bay length either in x or y directions. Figure 4.24 (b) compares the three specific cases with the three different out-of-plane stiffness of slabs with the similar bay length. For example, the ratio of the wall overstrength factor of Case2-1 to Case1-1 is equal to (1.36/1.26=1.08) at the base rotation of 0.015 rad; however, this ratio for Case2-2 to Case1-1 is equal to (1.44/1.26=1.14).

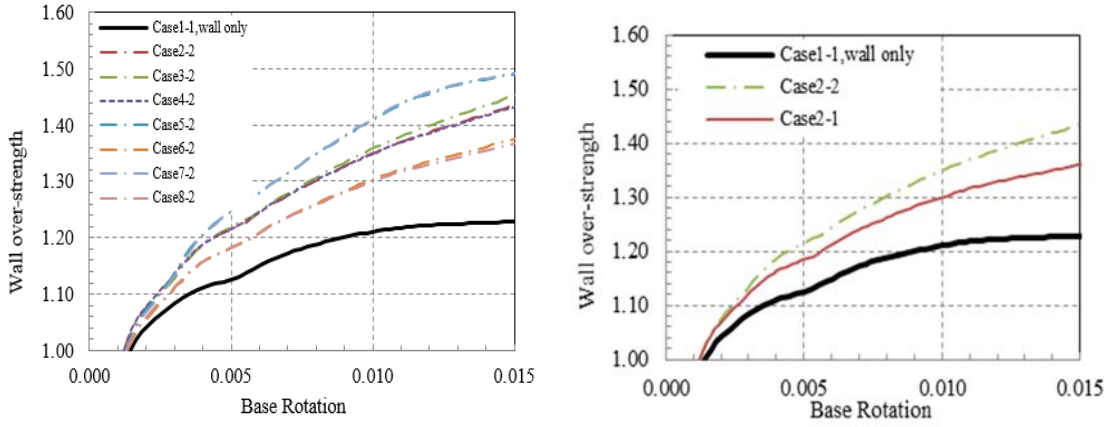

Figure 4.24: (a) Wall overstrength factor in Case2-2 to case8-2 **(b)** Wall overstrength factor in Case2-2, Case2-1 and Case1-1.

Table 4-14: Effect of slab flexural stiffness on the wall overstrength factor

Ω_w (Wall-L_x=6 L_y=6)	θ_b @ yielding point		θ_b=0.005	θ_b=0.01	θ_b=0.015
Case1-1, wall only	θ_y= 0.00123	1.0	1.153	1.241	1.259
Case2-3, EI_e=0.10 EI_g	θ_y= 0.00127	1.0	1.155	1.260	1.297
Case2-1, EI_e=0.25 EI_g	θ_y= 0.00123	1.0	1.184	1.301	1.360
Case2-2, EI_e=0.50 EI_g	θ_y= 0.00122	1.0	1.213	1.352	1.435

The average values of wall overstrength factor for all case studies with the same out-of-plane stiffness of slabs are provided in Table 4-15. First, the wall overstrength factor is calculated at a given base rotation for all case studies with the same flexural stiffness of slabs. Then, the average values were found and were presented in Table 4-15. For example, the average wall overstrength in a typical base rotation of 0.015 rad (this base rotation may be equivalent to base rotation demand we expect under the design base earthquake) reaches 1.906 which is quite large compared with typical values used in design.

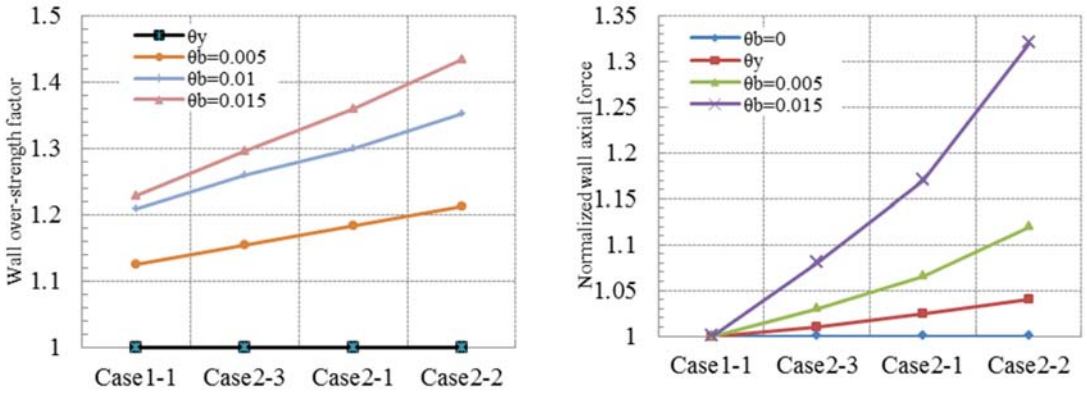

Figure 4.25: (a) Wall overstrength factor in four different cases in different base rotations (b) Normalized wall axial force in four different cases in different base rotations.

Another observation from the values in (from 0.25EIg to 0.50EIg) Table 4-15 is that 100% increase in the slabs out-of-plane stiffness of slabs resulted in a 15% increase in the wall overstrength factor. Figure 4.26 displays the increase in the wall overstrength factor with increasing slab out-of-plane stiffness in different base rotation levels. The wall overstrength factor for the Case1-1 (wall only) and average values of Case2-2 to Case2-8 are 1.229 and 1.906 respectively. The increase in the wall overstrength factor is equivalent to 55%. The estimated value of the wall overstrength factor is quite important in capacity design method to prevent occurrence of shear failure.

Table 4-15: Average overstrength factor in all cases with the same out-of-plane stiffness of slabs

Wall overstrength factor	θ_b @ yielding point		θ_b=0.005	θ_b=0.01	θ_b=0.015
Case1-1, wall only	0.00123	1.0	1.153	1.241	1.259
Cases with, EI_e=0.25 EI_g	0.00124	1.0	1.262	1.481	1.642
Cases with, EI_e=0.50 EI_g	0.00128	1.0	1.345	1.657	1.906

It is obvious from the graph in Figure 4.26 that with increasing flexural stiffness of slabs from 0.25EIg to 0.50EIg (doubling the flexural stiffness of slabs) the numerical value of average wall overstrength factor jumps from 1.65 to 1.9 (this is approximately equal to 15%).

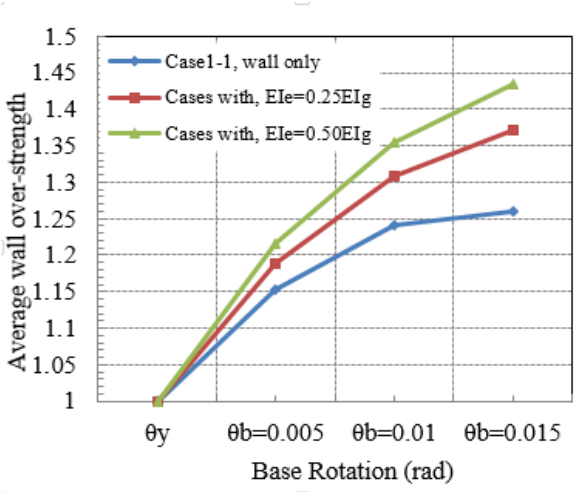

Figure 4.26: Average wall overstrength factor for different cases in different base rotations

4.5.8 Effect of Bay (Slab) Length on the Axial Force Amplification in Gravity Columns

Table 4-16 illustrates the increase in the axial force in one of the columns named C1. The location of this column was parallel to the structural wall in Y direction in the compression side. The numerical value in this table are represented the column axial force amplification at four different base rotation levels in Case1-1 to Case8-1. The maximum rise in the column C1 axial force at base rotation equal to 0.015 rad is for Case3-1. It should be highlighted that the distribution of axial force due to the system interaction between the adjacent columns are in-

deterministic problem. In other words, two-way flooring slabs have distributed the compatibility induced forces according the bay length in X and Y direction. Investigation of results shows that when the bay length in X direction is very short (such as Case5-1) the column perpendicular the structural wall will pick up more forces than the parallel column. Hence, the small increase was observed in axial force amplification in Case5-1. In this specific case, the axial force in a column perpendicular to the wall tension side reaches the axial tension forces. In other words, the induced axial forces are higher than the existing axial force in columns due to gravity loads equal to G+0.25Q.

For the above reason, to address the effect of bay length on the column C1 axial forces, the Cases with the same bay length in both directions were selected. Figure 4.27 (a) shows that column C1 axial force decrease with increasing the bay length. For example, the axial force amplification of column C1 in Case7-1, Case2-1 and Case8 is equal to 1.254, 1.171 and 1.129 respectively (at base rotation equal to 0.015). Figure 4.27 (b) also shows the similar observations in Case7-2, Case2-2 and Case8-2. However; the corresponding values are much higher than case studies with the lower value for the flexural stiffness of slabs.

Table 4-16: Axial force amplification in all cases with the same out-of-plane stiffness of slabs

Axial force amplification (Column C1)	θ_b @ yielding point		θ_b=0.005	θ_b=0.01	θ_b=0.015
Case 1-1, wall only	θ_y= 0.00123	1.0	1.0	1.0	1.0
Case2-1	θ_y= 0.00123	1.039	1.077	1.125	1.171
Case3-1	θ_y= 0.00126	1.100	1.190	1.300	1.410
Case4-1	θy= 0.00123	1.013	1.026	1.044	1.060
Case5-1	θ_y= 0.00127	1.006	1.015	1.026	1.036
Case6-1	θ_y= 0.00122	1.057	1.113	1.180	1.244
Case7-1	θ_y= 0.00129	1.060	1.116	1.186	1.254
Case8-1	θ_y= 0.00121	1.030	1.058	1.095	1.129

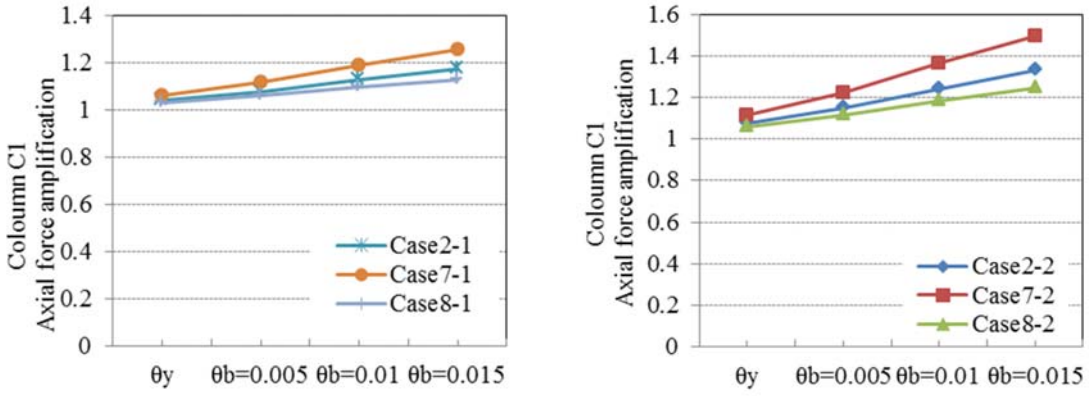

Figure 4.27: Effect of bay length on the column C1 axial force in case studies with (a) $EI_e=0.25EI_g$ (b) $EI_e=0.50EI_g$

4.5.9 Effect of Flexural Stiffness of Slabs on the Axial Force Amplification in Gravity Columns

Figure 4.28 shows the variation of axial force amplification in the column C1 at different base rotation levels in the different case studies. It is evident from Figure 4.28 (a) that once the flexural stiffness of slab is doubled in Case7-2 compared to Case7-1, the axial force amplification in the column C1 rise from 1.25 to 1.5 at base rotation equal to 0.015 rad. The similar observation is discernible from Figure 4.28 (b). However, due to large bay length of slabs in these cases, the corresponding values have changed from 1.129 to 1.247.

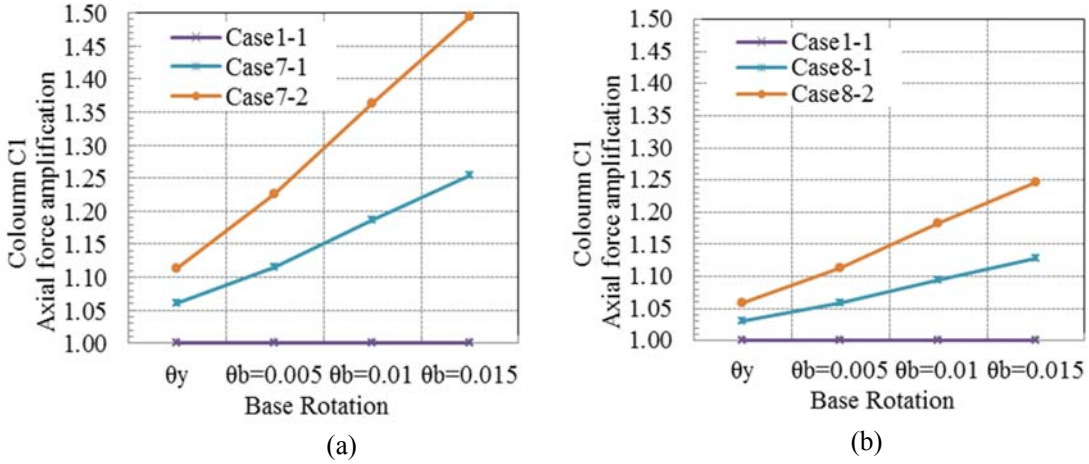

Figure 4.28: Effect of bay length on the column C1 axial force (a) Cases with 4 meter bay length (b) Cases with 8 meter bay length

4.5.10 Effect of Building (Shear Walls) Height on the System Overstrength Factor

One of the key variables for the calculation of system overstrength factor is the height of structural walls (number of floors). This is evident from the proposed closed form equations in Chapter 3. The height of structural walls could affect the system overstrength factor in two different ways. First, the vertical plastic displacement of structural walls (at the wall edges) increase with the height of building for a given base plastic rotation. Second, the accumulation of induced axial forces in gravity columns of tall buildings is higher compared the short buildings. It should be emphasized that we assume the gravity loads on the structural wall keep the same in these cases. Hence, the analysis repeated for the group one cases with different heights equivalent to 5 and 10 storey buildings. However, the axial forces on structural walls were modified to have the axial force on walls equal to the base case studies.

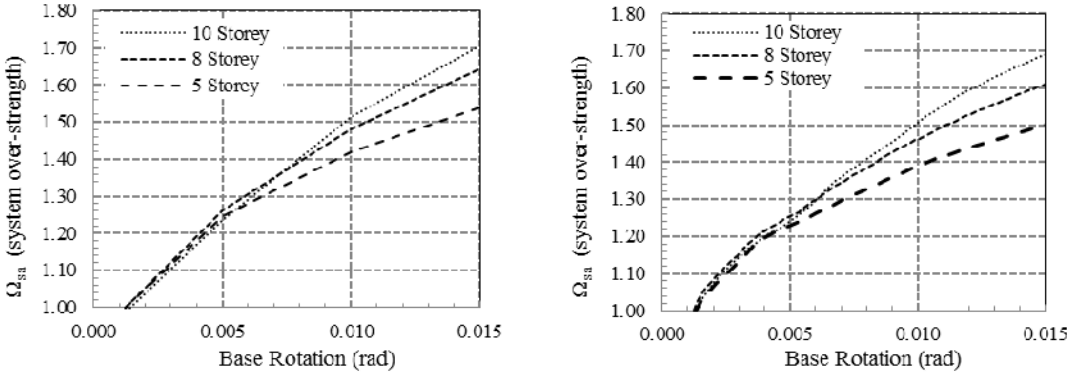

(a) (b)

Figure 4.29: Effect of height on the system overstrength factor (an averaged values over all cases (b) Case2-1 only with different height

Figure 4.29 shows the variation of system overstrength factor with height in group one case studies. Floor slabs in this group have an effective flexural stiffness equal to 0.25 times the gross flexural stiffness. To find a better overview on variation of system overstrength factor with height, system overstrength factor of each cases in a given base rotation are averaged over the all group one cases with the same height. Figure 4.29 (a) shows that up to the base rotation

equal to 0.005 rad system overstrength factor was not varied significantly with the building height. However, as the structural walls enter well into the nonlinear range, system overstrength of tall walls is higher than short walls. Figure 4.29 (b) also just indicate the variation of system overstrength factor for Case1-2 with three different height. For example, at the base rotation equal to 0.015 rad the system overstrength factor is equal to 1.50, 1.61 and 1.69 for 5 storey, 8 storey and 10 storey buildings respectively.

4.6 Conclusion

This chapter has explored the effect of wall-slab-gravity system interaction on the overall behaviour of shear wall building systems. The out-of-plane stiffness of slabs can induce some additional axial forces in the gravity columns and this interaction can increase the system moment capacity and the corresponding overstrength of the whole structure as well as structural walls. Results of analysis demonstrated that the average system over strength of the first and second group case studies (excluding Case1-1) were 1.642 and 1.906 (at base rotation level equal to 0.015 rad) respectively. However, the corresponding average overstrength of structural walls were equal to 1.37 and 1.43 at this base rotation. Average increase of compressive axial force in one of the representative columns (adjacent to the structural wall) at the base rotation of 0.015 rad was equal to 1.19 and 1.36 in the first and second group case studies. Furthermore, results show that the system overstrength factor for tall structural walls is greater than short ones having a same section and axial forces. At base rotation equal to 0.015 rad the representative value of system overstrength was equal to 1.53, 1.63 and 1.7 for the group one case studies.

In capacity design philosophy, this overstrength may affect the strength hierarchy of different failure modes of the structural walls mainly due to additional shear force demand induced in the different storeys of the structural walls. This system interaction effect requires additional

allowance in base shear demand calculation and shear force envelope proposed for the structural walls. The average value of system overstrength factor and wall overstrength factor for a typical configuration of slabs are demonstrated in this chapter.

4.7 References

Adebar, P., and Bohl, A. (2011). Plastic hinge lengths in high-rise concrete shear walls. *ACI Structural Journal*, 148-157.

Antoniou, S., Rovithakis, A., and Pinho, R. (2002). Development and verification of a fully adaptive pushover procedure. In *Proceedings of the Twelfth European Conference on Earthquake Engineering*.

Aktan, A. E., and Bertero, V. V. (1984). Seismic response of R/C frame-wall structures. *Journal of Structural Engineering*, *110*(8), 1803-1821.

ATC-40 (1996). *Seismic evaluation and retrofit of concrete buildings*. Redwood City, California: Applied Technology Council, Seismic safety commission.

Building Seismic Safety Council (2004). *NEHRP recommended provisions for seismic regulations for new buildings and other structures* (FEMA 450). Retrieved from https://www.nehrp.gov/pdf/fema450provisions.pdf .

Elnashai, A. S., and Mwafy, A. M. (2002). Overstrength and force reduction factors of multistorey reinforced concrete buildings. *The structural design of tall buildings*, *11*(5), 329-351.

Fajfar, P., and Gašperšič, P. (1996). The N2 method for the seismic damage analysis of RC buildings. *Earthquake Engineering and Structural Dynamics*, *25*(1), 31-46.

FEMA 356 (2000). *Commentary for the seismic rehabilitation of buildings*. Washington, DC: Fedearl Emergency Management Agency.

FEMA 440 (2005). *Improvement of nonlinear static seismic analysis procedures*. Washington, DC: Fedearl Emergency Management Agency.

FEMA 695 (2009). *Quantification of building seismic performance factors*. Washington, DC: Fedearl Emergency Management Agency.

Hines, E. M., Restrepo, J. I., and Seible, F. (2004). Force-displacement characterization of well-confined bridge piers. *ACI Structural Journal, Vol. 101, No. 4,* pp. 537–548.

Humar, J. L., and Rahgozar, M. A. (1996). Concept of overstrength in seismic design. *Eleventh world conference on earthquake engineering*. 639, 1-8. Retrieved from http://www.iitk.ac.in/nicee/wcee/article/11_639.PDF .

Kabeyasawa, T., Shiohara, H., Otani, S., and Aoyama, H. (1983). Analysis of the full-scale seven-story reinforced concrete test structure. *Journal of the Faculty of Engineering*: *University of Tokyo, 37*(2), 431-478.

Krawinkler, H., and Seneviratna, G. D. P. K. (1998). Pros and cons of a pushover analysis of seismic performance evaluation. *Engineering structures*, *20*(4-6), 452-464.

Mander, J. B., Priestley, M. J., and Park, R. (1988). Theoretical stress-strain model for confined concrete. *Journal of structural engineering*, *114*(8), 1804-1826.

Mitchell, D., and Paultre, P. (1994). Ductility and overstrength in seismic design of reinforced concrete structures. *Canadian Journal of Civil Engineering*, *21*(6), 1049-1060.

Nassar, A. A., and Krawinkler, H. (1991). *Seismic demands for SDOF and MDOF systems* (Report No. 95). California: Stanford University, Blume Earthquake Engineering Center, Department of Civil Engineering.

New Zealand Society for Earthquake Engineering (NZSEE), (2006). *Assessment and Improvement of the Structural Performance of Buildings in Earthquake*. The New Zealand Society for Earthquake Engineering.

NZS1170.5 (2004). Concrete Structures Standard, NZS 1170.5:2004 Parts 1 and 2 Standards New Zealand.

NZS3101 (2006): Concrete Structures Standard, NZS 3101:2006 Parts 1 and 2 Standards New Zealand.

Panagiotou, M., Restrepo, J. I., and Conte, J. P. (2010). Shake-table test of a full-scale 7-story building slice. Phase I: Rectangular wall. *Journal of Structural Engineering*, 137(6), 691-704.

Park, R. (1996). Explicit incorporation of element and structure overstrength in the design process. *Proceedings of the 11th WCEE. IAEE.* Acapulco, Mexico.

Paulay, T., and Uzumeri, S. M. (1975). A critical review of the seismic design provisions for ductile shear walls of the Canadian code and commentary. *Canadian Journal of Civil Engineering*, *2*(4), 592-601.

Priestley, M. J. N. (1997). Displacement-based seismic assessment of reinforced concrete buildings. *Journal of earthquake engineering*, *1*(01), 157-192.

Priestley, M. J. N., Calvi G. M., and Kowalsky M. J. (2007). *Displacement-based seismic design of structures*. Pavia, Italy: IUSS Press.

SAP2000, CSI, S. (2014): Ver. 17.1.1, integrated finite element analysis and design of structures basic analysis reference manual. Berkeley (CA, USA), Computers and Structures INC.

5 Investigation of the System Overstrength in Multi-storey Shear Wall Buildings under Dynamic Excitation

5.1 Introduction

Under high-intensity earthquakes, multi-story RC shear walls might respond inelastically due to the change in the material and geometric properties. Nonlinear response history analysis that takes the material and geometric nonlinearity of structures into account has been commonly utilized for nonlinear seismic response computation. Hence, in this study all of the material and geometric nonlinearity in the whole structure is reflected in a three-dimensional nonlinear finite element model that was previously verified. The nonlinearities are simulated during the nonlinear direct-integration time history analysis available in SAP2000 software. Multilayered nonlinear shell elements modeled with nonlinear material behavior are used to simulate the reinforced concrete structural walls and linear shell elements are used to model the floor slabs. The gravity columns are idealized as axial springs with elastic behavior in tension and compression. A detailed explanation of the finite element model was presented in the previous chapter. The above mathematical model is able to account for material nonlinearity during the nonlinear direct-integration analysis in conjunction with P-delta effect associated with the geometrical nonlinearity provided by the SAP2000 software.

5.2 Description of Case Studies

The case study buildings, specifications are given in Table 5-1. The dynamic response of three case study shear wall buildings is investigated in this chapter. These buildings have the same geometry with different out-of-plane stiffness of floor slabs. The plan dimensions and design information of these case study buildings have been already provided in Chapter 4. The results of pushover analysis presented in the previous chapter indicated that the system overstrength factor highly depends on the floor slab flexural stiffness. The system overstrength factors are presented in Table 5-2 for the three case study buildings at four different base rotations. Table 5-2 displays the numerical values for the system-overstrength factor which were

estimated by employing the pushover analysis results under constant force distribution proportional to the first elastic mode shape.

Table 5-1: Variables in the first group of case study buildings

Case	Slab flexural stiffness	Slab length in X direction(L_x) (m)	Slab length in Y direction(L_y) (m)
Case1-1/wall only	0	6	6
Case2-2	$0.25EI_g$	6	6
Case2-3	$0.50EI_g$	6	6

Table 5-2: Effect of slab flexural stiffness on the system overstrength factor (excluding P-Δ)

Ω_s (L_x=6 L_y=6)	θ_b @ yielding point (rad)		θ_b=0.005 (rad)	θ_b=0.01 (rad)	θ_b=0.015 (rad)
Case1-1, wall only	θ_y= 0.00123	1.0	1.126	1.210	1.229
Case2-2, EI_e=0.25 EI_g	θ_y= 0.00123	1.0	1.252	1.465	1.612
Case2-3, EI_e=0.50 EI_g	θ_y= 0.00122	1.0	1.336	1.643	1.884

θ_b: Base rotation (rad) θ_y: Yield base rotation (rad)

We have explained the importance of wall edge vertical deformations on the floor slab-wall-gravity columns interaction in the previous chapter. For a given structural wall, according to the results of pushover analysis, the wall vertical edge deformation under lateral force does not change significantly with increase in the flexural stiffness of slabs (sectional flexural stiffness of the floor slab as well as slab length). However, it has been confirmed that vertical deformation compatibility between the floor slabs and structural walls in their connection region causes a significant system overstrength factor in the case study buildings with the larger floor slab flexural stiffness.

It is worth mentioning that the focus of this study is not the prediction of seismic demand in the case study buildings for a given seismic hazard level. Hence, the different methodologies available for the scaling and selection of ground motion records to conduct the nonlinear response history analysis are not investigated too deeply in this chapter. The scaling and

selection process of ground motion records under a specific seismic hazard level is of great importance in the vulnerability or risk assessment. In risk assessment of buildings, we seek to find the suite of ground motions need to be representative of the site location for a given seismic hazard level. However, in this thesis, we only intend to investigate the dynamic response of the system under naturally recorded or artificial ground motions at a predefined base rotation. Hence, we start increasing the intensity of ground motions to achieve a target maximum transient base rotation in the structural walls. In other words, to be consistent with the pushover analysis results, the scale factor (SF) for a given ground motion has been selected such that the maximum transient base rotation in nonlinear response history analysis reaches the specific values equal to 0.005, 0.01 and 0.015 rad respectively. Detail discussions and results are only presented for the base rotation equal to θ_b=0.01 (rad). This level of base rotation can be representative of typical value expected under a design base earthquake. It will be illustrated that this level of base rotation in the specific case studies is equivalent approximately up to 0.02 global drift. This procedure is repeated for each case study building separately. Although dynamic analysis under a large number of ground motions can improve the accuracy of results by increasing the chance of finding the best average values for the responses, in this chapter very limited number of records has been used due to the requirement of computationally expensive models. However, it is interesting to highlight that a number of response parameters are not found to be very sensitive to the ground motion characteristics. In this study, we intend to impose a specific base rotation in all case studies under the dynamic excitation by manipulating the scale factor. A scale factor is a numerical scalar value. Each ground motion time series is multiplied by this scalar value. This scale factor has been selected carefully to induce the target base rotation with many trial and errors. The objective of this study is to understand the mechanism of wall-slab and gravity columns interaction at the different base rotation/drift levels under earthquake excitations.

5.3 Equation of Motion and Distribution of Mass

All realistic physical structures have an infinite number of dynamic degrees of freedom. However, only a limited number of degrees of freedom can be used in mathematical models used to represent a given structure. A mathematical model with a limited number of nodal points is selected to represent the case study buildings considered herein. Each node point may have up to six degrees of freedom, three translations and three rotations. A detailed description of degrees of freedom in the elements employed for the analysis in this project has been presented in chapter 2.

Selection of the nodes and the corresponding degrees of freedom greatly depends on the degree of complexity of the structure, the characteristics of ground motion, and the precision with which the response calculations are to be made. However, engineering judgment plays an important role in the selection of the nodes and the corresponding degrees of freedom. If the mathematical model consisting of a total of n degrees of freedom is subjected to a ground motion, the equations of motion in a given direction for the system can be expressed in a matrix form as

$$[\mathrm{M}]\{\ddot{\mathrm{x}}\} + [\mathrm{C}]\{\dot{\mathrm{x}}\} + [\mathrm{K}]\{\mathrm{x}\} = -[\mathrm{M}]\ddot{a}_{\mathrm{g}}(t) \quad (5.1)$$

where:

$\{\ddot{x}\}, \{\dot{x}\}\ and\ \{x\}$ are vectors of relative accelerations, velocities and displacements, respectively, at time t.

[M] = Mass matrix

[C] = Damping matrix

[K] = Stiffness matrix

$\ddot{a}_g(t)$ = Time history of ground or support motion

By solving Equation (5.1), the relative accelerations of the mass points are obtained. The absolute accelerations of these nodes, which may be necessary for the design of acceleration sensitive non-structural elements, can be obtained by the Equation (5.2)

$$\{\ddot{X}\} = \ddot{a_g}(t) + \{\ddot{x}\} \quad (5.2)$$

, where $\{\ddot{X}\}$ = Absolute acceleration vector at time t.

In linear systems, the matrix [M], [C] and [K] remain constant in each time step but in nonlinear systems the matrix [C] and [K] can change from one-time step to another time step. Detailed description of numerical methods to solve the above dynamic equation of motion can be found in Chopra (2001).

In a nonlinear dynamic analysis, the variation of stiffness matrix [K] in each time step follows the force/resistance deformation relationship which is normally well established. However, the variation of damping matrix [C] in each time step is very critical to get reliable results in nonlinear systems.

In a dynamic analysis under a given ground motion record, it is quite critical to decide how the mass of the system should be distributed on the specific dynamic degrees of freedom. In the first part of this study, we only distribute the horizontal mass at the floor level without assigning any vertical mass on the nodes. It is also important to consider that in multi-storey shear wall buildings the distribution of horizontal mass may differ from the vertical mass distribution. The reason behind this can be attributed to the role of gravity columns (or frames) on resisting the vertical mass. While the structural walls must resist the whole horizontal mass of floors in each direction, both the gravity columns and structural walls resist the vertical mass (Figure 5.1).

As demonstrated later, including vertical mass on degrees of freedom can have a significant impact on the axial force amplification in the structural walls even in Case1-1 (wall-only). In the next section, a number of engineering demand parameters (EDP) are presented for the case study buildings with only horizontal mass distributed on their nodes. The following sections

demonstrate the results of nonlinear response history analysis by assuming the Rayleigh damping model at two different modes to solve the equation of motions. The two options associated with the two damping models are named as Option A and Option B from now on. Detail information of these options are explained in the next section.

Figure 5.1 illustrates a typical plan of the case study buildings used in this chapter. Case studies were subjected to three different ground motions in the Y direction. The portion of the floor contributing to the horizontal inertia mass and vertical inertia mass is displayed with different hatches on Figure 5.1. Although we assume that only horizontal mass exists in each direction and vertical mass is equal to zero, we are taking the gravity loads (dead load plus 25% of live load) on the walls and columns into account in the analysis. The gravity loads are applied gradually (pseudo static) before starting the nonlinear response history analysis.

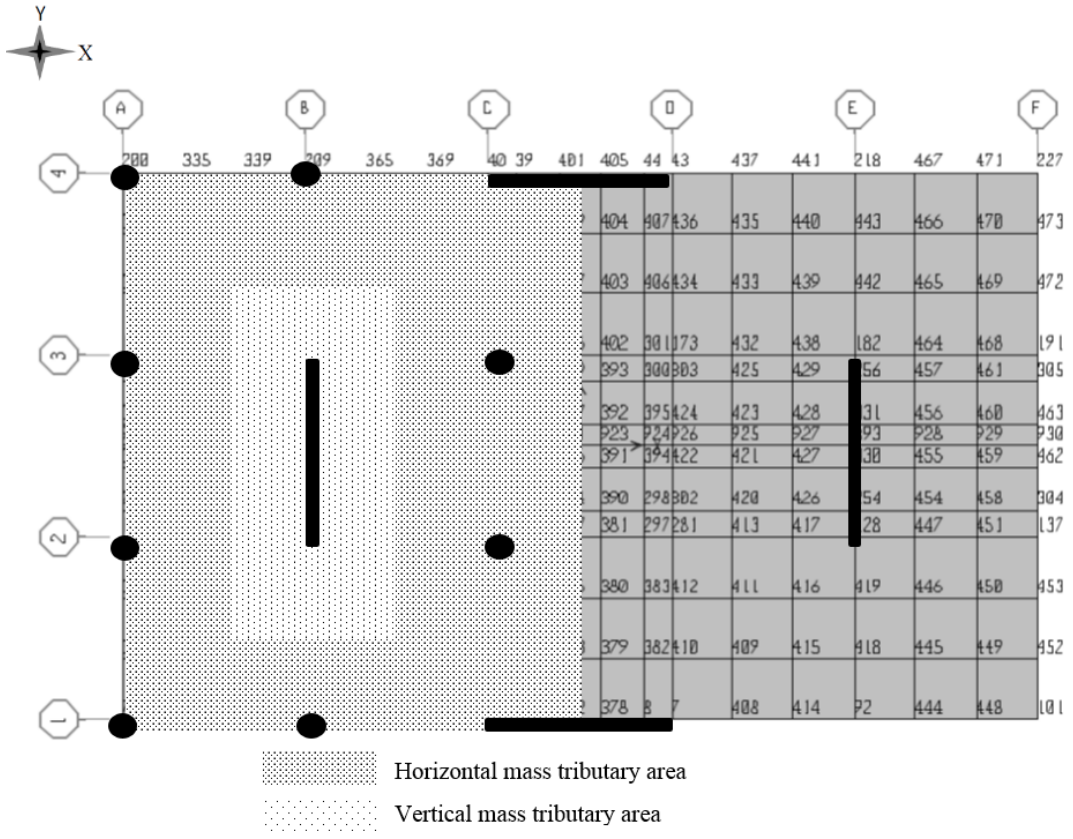

Figure 5.1: Typical plan and representation of vertical and horizontal mass distribution in the case study buildings

Table 5-3 lists the mass distributed on each floor. The current mass distribution assumes zero vertical mass. In the next stage vertical mass will also be assigned to the floors to see any possible changes in the results. The inclusion of vertical mass in the model may change the amplification of axial forces on the structural walls.

Table 5-3: Vertical and horizontal mass distribution in case study buildings

All case studies	Mass X ($kN.s^2/m$)	Mass Y ($kN.s^2/m$)	Mass Z ($kN.s^2/m$)
Floor 8	463.032	463.032	0.0
Floor 7	463.032	463.032	0.0
Floor 6	463.032	463.032	0.0
Floor 5	463.032	463.032	0.0
Floor 4	463.032	463.032	0.0
Floor 3	463.032	463.032	0.0
Floor 2	463.032	463.032	0.0
Floor 1	463.032	463.032	0.0

5.3.1 Damping

For dynamic analysis of elastic structures, it is a common practice to specify an elastic viscous damping to the mathematical model to account for energy dissipation through the system. In dynamic analysis of inelastic structures, that elastic energy dissipation is still present and is added to the energy dissipation due to inelastic behavior of materials. Inelastic energy dissipation is modeled directly in a nonlinear dynamic analysis. For modelling of elastic energy dissipation, elastic viscous damping is still a powerful tool; however, since the direct time integration analysis does not make use of natural modes of vibration to solve the equation of motion, it is not practical to specify a modal damping in each mode separately. SAP2000 uses Rayleigh damping model in the form of "αM+βK", which assumes that the whole structure has a constant damping matrix, C, given by:

$$C= \alpha M+\beta K \tag{5.3}$$

Where M is the structure mass matrix, K is the initial elastic stiffness matrix; α and β are multiplying factors. In Equation (5.3) α and β are mass and stiffness proportionality factors, respectively.

Relationships between the modal equations and orthogonality conditions allow this equation to be rewritten as:

$$\xi_n = \frac{1}{2\omega_n}\alpha + \frac{\omega_n}{2}\beta \tag{5.4}$$

where ξ_n is the critical damping ratio, and ω_n is the natural frequency ($\omega_n = \frac{2\pi}{T_n}$).

If the damping ratios (ξ_i and ξ_j) associated with two specific frequencies (ω_i and ω_j), or modes, are known, the two Rayleigh damping factors (α and β) can be evaluated by the solution of a pair of simultaneous equations, given mathematically by:

$$\begin{bmatrix}\xi_i \\ \xi_j\end{bmatrix} = \frac{1}{2}\begin{bmatrix}\frac{1}{\omega_i} & \omega_i \\ \frac{1}{\omega_j} & \omega_j\end{bmatrix}\begin{bmatrix}\alpha \\ \beta\end{bmatrix} \tag{5.5}$$

When damping for both frequencies is set to an equal value, the conditions associated with the proportionality factors can be further specified from Equation (5.5). If the first and second mode frequencies, ω_1 and ω_2, are known, and both of them have the same damping ratio, the proportionality factors may be computed from the following expression (Clough and Penzien, 2003):

$$\begin{Bmatrix}\alpha \\ \beta\end{Bmatrix} = \frac{2\xi}{\omega_1+\omega_2}\begin{Bmatrix}\omega_1\omega_2 \\ 1\end{Bmatrix} \tag{5.6}$$

Note that α and β are directly proportional to ξ. It can be shown easily that to increase the target damping from 2 percent to 5 percent of critical, all that is required is a multiplying factor of 2.5 on α and β.

It is evident that αM damping corresponds to more damping in lower (longer period) modes and less damping in higher (shorter period) modes, with the relationship:

$$\xi_i = \alpha\frac{T_i}{4\pi} \tag{5.7}$$

Where T_i= period of mode "i" and ξ_i = proportion of critical damping in this mode. It can also be shown that βK damping corresponds to less damping in lower modes and more damping in higher modes, with the relationship:

$$\xi_i=\beta\frac{\pi}{T_i} \tag{5.8}$$

By combining αM and βK damping it is possible to have almost constant damping over a significant range of periods, as indicated in Figure 5.2.

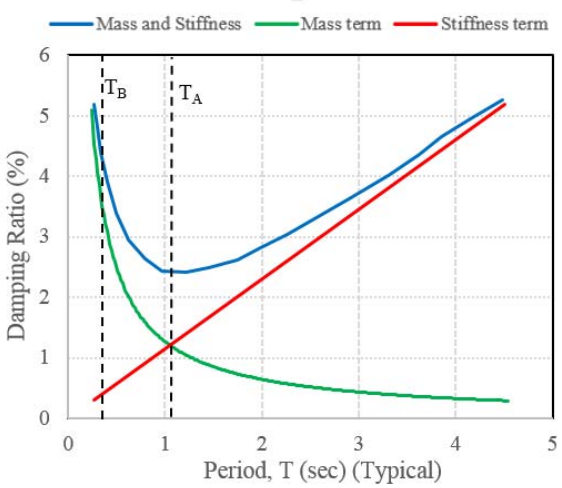

Figure 5.2: Classical Rayleigh damping model

In SAP2000 procedure, instead of specifying values for α and β, two periods of T_A and T_B and the damping percentages at these ratios should be specified. Then the values of α and β will be calculated according to the above-explained formulation.

It is apparent that Rayleigh damping can be specified exactly at only two periods in order to solve for α and β in the above equations. A typical choice for T_A and T_B is using 1_{st} and 2_{nd} mode or any other higher mode respectively. It is evident from Figure 5.2 and above formulation that is not possible to get a same damping ratio in the all modes. However, by choosing the appropriate values for α and β it is possible to have almost nearly constant damping over the range of specified periods, as indicated in Figure 5.2. SAP2000 manual

recommends the value of $0.9T_1$ and $0.25T_1$ (or the shortest period of structure which may contribute to the response) as a typical value for the damping purpose. T_1 is the first mode period of the structure.

The dynamic properties of the case study shear wall buildings are summarized in Table 5-4. Mode shapes are normalized to have the unit modal amplitude at roof level. It is evident from the numerical values of Table 5-4 that the presence of flexural stiffness of slab in the model named as Case2-3 decrease the first mode period only by 3.4 % which is not very significant. The remaining higher modes are almost the same.

Table 5-4: Dynamic properties of case study buildings

Case	Period (Sec)			Modal Participation Factor (Γ_i)			Modal Mass Ratio (α_i)		
	T_1	T_2	T_3	Γ_1	Γ_2	Γ_3	(α_1)	(α_2)	(α_3)
Case1-1	0.822	0.154	0.068	1.44	0.63	0.28	0.68	0.22	0.064
Case2-2	0.807	0.154	0.068	1.44	0.63	0.28	0.68	0.22	0.063
Case2-3	0.794	0.153	0.068	1.39	0.63	0.28	0.68	0.22	0.063

The configuration, member details and dynamic properties of the case study buildings are presented in detail in Chapter 4. Both pushover and nonlinear response history analyses were performed using nonlinear behavior of concrete (confined and unconfined) and reinforcing bar materials including P-Delta effects. The nonlinear behavior of concrete (confined and unconfined) and reinforcement were modeled as discussed in Chapter 3 and Chapter 4.

The targeted structural frequencies and the resulting damping proportionality factors are shown in Table 5-5 for the two different options. Two different alternatives have been considered to model damping in this study. While Option A uses the global initial stiffness and mass matrix to form the damping matrix, Option B employs the initial stiffness and mass matrix at the element level (or material level) to generate the damping matrix. The latter approach is similar

to the method developed by Puthanpurayil et al., (2016) to formulate the damping in the element level.

When it is assumed that the damping matrix is proportional to mass and initial stiffness (at the global level), artificial damping may be generated in the higher modes (with higher frequencies or lower periods of vibration) (Puthanpurayil et al., 2017; Charney, 2008), with the effective damping forces increasing several hundred percent. Hence, in some cases, the use of initial stiffness proportional damping at global level may produce extreme errors. When the damping formulation is based on initial stiffness, the best approach to avoid these artificial forces is to employ the material level damping to differentiate between the yielded and elastic materials. In the material (element) level damping model, we provide a stiffness proportional damping multiplier equal to zero for all yielding materials (elements) having substantial initial stiffness. The use of tangent stiffness proportional damping, when available, may also bypass this problem partially.

Hence, the stiffness proportional damping factor must not be included in the yielded elements used to represent the vertical yielding of structural walls in the case study buildings. In this project, these elements were located at the potential plastic hinge regions. These materials have a relatively high initial stiffness before yielding and small post-elastic stiffness after yielding. For example, in a structural wall with vertical reinforcement, before the rebar yields in the vertical direction, there is virtually no vertical velocity in the nodes due to relatively high vertical initial stiffness. After yielding, the vertical velocity (the rate of change in the vertical deformation of wall) is significant because the material post-yield stiffness is very low and the rate of change in deformation (velocity) is very high. If a stiffness proportional damping factor is used for yielding material large viscous axial forces (damping forces) will develop in the element.

These artificial viscous axial forces are the product of the axial velocity, the initial vertical stiffness of the materials and the stiffness proportional damping factor. The numerical values of these damping forces can be quite large. These viscous axial forces occur in phase with the plastic vertical movement; hence the plastic axial stiffness forces and the viscous axial forces are additive. These large axial forces produce artificially high base moments. The axial amplification factor has been reported separately in the following section. In a similar fashion, the use of stiffness proportional damping in discrete lumped plastic hinges can produce a grossly inaccurate analysis result. The reader can see (Chrisp, 1980; Carr, 1997; Charney, 2008; Puthanpurayil et al., 2011; and Carr and Puthanpurayil 2017) for further details.

Here, two distinctive approaches are used to incorporate damping in the analytical model. The first approach is named as damping model A. In this approach, Rayleigh damping in the mathematical model was based on the global initial stiffness matrix and mass matrix. The damping ratios attributed to each mode of vibration are illustrated in Table 5-5.

In the second approach which is named as damping model B, the damping model is assigned to the structural system at the local (material) level, not the global level. In other words, the damping ratios are allocated to the steel and concrete materials separately according to the expected nonlinearity in the structure. In other words, different coefficients are used for concrete and reinforcement in the potential plastic hinge region and remaining part of the structure. To avoid above mentioned spurious damping in the model due to yielding of elements in the plastic hinge regions, the damping ratio in the materials (rebars and concrete) which are expected to yield has been assigned only proportional to the mass (ATC-72-1, 2010). Since the first elastic mode of case study buildings were changed slightly due to stiffness of floor slabs corresponding value of damping parameters in Table 5-5 were adjusted accordingly.

Table 5-5: Two types of damping models for the nonlinear dynamic analyses

Damping		α (sec^{-1})	β (sec)
Damping model A α[M]+β[K]-Global T_1=0.8217, T_2=0.1541 ζ=2.5%	All materials	0.322	1.033E-3
Damping model B α[m]+β[k]-Local T_1=0.8217, T_2=0.1541 ζ=2.5%	Non-Yielding material	0.322	1.033E-3
	Yielding material	0.322	0

5.4 Hysteresis Rules for Material Nonlinearity

In a dynamic analysis, hysteresis loops are described by a hysteresis model and its corresponding rules, which define the load reversal paths within the hysteresis loops. These hysteresis loops depend on material properties and type of loading. They reflect the force-deformation (resistance-deformation) characteristics of structural members (sections or fibers) subjected to cyclic loading.

Resistance-deformation relationship under monotonically increasing loading is called the skeleton curve or backbone curve. The skeleton curve provides an envelope of the hysteresis resistance-deformation relationship. The skeleton curve for the reinforced concrete member is normally represented by a trilinear relation with stiffness changes at flexural cracking and tensile yielding of longitudinal reinforcement. The skeleton curve of a member must be defined on the basis of mechanical properties of constitutive materials and geometry of the member. Some researchers suggest the use of a bilinear relation with a stiffness change at yielding, ignoring the initial un-cracked stage, because a reinforced concrete member subjected to light or moderate axial force can be easily cracked by shrinkage, accidental gravity loading or dominantly by previous frequent wind and ground motions (under the serviceability limit state design actions).

The state of the art is not sufficient to determine precisely the ultimate point on the hysteresis curve, i.e. the deformation at which the resistance of a member starts to decay, according to mechanics of materials. The force-deformation relation after the onset of strength decay is normally not modeled because the behavior is strongly dependent on a particularly localized deterioration of materials.

In order to appropriately select the hysteresis type in nonlinear analyses, SAP2000 provides two hysteresis types at the material level for reinforcement and concrete: Kinematic hysteresis, Takeda hysteresis. The following describes the hysteretic models which were preprogrammed into SAP2000. Although these simplified models employ simple rules for cyclic behavior of steel and concrete under reversed loadings, the prediction of global demands is in the acceptable range compared with other uncertainties which exist in our modelling approach. Moreover, in the context of dynamic analysis, hysteresis loops should be able to represent the appropriate dissipation of energy in the system. Hence, the ability of hysteresis loops to follow the exact cyclic behavior of the material is not of too much interest in this project. Thus, as far as our mathematical model is able to predict the global demands, it can be deemed acceptable for this project. Chapter 3 provides detail information regarding the verification of numerical model employed in this project. Results of a shake table experimental testing at the system level were employed to confirm the validity of the numerical model.

5.4.1 Multi-Linear Kinematic Hysteresis Loop

There are two types of hardening material models available in SAP2000. The isotropic hardening model and the kinematic hardening model are two most common models used to model metal (steel) type behavior. However, if one takes a reinforcement specimen and loads it in tension into the plastic range, and then unloads it and continues on into compression, one finds that the yield stress in compression is not the same as the yield strength in tension, as it would have been if the specimen had not first been loaded in tension. In fact, the yield point,

in this case, will be significantly less than the corresponding yield stress in tension. This reduction in yield stress is known as the Bauschinger effect. The effect is illustrated in Figure 5.3. The dotted lines are two extreme cases which are used in the plasticity models; the first is the isotropic hardening model, in which the yield stress in tension and compression are maintained equal, and the second being the kinematic hardening, in which the total elastic range is maintained a constant value throughout the deformation.

Figure 5.4 (a) is representative of uniaxial stress strain curve for isotropic hardening rule. If the part is taken beyond the yield stress, it begins to deform plastically. If taken to a maximum stress (point A) and the load is released, it unloads along the dashed line. If the part is loaded again, no additional plastic deformation occurs until the stress reaches point A. If the part is put into compression, it compresses elastically along the dashed line until it reaches point B, and then it yields in compression. With isotropic hardening, the change in stress from point A to point B is twice the maximum stress previously obtained.

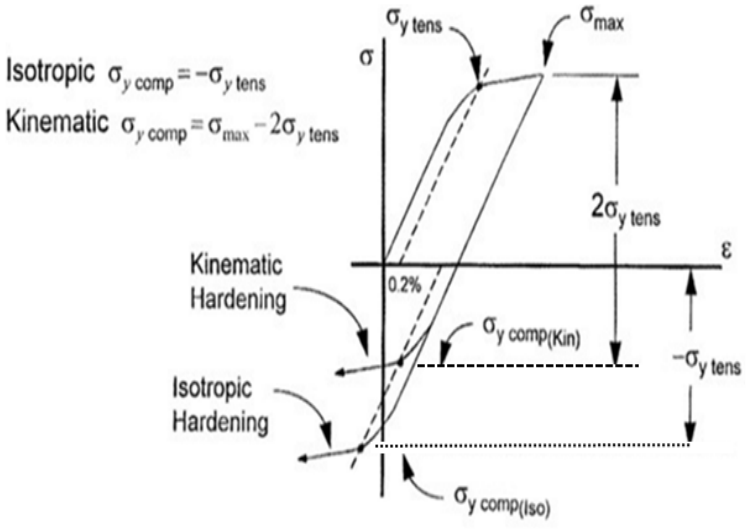

Figure 5.3: Hardening rules

The multilinear Kinematic model, based on the kinematic hardening behavior commonly observed in the metals, presents a nonlinear force-deformation relationship under the monotonic loading provided by a multilinear curve described by a set of user-defined points, as seen in Figure 5.4 (b). The kinematic hardening rule assumes that yield stress following the inelastic deformation is degraded, unlike the isotropic hardening rule that assumes the symmetrical behavior in tension and compression. The kinematic hardening model is preferred for the analysis involving cyclic loading to account for Bauschinger effect in reinforcement bars. Figure 5.4 (b) represents a typical uniaxial stress-strain curve.

In Figure 5.4, the first slope on either side of the origin is elastic, and the remaining parts of the curve define the plastic deformation. Upon reversals of deformation, the hysteresis rule follows the two elastic segments of the curve from either side of the origin before initiating plastic deformation in the reverse direction. Once initiated, plastic deformation in one direction of loading forces the yielding in the reverse direction of loading to occur earlier.

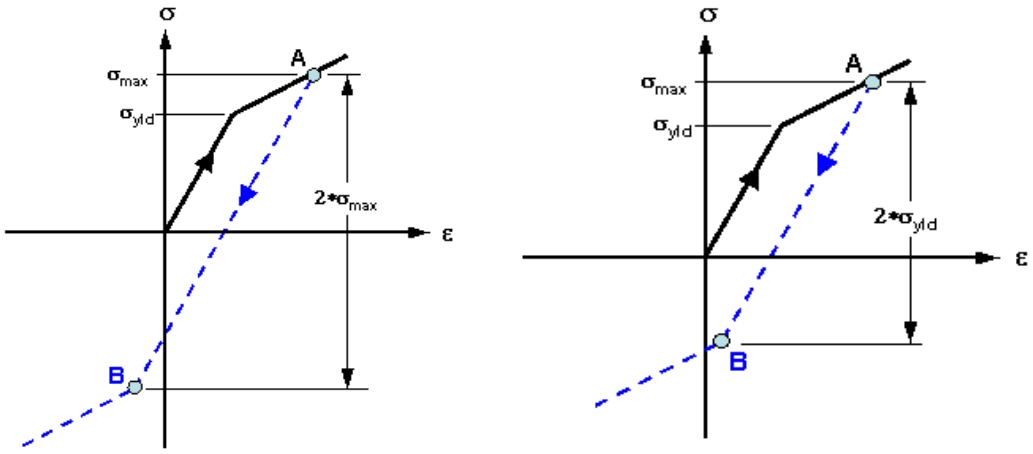

(a) (b)

Figure 5.4: (a) Isotropic hardening rule (b) Kinematic hardening rule

To appropriately illustrate the behavior of load reversal paths under cyclic loading with increasing displacement magnitude, Figure 5.5 defines the origin as point 0, the points on the positive axis as 1, 2, 3 from the origin, and the points on the negative axis as -1, -2, -3 from the origin. In Figure 5.5, the loading is initially elastic and is described from point 0 to point 1 on the curve.

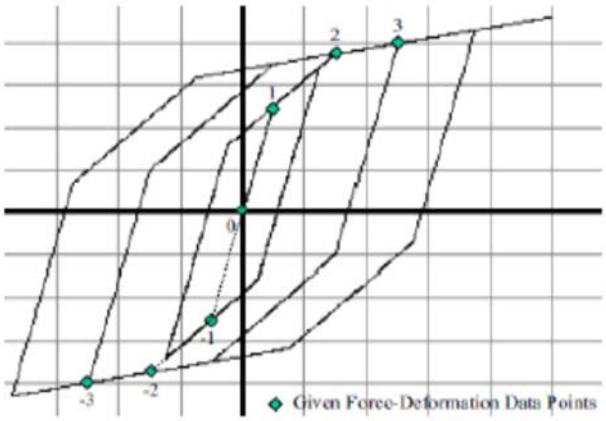

Figure 5.5: Multilinear Kinematic plasticity for uniaxial deformation

- As loading increases from point 1 to point 2, the onset of plastic deformation begins and is described by the movement from point 1 toward point 2 on the curve. In effect, points -1 and 0 are pulled by point 1, moving the same amount in the force and

deformation directions. The movement of point 0 along with points -1 and 1 occurs to preserve the elastic slopes.

- Upon load reversal, unloading occurs along the shifted elastic line from point 1 to point-1 and then toward point -2, which will not move until it is forced by loading in the negative direction, or until loading in the positive direction forces movement in point 2, which consequently pulls point -2 by an identical amount.
- Upon reversal of the load once more, point 1 is advanced toward point 2, and together they are forced toward point 3, thereby pulling along with them points -1 and -2. Throughout the rest of the analysis, the procedure described above is continued. Beyond points 3 and -3 the slopes are maintained even as these points carry on shifting with the furthering of the analysis.

It is worth mentioning that the employed idealized mathematical model does not account for opening and closing of cracks in analysis. RC members commonly illustrate stiffness reduction during the unloading and reloading due to evolution of cracks and corresponding damage in concrete. To account for this type of behavior in flexural RC members the Takeda hysteresis rule is assigned to rebars instead of the Kinematic rule. Detailed description of the Takeda rule is presented in the next section.

5.4.2 Multilinear Takeda Hysteresis Loop

The hysteresis model developed by Takeda et al. (1970) is based on the experimental behavior observed on a number of medium-size reinforced concrete members subjected to lateral load reversals with light to medium amount of axial load. The Takeda model simulates dominantly flexural behavior. Simplified Takeda hysteresis models were proposed by Otani and Sozen (1972) and by Mondkar and Powell (1975), using a bilinear backbone curve.

The multilinear Takeda model is identical to the multilinear Kinematic model in the specification of properties and overall shape similarities to the cyclic load behavior. The distinguishable factor between the two models lies in the multilinear Takeda model attributed to using a stiffness degrading hysteretic loop, as seen in Figure 5.6. The Takeda model includes stiffness changes at flexural cracking and yielding by using a multilinear skeleton force-deformation relationship.

A hysteresis model must be able to provide the stiffness and resistance under any displacement history. At the same time, the basic characteristics need to be defined by the member geometry and material properties. The current state of knowledge is sufficient to define flexural hysteresis models. However, it is not sufficient to determine the degree of stiffness degradation due to the deterioration of shear-resistance in the past-yielding phase and rebar-concrete bond mechanisms.

The Takeda model is able to account for the stiffness changes at flexural cracking and yielding, and also strain-hardening characteristics. The unloading stiffness reduced by an exponential function of the previous maximum deformation. Takeda et al. (1970) also prepared a set of rules for load reversals within the outermost hysteresis loops.

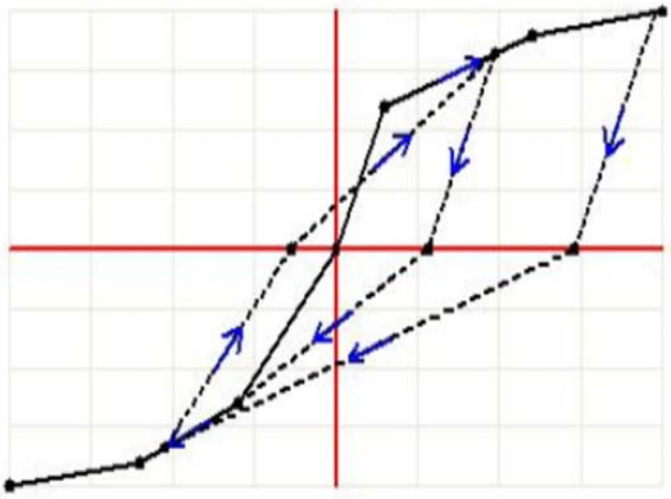

Figure 5.6: Multilinear Takeda plasticity for the uniaxial deformation

The behavior of the multilinear Takeda model differs from that of the multilinear Kinematic model particularly in the unloading path, as seen in Figure 5.6. When crossing the horizontal axis, the multilinear Takeda model curve follows a secant path to the backbone force deformation relationship upon unloading in the reversed direction. SAP2000 implements Takeda model with a fixed value for the unloading stiffness. The full description of this model is provided by Takeda et al. (1970).

5.5 Ground Motion Selection and Scaling

5.5.1 Ground Motion Selection

Nonlinear response history analysis of structures is highly sensitive to the structural modelling and ground motion characteristics. Therefore, it is broadly accepted to use a set of representative ground motion records that account for uncertainties in their severity, frequency and duration characteristics. However, there is no universally accepted procedure to find the best suit of ground motion records to predict the deformation response and failure modes of the structures in a specified hazard level. Thus, for sake of simplicity, nonlinear seismic demand (mostly deformation or ductility demand) prediction is generally performed iteratively by pushover analysis. This method compares the push over capacity curve with the smoothed response spectra (i.e. the demand spectrum) to obtain the performance point. It should be highlighted that description of a method to find the nonlinear deformation demand by the intersection of the pushover curve and smoothed demand curve is out of the scope of this chapter. In this study, the accuracy of results found by pushover analyses (under the invariant lateral load pattern) is compared with responses which were obtained from the response history analysis under the randomly selected ground motion excitations.

According to the general principle of structural dynamics, the dynamic responses of a system subject to an arbitrary ground motion are sensitive to the frequency content of the records.

However, the degree of uncertainty in prediction of different engineering demand parameters can vary significantly. For example, estimation of the inelastic inter-storey drift in structural walls has less degree of uncertainty compared to the prediction of the shear force distribution over the height. Hence, it is critical to determine the main engineering demand parameters which are of main interest of this project. The principal engineering demand parameters in this investigation are the base moment and base rotation. Although the required scale factor to achieve a specified base rotation in the case study buildings under a given record varies significantly, the overall trend of response envelope for the base moment versus base rotation curve is not sensitive to the type of records. However, the shape and number of loops inside the base moment versus base rotation curve are quite different for each ground motion record. It is worth mentioning that unlike the envelope curve for the base moment versus base rotation, the envelope of system base shear versus base rotation can significantly vary for different records. This is mostly due to the nature of the records and higher mode effects.

It may be questioned why cyclic push-pull analysis was not employed to conduct nonlinear analysis in this project. To answer this question, it should be highlighted that in structural walls, moment distribution depends on the distribution of inertia forces on the floors over the height of building (mostly aligned with the fundamental mode) while the shear distribution may reach much higher values due to higher mode effects. Besides, it is important to draw the attention to the fact that the distribution of mass over the height and dynamic characteristics of the structural wall determine the shear response and its distribution over the floors. Additionally, the vertical deformations of structural walls (upward movement of structural walls due to movement of neutral axis and cyclic elongation) which induce the system overstrength most likely achieve the different values through the dynamic analysis.

Moreover, during dynamic response, shear force and moment response are not always in phase with each other. This means that, contrary to the static conditions, maximum moment and

maximum shear force do not necessarily occur simultaneously. Consequently, the structural wall with a given base section flexural capacity may be subjected to different distribution of shear force over the building height. Dynamic analysis enables us to find the shear force demand on the wall sections in each floor depending on the earthquake excitation. All these dilemmas urge us to conduct dynamic analysis instead of pushover analysis to find the system overstrength factors.

As will be demonstrated later, ductile response at the base of structural walls produces an envelope of base moment versus base rotation hysteresis loops that are irrelevant of distribution of lateral force over the height of the building in the inelastic phase. However, the results show that different loops can form inside the hysteresis envelope curves.

The ground motion records used in this study include El Centro (ELC) (Imperial Valley, 18 May 1940, NS component), Sylmar Olive View Med (SOVM) 360^{o} component (record from the 1994 Northridge earthquake) and Taft (was recorded at Kern County in 1952) earthquakes. These records were not modified to match with any spectrum because the objective of this investigation was to investigate the dynamic behavior of system up to a specified base rotation level. The peak ground accelerations (PGAs) of the selected ground motions are within 0.319g to 1.17g. The El-Centro record used here is a widely known ground motion which includes most of the frequency ranges in its frequency content. The description and specification of these ground motions have been explained in the next section.

This study investigates the lateral pushover response of case study shear wall buildings at various degrees of inelastic deformation levels represented by target base rotation. Three base rotation levels were considered as illustrated in Figure 5.7.

For each case study building, each ground motion record was scaled to obtain the pre-determined base rotation for the system considered. The 5% damped elastic pseudo-acceleration response spectra of the ground motions are given in Figure 5.8, Figure 5.9 and

Figure 5.10. The acceleration- time histories of ground motion records are also shown in these figures. The first ground motion was recoded in El-Centro (ELC) station in Imperial Valley earthquake. The duration of record was 31.14 second with the absolute maximum peak ground acceleration equal to 0.32g. The pseudo acceleration and displacement spectrum of this record are illustrated in Figure 5.8.

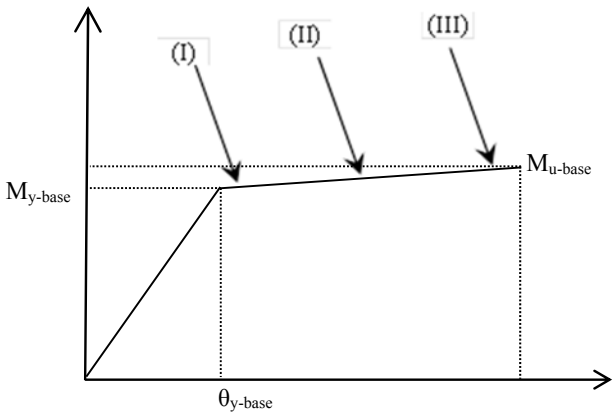

Base Rotation	Value (rad)
I	0.005
II	0.01
III	0.015

Figure 5.7: Predetermined base rotation levels for the dynamic analysis

The whole time series of records are scaled up or down with the same scale factor. However, for a given record, the number of iterations to reach a specified base rotation and the required scale factor is notably different.

The ELC record has the maximum and minimum acceleration equal to +0.2984g and -0.3188g respectively. The pseudo acceleration and displacement response spectra illustrate the maximum value of (0.5sec, 0.91g) and (2.8sec, 0.30m) respectively. It is evident that the response spectral of all three records are jagged in nature but have different shapes. Hence, it makes the prediction of response parameters quite challenging.

For practical purpose, a smooth spectrum is utilized in design to facilitate the prediction of demand at a given elastic period. Most of the probabilistic approaches have been developed to

quantify engineering demand parameters in terms of mean and standard deviations to appreciate these variations.

El Centro record (ELC)

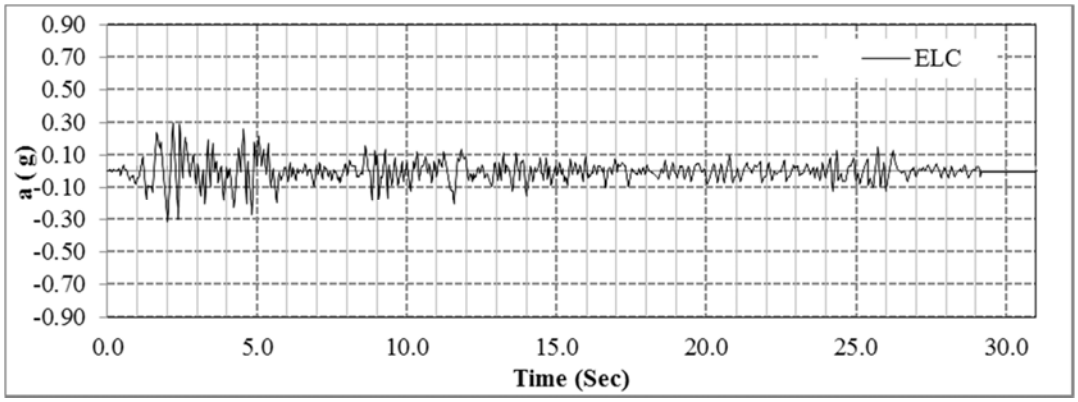

$a_{max(+)}$= +0.2984g
$a_{max(-)}$= -0.31882g
t=31.14 sec

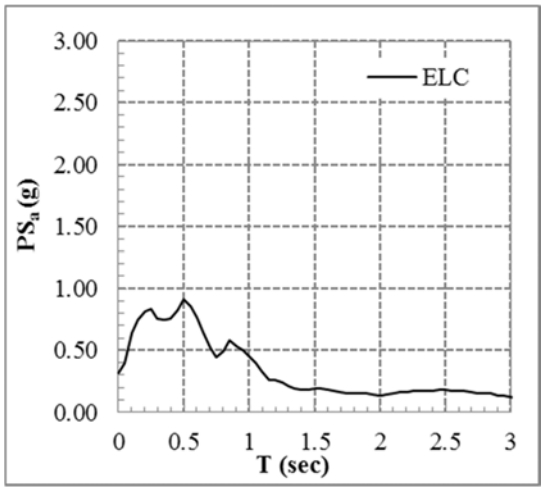

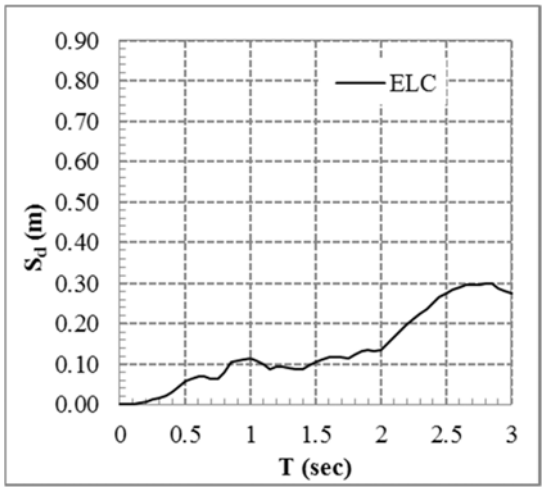

Figure 5.8: El Centro record and its spectrum

The SOVM record has the maximum and minimum accelerations equal to +0.8434g and -0.5895g respectively. The duration of the ground motion was 40.02 seconds. The pseudo acceleration and displacement response spectra illustrate the maximum values of (0.35s, 2.8g) and (2.5s, 0.78m) respectively.

Sylmar Olive View Med 360° record (SOVM)

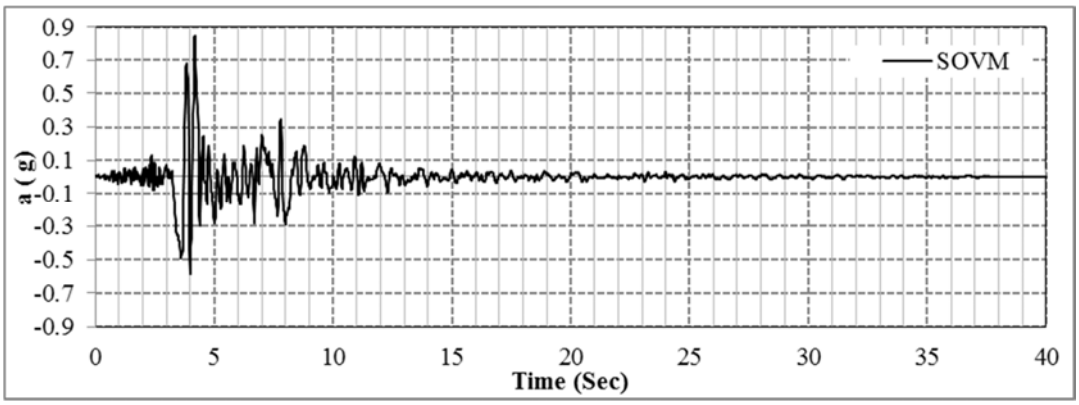

$a_{max(+)}$=+0.8434g
$a_{max(-)}$=-0.5895g
t=40.02 sec

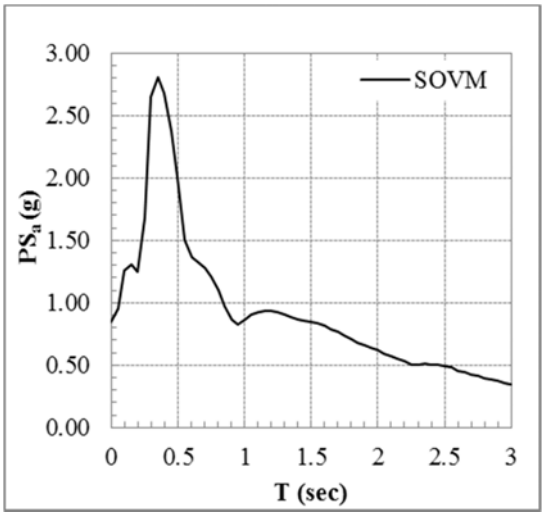

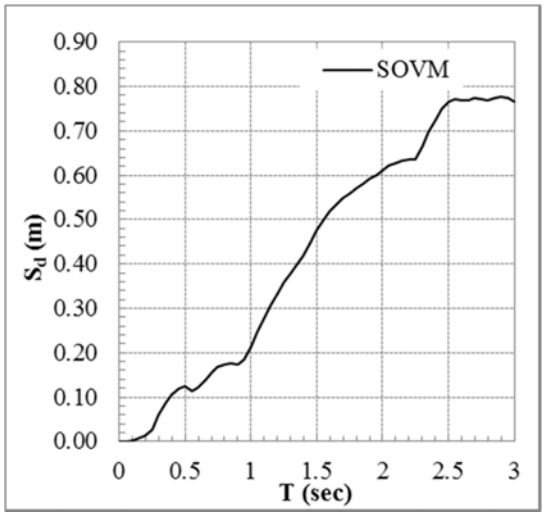

Figure 5.9: Sylmar Olive View Med 360° record and its spectrum

The TAFT record has the maximum and minimum acceleration equal to +0.1449g and -0.1589g respectively. The duration of ground motion was 58.02 second. The acceleration and displacement response spectra illustrate the maximum value of (0.3s, 0.6g) and (3.0s, 0.09m) respectively.

Taft record (TAFT)

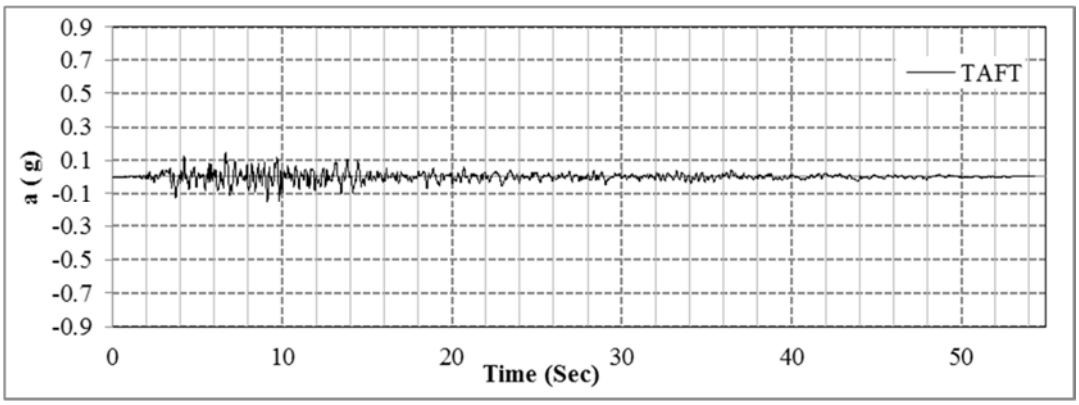

$a_{max(+)}$=+0.1449g
$a_{max(-)}$=-0.1589g
t=58.02 sec

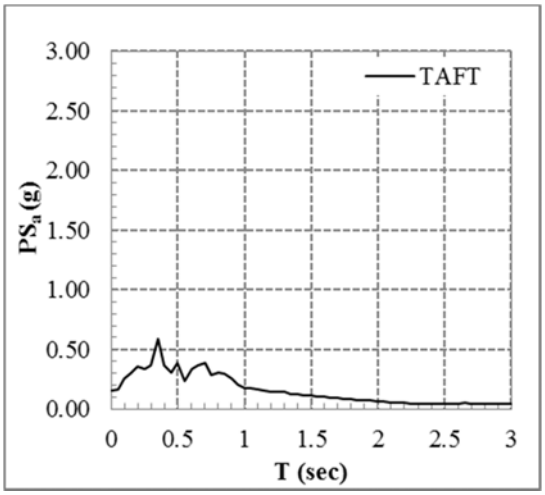

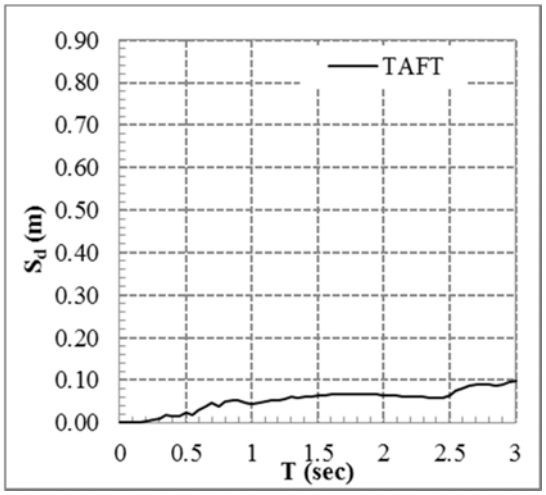

Figure 5.10: Taft record and its spectrum

5.5.2 Ground Motion Scaling

As the ground motions were chosen to conduct nonlinear response history analyze, they should be selected to have properties that are essential for forcing the structural response into the nonlinear phase; not just on their seismological features. It was noted that the important properties of ground motion records can change depending on the structure and the desired

response parameter, so seismologists must know something about the structure to be able to select an appropriately small number of representative records.

Currently, there is no consensus on the best approach for selection of appropriate suites of acceleration time series for use in nonlinear dynamic analyses. Selecting an appropriate method requires communication between the seismologist and the structural engineer to establish which aspects of ground motion are important to the structure and what is the goal of the analysis. Hence, before developing the selection and scaling criteria, it is necessary to determine the intended use of the records and the intent of the nonlinear dynamic analysis. The objective of this study is to investigate the system-over strength in different degrees of nonlinearity in the system; not the prediction of the structural response under a specified hazard level.

Results for the different type of engineering demand parameters are presented in the next section. The observation of outputs confirmed that damping model A results in spurious amplification of the wall axial force due to the nature of damping model employed in the analysis. This axial force amplification cause an unjustifiable increase in the base moment resistance which does not have any physical interpretation. To eliminate the effect of this damping in the mathematical model, damping model B was employed in the later analysis.

5.6 Engineering Demand Parameters

One of the important aspects of nonlinear time history analysis is to obtain the cyclic energy dissipation of system subjected to the ground motions. The resulted curves for base moment versus base rotation for the different case studies under dynamic excitation were presented in upcoming figures once the analysis scale factor was manipulated to achieve the peak base rotation of 0.01 rad. The pushover analysis results are also presented for the case studies. It is quite important to mention that the employed dynamic analysis can overcome the deficiency of static pushover analysis which has been highlighted in detail earlier. The static pushover

analysis assumes the load shape factor constant and proportional to the first elastic mode response while in dynamic analysis the system dynamic properties are updated in each step of the analysis. While the system base moment overstrength at a specified base rotation level is not dependent on the ground motions, the system base shear overstrength may highly be affected by the type of record employed in the analysis.

The key variables in this investigation are the variation of structural wall vertical deformation at each story over the time and base rotation. Figure 5.11 illustrates specific location of nodes at the roof level and the base gage length used to obtain the above engineering demand parameters.

5.6.1 EDP for the Case1-1

Figure 5.12 (a) displays the base moment versus base rotation for the Case1-1 under the ELC record. The ELC record was scaled by iterations to impose the maximum base rotation equal to 0.01 rad in this structure. The maximum base moment during the response history analysis reached to the maximum of 99.84 MN.m. This is equal to system overstrength factor equal to 1.6 based on calculated the yield moment equal to 69.15 MN.m. The ratio of this value to the corresponding maximum strength from the pushover analysis is equal to 1.28. However, it is evident that dynamic model with damping values according to damping model A resulted in higher overstrength factor due to the introduction of additional damping axial forces in the mathematical model of the structure. Figure 5.12 (b) and Figure 5.12 (c) show the response histories of base rotation and global drift. The base rotation is estimated over a gage length equal to $0.355L_w$. The reason why this length was chosen to estimate the base rotation has been discussed in the previous chapter.

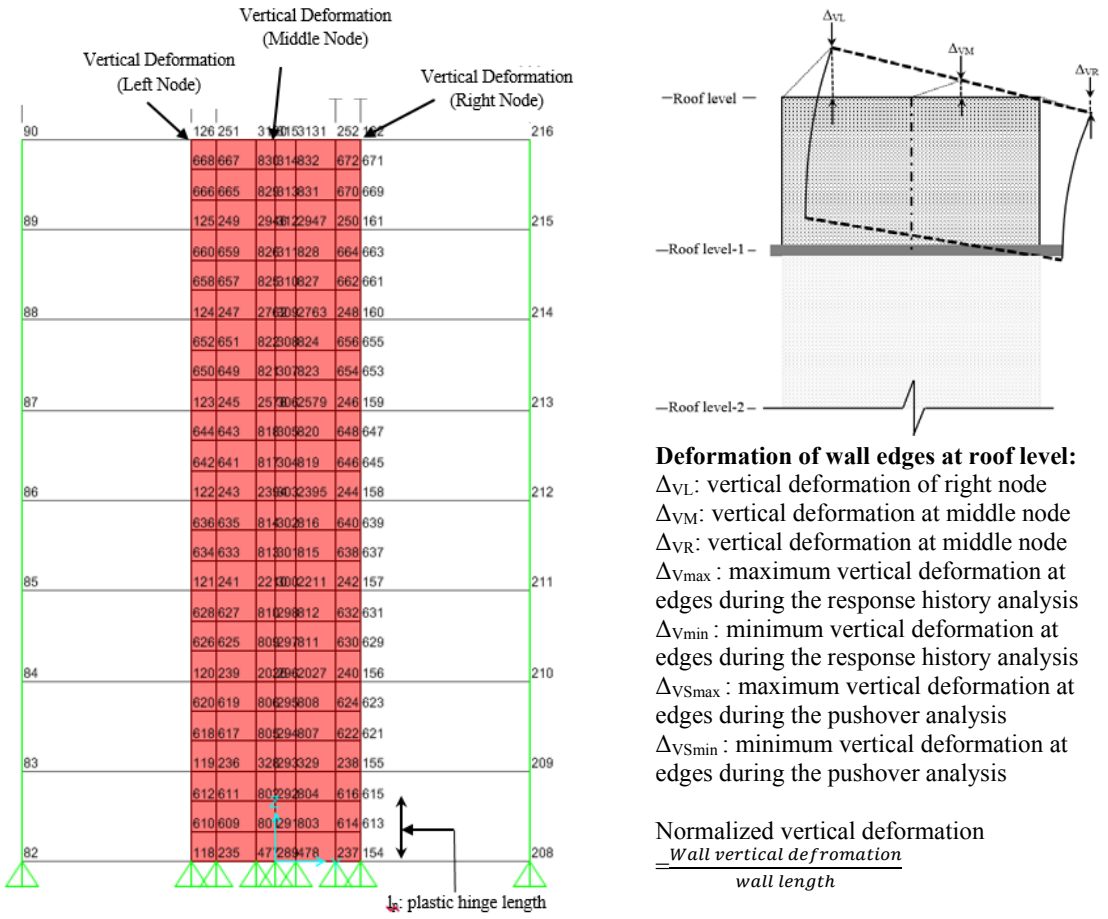

Figure 5.11: Vertical deformation and base rotation indexes

The extent of system interaction is also the function of wall edges vertical deformation response history. Hence, the response histories of wall vertical deformation along the right edge, left edge and the middle node at the roof level were recorded and illustrated in Figure 5.12 (d). While the model for the Case1-1 under the scaled ELC record reached the max base rotation equal to 0.01 rad the maximum global drift value reached the peak value of 0.02 (see Figure 5.12 a and b). This observation confirms that the ratio of system global drift to the base rotation is equal to 2 for this specific analysis. Although it shows that the maximum global drift and maximum plastic hinge rotation did occur concurrently, this conclusion might not valid for high rise buildings (White and Adebar 2004). The implication of their observations were the relation between the maximum global drift and maximum plastic hinge rotation is not always

similar to the equations commonly found by static analysis based on the first mode deformation pattern. The structural wall left and right edge normalized vertical deformation at the roof level reached to the value of 0.0125 and 0.0225 respectively. Figure 5.13 plots the variation of wall left and right edge normalized vertical deformation at the roof versus the base rotation. The maximum transient values as well as residual vertical deformation of the middle node plays an important role in the interaction mechanism of the structural walls. Figure 5.13 also illustrates that maximum and residual normalized vertical deformations of the middle node at the roof level for Case1-1 under the ELC records are equal to 0.0097 and 0.0021 respectively.

The system responses for Case1-1 under the SOVM and Taft records are presented in Figure 5.15 to Figure 5.20. Although the base moment versus base rotation hysteresis loops are quite different in these records the overstrength factor at the target base rotation is very close. The reason for this is attributed to the having the same envelope curve for base moment versus base rotation due to ductile response in the plastic hinge region.

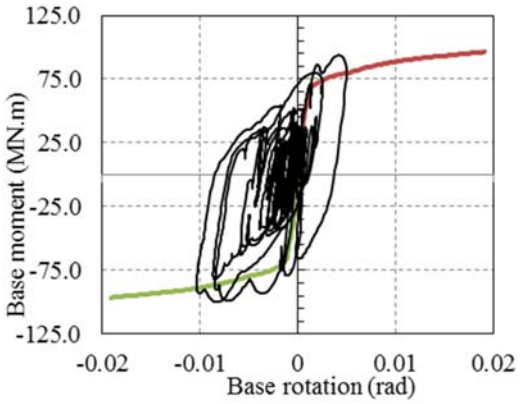

(a)

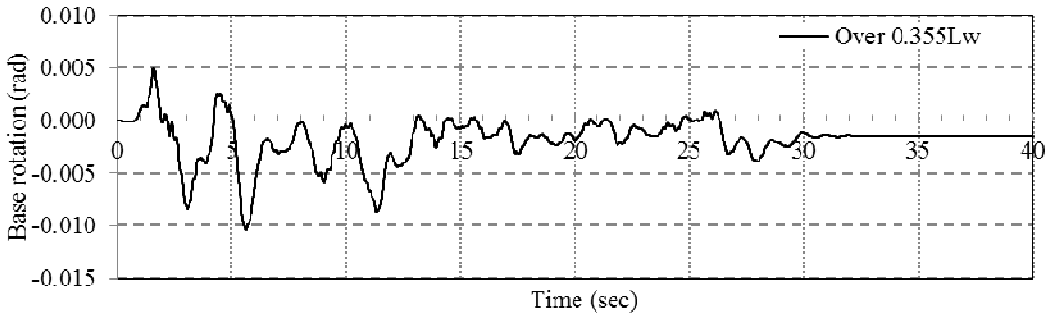

(b) Base rotation time history

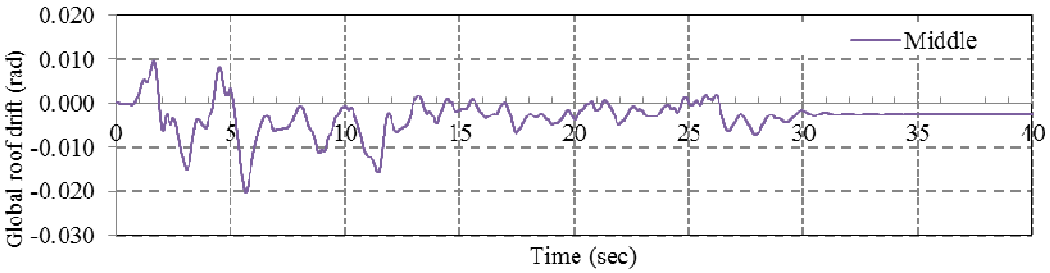

(c) Global drift time history

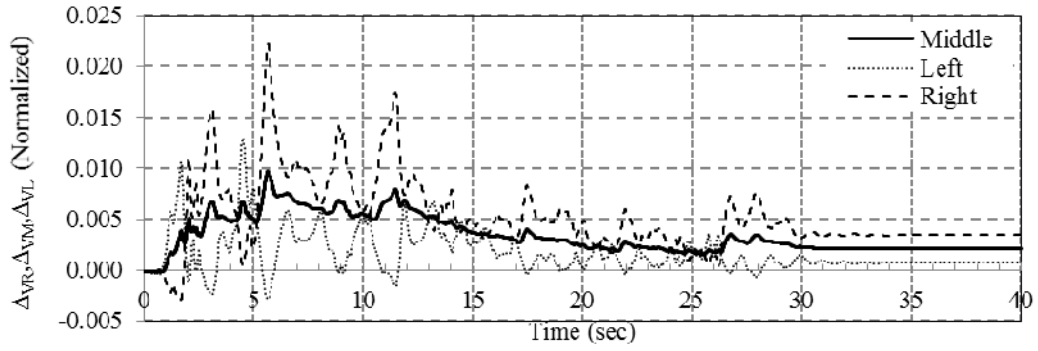

(d) Normalized vertical deformation time history

Figure 5.12: EDP response history and moment-rotation hysteresis loops for the Case1-1 under ELC record - Damping model A

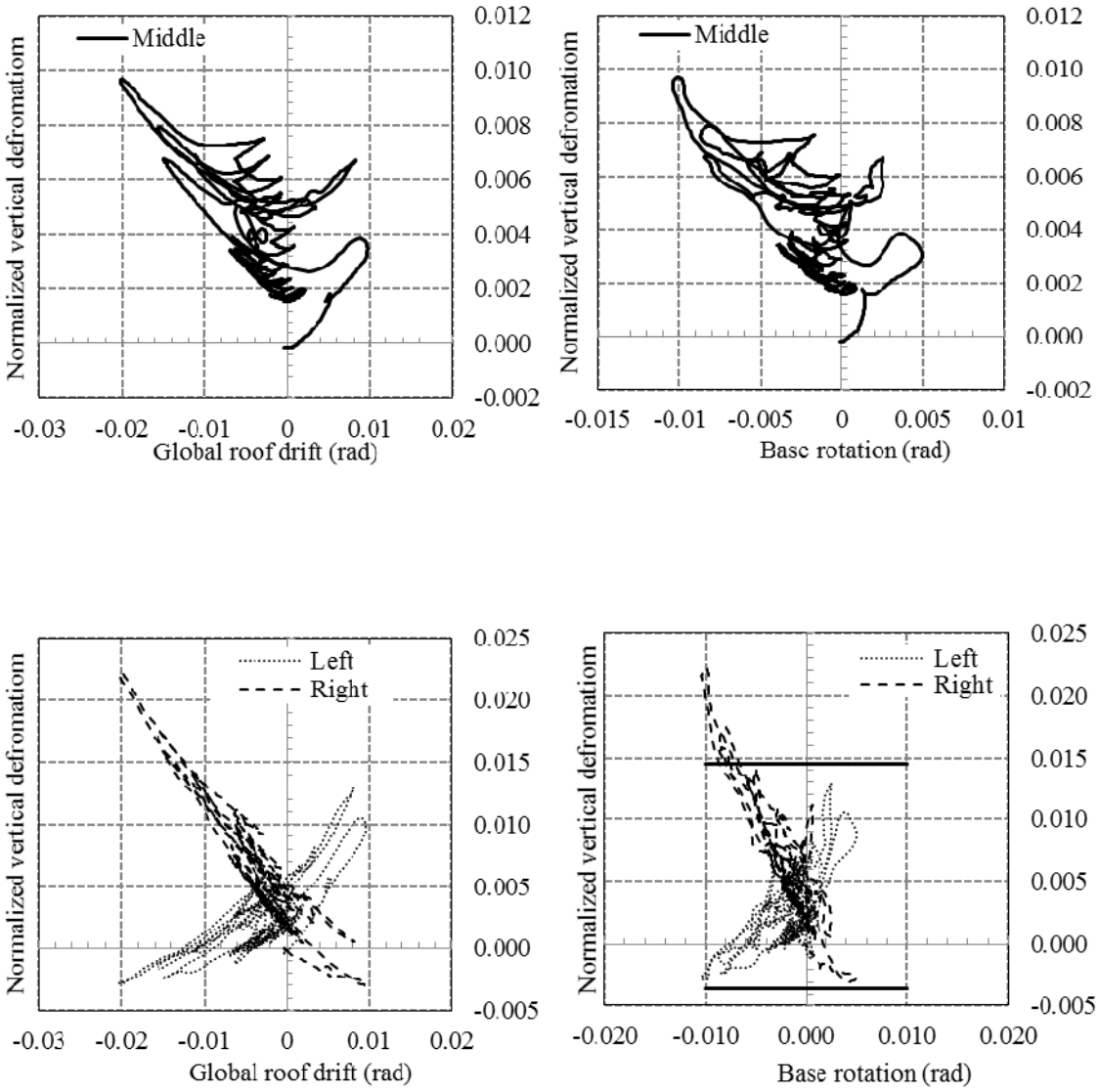

Figure 5.13: Normalized roof level vertical deformation versus the base rotation/global drift for the Case1-1 under ELC record - Damping model A.

The values of important engineering demand parameters are listed in Table 5-6 for the Case1-1 building under the three different records.

Table 5-6: Selected normalized engineering demand parameters for the Case1-1, Damping model A Θ_b=0.01 rad

Case1-1	Max M_{ub}(MN.m)	Maximum Vertical Deformation (normalized)			Residual Vertical Deformation (normalized)			Normalized Axial Force Amplification
		(Middle)	(Left)	(Right)	(Middle)	(Left)	(Right)	
ELC	99.84	0.0097	0.0129	0.0222	0.0021	0.0007	0.0034	1.40
SOVM	103.27	0.0084	0.0169	0.0191	0.0021	0.0017	0.0026	1.51
TAFT	107.35	0.0094	0.0213	0.0196	0.0033	0.0029	0.0037	1.49
Pushover	88.60	-	0.0145	0.0145	-	-	-	1.0

It is interesting to find that the axial force amplification has increased the moment strength of the system. The employed nonlinear shell element is able to account for the axial-flexural interaction in its formulation. Hence, the increase in axial force leads to increase in the structural wall's moment resistance. It is worth mentioning that this phenomenon is against our expectation because no vertical mass was assigned to the floor nodes in the mathematical model of Case1-1. Further investigation shows that this phenomenon is purely attributed to spurious damping forces, not the inertia forces. To overcome this issue in the nonlinear analysis of structural walls, use of damping model B is recommended. However, for a few case studies, the result of damping model A also presented along with damping model B to scrutinize the effect of damping model on different engineering demand parameters. Needless to say, the results of analyses obtained by employing damping model B are used to evaluate the system overstrength factor.

To verify this effect, moment curvature analysis has been conducted on the wall base section to find the approximate increase in its moment resistance due to the spurious axial force amplification. In Case1-1 the normalized axial force amplification is equal to 1.4. Hence, the moment curvature analysis of the section under this new increased axial force amplification

has been conducted. The result of moment curvature analysis is illustrated in Figure 5.14 and it confirms similar increase in the section moment strength due to increase in the axial forces. However, it should be highlighted that Case1-1 is the system with the wall only and the flexural stiffness of slabs are assumed to be zero. As we have already discussed, it needs further investigation by experimental tests to confirm the possible amplification in the axial force due to this kind of damping forces. One does not expect any increase of the axial force in the structural wall not only in the static analysis results but also in the dynamic analysis results because structural walls are called isolated walls without any slab in Case1-1. Hence, to avoid this unexpected phenomenon in the analysis, we use the alternate approach to model damping in the numerical model which has been introduced earlier as damping model B.

Figure 5.14 shows the moment curvature analysis of the wall base section under the two different axial forces. In the moment curvature analysis of the structural wall base section, material properties were taken similar to the material models employed in the dynamic analysis. The continuous moment curvature curve was idealized to form an elastic-plastic bilinear curve to find the plastic moment strength. The idealization method has been conducted according to the Caltrans, S.D.C. (2010) manual. The flexural strength of the section with the amplified axial force reached 44.6 MN.m. This value is 12 percent higher than the initial flexural strength of the wall section with the gravity loads only.

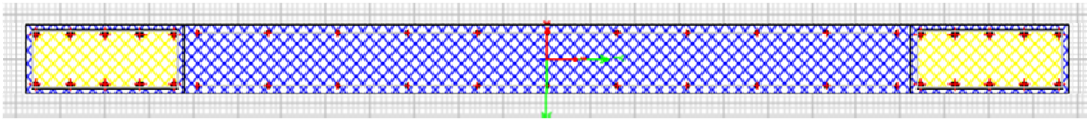

structural wall section

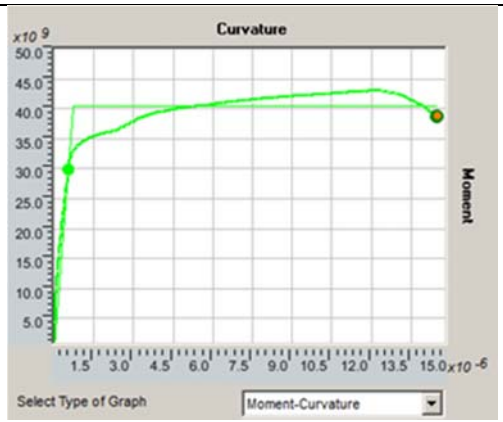

N_1=5441.5 kN

M_{ub1} (Idealized)=40.1 MN.m

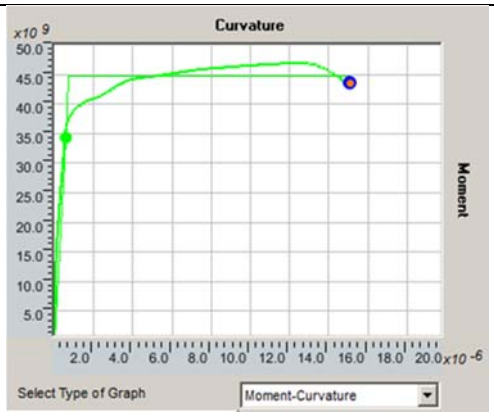

N_2=5441.5*1.4=7618.1 kN

M_{ub2}(Idealized)=44.6 MN.m

M_{ub2}/ M_{ub1}=1.12

Figure 5.14: Moment curvature analysis under the increased axial force

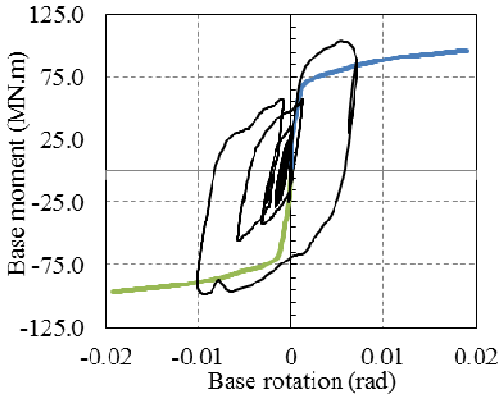

(a)

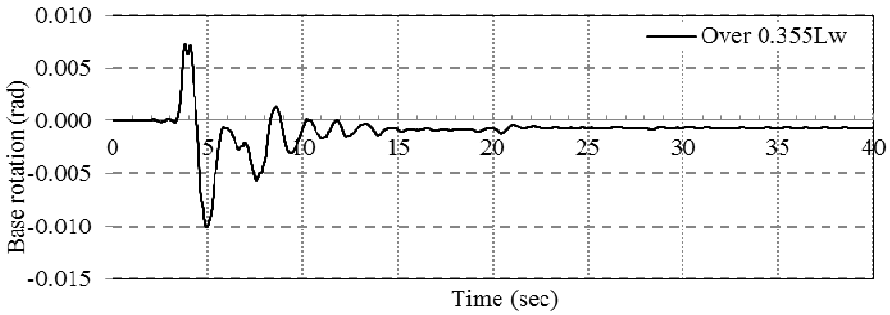

(b) Base rotation time history

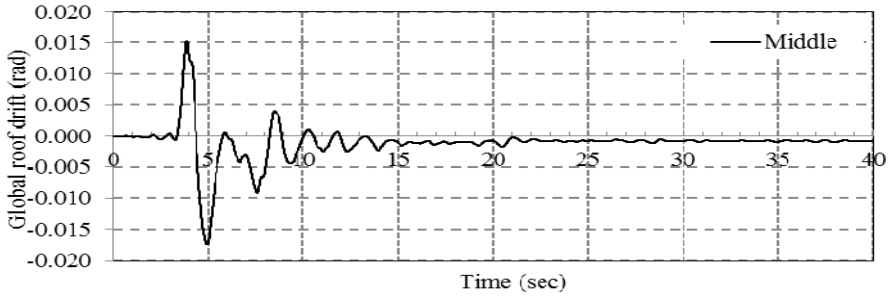

(c) Global drift time history

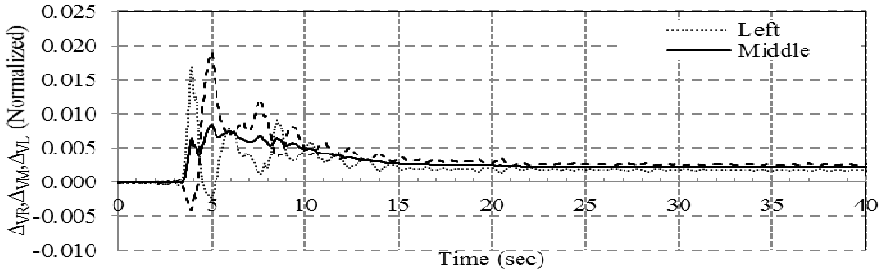

(d) Normalized vertical deformation time history

Figure 5.15: EDP response history and moment-rotation hysteresis loops for the Case1-1 under SOVM record - Damping model A

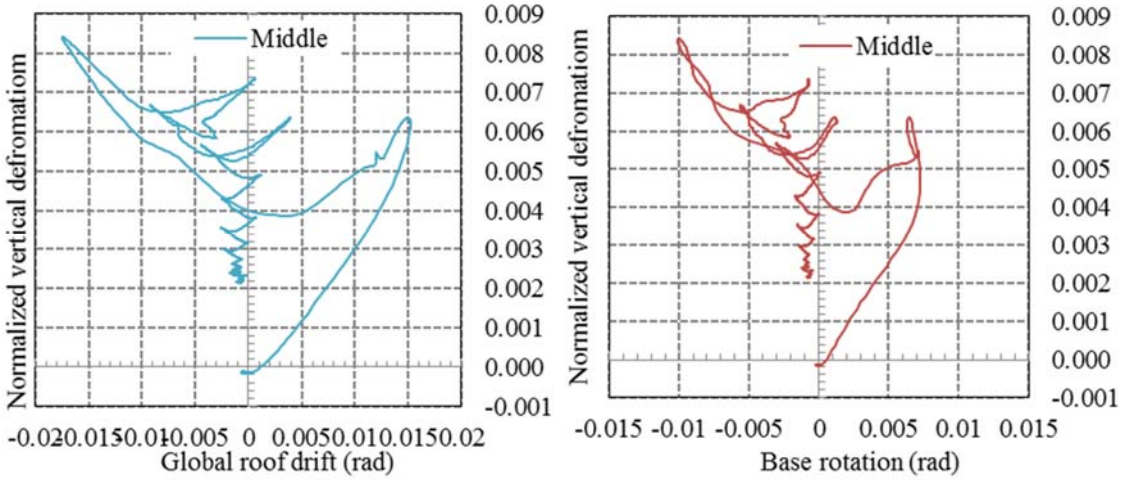

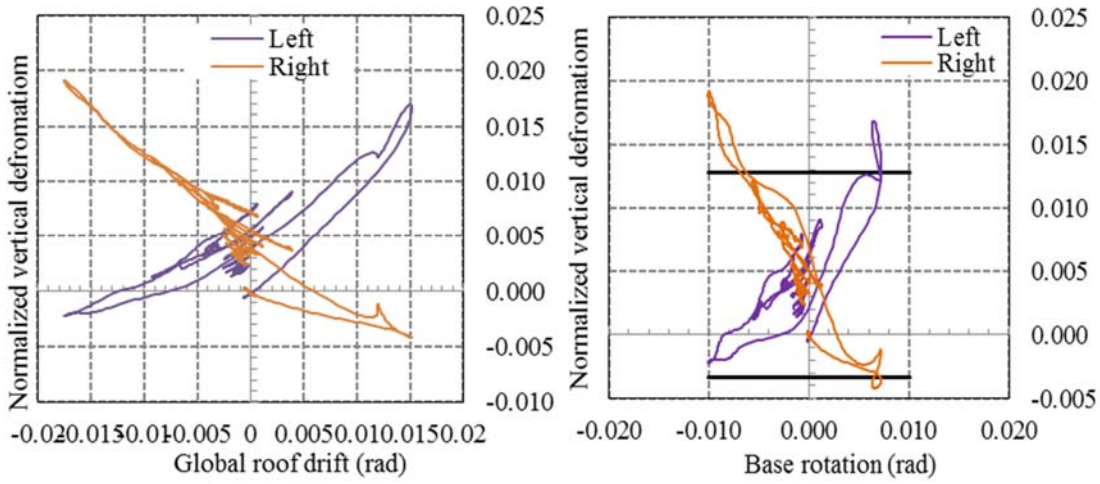

Figure 5.16: Normalized roof level vertical deformation versus the base rotation/global drift for the Case1-1 under SOVM record - Damping model A

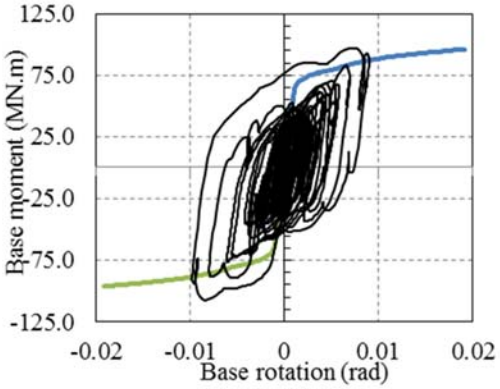

(a)

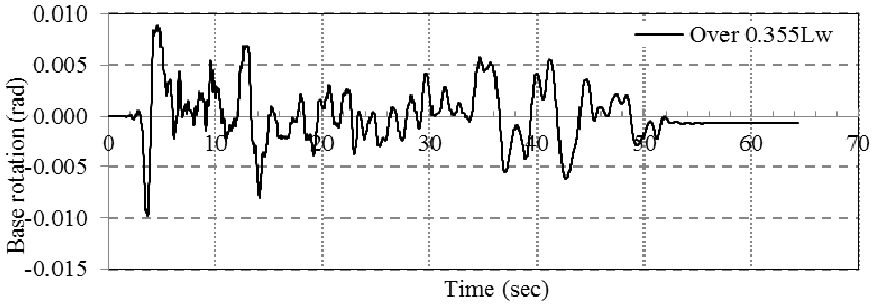

(b) Base rotation time history

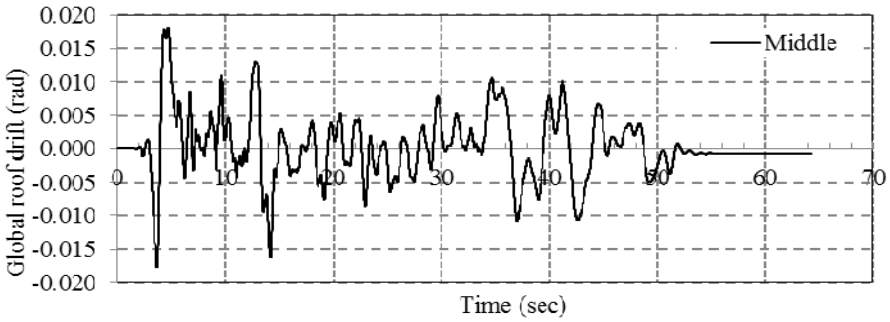

(c) Global drift time history

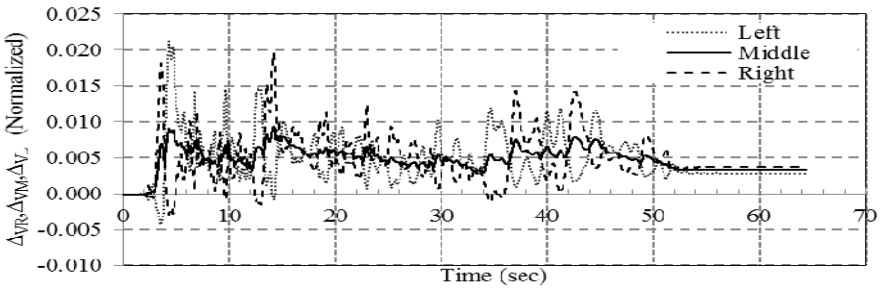

(d) Normalized vertical deformation time history

Figure 5.17: EDP response history and moment-rotation hysteresis loops for the Case1-1 under TAFT record - Damping model A.

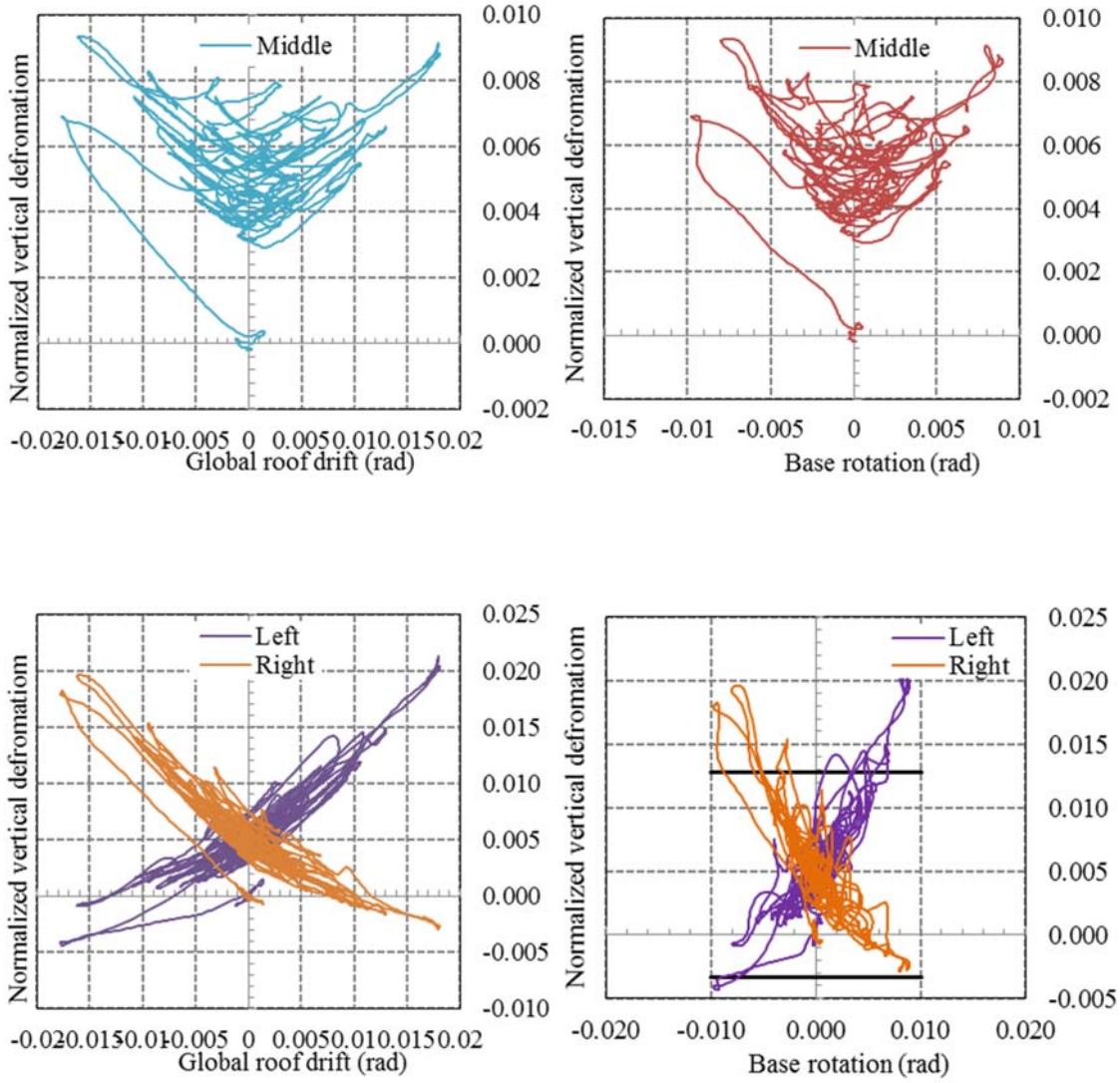

Figure 5.18: Normalized roof level vertical deformation versus the base rotation/global drift for the Case1-1 under TAFT record - Damping model A

5.6.2 EDP for the Case2-2

To investigate the response parameters due to change in flexural stiffness of slabs, Case2-2 and Case2-3 buildings were subjected to the same ground motions. However, the scale factors were modified to push the structure to the predefined base rotation equal to 0.01 rad. Results from the pushover analysis in the previous section confirmed that the system overstrength increased with increase in the flexural stiffness of slabs. Nonlinear response history analysis also shows the similar trend in the system-over strength increase. The Case2-2 under the ELC record at base rotation equal to 0.01 rad shows the system base moment equal to 123.25 MN.m compared to 99.83 MN.m in Case1-1. The system base moment versus the base rotation curves along with the pushover envelope curve are displayed in Figures.

The key results related to the desired engineering parameters for the Case2-2 buildings are presented in Table 5-7.

Table 5-7: Selected normalized engineering demand parameters for Case2-2, Damping model A - Θ_b=0.01 rad

Case2-2	Max M_{ub}(MN.m)	Max. Vertical (normalized)			Residual Vertical (normalized)			Normalized Axial Force Amplification
		(Middle)	(Left)	(Right)	(Middle)	(Left)	(Right)	
ELC	123.25	0.007	0.011	0.017	0.0017	0.0010	0.0023	1.47
SOVM	125.04	0.007	0.013	0.016	0.0014	0.0021	0.0021	1.59
TAFT	131.00	0.007	0.018	0.010	0.0011	0.0013	0.0009	1.61
Pushover	114.00	-	0.012	0.012	-	-	-	1.00

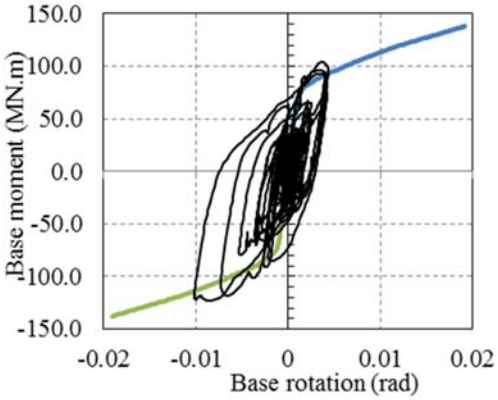

(a)

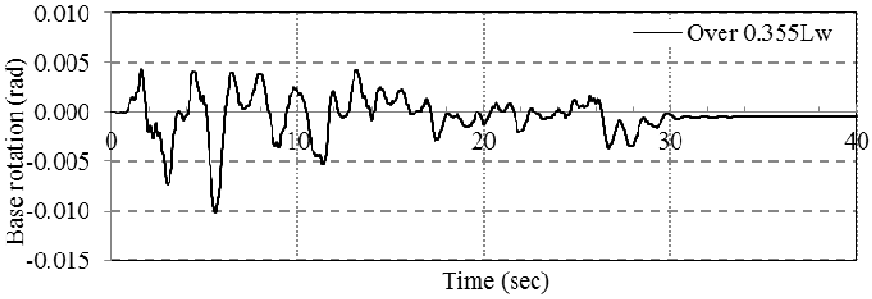

(b) Base rotation time history

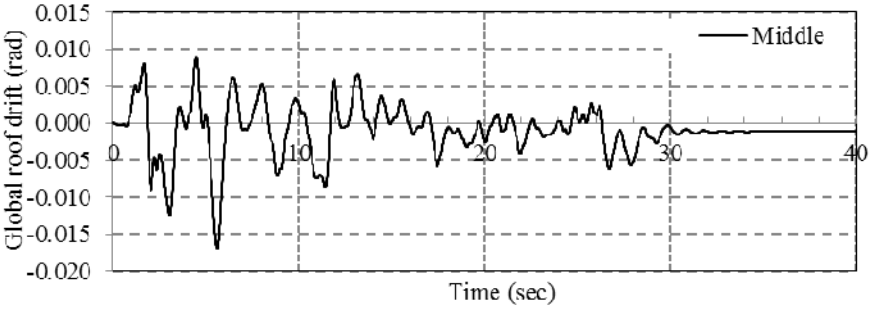

(c) Global drift time history

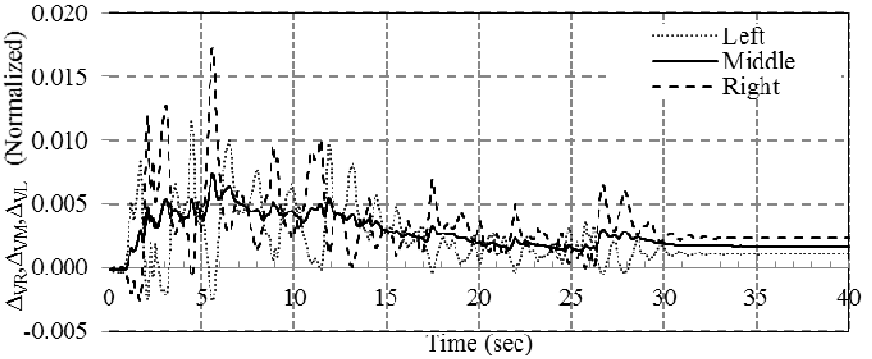

(d) Normalized vertical deformation time history

Figure 5.19: EDP response history and moment-rotation hysteresis loops for the Case2-2 under ELC record - Damping model A

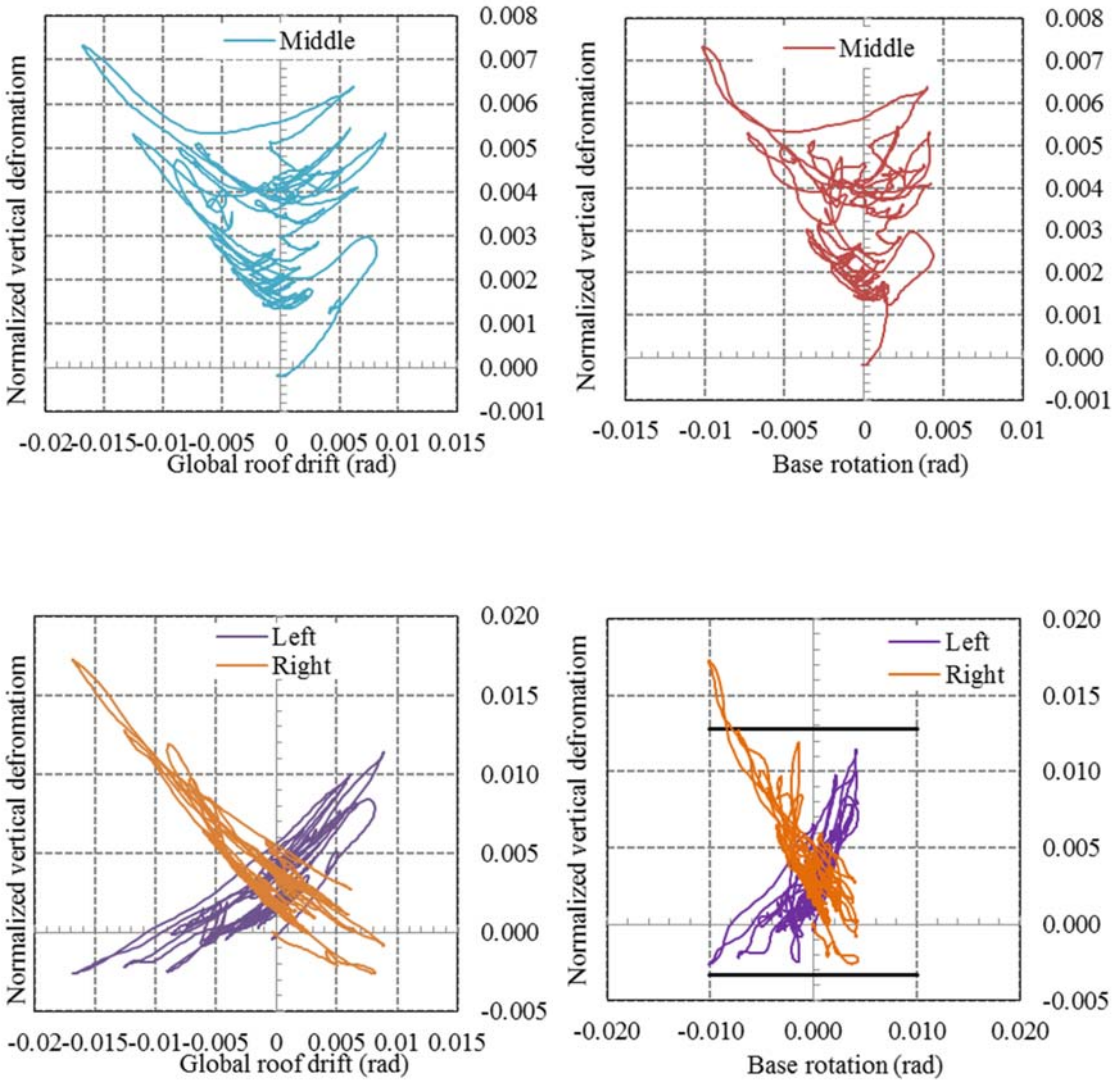

Figure 5.20: Normalized roof level vertical deformation versus the base rotation/global drift for the Case2-2 under ELC record - Damping model A

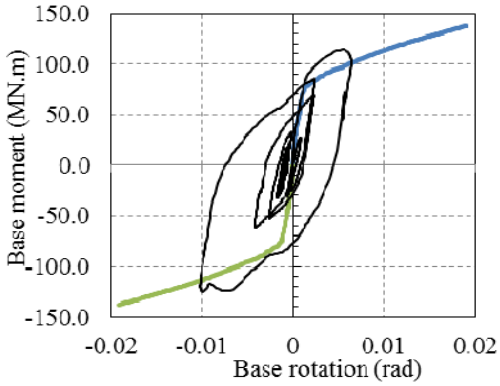

(a)

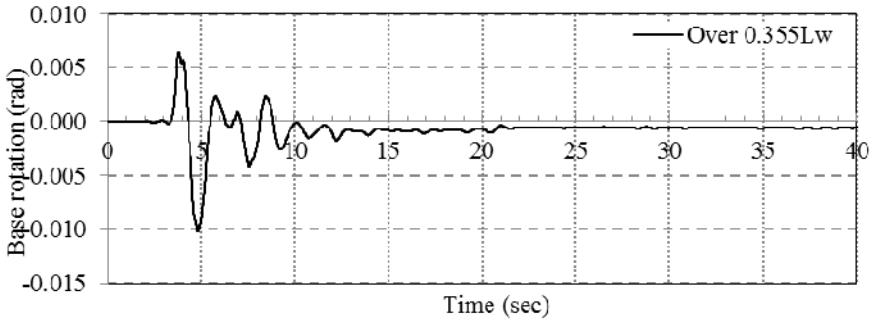

(b) Base rotation time history

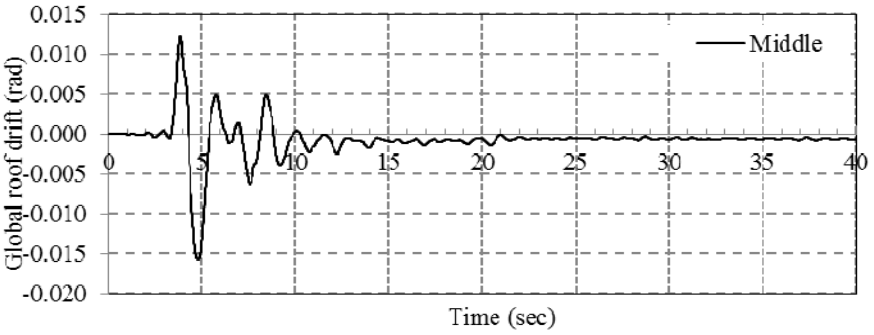

(c) Global drift time history

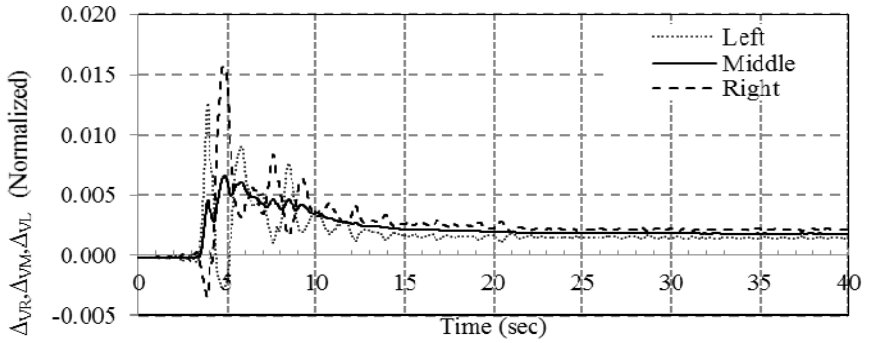

(d) Normalized vertical deformation time history

Figure 5.21: EDP response history and moment-rotation hysteresis loops for the Case2-2 under SOVM record - Damping model A

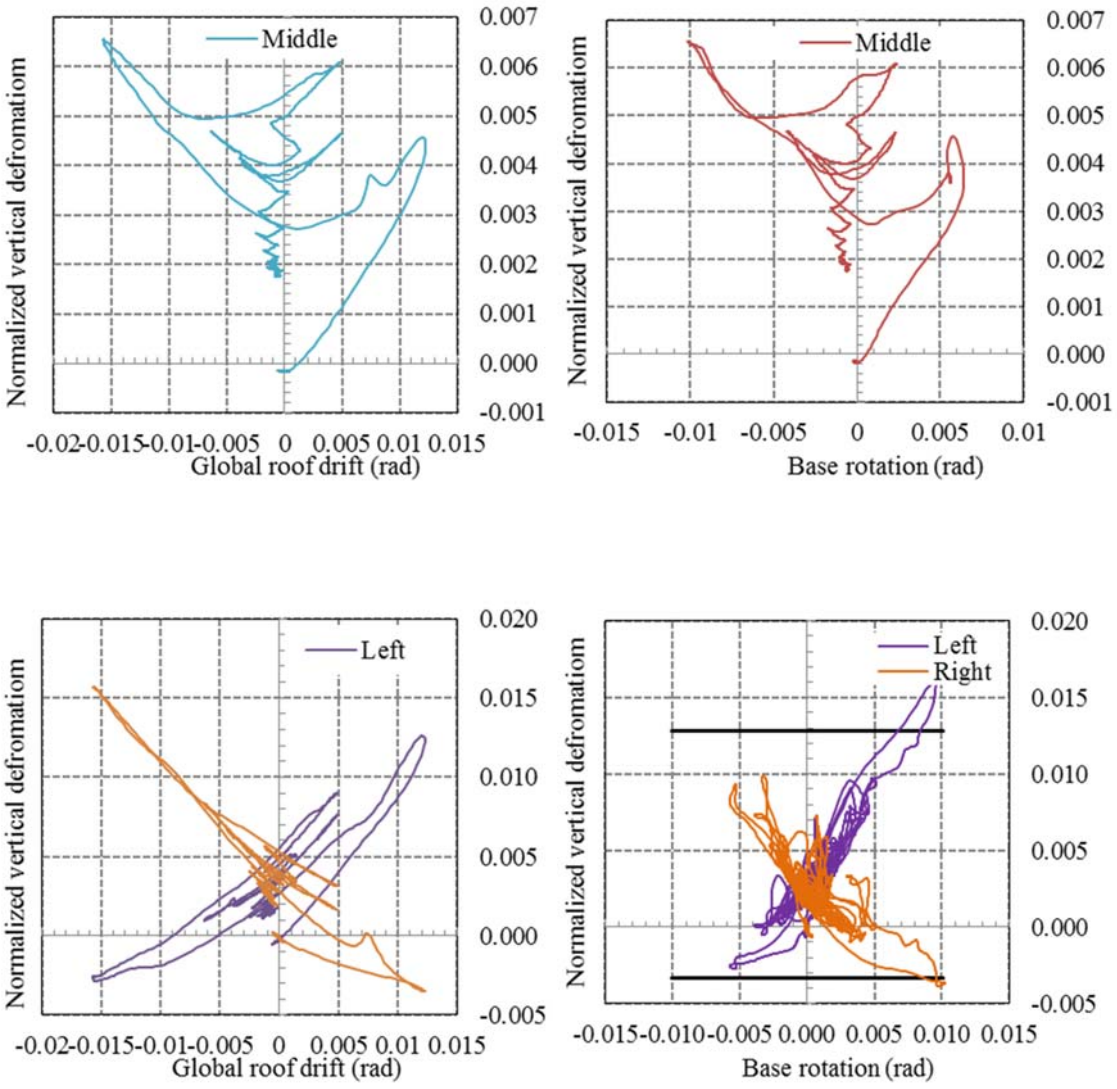

Figure 5.22: Normalized roof level vertical deformation versus the base rotation/global drift for the Case2-2 under SOVM record - Damping model A

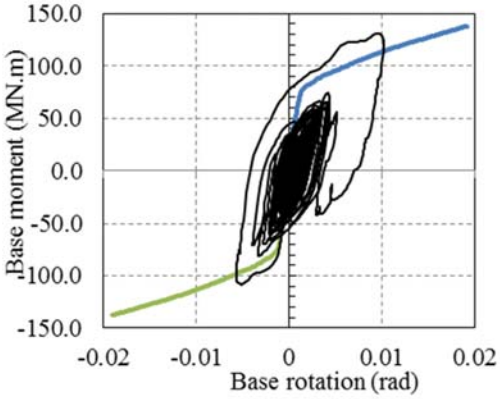

(a)

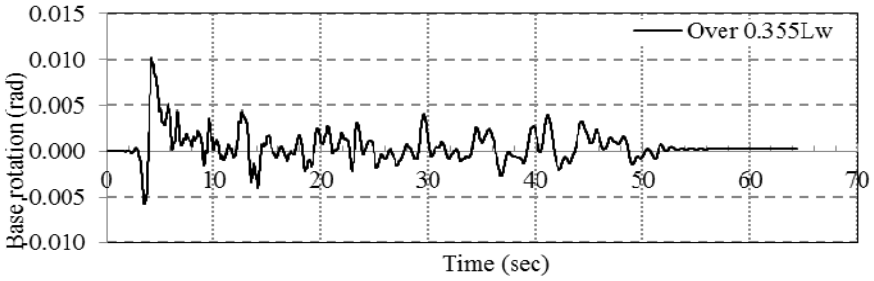

(b) Base rotation time history

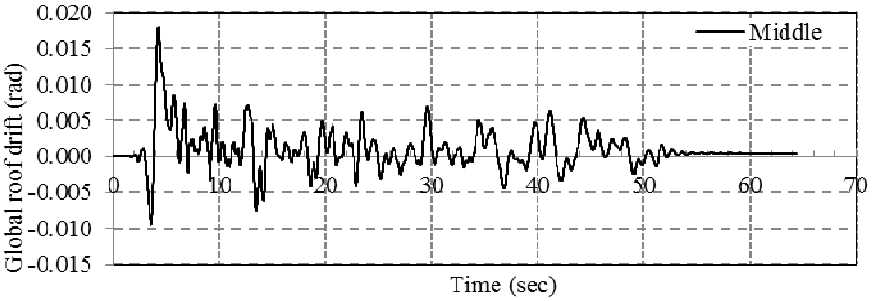

(c) Global drift time history

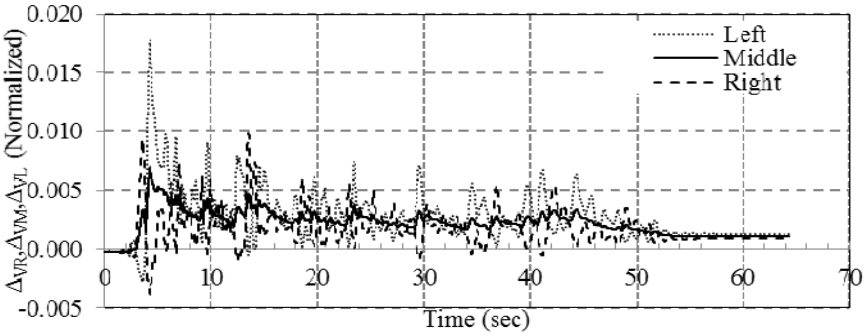

(d) Normalized vertical deformation time history

Figure 5.23: EDP response history and moment-rotation hysteresis loops for the Case2-2 under TAFT record - Damping model A

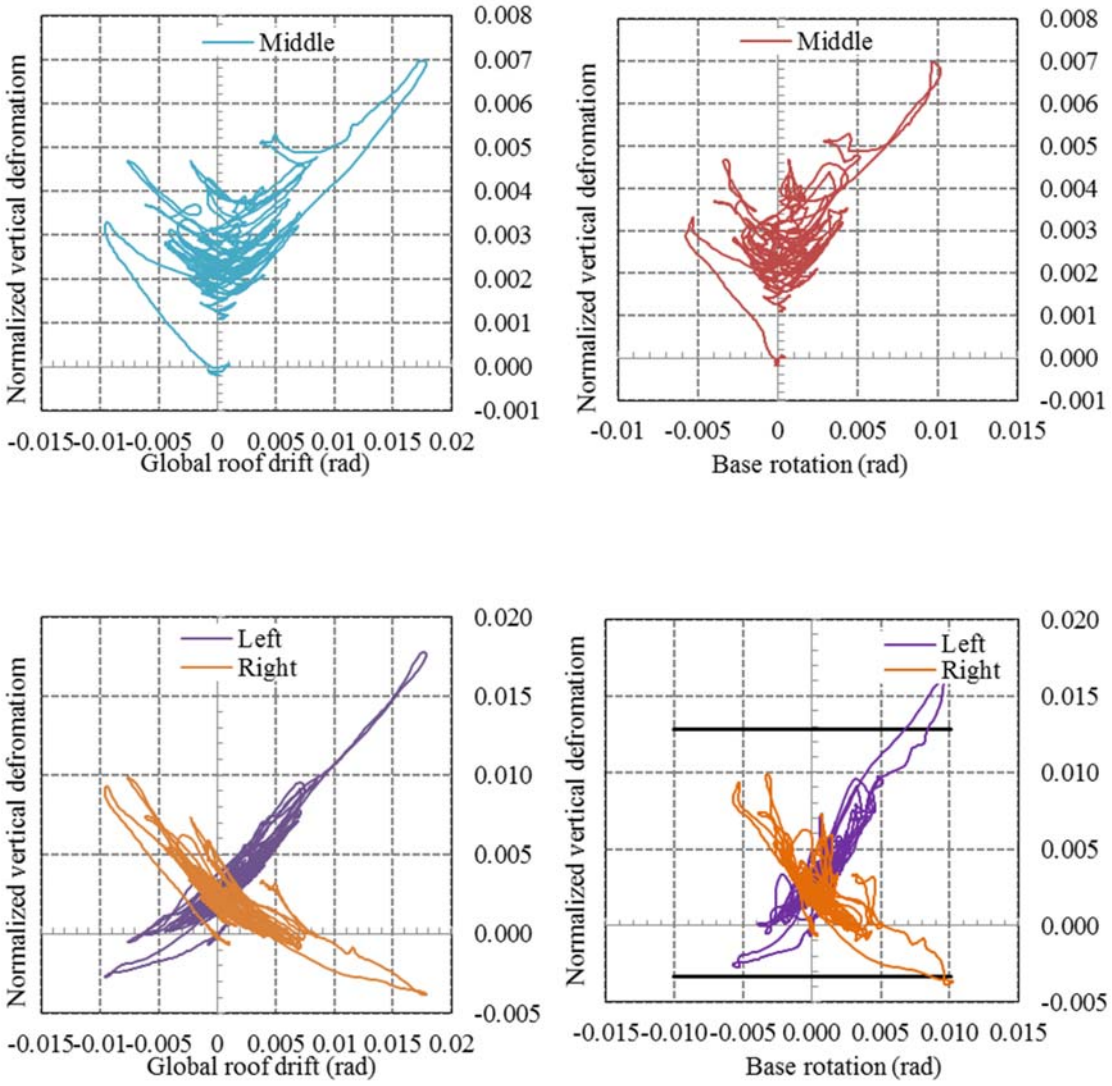

Figure 5.24: Normalized roof level vertical deformation versus the base rotation/global drift for the Case2-2 under TAFT record - Damping model A

5.6.3 EDP for the Case2-3

The Case2-3 building under the ELC record at 0.01 rad base rotation equal to shows the system base moment equal to 148.96 MN.m compared to 99.83 MN.m in Case1-1. The system base moment versus base rotation along with pushover analysis results are displayed in Figures.

The engineering parameters for Case2-3 are presented in Table 5-8. The first observation shows that the at the base rotation equal to 0.01 rad, the system overstrength has increased due to increase in flexural stiffness of slab. However, in this model increase in the base moment resistance stems from the effect of out-of-plane flexural stiffness of slabs as well as the spurious axial force amplification. Hence, unlike in the Case1-1, to separate the contribution of the flexural stiffness of the slabs from the contribution of increased axial force on the structural walls to the system overstrength factor, further analysis is needed. However, the general trend shows an increase in the system overstrength factor due to the flexural stiffness of slabs.

Table 5-8: Selected normalized engineering demand parameters for the Case2-3, Option A damping model-Θ_b=0.01 rad

Case2-3	Max M_{ub}(MN.m)	Max vertical deformation (normalized)			Residual vertical deformation (normalized)			Normalized Axial Force Amplification
		(Middle)	(Left)	(Right)	(Middle)	(Left)	(Right)	
ELC	148.96	0.006	0.012	0.015	0.0016	0.0013	0.0019	1.65
SOVM	148.88	0.006	0.011	0.014	0.0016	0.0012	0.0020	1.68
TAFT	151.80	0.006	0.014	0.007	0.0005	0.0007	0.0004	1.66
Pushover	137.11	-	0.012	0.012	-	-	-	1.0

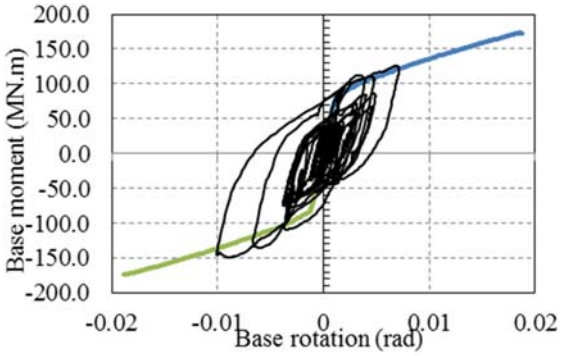

(a)

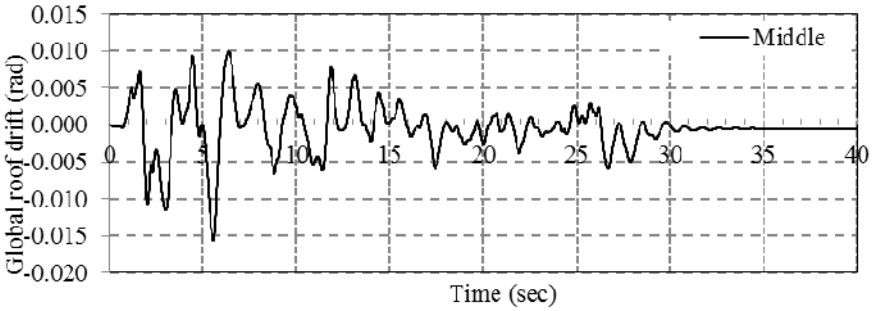

(b) Base rotation time history

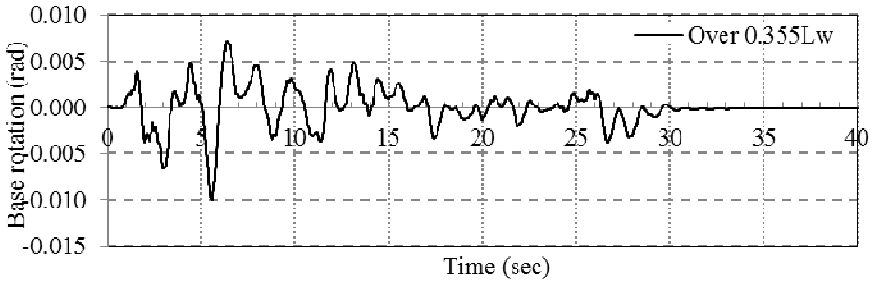

(c) Global drift time history

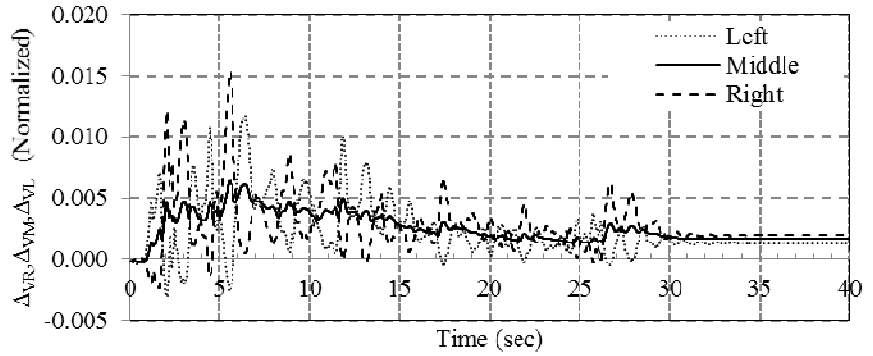

(d) Normalized vertical deformation time history

Figure 5.25: EDP response history and moment-rotation hysteresis loops for the Case2-3 under ELC record - Damping model A

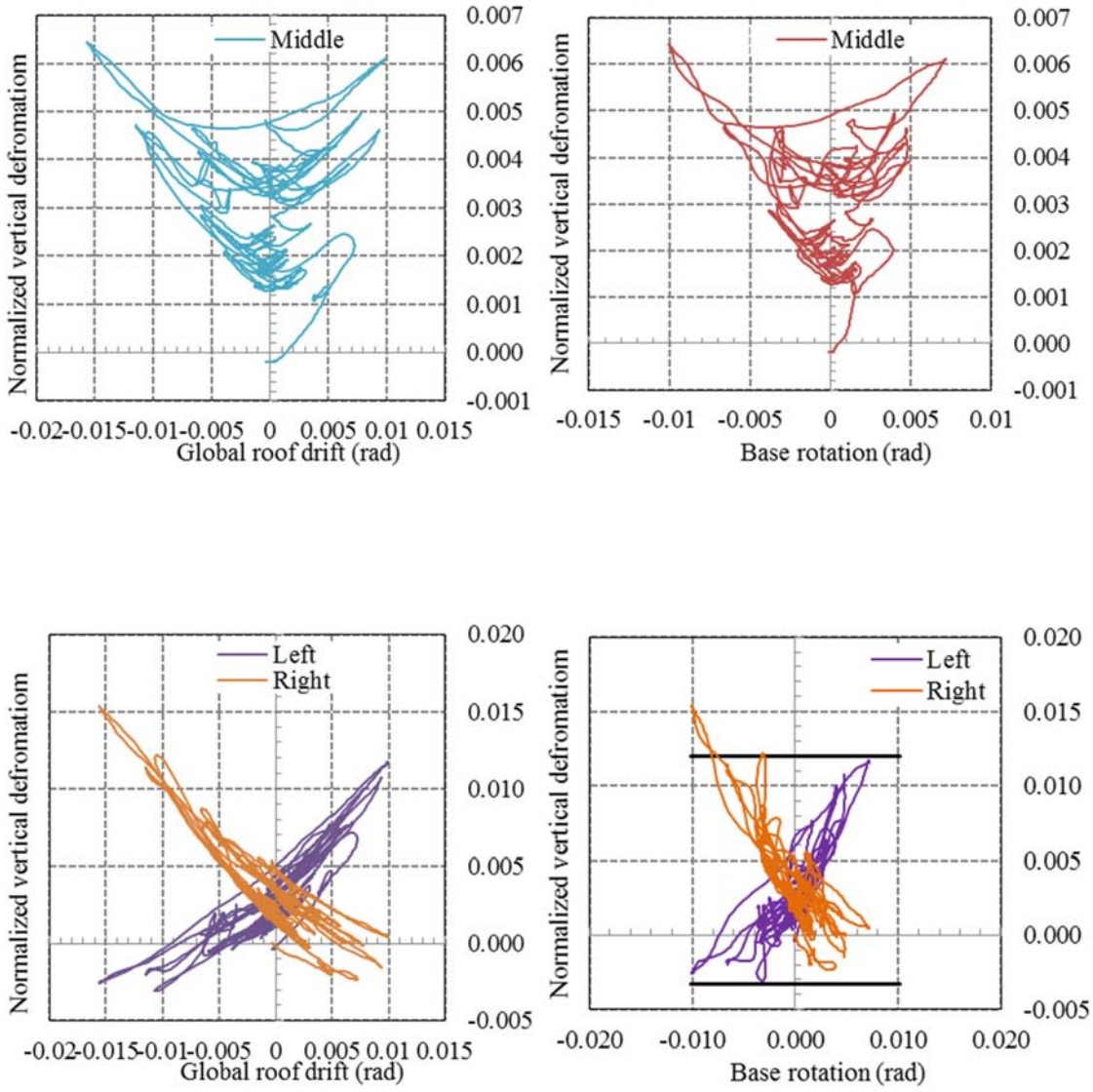

Figure 5.26: Normalized roof level vertical deformation versus the base rotation/global drift for the Case2-3 under ELC record - Damping model A

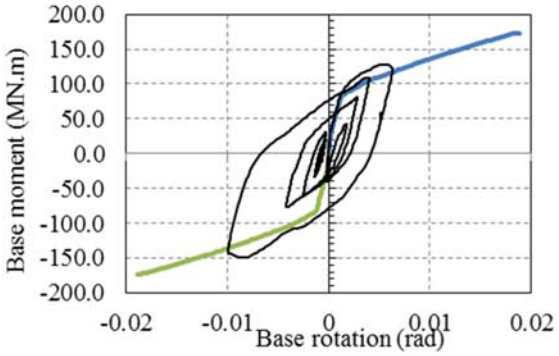

(a)

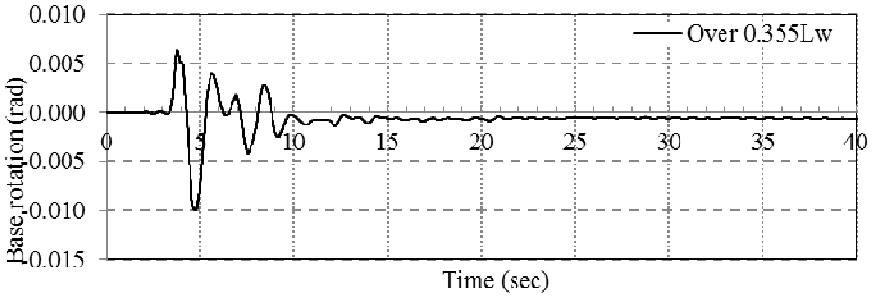

(b) Base rotation time history

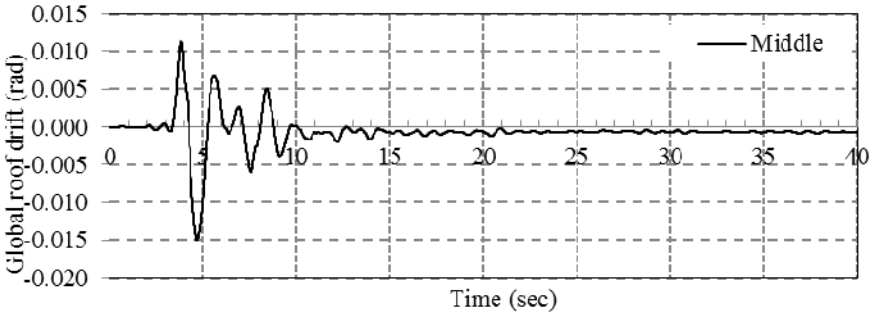

(c) Global drift time history

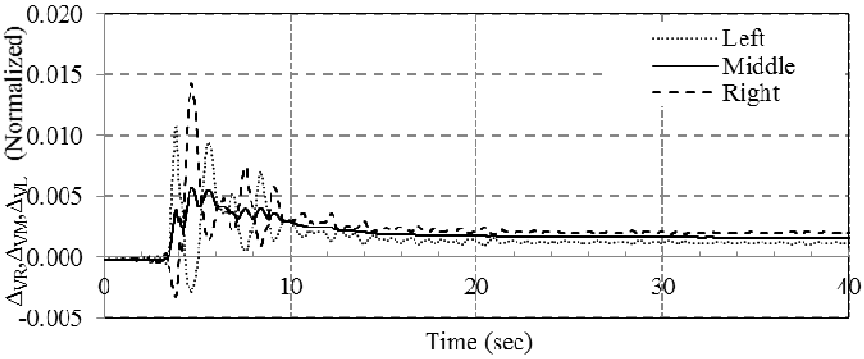

(d) Normalized vertical deformation time history

Figure 5.27: EDP response history and moment-rotation hysteresis loops for the Case2-3 under SOVM record - Damping model A

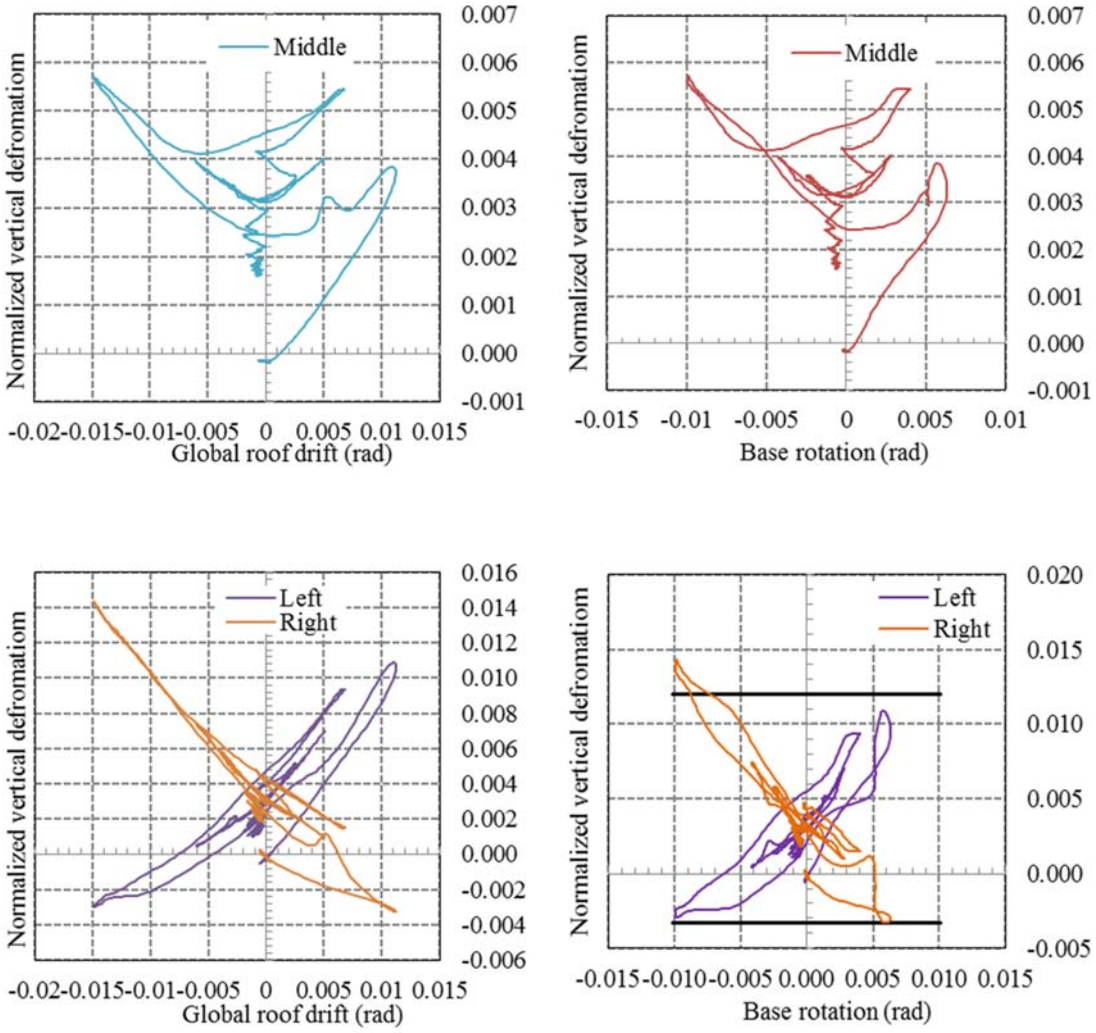

Figure 5.28: Normalized roof level vertical deformation versus the base rotation/global drift for the Case2-3 under SOVM record - Damping model A

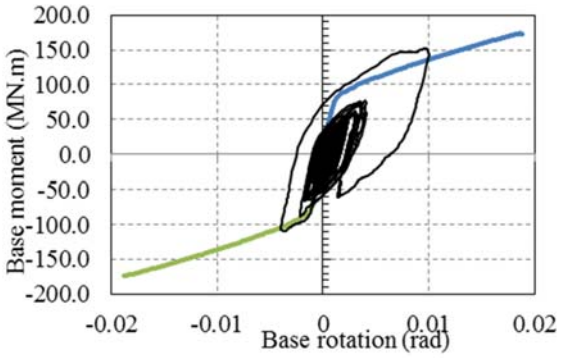

(a)

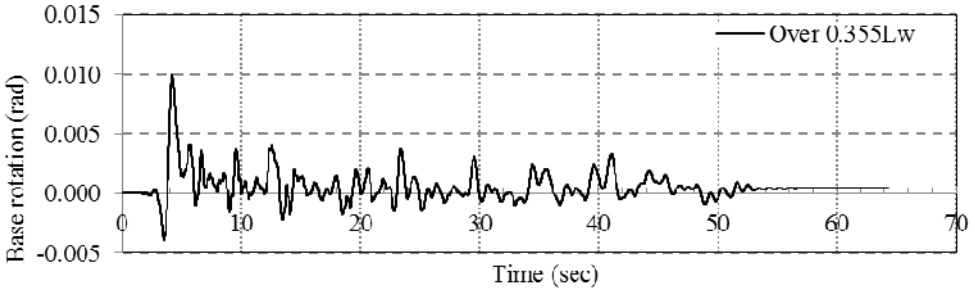

(b) Base rotation time history

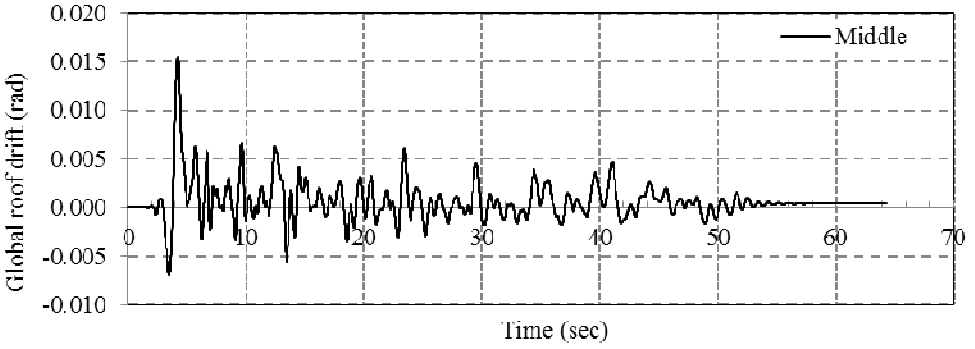

(c) Global drift time history

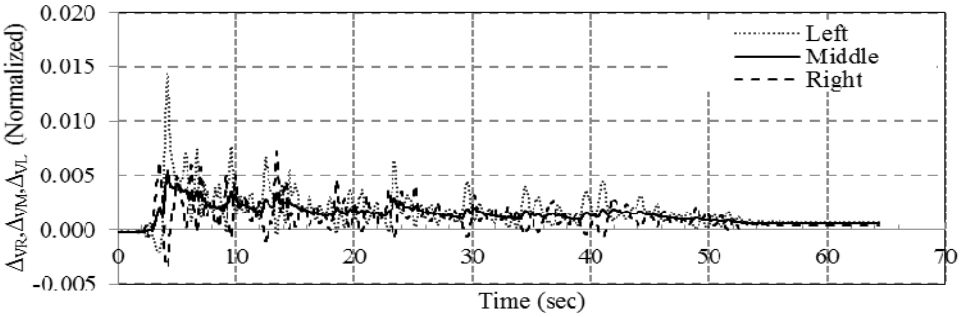

(d) Normalized vertical deformation time history

Figure 5.29: EDP response history and moment-rotation hysteresis loops for the Case2-3 under TAFT record - Damping model A

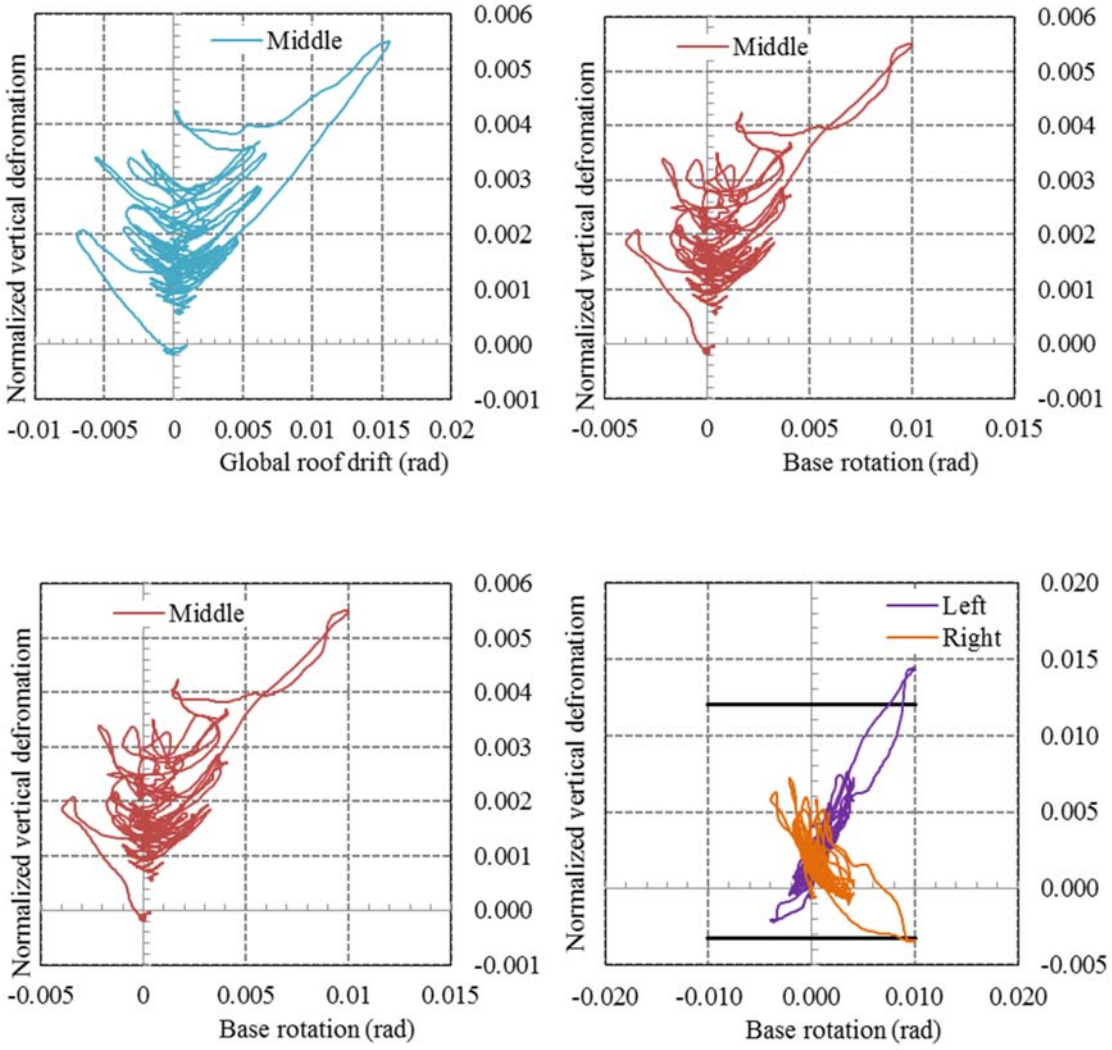

Figure 5.30: Normalized roof level vertical deformation versus the base rotation/global drift for the Case2-3 under TAFT record - Damping model A

Table 5-9: Maximum moment resistance at the base rotation equal to 0.01 (rad) - Damping model A

Case No.	M_{yb} (MN.m)	Analysis Input	M_{ub1} (MN.m)	Ratio of M_{ub1}/M_{yb}	M_{ub2} (Excluding p-delta) (MN.m)	Ratio of M_{ub2}/M_{yb}
Case1-1	69.15	ELC	99.84	1.44	94.32	1.36
	69.15	SOVM	103.27	1.49	97.56	1.41
	69.15	TAFT	107.35	1.55	101.41	1.47
	69.15	Pushover	88.6	1.28	83.70	1.21
Case2-2	74.70	ELC	123.12	1.65	118.15	1.58
	74.70	SOVM	125.04	1.67	119.99	1.61
	74.70	TAFT	131	1.75	125.71	1.68
	74.70	Pushover	114	1.53	109.40	1.46
Case2-3	80.89	ELC	148.96	1.84	144.39	1.79
	80.89	SOVM	148.87	1.84	144.31	1.78
	80.89	TAFT	151.79	1.88	147.14	1.82
	80.89	Pushover	137	1.69	132.80	1.64

Table 5-9 summarizes the numerical value of the system base moment for the three different cases under the three ground motions. The ratio of the system moment strength at the base rotation equal to 0.01 rad to the yield base moment is calculated and presented accordingly. This ratio is named as the system overstrength factor at the specified base rotation. For all cases, the results obtained from the dynamic analyze led to higher values compared to the pushover results. Based on the numerical values which are presented in Table 5-10, the percentage difference between these moment predictions from pushover analysis results and dynamic analysis for Case1-1, Case2-2 and Case2-3 were (1.41-1.21)/1.21=16.5%, (1.62-1.46)/1.46=11% and (1.80-1.64)/1.64=8.7%, respectively. It was observed that in Table 5-6, Table 5-7 and Table 5-8 increasing the flexural stiffness of slabs reduces the extent of axial force amplification. This is expected because stiffer slabs constrain the movement of the wall in the vertical direction. However, as already explained, the higher moment resistance occurred mainly due to axial force amplification, was mainly attributed to spurious damping forces in the system. These differences cannot be justified when compared to the experimental tests.

These effects occur mostly due to the damping model employed in the numerical computation to solve the dynamic equation of motion.

Table 5-10: Maximum moment resistance at the base rotation of 0.01 (rad) - Damping model A

Case No.	M_{yb}(MN.m)	Analysis Input	Mean M_{ub1} (MN.m)	Ratio of M_{ub1}/M_{yb}	M_{ub2}(Excluding p-delta)(MN.m)	Ratio of M_{ub2}/M_{yb}
Case 1-1	69.15	NTH	103.4866667	1.50	97.76	1.41
	69.15	Pushover	88.6	1.28	83.70	1.21
Case 2-2	74.7	NTH	126.3866667	1.69	121.29	1.62
	74.7	Pushover	114	1.53	109.40	1.46
Case 2-3	80.89	NTH	149.8733333	1.85	145.28	1.80
	80.89	Pushover	137	1.69	132.80	1.64

On the other hand, Table 5-11 compares the maximum and minimum transient normalized wall edge vertical deformations at the roof in the three case studies. The ratio of the vertical deformation calculated by the dynamic analysis to those obtained from the pushover results (Δ_{vsmax}, Δ_{vsmin}) shows that the minimum normalized wall edge vertical deformation (at the roof level) under the ELC record was under-predicted for all three cases. However, according to the average values presented in Table 5-12 the prediction on average is close enough to the pushover results. On the other hand, the maximum normalized wall edge vertical deformation was over-estimated by the dynamic analysis. The extent of overestimation of these maximum values reduced with increasing flexural stiffness of the slabs. The average ratio of the maximum normalized wall vertical deformation found from the dynamic analysis to the pushover results for the Case1-1, Case2-2 and Case2-3 models was 1.402, 1.328 and 1.194, respectively.

Table 5-11: Vertical edge deformation at base rotation equal to 0.01 (rad) - Damping model A

Case No.	Analysis Input	Δ_{vmax}	Ratio of $\Delta_{vmax}/\Delta_{vsmax}$	Δ_{vmin}	Ratio of Δ_{vmin}/V_{vsmin}
Case1-1	ELC	0.022	1.517	-0.003	0.833
	SOVM	0.019	1.310	-0.004	1.111
	TAFT	0.02	1.379	-0.004	1.111
	Pushover	0.0145	1.000	-0.0036	1.000
Case2-2	ELC	0.017	1.328	-0.003	0.882
	SOVM	0.016	1.250	-0.004	1.176
	TAFT	0.018	1.406	-0.004	1.176
	Pushover	0.0128	1.000	-0.0034	1.000
Case2-3	ELC	0.015	1.250	-0.003	0.909
	SOVM	0.014	1.167	-0.003	0.909
	TAFT	0.014	1.167	-0.003	0.909
	Pushover	0.012	1.000	-0.0033	1.000

Table 5-12: Vertical edge deformation at base rotation equal to 0.01 (rad) - Damping model A

Case No.	Analysis Input	Δ_{vmax}	Ratio of $\Delta_{vmax}/\Delta_{vsmax}$	Δ_{vmin}	Ratio of $\Delta_{vmin}/\Delta_{vsmin}$
Case1-1	NTH	0.0203	1.402	-0.0037	1.019
	Pushover	0.0145	1.000	-0.0036	1.000
Case2-2	NTH	0.017	1.328	-0.0037	1.078
	Pushover	0.0128	1.000	-0.0034	1.000
Case2-3	NTH	0.0143	1.194	-0.003	0.909
	Pushover	0.012	1.000	-0.0033	1.000

5.6.4 Revised Damping Model

As stated previously, damping model A generated spurious damping forces in the structural walls. According to Rayleigh damping formulation based on the global initial stiffness of the model, vertical yielding of structural walls (yielding of vertical reinforcement) has been generated the axial damping forces. No experimental tests at the system level are available to justify this level of axial force amplification due to damping forces. It also was not feasible in the current version of the software to differentiate between the damping forces and stiffness forces from the outputs. However, as previously discussed using the material level damping model named as damping model B in the previous section is a superior approach. A summary

of analysis results using damping model B is presented in Table 5-13 to compare them with pushover results as well as damping model A outputs. Detailed results of analyze based on damping model B model are presented in Appendix A.

Table 5-13: Maximum moment resistance at base rotation equal to 0.01 (rad) - Damping model B

Case No.	M_{yb} (MN.m)	Analysis Input	M_{ub1} (MN.m)	Ratio of M_{ub1}/M_{yb}	M_{ub2} (Excluding p-delta) (MN.m)	Ratio of M_{ub2}/M_{yb}
Case1-1	69.15	ELC	87.56	1.27	82.72	1.20
	69.15	SOVM	89	1.29	84.08	1.22
	69.15	TAFT	90.4	1.31	85.4	1.24
	69.15	Pushover	88.6	1.28	83.7	1.21
Case2-2	74.7	ELC	114.83	1.54	110.20	1.48
	74.7	SOVM	115.00	1.54	110.36	1.48
	74.7	TAFT	114.30	1.53	109.70	1.47
	74.7	Pushover	114.00	1.53	109.40	1.46
Case2-3	80.89	ELC	139.9	1.73	135.60	1.68
	80.89	SOVM	137.5	1.70	133.28	1.65
	80.89	TAFT	137.7	1.70	133.48	1.65
	80.89	Pushover	137.0	1.69	132.8	1.64

Table 5-14: Maximum moment resistance at base rotation equal to 0.01 (rad) - Damping model B

Case No.	M_{yb} (MN.m)	Analysis Input	Mean M_{ub1} (MN.m)	Ratio of M_{ub1}/M_{yb}	M_{ub2} (Excluding p-delta) (MN.m)	Ratio of M_{ub2}/M_{yb}
Case1-1	69.15	NTH	88.99	1.29	84.10	1.22
	69.15	Pushover	88.6	1.28	83.7	1.21
Case2-2	74.7	NTH	114.71	1.54	110.10	1.47
	74.7	Pushover	114.00	1.53	109.40	1.46
Case2-3	80.89	NTH	138.35	1.71	134.11	1.66
	80.89	Pushover	137	1.69	132.80	1.64

Table 5-15: Vertical edge deformation at base rotation equal to 0.01 (rad) - Damping model B

Case No.	Analysis Input	Δ_{vmax}	Ratio of $\Delta_{vmax}/\Delta_{vsmax}$	Δ_{vmin}	Ratio of Δ_{vmin}/V_{vsmin}
Case1-1	ELC	0.0197	1.36	-0.0025	0.69
	SOVM	0.0158	1.09	-0.0023	0.64
	TAFT	0.0159	1.10	-0.0029	0.81
	Pushover	0.0145	1.00	-0.0036	1.00
Case2-2	ELC	0.0159	1.24	-0.0022	0.65
	SOVM	0.0143	1.12	-0.0025	0.74
	TAFT	0.0147	1.15	-0.0021	0.62
	Pushover	0.0128	1.00	-0.0034	1.00
Case2-3	ELC	0.0151	1.26	-0.0021	0.64
	SOVM	0.0136	1.13	-0.0026	0.79
	TAFT	0.0130	1.08	-0.0019	0.58
	Pushover	0.0120	1.00	-0.0033	1.00

Table 5-16: Vertical edge deformation at base rotation equal to 0.01 (rad) - Damping model B

Case No.	Analysis Input	Δ_{vmax}	Ratio of $\Delta_{vmax}/\Delta_{vsmax}$	Δ_{vmin}	Ratio of $\Delta_{vmin}/\Delta_{vsmin}$
Case1-1	NTH	0.0171	1.18	-0.0026	0.71
	Pushover	0.0145	1	-0.0036	1
Case2-2	NTH	0.0150	1.17	-0.0023	0.67
	Pushover	0.0128	1	-0.0034	1
Case2-3	NTH	0.0139	1.16	-0.0022	0.67
	Pushover	0.012	1	-0.0033	1

The results with damping model B damping model for the system overstrength factor matches well with the pushover analysis results (see Table 5-14). The different between the predictions of system overstrength by the pushover analysis and dynamic analysis is less than 1.5 percent. This observation confirms that there is no spurious damping in this analytical model and all axial forces induced in the structural walls can be attributed to the system interaction effects.

Hence, it is quite justified to use these results with confidence. A summary of averaged results for the normalized maximum and minimum wall vertical deformations is displayed in Table 5-16. While in the dynamic analyses of the case studies, the minimum vertical deformation was under-predicted by 30 percent compared to the pushover analysis results, the maximum vertical deformation was over-predicted by up to 17 percent.

Figure 5.31 (a) shows that the system overstrength with damping model A analysis method is higher than pushover results in all cases (and all ground motions). At a base rotation equal to 0.01 rad, the increase in the predicted system overstrength for the Case1-1, Case2-2, and Case2-3 is equal to 16 percent, 11 percent and 9.7 percent, respectively. On the other hand, Figure 5.31 (b) illustrates that the corresponding values in damping model B analysis method are equal to 0.8 percent, 0.8 percent, and 1.2 percent. It is hence concluded that damping model B provides a reliable prediction of the system-over strength factor.

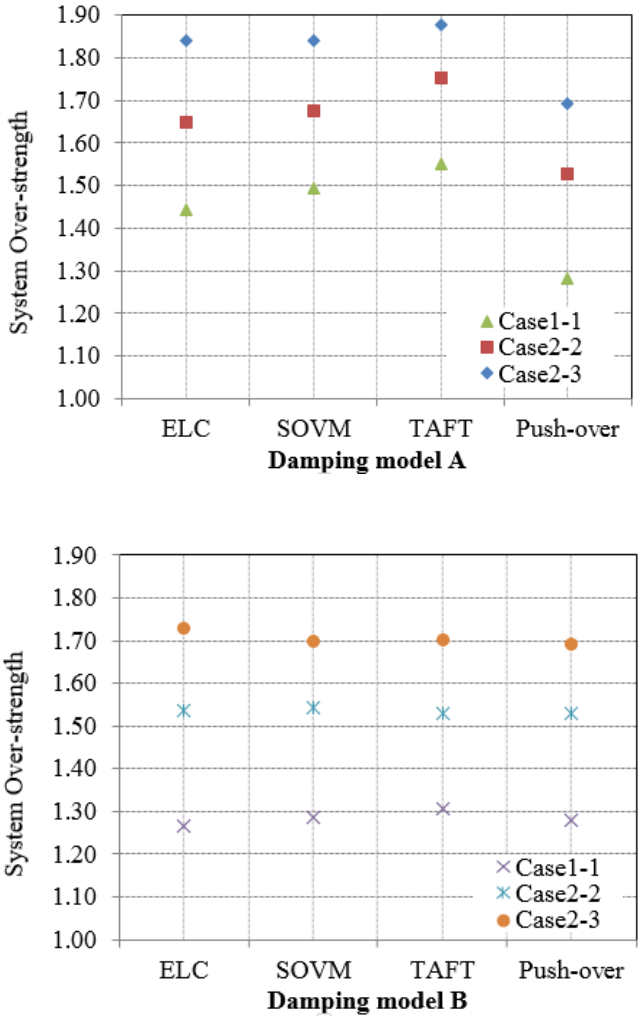

Figure 5.31: System overstrength for damping model A and damping model B (base rotation equal to 0.01 rad)

Figure 5.32 plots the maximum and minimum vertical wall deformations at the roof level at the base rotation equal to 0.01 rad obtained by damping model A and damping model B analysis methods.

It is evident that damping model A overestimates the maximum wall vertical deformation compared to the pushover results for the Case1-1, Case2-2, and Case2-3 by respectively 40%, 32.8% and 19.4% on average. However, the corresponding values obtained from damping model B analysis method are equal to 18%, 17% and 16%, respectively.

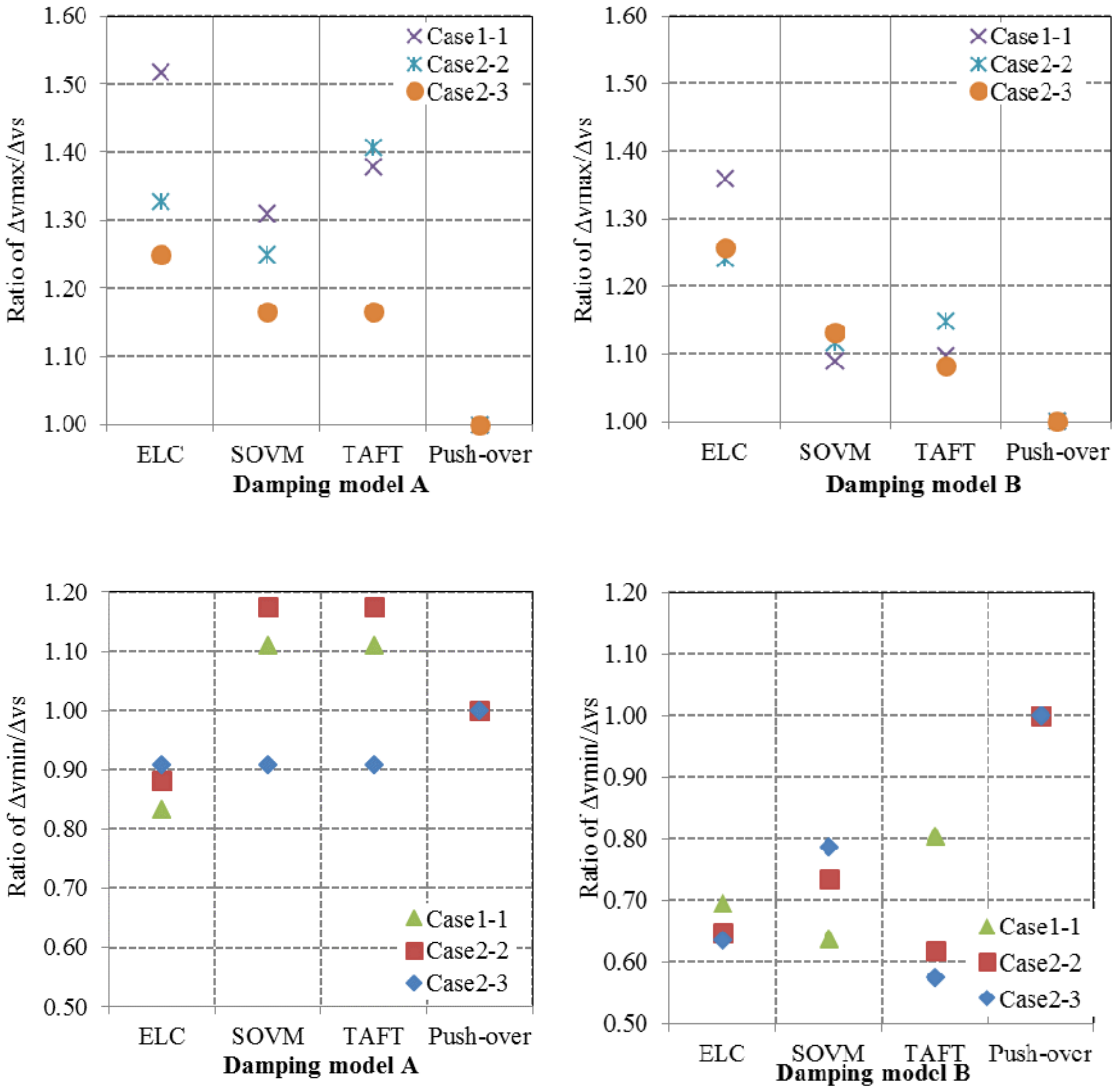

Figure 5.32: Ratio of maximum and minimum wall vertical deformation to pushover analysis at roof level (base rotation equal to 0.01 rad) for damping model A and damping model B

The minimum vertical deformation found from the analysis is also compared to the pushover results in Figure 5.32. It seems that damping model A analysis method results are closer to the pushover results, and damping model B analysis method underestimates the above value for the Case1-1 by 29 percent and for the Case2-2 and Case2-3 by 23 percent.

5.7 Conclusion

This chapter investigated the effect of wall-floor slab-gravity column interaction in shear wall buildings under three different ground motion time histories. Dynamic analysis of three case study buildings has been conducted with different levels of base rotation targets to investigate the system over strength factor. Results of dynamic analysis demonstrated that using the Rayleigh damping model at the global level generated a spurious axial force (damping term) in isolated shear walls. The amplified axial forces caused increase of flexural strength up to 26 percent in the case studies at base rotation equal to 0.01 rad. Hence, a new alternative damping model (damping model B) was proposed by assigning different damping coefficients to the materials located in the plastic hinge region where significant nonlinear response is expected.

It has been found (the results of damping model B) that the system overstrength of the case study buildings (excluding Case1-1) varied from 1.46 to 1.68 at a base rotation of 0.01 rad (as a representative base rotation) depending mainly on the stiffness of the floor slabs. The corresponding value for the overstrength of structural wall itself increased from 1.21 to 1.38. Moreover, the results show that the axial force amplification (without vertical mass) in structural walls for the case study buildings varied from 1.07 to 1.25 at base rotation of 0.01 rad.

The results obtained for the maximum vertical deformation of wall edges at the roof level from the dynamic analysis agrees reasonably well enough with the corresponding pushover analysis results.

Results of different engineering demand parameters employing damping model B were presented in Appendix A. A comparison of the results obtained from two different damping models confirms that spurious damping forces can cause higher value of spurious flexural strength.

5.8 References

ATC-72-1 (2010). *NEHRP recommended provisions for seismic regulations for new buildings and other structures*. Redwood City, California: Applied Technology Council.

Caltrans, S. D. C. (2010). *Caltrans seismic design criteria version 1.6*. Sacramento, CA: California Department of Transportation.

Carr, A. J. (1997). Damping models for inelastic structures. *Proceedings of Asia Pacific vibration conference*.Kyongju, Korea.

Carr, A. J., and Puthanpurayil, A. M. (2017). Inherent Damping in Nonlinear Time-History Analyses: A Recommended Modelling Approach. In *International Conference on Earthquake Engineering and Structural Dynamics* (pp. 87-103).

Charney, F. A. (2008). Unintended consequences of modelling damping in structures. *Journal of structural engineering*, *134*(4), 581-592.

Chopra, A. K. (2001). *Dynamics of structures: theory and applications to earthquake engineering*. Upper Saddle River, NJ: Prentice-Hall.

Chrisp, D. J. (1980). *Damping models for inelastic structures* (Master thesis). University of Canterbury, Christchurch, New Zealand.

Clough, R. W., and Penzien, J. (2003). Dynamics of structures. Computers and Structures, Inc.

Otani, S., and Sozen, M. A. (1972). *Behavior of multistory reinforced concrete frames during earthquakes* (structural research series NO. 392). Urbana, Illinois: University of Illinois Engineering Experiment Station. Retrived from: https://www.ideals.illinois.edu/bitstream/2142/13805/2/SRS-392.pdf

Mondkar, D. P., and Powell, G. H. (1975). *Static and dynamic analysis of nonlinear structures* (Report No. EERC 75-10). Berkley, California: University of California, Earthquake Engineering Research Centre.

Puthanpurayil, A. M., Dhakal, R. P., and Carr, A. J. (2011). Modelling of In-Structure Damping: A Review of the State-of-the-art. *Proceedings of the Ninth Pacific Conference on Earthquake Engineering*. Auckland, New Zealand.

Puthanpurayil, A. M., Lavan, O., Carr, A. J., and Dhakal, R. P. (2016). Elemental damping formulation: an alternative modelling of inherent damping in nonlinear dynamic analysis. *Bulletin of Earthquake Engineering*, *14*(8), 2405-2434.

SAP2000, CSI, S. (2016): Ver. 17.1.1, integrated finite element analysis and design of structures basic analysis reference manual. Berkeley (CA, USA), Computers and Structures INC.

Takeda, T., Sozen, M. A., and Nielsen, N. N. (1970). Reinforced concrete response to simulated earthquakes. *Journal of the Structural Division*, *96*(12), 2557-2573.

White, T., and Adebar, P. (2004). Estimating rotational demands in high-rise concrete wall buildings. In *13th World Conference on Earthquake Engineering*, Vancouver, BC.

6 Outline of the Proposed Simplified Methodology to Estimate the System Overstrength Factor in Multi-Storey Shear Wall Buildings

6.1 Introduction

The importance of system overstrength in capacity design of ductile multi-storey shear wall buildings, due to the presence of flooring slabs, has been addressed extensively in the previous chapters. It has been confirmed that the system overstrength due to the presence of flooring slabs depends mainly on the structural wall height, flexural stiffness of the floors (slabs), spatial bay length (wall distance to the surrounding columns) and the target global drift ratio of structural walls (or the corresponding wall base rotation). It is also useful to highlight that the maximum global drift of a ductile RC multi-storey shear wall building under a specified level of seismic excitation depends on its dynamic properties and ground motion characteristics.

Additionally, it has also been demonstrated that the contribution of floors to the system response starts being significant once the yielding of tension rebar's occurred at the base section of structural walls. However, in order to develop a simplified method to account for the effect of the system overstrength factor in a design process, we assumed that the maximum global drift capacity of the building is attained under any arbitrary seismic excitation.

Drift dependency of the system overstrength (significantly in the nonlinear range) implies that the system overstrength factor in a ductile multi-storey RC shear wall building, under specific level of excitation, also depends on the dynamic characterization of building such as its elastic period and damping. However, for design purpose, the maximum usable plastic rotation at the base of structural walls is used here to estimate the system overstrength factor conservatively. In other words, the proposed method gives an upper bound value of the system over strength factor since it employs the ultimate curvature capacity of the wall base section independent of the seismic demand imposed on the system. Hence, for a given demand spectrum, one can employ the capacity demand spectrum method (ATC-40): to find the maximum lateral displacement (and consequently the maximum base rotation) of structural walls under a

specified demand spectrum. This method allows a user to employ a smaller value for the system overstrength factor since the wall base rotation demand under a design level earthquake may be much less than the ultimate base rotation capacity of the wall.

In this chapter, the method proposed in Chapter 4 is presented step by step to obtain a system overstrength factor. It shows how one can account for the system overstrength factor of a multi-storey shear wall building in a design office. Due to the complexity due to a number of variables involved in the method, the application of the simplified method may be limited only to buildings with similar configuration to those investigated in this study. Although this simplified method has been verified extensively with a detailed numerical analysis, in case of complex geometries a three- dimensional pushover analysis is highly recommended.

6.2 Outline of the Simplified Methodology

Figure 6.1 shows how one can follow the method step by step to find an upper bound value of the system overstrength in a ductile multi-storey shear wall building. Detailed explanation and background on the employed formulation have been presented in Chapter 4. The diagram highlights the input variables as well as closed form analytical solution to estimate the system overstrength factor for a given RC multi-storey shear wall building.

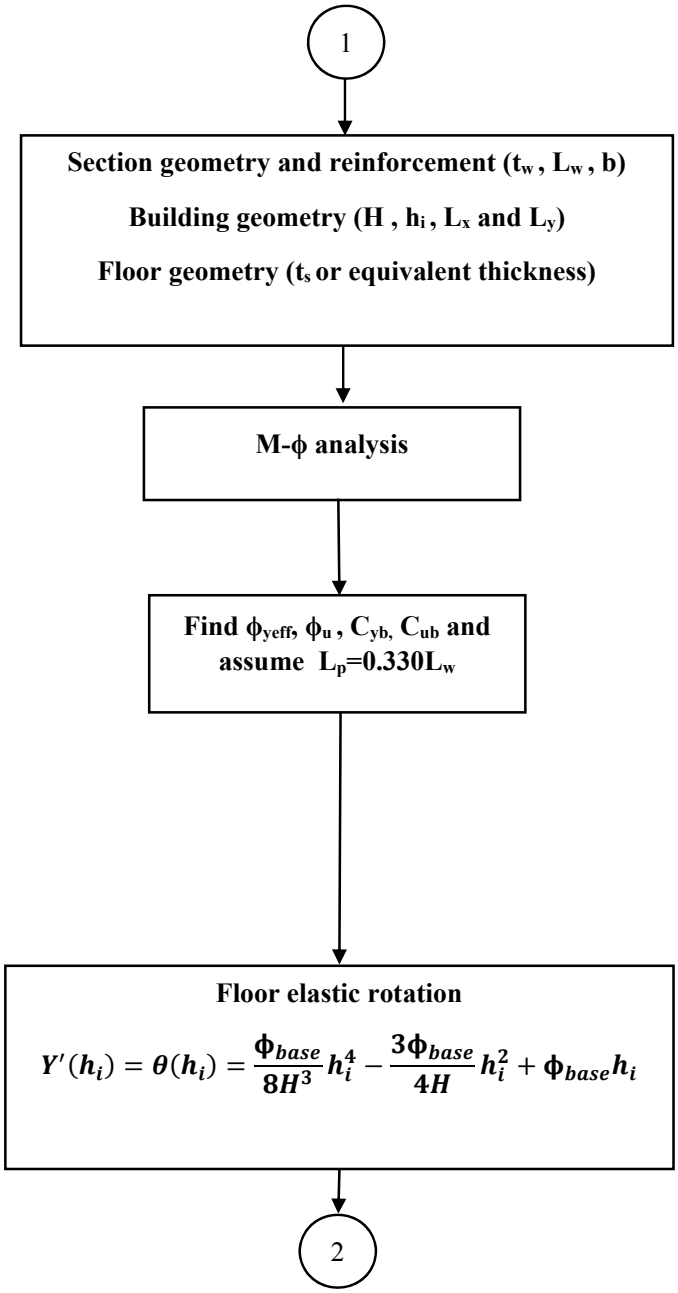
1
Section geometry and reinforcement (t_w , L_w , b)
Building geometry (H , h_i , L_x and L_y)
Floor geometry (t_s or equivalent thickness)
M-ϕ analysis
Find ϕ_{yeff}, ϕ_u , C_{yb}, C_{ub} and assume L_p=0.330L_w
Floor elastic rotation
$Y'(h_i) = \theta(h_i) = \frac{\phi_{base}}{8H^3} h_i^4 - \frac{3\phi_{base}}{4H} h_i^2 + \phi_{base} h_i$
2

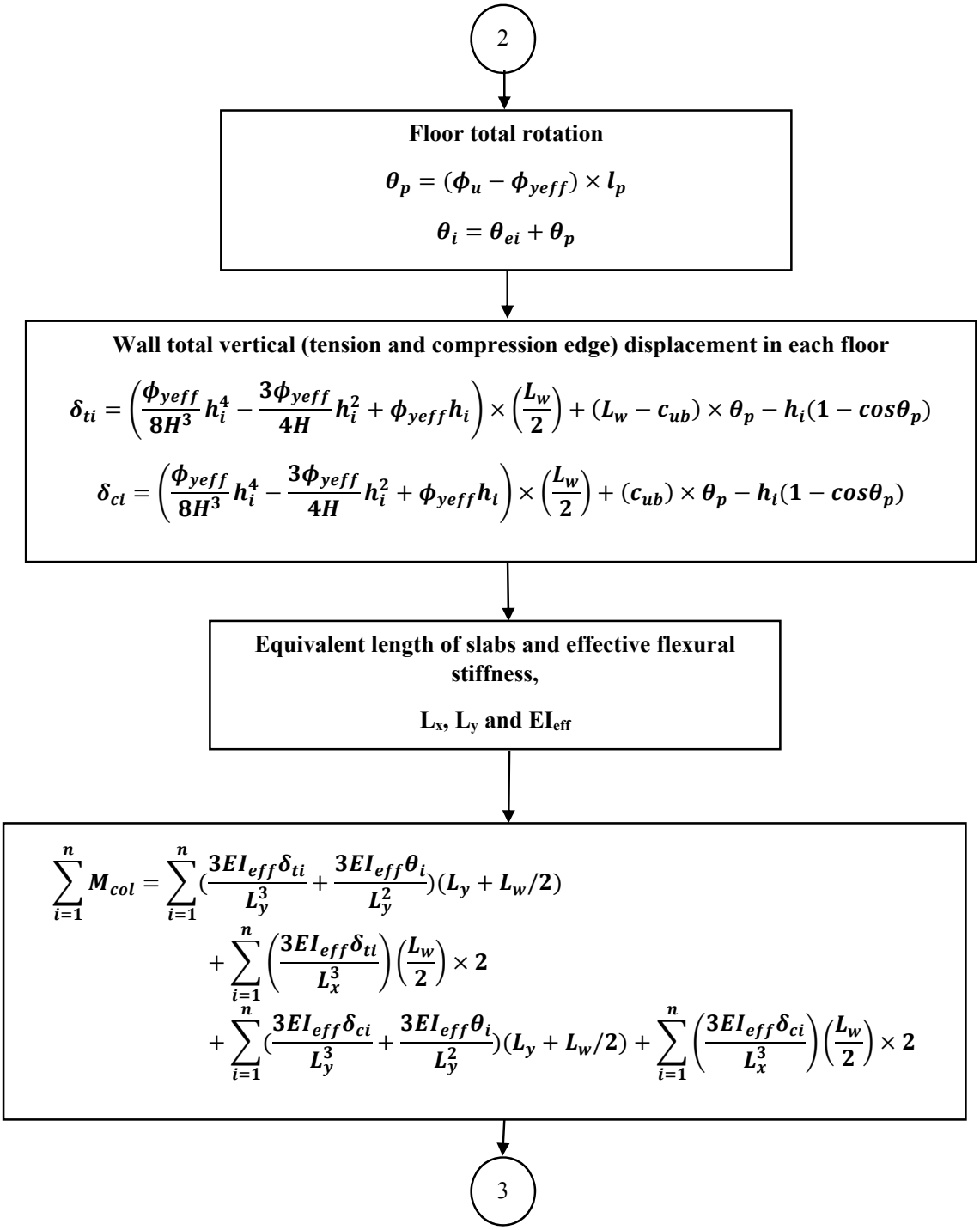
2
Floor total rotation
$\theta_p = (\phi_u - \phi_{yeff}) \times l_p$
$\theta_i = \theta_{ei} + \theta_p$
Wall total vertical (tension and compression edge) displacement in each floor
$\delta_{ti} = \left(\frac{\phi_{yeff}}{8H^3} h_i^4 - \frac{3\phi_{yeff}}{4H} h_i^2 + \phi_{yeff} h_i\right) \times \left(\frac{L_w}{2}\right) + (L_w - c_{ub}) \times \theta_p - h_i(1 - cos\theta_p)$
$\delta_{ci} = \left(\frac{\phi_{yeff}}{8H^3} h_i^4 - \frac{3\phi_{yeff}}{4H} h_i^2 + \phi_{yeff} h_i\right) \times \left(\frac{L_w}{2}\right) + (c_{ub}) \times \theta_p - h_i(1 - cos\theta_p)$
Equivalent length of slabs and effective flexural stiffness,
L_x, L_y and EI_{eff}
$\sum_{i=1}^{n} M_{col} = \sum_{i=1}^{n} (\frac{3EI_{eff}\delta_{ti}}{L_y^3} + \frac{3EI_{eff}\theta_i}{L_y^2})(L_y + L_w/2) + \sum_{i=1}^{n} \left(\frac{3EI_{eff}\delta_{ti}}{L_x^3}\right)\left(\frac{L_w}{2}\right) \times 2 + \sum_{i=1}^{n} (\frac{3EI_{eff}\delta_{ci}}{L_y^3} + \frac{3EI_{eff}\theta_i}{L_y^2})(L_y + L_w/2) + \sum_{i=1}^{n} \left(\frac{3EI_{eff}\delta_{ci}}{L_x^3}\right)\left(\frac{L_w}{2}\right) \times 2$
3

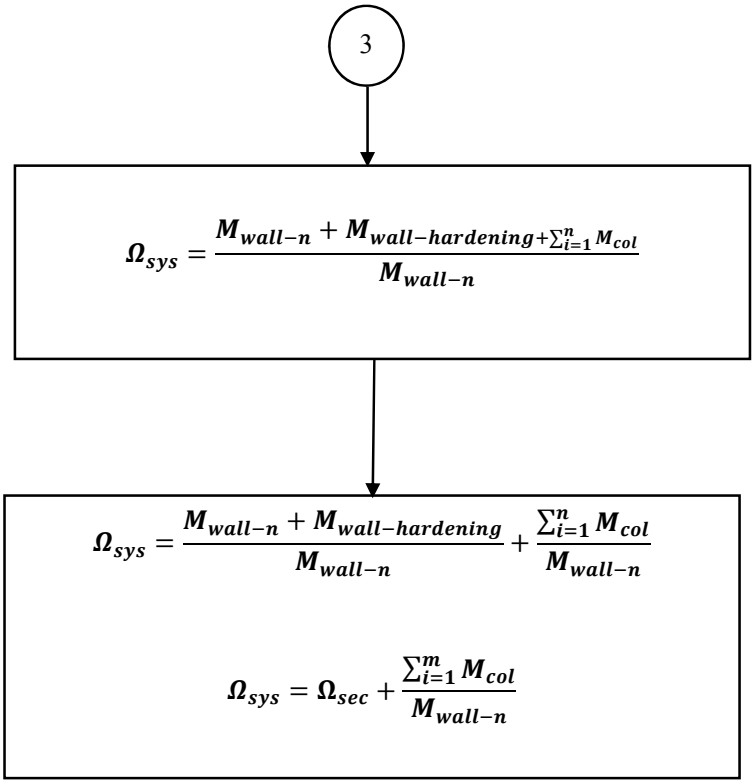

Figure 6.1: Outline of the step by step method to obtain the system overstrength factor

It is quite evident from the last equation in Figure 6.1 that the system overstrength increases the slope of the post-yield segment of the force versus deformation (or corresponding moment versus rotation) curve for a given structural wall. The system overstrength introduces an additional lateral strength on top of the sectional flexural overstrength. Flexural overstrength of a wall section originates mainly from the strain hardening of the reinforcing bars, difference between the expected and characteristics values of material properties and design strength reduction factors.

Although in general, this additional overstrength of the system (due to the contribution of the floor slabs) is desirable to resist additional lateral actions, it may raise a concern when the capacity design principle is employed to inhibit the shear failure along the wall height. Therefore, on one hand, the standard practice to neglect the contribution of the floor systems in the seismic response seems conservative, while on the other hand, care should be taken when

capacity design is employed to prevent shear failure. The following example shows an application of the proposed method in a five story shear wall building.

6.3 Example: Calculate the system overstrength of five storey shear wall building at the drift level associated with wall base ultimate rotation (or curvature)

The building plan is shown in Figure 6.2. The example building has barbell type shear walls resisting the seismic forces in Y direction and RC perimeter moment frames in the other direction (X). This building is designed according to the NZ seismic standards (NZS1170.5:2004). The design period of the structure was calculated by Eigen value analysis according to the stiffness values recommended in NZS3101:2006 for RC elements. All other design information is demonstrated in Table 6-1. The floor stiffness was neglected in the calculation of building period. Floor systems comprised of equivalent flat slabs in both directions. According to capacity design principle, we assume that the slabs are reinforced enough to prevent any slab to column punching shear failure or any other non-ductile failures inside the floors. The base section of the walls and reinforcement bars are shown in Figure 6.3. Wall section has thicker boundary elements and, is confined with stirrups and ties of T12 bars spaced at 75 mm.

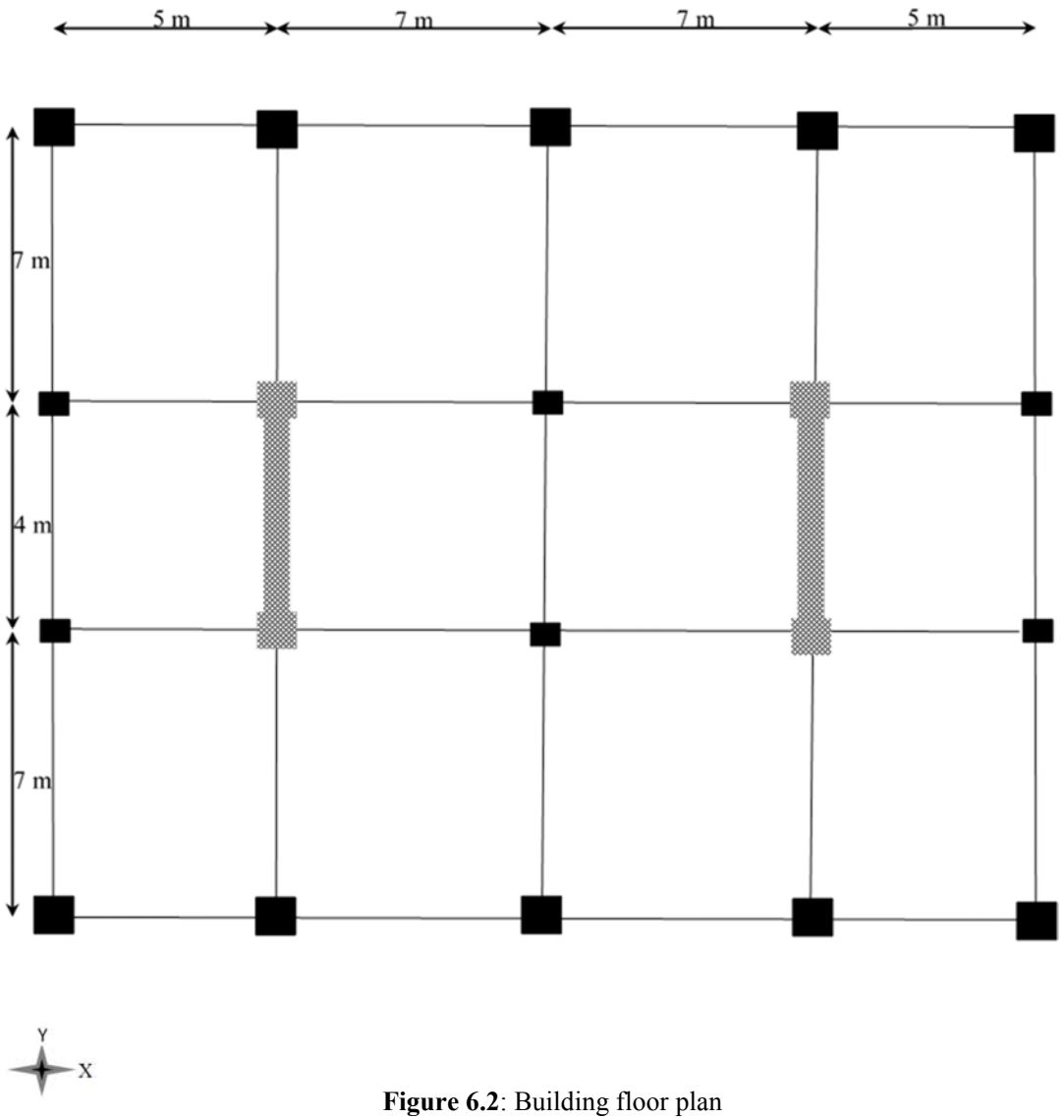

Figure 6.2: Building floor plan

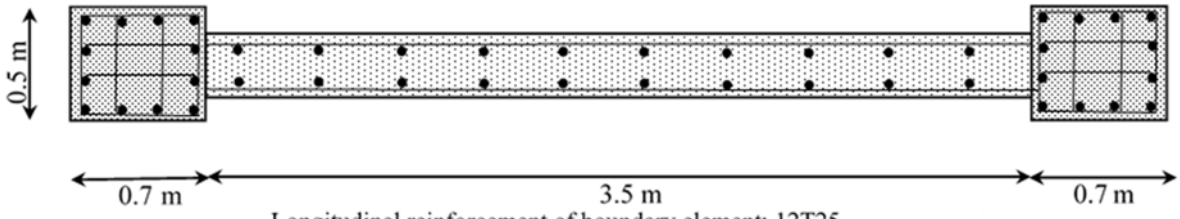

Longitudinal reinforcement of boundary element: 12T25
Confinement and anti-buckling ties of boundary element: T12@75mm
Longitudinal reinforcement of web: T16@300
Shear reinforcement of web: T16@300

Figure 6.3: Wall base section

Table 6-1: Design information

Barbell type wall section	3500*300 + 700*500	Near fault factor	1.0
Typical floor height	3.5 m	Seismic weight on each wall	8429.5 kN
f_c	30 MPa	Soil type	D
f_{yl}, f_{yh}	500, 300 MPa	Near fault factor	1.0
Gravity columns	400x400 mm	Zone factor	0.4
Slab thickness	200 mm	Return period factor	1.0
Gravity load on each wall base	3009 kN	Structural ductility	3.5
Period (Y direction)	0.75 sec		

Moment curvature analysis of the wall base section has been conducted using the material stress and strain law for the unconfined, confined concrete and reinforcement. Section designer tool in SAP2000 is used to find the moment curvature of wall base section. Mander et al., 1988 and Thompson and Park 1978 model are used for nonlinear behaviour of concrete (confined and unconfined) and reinforcing steel bar respectively. The strain limits for the reinforcement and confined concrete are based on the Priestley et al. (2007) recommendations. Table 6-2 indicates the results obtained from a moment curvature analysis of the wall base section. An idealized bilinear curve has been built to find the effective curvature point (or significant yield point) and slope of the strain hardening part (post-yield) as well as the ultimate point on this curve. The slope of post-yield response (force displacement or moment curvature curve) is one of the key variables to obtain the section overstrength factor. Table 6-2 shows that the estimated flexural overstrength of the wall section at the ultimate point is equal to 1.285 based on the employed idealization method.

Table 6-2: Moment curvature analysis results

Output of Section Analysis		
Gravity load on wall	-3009	kN
L_w	5200	mm
f_c	30	MPa
f_y	500	MPa
f_u	607.6	MPa
E_c	25743	MPa
E_s	200000	MPa
ε_y	0.0025	1/mm
ε_{us}	0.06	1/mm
ε_{ucu}	0.004	1/mm
ε_{ucc}	0.015	1/mm
ϕ_y (point A)	0.708	1/km
C_{yb}	1270.67	mm
C_{yb}/L_w	0.244359615	
M_y (point A)	20138	kN.m
M_n (point B)	22101	kN.m
ϕ_{yeff} (point B)	0.777	1/km
ϕ_u (point C)	14.11	1/km
C_{ub}	770	mm
M_u (point C)	28404	kN.m
C_{ub}/L_w	0.148076923	
L_p	1752.4	mm
Θ_p	0.02353	rad
$\Omega_{section}$	1.285	

Hence, to prevent shear failure according to the capacity design principle, shear capacity in the plastic hinge region of the wall should be greater than the shear demand equivalent to the overstrength actions due to flexural yielding of the wall base section.

It should be highlighted that any other source of shear demand amplification (such as dynamic shear amplification due to higher mode effects) are neglected for simplicity of calculations. According to the NZS3101:2006, the shear demand on the cantilever walls is calculated as:

$$V^*_{wall}=\omega_v\varphi_o V^*_E \quad (6.1)$$

ω_v: dynamic amplification factor (higher elastic modes)

$$\omega_v= 1.3+n/30 < 1.8 \quad (6.2)$$

n: number of stories

φ_0= Isolated wall sectional overstrength factor (flexural) at the base section (this factor account for the effect of strain hardening of reinforcement rebars, concrete confinement, design strength reduction factor and difference between the expected and characteristic value for the material properties)

However, the results of the extensive numerical investigation in this thesis, as well as results of experimental tests, have confirmed that system overstrength due to the spatial interaction of floor slabs, frames, and structural walls should be included in the above formulation.

Figure 6.4 indicates the results of moment curvature analysis of wall base section up to ultimate curvature capacity of the base section. In this particular example, the ultimate point is obtained once the tensile strain in the reinforcing bars reached the threshold value of 0.06. At this point, the corresponding concrete compressive strain was equal to 0.00763 in the confined zone.

The numerical value of the section over strength highly depends on how one idealizes the moment curvature curve. Different methods have been proposed in the literature to idealize the moment curvature curve. Figure 6.4 below shows the employed methodology to idealize the moment curvature by equating the area (A_1=A_2) between the curve and the horizontal straight line (segment BC) passing through the segment OAB. The point A on the moment curvature curve is associated with the point once the first raw reinforcing rebars inside the boundary element yielded in tension.

The second simple method to bi-linearize the curve is to connect the point A (first yield curvature associated with yielding of the first rebar in tension) to the point C as ultimate curvature capacity. While the idealization of the curve as segment OAC leads to sectional over

strength equal to 1.41, the idealization of the curve with segment OBC results in the sectional over strength equivalent to 1.285.

In this thesis, the first method has been used to bi-linearize the moment curvature curve since this method has been widely accepted for idealizing moment curvature curves.

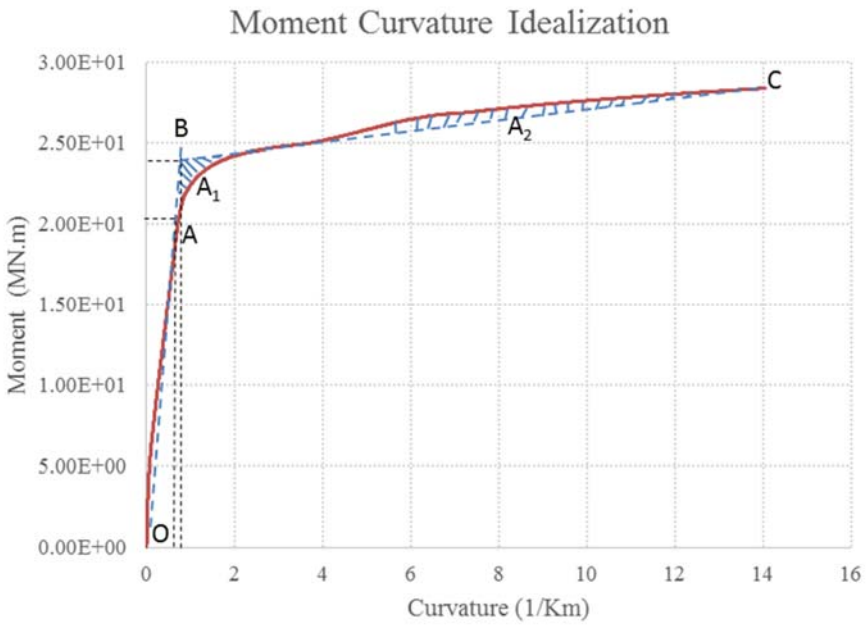

Figure 6.4: Idealized moment curvature curve of example wall base section

Table 6-3 to Table 6-8 in the following pages indicates step by step application of the method to estimate the system overstrength factor for the example building.

Table 6-3: Building geometry and floor specification

Building Geometry	Five Storey	Units
H	17.5	m
h_1	3.5	m
h_2	7.0	m
h_3	10.5	m
h_4	14.0	m
h_5	17.5	m
$L_{x\text{-}1}$	7.0	m
$L_{x\text{-}2}$	4.0	m
$L_{y\text{-}1}$	7.0	m
$L_{y\text{-}2}$	5.0	m
$L_{x\text{-}eff}$	5.5	m
$L_{y\text{-}eff}$	6.0	m
Slab Thickness	0.20	m
$E_cI_{g\text{-}x}$	94391000	$N.m^2$
$E_cI_{g\text{-}y}$	102972000	$N.m^2$
$E_cI_{eff\text{-}x}$	23597750	$N.m^2$
$E_cI_{eff\text{-}y}$	25743000	$N.m^2$

Table 6-4: Floor elastic rotation

$$Y'(h_i) = \theta(Z) = \frac{\emptyset_{base}}{8H^3} {h_i}^4 - \frac{3\emptyset_{base}}{4H} {h_i}^2 + \emptyset_{base} h_i$$

Elastic Floor Rotation			Floor edge vertical movement	
Floor	h_i	Floor rotation(rad)	(Up) (mm)	(Down)(mm)
0	0	0	0	0
1	3.5	0.00273	7.109	7.109
2	7	0.00455	11.830	11.830
3	10.5	0.00556	14.462	14.462
4	14	0.00596	15.506	15.506
5	17.5	0.00602	15.665	15.665

Table 6-5: Floor plastic rotation

Plastic Floor Rotation	Θ_p=0.02353	Floor rotation(rad)	Floor edge vertical movement	
Floor	h_i (m)		(Up) (mm)	(Down) (mm)
0	0	0.0235	0	0
1	3.5	0.0235	104.242	18.120
2	7	0.0235	104.241	18.121
3	10.5	0.0235	104.240	18.122
4	14	0.0235	104.239	18.123
5	17.5	0.0235	104.238	18.124

Table 6-6: Vertical displacement of wall edges

$$\delta_{ti} = \left(\frac{\phi_{eff}}{8H^3}h_i^4 - \frac{3\phi_{eff}}{4H}h_i^2 + \phi_{yeff}h_i\right) \times \left(\frac{L_w}{2}\right) + (L_w - c_{ub}) \times \theta_p - h_i(1 - cos\theta_p)$$

$$\delta_{ci} = \left(\frac{\phi_{yeff}}{8H^3}h_i^4 - \frac{3\phi_{yeff}}{4H}h_i^2 + \phi_{yeff}h_i\right) \times \left(\frac{L_w}{2}\right) + (c_{ub}) \times \theta_p - h_i(1 + cos\theta_p)$$

Total Floor Rotation		Floor rotation(rad)	Floor edge vertical movement	
Floor	h_i(m)		(Up)(m)	(Down)(m)
0	0	0.02353	0	0
1	3.5	0.02627	0.1113	0.0252
2	7	0.02808	0.1160	0.0299
3	10.5	0.02909	0.1187	0.0325
4	14	0.02949	0.1197	0.0336
5	17.5	0.02956	0.1199	0.0337

Table 6-7: Additional moment capacity due to interaction

$$\sum_{i=1}^{n} M_{col} = \sum_{i=1}^{n}\left(\frac{3EI_{eff}\delta_{ti}}{L_y^3} + \frac{3EI_{eff}\theta_i}{L_y^2}\right)(L_y + L_w/2) + \sum_{i=1}^{n}\left(\frac{3EI_{eff}\delta_{ti}}{L_x^3}\right)\left(\frac{L_w}{2}\right) \times 2 + \sum_{i=1}^{n}\left(\frac{3EI_{eff}\delta_{ci}}{L_y^3} + \frac{3EI_{eff}\theta_i}{L_y^2}\right)(L_y + L_w/2) + \sum_{i=1}^{n}\left(\frac{3EI_{eff}\delta_{ci}}{L_x^3}\right)\left(\frac{L_w}{2}\right) \times 2$$

Floor	h_i(m)	M_{floor} (kN.m)	$M_{cumulative}$ (kN.m)
1	3.5	1691.338014	9175.52276
2	7	1808.246612	7484.184746
3	10.5	1873.425742	5675.938134
4	14	1899.290476	3802.512392
5	17.5	1903.221916	1903.221916
	Sum	9175.52276	

Table 6-8: System overstrength factor

$\Omega_{sys} = \Omega_{sec} + \frac{\sum_{i=1}^{m} M_{col}}{M_{wall-n}}$	
Ω_{sys}	1.688

The above calculation shows how one can predict the upper bound value of the system overstrength factor at a drift level associated with the ultimate curvature of a wall base section by employing the proposed simplified method. The obtained system overstrength factor is taken as an upper bound value since this value was found at the ultimate curvature capacity of the base section.

The estimated numerical value of system overstrength shows that the system overstrength for the example building is equal to 1.688 at the drift level associated with the ultimate rotation capacity of the wall base section. However, the sectional overstrength was only equal to 1.285 according to the numerical value presented in Table 6-2.

The ratio of system overstrength to the section overstrength factor is about 1.32.

The slope of post-yield response of the section (on moment curvature curve) was obtained equal to ((28404-22101)/ (14.11-0.777))/ (22101/0.777) = 0.0166 by bi-linearization of moment curvature curve. Hence, the percentage of the post-yield slope normalized to initial (effective) stiffness is equal to 1.66%. However, the corresponding value once the system overstrength was included in calculations is 4.0%.

According to the capacity design principle, non-ductile failure mechanisms such as shear failure should be avoided along the height of the wall. Design standards use only the section overstrength factor to calculate the maximum probable moment capacity of the wall base sections. However, it has been confirmed here that another source of overstrength will be mobilized due to three-dimensional interaction of floor slabs, walls, and frames. Hence, the

design implication of this value is that if one intends to prevent shear failure along the heights of the wall according to the capacity design principal, he/she should provide some allowance, on top of sectional over strength, for this additional system overstrength factor.

6.4 Calculation of System-Overstrength under the DBE and MCE Level Seismic Demand

As already mentioned, the system overstrength can significantly increase the post- yield slope of the force deformation curve obtained the multi-storey shear wall buildings. However, the increased post-yield slope of force-deformation curve implies that for a given target drift higher external force can be applied to the system.

It is worth mentioning that upper bound system overstrength factor has been found for the example building at the ultimate curvature capacity of the wall base section. However, the system overstrength factor under DBE or MCE level seismic excitations may be less than this upper bound value.

6.4.1 Capacity Spectrum Method

In this section, the lateral displacement of a system under DBE and MCE level ground motions will be determined from the smoothed demand spectrum at two hazard levels. Capacity Spectrum Method (ATC-40) will be employed to find the target displacement of the system under a given demand spectrum with an iterative procedure.

It should be emphasized that the force deformation response of the prismatic shear walls was established using the wall base section idealized moment curvature curve. In doing so, the interrelation between the base plastic curvature and plastic displacement profile were found according to the plastic hinge analysis method.

It is useful to say that significant uncertainty exists on how one can obtain the displacement demand of nonlinear MDOF system under earthquake excitations. Although many assumptions

exist in the CSM method, it is widely accepted that the CSM method is the most practical way to find the ultimate displacement of ductile structures under a given demand spectrum. Moreover, the formulation based on the assumption of equal displacement or equal energy rules do not account for the effect of change in the post-yield stiffness of yielding structures explicitly.

Closed form equations are proposed in Chapter 3, to interrelate the base section effective yield curvature with the roof (or at effective height) displacement. Hence, using the polynomial deformation profile (shape function) for the structural wall deformation (prismatic wall with constant flexural stiffness EI and mass m), the effective mass in the first mode and the mode participation factor can be calculated as:

$$PF_1 = \left[\frac{\sum_{i=1}^{n}(w_i\Phi_{i1})/g}{\sum_{i=1}^{n}(w_i\Phi_{i1}^2)/g}\right] \tag{6.3}$$

$$\alpha_1 = \frac{\left[\sum_{i=1}^{n}(w_i\Phi_{i1})/g\right]^2}{[\sum_{i=1}^{n}w_i/g][\sum_{i=1}^{n}(w_i\Phi_{i1}^2)/g]} \tag{6.4}$$

$$S_a = \frac{V/W}{\alpha_1} \quad \text{and} \quad S_d = \frac{\Delta_{roof}}{PF_1\Phi_{roof,1}} \tag{6.5}$$

$$T_1 = 2\pi\sqrt{\frac{S_d}{S_a}} \tag{6.6}$$

where:

PF_1: modal participation factor for the first natural mode.

α_1: modal mass coefficient for the first natural elastic mode.

w_i/g: mass assigned to level i.

ϕ_{i1}: amplitude of mode 1 at level i.

n: level n (upper floor).

V: base shear.

W: building weight.

Δ_{roof}: roof displacement.

S_a: spectral acceleration.

S_d: spectral displacement.

T_1: first natural fundamental mode

According to the CSM method documented in ATC-40, establishing the equivalent single degree of freedom systems for multi-storey structural walls require knowledge of the target displacement in the capacity spectrum curve. Target displacement demand can be found in an iterative procedure. The equivalent damping of the system calculated according to the idealized hysteresis loop shown in Figure 6.5. Detailed information on this method can be found in ATC-40.

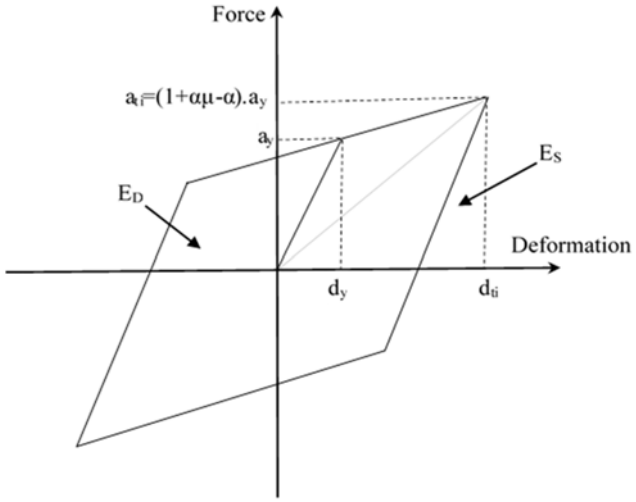

Figure 6.5: The method of equivalent damping ratio

$$T_{eq} = T_1\sqrt{\frac{\mu}{1+\alpha(\mu-1)}} \tag{6.7}$$

$$\hat{\zeta}_{eq} = \zeta + \kappa\zeta_{eq} \qquad \text{and} \qquad \zeta_{eq} = \frac{2}{\pi}\frac{(\mu-1)(1-\alpha)}{\mu(1+\alpha\mu-\alpha)}, \tag{6.8}$$

where T_{eq} is the natural vibration period of the equivalent linear system, T_1 is the natural vibration period of the system vibrating within its linearly elastic range, μ is the displacement ductility factor, α is the post-yield stiffness to elastic stiffness, $\hat{\zeta}_{eq}$ is the equivalent viscous damping ratio of the nonlinear system, ζ is the viscous damping ratio of the bilinear system

vibrating within its linearity elastic range, ζ_{eq} is the additional equivalent viscous damping ratio of the nonlinear system, and κ is the damping modification factor (ATC-40).

With the knowledge of the equivalent period and the equivalent damping at the assumed target displacement, the displacement demand can be calculated. An iterative method is required to match the calculated and assumed displacement demand.

There are various expressions in the literature in order to reduce the elastic response spectra to different levels of damping. The equivalent viscous damping values obtained from Equation 6.9 can be used to estimate spectral reduction factors. Spectral reduction factors are used to decrease the elastic (5% damped) response spectrum for damping greater than 5% of critical damping. In this work, the following expression is used to create a highly damped displacement spectrum, $S_{d,\xi}$, from the 5% elastic spectral displacement demands, $S_{d,5\%}$:

$$S_{d,\zeta} = S_{d,5\%}[\frac{7}{2+\hat{\xi}_{eq}}]^{0.5} \tag{6.9}$$

However, as stated earlier, an iteration is required to reach a displacement on the capacity spectrum curve which produces the same displacement demand corresponding to the equivalent damping and equivalent period. It is useful to highlight that the two latter variables are functions of the chosen displacement (ductility) on the capacity spectrum curve. Hence, a spreadsheet has been developed to find the displacement demand by an iterative procedure.

A key step in the above procedure is how to find the force deformation curve of a multi-storey shear wall building utilizing the idealized moment curvature curve for the wall base section. For this, an equivalent single degree of freedom system model is established for the multi-storey shear wall building using the effective mass, mode participation factor and effective height. Figure 6.6 shows a single multi-storey wall of height H, length L_w, and thickness t_w, subjected to lateral inertial forces associated with the floor masses. A capacity curve is to be

developed for response associated with the first mode, for which lateral forces along the height of the wall are proportional to the product of the fundamental mode shape amplitude and the mass at each floor. The story shears, wall moments, and the deflected shape caused by the lateral forces are also illustrated. The key coefficients to convert the prismatic multi-storey shear wall building with uniform stiffness and mass distribution to an idealized single degree of freedom are also shown in Figure 6.7. To capture the more realistic response in the elastic range, a higher degree polynomial proposed in Chapter 3 was used to reproduce the shape of the first mode in structural walls. The numerical values of coefficients are populated for different multi-storey shear wall buildings with different number of stories in Table 6-9. The numerical values in this table are found using the equations presented in Figure 6.7 and assuming uniform distribution of mass and flexural stiffness over the wall height.

Table 6-9: Curvature modification, mode participation factor, effective mass and effective height for a cantilever prismatic wall

n (number of stories)	λ	PF_1	α_1	H_{eff}/H
1	1.2121	1	1	1
2	1.1078	1.2017	0.8074	0.8721
3	1.0725	1.2911	0.7399	0.8278
5	1.0656	1.3737	0.6882	0.8000
8	1.0265	1.4408	0.6602	0.7670
10	1.0208	1.4629	0.6511	0.7590
15	1.0129	1.4941	0.6391	0.7480

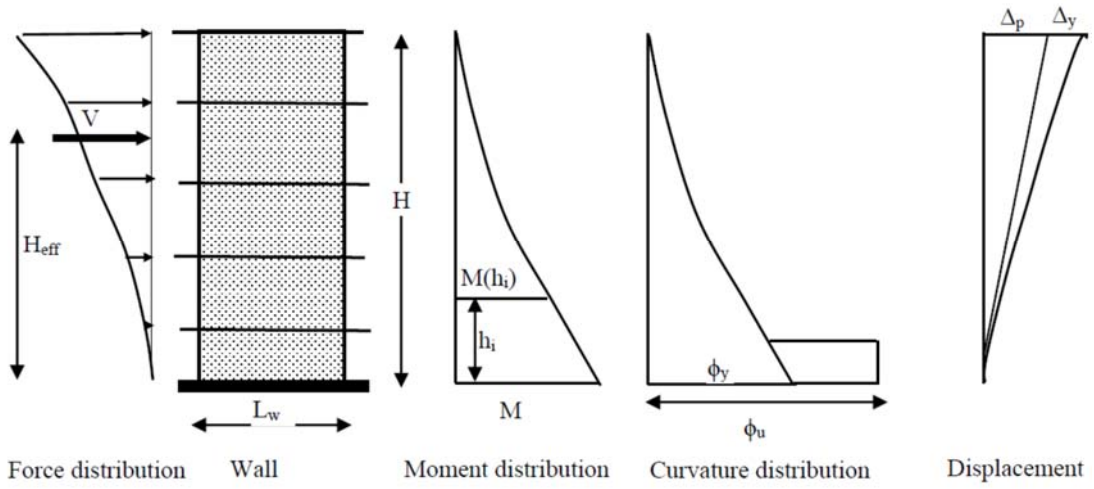

Figure 6.6: Distribution of lateral force, moment and curvature in multi-storey shear wall

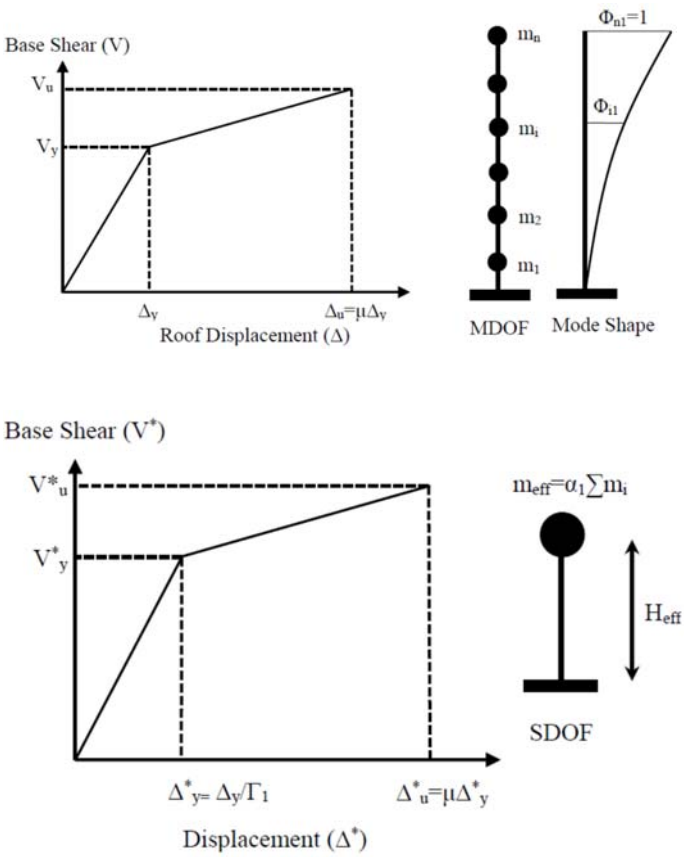

$$\Delta(h_i) = \frac{\Delta_{roof}}{11H^5} h_i^{\,5} - \frac{10\Delta_{roof}}{11H^3} h_i^{\,3} + \frac{20\Delta_{roo}}{11H^2}$$

$$\Delta_{y(roof)} = \frac{11H^2}{40} \phi_{yeff} \times \lambda$$

$$\Delta_y^* = \frac{\Delta_y}{PF_1} = s_d$$

$$V_y^* = \frac{M_n}{H_{eff}} \quad or \; V_u^* = \frac{M_u}{H_{eff}}$$

$$\alpha_1 = \frac{[\sum_{i=1}^{n}(w_i \Phi_{i1})/g]^2}{[\sum_{i=1}^{n} w_i/g][\sum_{i=1}^{n}(w_i \Phi_{i1}^2)/g]}$$

$$PF_1 = \left[\frac{\sum_{i=1}^{n}(w_i \Phi_{i1})/g}{\sum_{i=1}^{n}(w_i \Phi_{i1}^2)/g}\right]$$

$$H_{eff} = \left[\frac{\sum_{i=1}^{n}(w_i \Phi_{i1})/g \times h_i}{\sum_{i=1}^{n}(w_i \Phi_{i1})/g}\right]$$

$$\lambda = PF_1 \times (\frac{40}{33}) \times (\frac{H_{eff}}{H})^2$$

$$S_a = \frac{V_y^*}{\alpha_1 \sum m_i}$$

$$T_1 = 2\pi \sqrt{\frac{S_d}{S_a}}$$

$$\theta_p = (\phi_u - \phi_{yeff}) \times l_p$$

$$\Delta_p = \theta_p (H - \frac{l_p}{2})$$

Figure 6.7: Conversion of MDOF multi-storey shear wall to SDOF

The demand spectrum for earthquakes at DBE level and MCE level are shown in Figure 6.8. These curves are demand spectrum (5% damping) for the soil type D with zone factor equal to 0.4 according to NZS1170.5:2004 standard. It should be mentioned that MCE level spectrum obtained simply by multiplying the DBE spectrum in 1.8 according to NZS 1170.5:2004 standard.

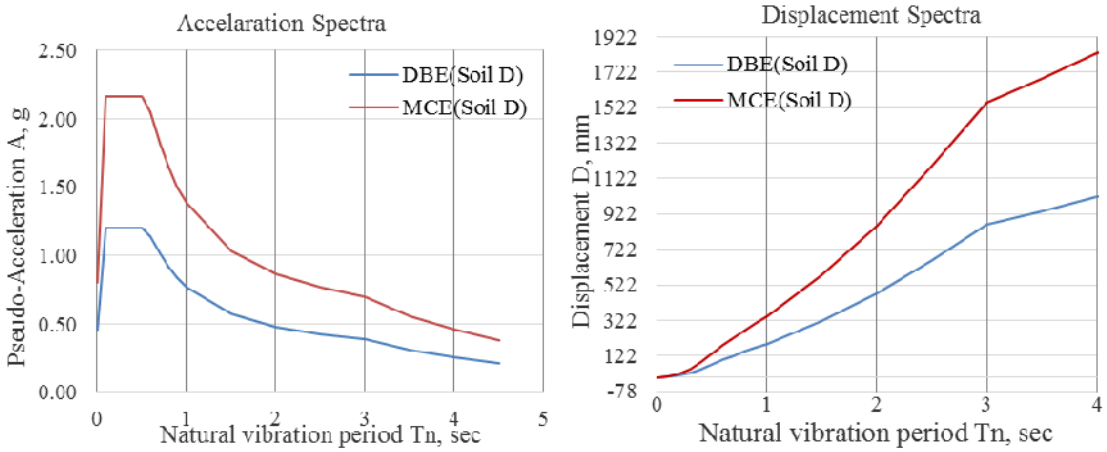

Figure 6.8: Response spectrum for DBE and MCE level

Table 6-10 displays the final results obtained for the example building under DBE level spectrum demand. It is evident that the system overstrength factor under the DBE level earthquake (1.19) is quite small compared to the value obtained at the ultimate curvature capacity of the base section (1.69).

As showing in Table 6-11, the overstrength factors due to sectional overstrength and system overstrength for the example building under MCE level are 1.37 and 1.74, respectively.

Table 6-12 presents a summary of the results under the two level earthquakes with and without the system interaction. Results confirm that system overstrength factor and sectional overstrength factor under the MCE level earthquake attained higher value compared to the values obtained at the ultimate curvature capacity of the base section. This is likely due to the

underestimation of ultimate displacement capacity of structural walls employing plastic hinge analysis. The appropriate effective plastic hinge length is a key variable to obtain the ultimate displacement capacity of structural walls in this method.

Table 6-10: Overstrength factor with and without floor interaction under DBE

	T_1(sec)	T_{eq}(sec)	a	ζ_{eq}(%)	Δ^*_u(m)	Ω_{sys}
Only section overstrength	0.86	1.342	0.048	28.2	0.134	1.08
System overstrength	0.86	1.285	0.116	24.7	0.136	1.19

Table 6-11: The overstrength factor with and without floor interaction under MCE

	T_1(sec)	T_{eq}(sec)	a	ζ_{eq}	Δ^*_u(m)	Ω_{sys}
Only sectional overstrength	0.86	2.172	0.048	31.3	0.446	1.37
System overstrength	0.86	1.778	0.116	23.7	0.380	1.74

Table 6-12: The system overstrength factor at three different drift limits

	At DBE level	At MCE level	At ultimate base rotation capacity
Without slab	1.08	1.37	1.285
With slab	1.19	1.74	1.689

6.5 Conclusion

This Chapter complements the findings of the three earlier chapters presented in the Thesis (chapters 4, 5, and 6). It focused on outlining the recommendations for improved capacity design principles for multi-storey shear wall buildings. An improved capacity design method has been proposed considering the effect of floor systems on seismic behaviour of typicall ductile RC shear wall buildings commonly used in NZ. A method was also developed to determine the system overstrength factor when the first plastic hinge formed at a wall base.

The proposed method was verified using the results of nonlinear time history analysis and parametric studies using an experimentally validated constitutive shear wall model. The

method was also implemented in real building to validate its feasibility in the context of three-dimensional reinforced concrete shear walls considering three-dimensional spatial interaction of floor system with structural walls and frames. More details of the developments and the applications of the proposed design method were presented in Chapters 4, 5 and 6.

6.6 References

ATC-40 (1996). *Seismic evaluation and retrofit of concrete buildings*. Redwood City, California: Applied Technology Council, Seismic safety commission.

Mander, J. B., Priestley, M. J., and Park, R. (1988). Theoretical stress-strain model for confined concrete. *Journal of structural engineering*, *114*(8), 1804-1826.

NZS1170.5 (2004). Strcutral Deisng Actions, NZS 1170.5:2004 Parts 1 and 2 Standards New Zealand.

NZS3101 (2006). Concrete Structures Standard, NZS 3101:2006 Parts 1 and 2 Standards New Zealand.

Priestley, M. J. N., Calvi G. M., and Kowalsky M. J. (2007). *Displacement-based seismic design of structures*. Pavia, Italy: IUSS Press.

Thompson, K. J., and Park, R. (1978). Stress-strain model for grade 275 reinforcing steel with cyclic loading. *Bulletin of the New Zealand Society for Earthquake Engineering.New Zealand*, *11*(2), 101.

7 Concluding Remarks and Research Recommendations

7.1 Concluding Remarks

This thesis sought to shed light on the three-dimensional spatial interaction between structural walls, gravity columns, and flooring systems in multi-storey shear wall buildings. The outcome of this thesis will improve the capacity design of multi-storey structural walls. The aims of the thesis were i) to gain insight into the mechanism of three-dimensional spatial interaction; ii) to identify the key variables involved in this phenomenon; iii) to quantify the system overstrength factor in typical multi-storey shear wall buildings, and iv) to investigate its implication on capacity design of structural walls. The following steps were taken to achieve these objectives:

- A review of all modelling approaches available for the numerical modelling of structural walls; specifically the ones proposed for three-dimensional analysis of shear walls under dynamic excitation
- Verification and validation of a numerical modelling approach using experimental results of wall specimens tested under both static and dynamic loadings.
- Evaluating capability of the modelling approach in the prediction of key engineering demand parameters obtained from the results of large-scale multi-storey wall specimen tested under seismic shaking, and identifying the governing parameters.
- Designing a different typical multi-storey shear wall building for a parametric study of three-dimensional spatial interaction to investigate the variation of system overstrength factor and axial force amplification in structural walls and columns.
- A parametric study on different variables affecting the interaction mechanism between structural walls, flooring systems and frames, and close scrutiny of key parameters including the bay length, the floor stiffness and the wall height on the system overstrength factor, and amplification of axial forces in the wall and the columns.

The conclusions resulted from different parts of this research are included at the end of each chapter, and the overall findings are presented herein along with the corresponding objectives presented in Chapter 1.

Objective 1: To obtain a variation of system overstrength factor in typical configuration of multi-storey shear wall buildings

The system overstrength factor in multi-storey shear wall buildings due to the three-dimensional spatial interaction mechanism and its controlling parameters was studied by employing the validated numerical model. Vertical deformation of structural walls can trigger the out-of-plane/torsional stiffness of floor slabs and/or axial stiffness of columns. This phenomenon introduces an additional lateral resistance to the ductile multi-storey shear wall buildings. It can be confirmed by the aid of the numerical simulation (and a shake table testing of full-scale multi-storey shear wall building conducted by other researchers) that the contribution of floor systems and gravity columns to the system lateral strength is significant in the post-yield stage of ductile structural walls. Then, this additional lateral resistance can be defined as a system overstrength factor of multi-storey shear wall buildings. It was also shown that quantifying the system overstrength in multi-storey shear wall buildings played a crucial role for capacity design of structural walls.

The results indicated that the flexural/torsional stiffness of floor systems, target (design) plastic rotation of the wall base section, distance of frames from the structural walls, and height of structural walls play a significant role in the 3D spatial interaction mechanism and consequently the magnitude of the system overstrength factor. For the case study buildings analysed in this thesis, the values of system overstrength factor at three different base rotation levels are postulated in tables for practical application. The proposed values accounted only for the system overstrength due to the sectional strain hardening effect as well as the effect of

spatial interaction between the structural walls, floor system, and columns. Overstrength actions associated with the difference between the expected and characteristic material properties should be calculated and considered separately by the designer. The analysis results indicated that the system overstrength factor for the case studies varied from 1.36 to 1.50 at design base rotation equal to 0.015 rad. For the design base rotation other than 0.015 rad, one can refer to the tables presented in chapter 4.

Further investigation confirmed that for the same base section and axial forces the system overstrength factor increases with the height of structural walls. Proposed analytical equations also demonstrated that by increasing the number of floors, the induced axial forces in the gravity columns increases. Hence, the system overstrength factor for the 5, 8 and 10 stories case study walls were also presented in different tables. For example, the system overstrength factor of three case studies (with the same floor flexural stiffness, bay length and axial force) were equal to 1.63, 1.76 and 1.82 at base rotation level equal to 0.015 rad.

The main findings under this objective are:

- Average system overstrength factors at a design base rotation equal to 0.015 rad for the typical case studies investigated in this study are:

Case studies	At base rotation =0.015 rad
With Slab (EI_e=0.25EI_g)(five storey)	1.54
With Slab (EI_e=0.25EI_g)(eight storey)	1.64
With Slab (EI_e=0.25EI_g)(ten storey)	1.70

- A closed form equation is developed to estimate the elastic floor rotation in each level $\left\{Y'(Z) = \theta(Z) = \frac{\emptyset_{base}}{8H^3}Z^4 - \frac{3\emptyset_{base}}{4H}Z^2 + \emptyset_{base}Z\right\}$.

  This equation along with other equations which were presented in chapter 3 can be used to estimate the system overstrength factor.

Objective 2: To find the variation of axial force amplification in structural walls and gravity columns due to the three-dimensional spatial interaction of floor systems and frames

Another effect of the interaction between the structural walls, floor system, and frames is the variation of axial force in the structural wall and gravity columns. This varying axial force is induced due to the vertical stiffness (along the height) imposed by the floor system on the structural walls (or the vertical deformation compatibility between the structural walls and floor systems). Results of the numerical investigation confirmed that spatial interaction could increase the amount of axial force induced by deformation compatibility in the gravity columns. The columns close to the structural walls experienced a significant variation of axial forces during the system excitation compared to the columns far away from the structural walls. The axial force amplification in a representative column of the case studied building showed the variation of axial forces between 1.06 and 1.80 at the wall base rotation equal to 0.015 rad. Hence, different tables were generated to show the axial force variation in critical gravity columns of typical multi-storey shear wall buildings at different levels of wall base rotation. The amount of amplification has a key implication on shear strength design of gravity columns because the contribution of concrete to the shear resistance is a function of axial forces in columns.

However, the scrutiny of results obtained from the variation of axial forces in the structural wall itself revealed the variation of axial force (averaged over the case studies with the same floor stiffness) varied from 1.21 to 1.38 at base rotation level equal to 0.015 rad in base case studies.

Objective 3: To investigate the effect of out-of-plane stiffness of the floors on seismic response of multi-storey shear wall buildings

Out-of-plane stiffness of the floor systems (slabs) is another important parameter in the calculation of system-overstrength factor. Floor systems with higher flexural rigidity were found to induce larger axial forces into the gravity columns.

Although the deformation compatibility between the structural walls and floor system cause the floor system to bend (flexture) and/or twist (torsion), only the flexural stiffness of floor slabs was treated as a key variable in this thesis. The recommended values for out-of-plane stiffness of floor slabs at the ultimate limit state loads varied significantly in literature. Hence, three different numerical values were used for the flexural stiffness of floor slabs. This sensitivity analysis was carried out to quantify the variation of results to our assumption for the flexural stiffness of floor systems. The numerical values associated with this analysis were also presented in different tables in chapter 4.

It has been confirmed that this variable plays a key role in the extent of system overstrength generated due to the interaction mechanism throughout the building. For the base case studies with the floor slabs having the effective flexural stiffness equal to 0.25 and 0.5 times the gross stiffness, the average system overstrength factor was equal to 1.64 and 1.91 respectively at a design base rotation equal to 0.015 rad.

Objective 4: To explore the effect of different damping models in emulating the nonlinear response history of multi-storey shear wall buildings under dynamic excitation

Close scrutiny of results obtained from the dynamic analysis indicated that a common method employed to model the elastic damping in the nonlinear dynamic analysis of structural walls can induce high spurious damping force. These damping forces can reach up to 40 percent of gravity loads on structural walls. The spurious damping forces caused an increase in the base moment capacity of structural walls which was not realistic. Investigation on results of moment curvature analysis demonstrated that the wall base section, in all case studies, experienced an

increase in the flexural strength due to the spurious damping forces in all case studies. The cause for this was attributed to the traditional (Rayleigh) damping model employed in the global level. To overcome this issue, a material level damping model was used and all case studies were reanalyzed with the new damping model. In the author's knowledge, this is the first time that this type of damping model has been applied in nonlinear analysis of ductile walls. Further, to differentiate between the damping matrix of the yielded and elastic materials, we proposed a stiffness proportional damping multiplier equal to zero for all yielding materials (elements) having substantial initial stiffness. Comparison of results obtained from the pushover analysis with the dynamic analysis confirmed that the new damping model is effective in numerical modelling of ductile walls. Then, prototype buildings were excited under the ground motion records to reach a specific base rotation level by scaling a number of ground motion records. Significant trial and error was required to find the appropriate scale factors to reach a specified target (design) base rotation.

Objective 5: To develop a simplified method to quantify effects of interaction between structural walls, floor systems and frames in capacity design of structural walls

To improve the capacity design of ductile structural walls, a simplified methodology was proposed for the estimation of the system overstrength factor in multi-storey shear wall buildings. An attempt was made to find a displacement shape for the cantilever structural walls with uniform mass and stiffness. The proposed displacement pattern for the structural walls was employed to obtain the floor rotations and wall edge vertical deformations in every single floor. Then, the floor system in either direction was replaced with equivalent beam-type elements to impose the deformation compatibility equations. The results of the proposed hand calculation methodology demonstrated that assumption of half span in either direction for the equivalent beam led to a reasonable agreement with the numerical results.

The extensive moment curvature analysis was also conducted to establish a reliable effective curvature at the base section of walls for a given axial force, wall length, and reinforcement.

Hence, the floor rotations were obtained as a function of the wall base effective curvature, wall height and floor distance to the base. These floor rotations along with geometric deformation of wall panels in the plastic state were adopted to find the wall edge vertical deformations. The resulted vertical deformations were used to propose a simplified closed form formulation for calculating the system overstrength factor in multi-storey shear wall buildings.

At the end of this thesis, to demonstrate the practical application of the proposed method, the system overstrength factors of an example multi-storey shear wall were examined at these levels of responses: (i) at the ultimate base rotation capacity; (ii) at DBE (design base earthquake); and (iii) at MCE (maximum credible earthquake) level shakings. A summary of important findings from this study follows:

- System overstrength factors for the case study buildings at three different levels of shakings are:

	At DBE level	At MCE level	At ultimate base rotation capacity
Without floor slab	1.08	1.37	1.285
With floor slab	1.19	1.74	1.689

- The degree of spatial 3D interaction goes up with increasing flexural/torsional stiffness of the floor system, and consequently the system overstrength factor reduces when the flexural/torsional stiffness of floor system reduces.
- By increasing the height of structural walls, the system overstrength factor increases. In other words, low rise multi-storey structural walls may have less system overstrength factor in comparison to high rise structural walls.

- Reducing the target (design) base rotation demand leads to reduction in system overstrength factor.
- Reducing the distance of gravity columns from the structural walls results in a higher system overstrength factor.

In summary, the capacity design of ductile multi-storey RC structural walls should recognise, during the design phase, all sources of overstrength actions including the effect of the floor systems; otherwise the RC multi-storey structural walls might fail in shear before yielding in a ductile manner at the base plastic hinge. Currently, some design standards overlook the effect of system overstrength actions, which are induced due to the interaction between the floor systems, structural walls and gravity columns. Some other design standards aim to decouple the vertical displacement compatibility between the floor systems and RC structural walls. Enhanced capacity design procedures for multi-storey RC structural walls could recognise the system over-strength factor, by introducing an additional coefficient (an upper bound value) to the shear design equations for RC structural walls, to prevent shear failure.

7.2 Future Research Topics

There are many relevant research areas which could be investigated in a greater detail in future. Although an extensive investigation has been conducted in this project, numerous assumptions have been made during the development of closed form solutions as well as the numerical models for the proposed recommendations. One important area of research is to explore the system effects in multi-storey shear wall buildings under dynamic excitation. Several topics need to be investigated in future research projects:

1. This project only investigated simple configuration of walls in the plan. However, more complex geometry can exist in real buildings. Different wall configurations can be investigated in future studies.

2. The number of ground motions used in this study was limited since the objective was to address the interaction mechanism in detail. In this thesis, the emphasis was placed on understanding the system interaction mechanism and not much attention was paid on the effect of number of good motions and characteristics. Hence, extensive analysis can be conducted with a larger number of ground motions to obtain the median and variance of the results at different levels of seismic hazards.
3. Effect of material nonlinearity inside the floor systems including cracking and yielding can be addressed by a rigorous analysis method in future studies.
4. Effect of induced axial forces due to the spatial interaction of the floor system with columns and shear walls, on the shear strength of columns adjacent to the shear walls should be explored rigorously. Through such studies, one can find the upper and lower bound values for column shear strength according to variation of axial forces.
5. The effects of wall cross section type, cross sectional torsion, and irregular mass distribution can also be significant and need further investigations.
6. This research assumed that the wall foundations are adequate for transmission of the induced base shears and moments and that they are fixed at their base. Therefore, more detailed investigation on the effects of foundation strength and rigidity should be considered in future studies.

APPENDIX-A

A summary of nonlinear response history analysis results is presented in this section for analyses employing Damping model B. The definition of parameters for this type of damping model was introduced in Chapter 5. This damping model employs different damping parameters for yielding and non-yielding materials.

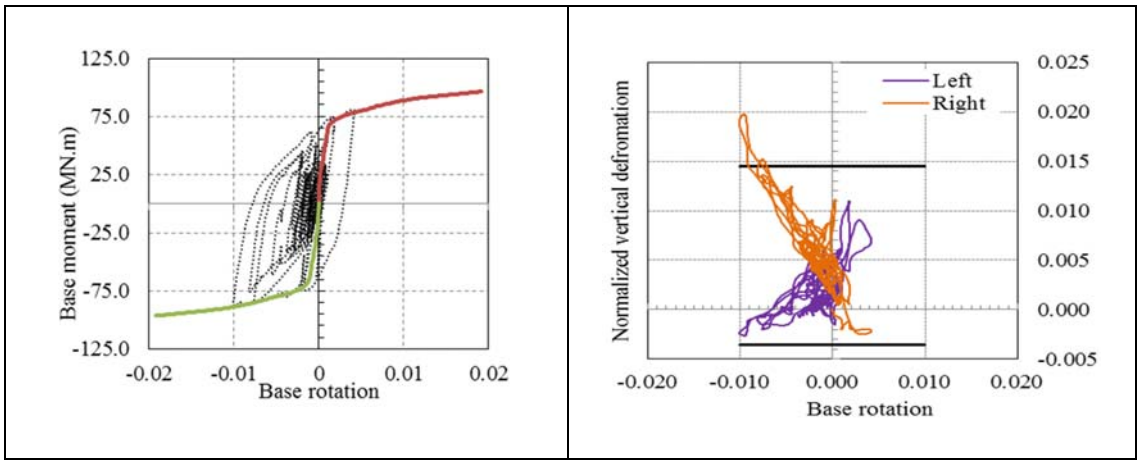

Case1-1- Damping model B, analysis results-ELC

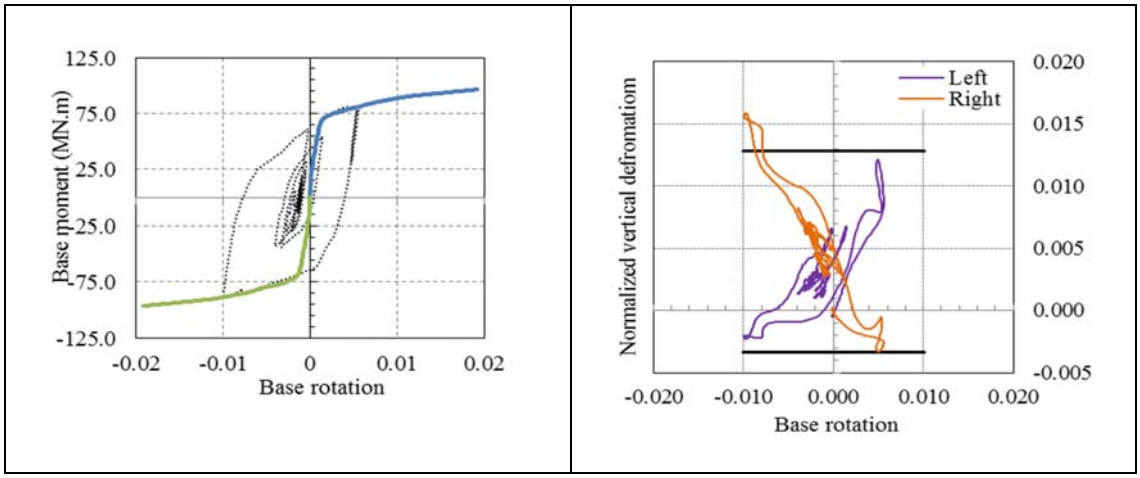

Case1-1- Damping model B, analysis results-SOVM

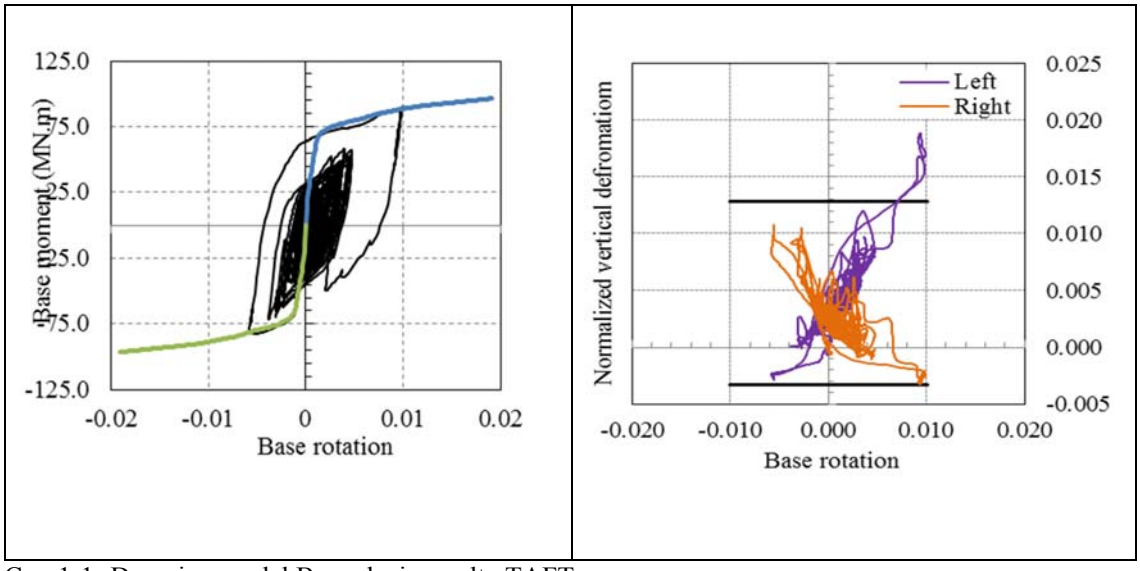

Case1-1- Damping model B, analysis results-TAFT

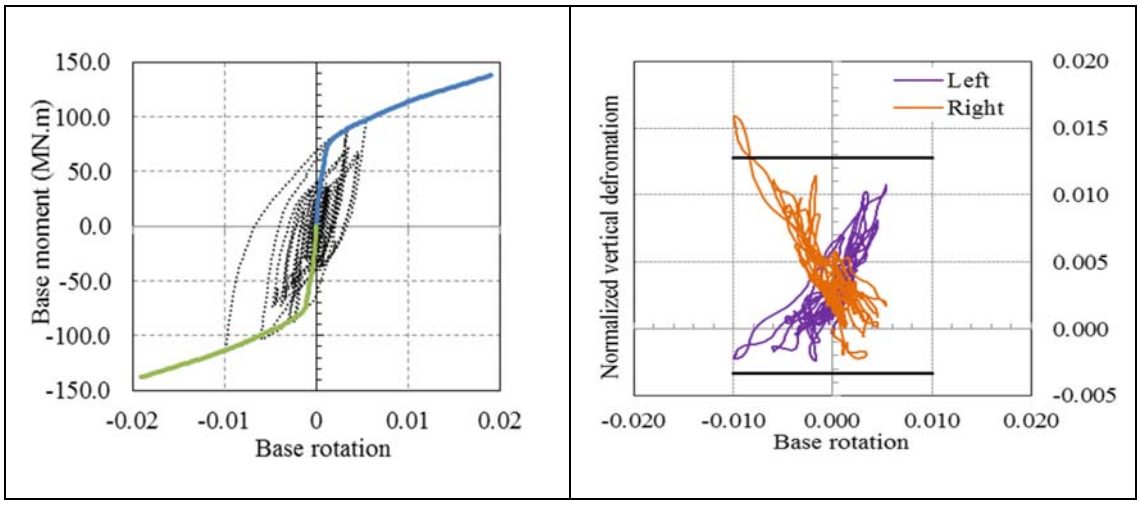

Case2-1- Damping model B, analysis results-ELC

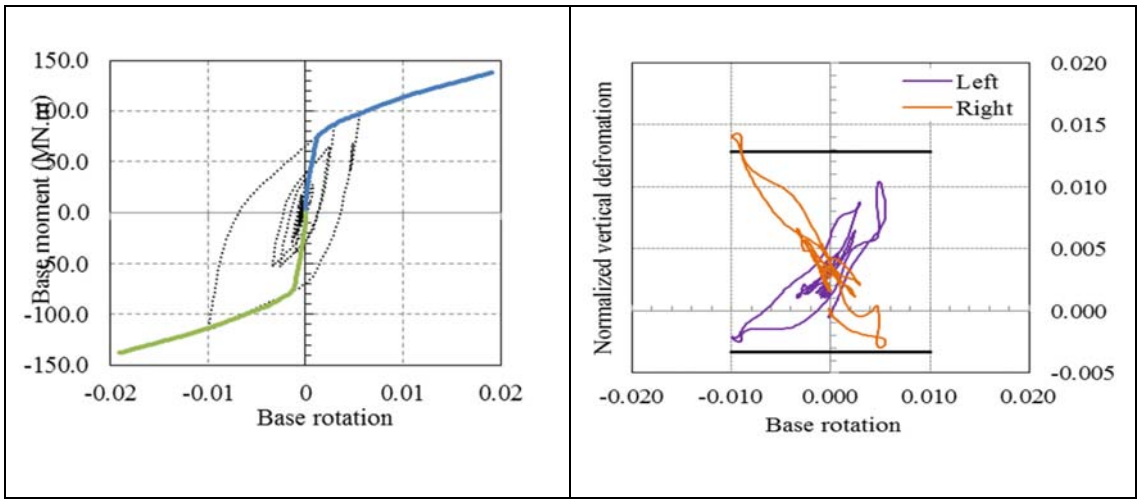

Case2-1- Damping model B, analysis results-SOVM

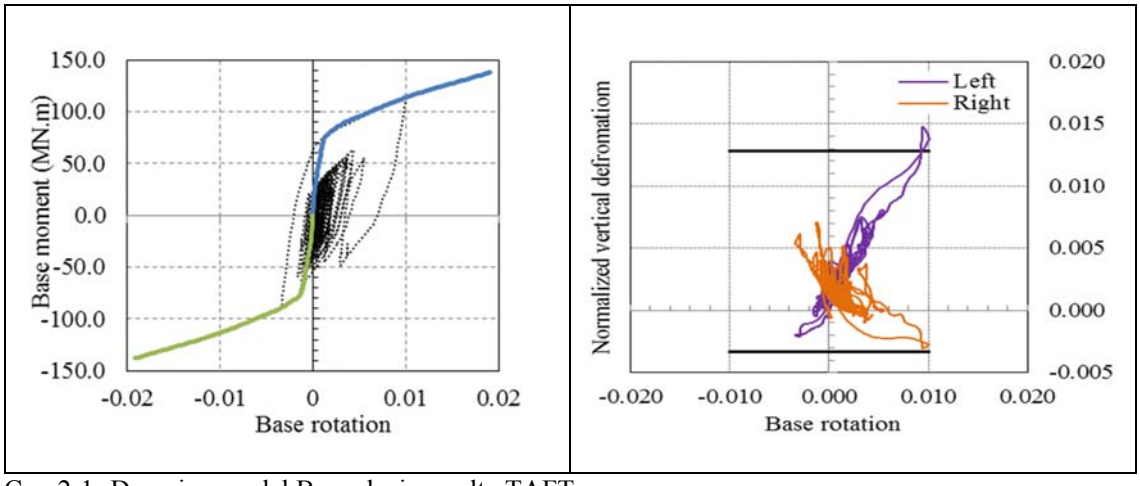

Case2-1- Damping model B, analysis results-TAFT

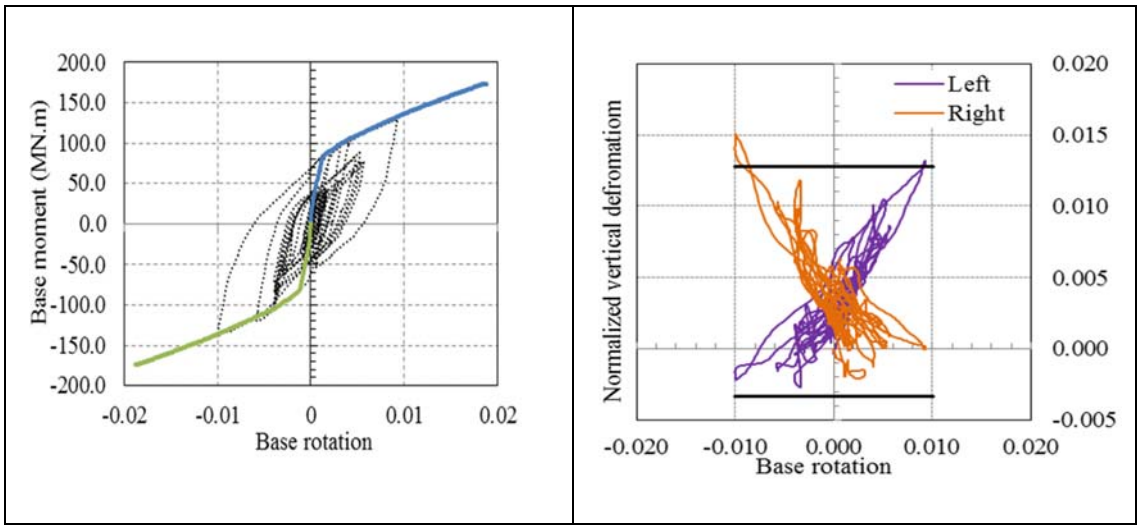

Case2-2- Damping model B, analysis results-ELC

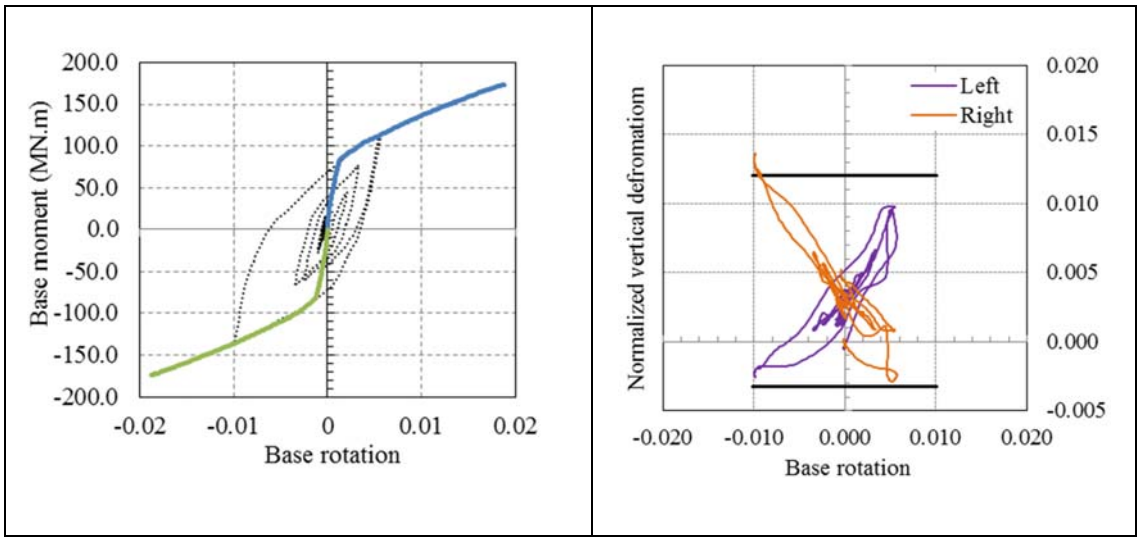

Case2-2- Damping model B, analysis results-SOVM

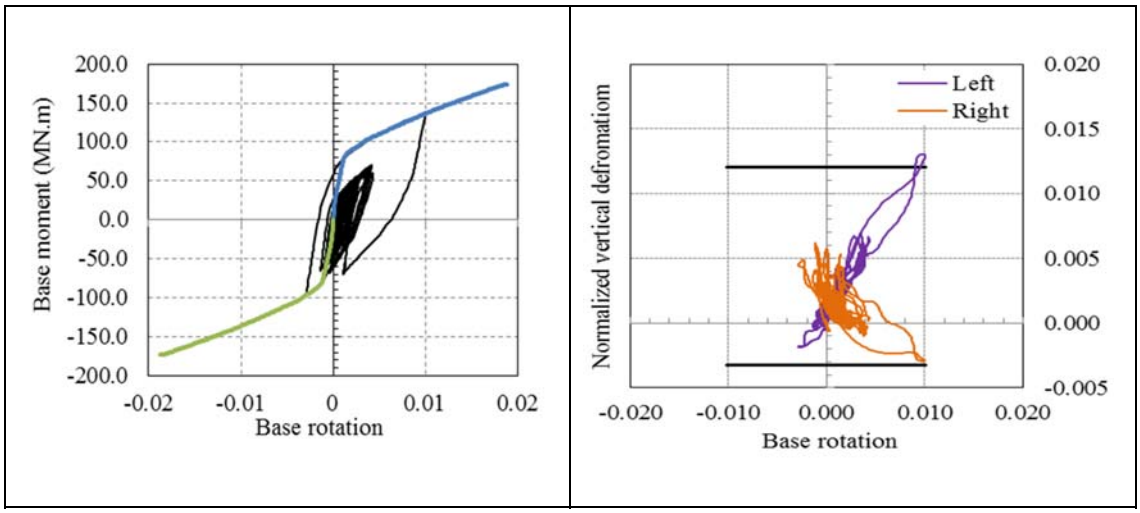

Case2-2- Damping model B, analysis results-TAFT